THE
PHYSICAL REVIEW
A Journal of Experimental and Theoretical Physics
VOL. 46, NO. 10 NOVEMBER 15, 1934 SECOND SERIES

Depth Distribution of Origins of Characteristic X-Rays from Thick Targets

PAUL KIRKPATRICK AND DONALD G. HARE, *Stanford University*
(Received October 3, 1934)

If I is the intensity of any x-ray wave-length as observed in a direction making an angle ϕ with the face of the (thick) target in which the radiation originates, then

$$S_T = \frac{-1}{\mu}\left(\frac{d \log I}{d \csc \phi}\right)_{\csc \phi = 0}$$

is the depth of the *centroid of the x-ray luminosity distribution* in the target. This depth is greater than the effective mean depth of production by an amount which depends upon the angle of observation and the form of the luminosity distribution. For large angle observation of Ag $K\alpha$ at 100 kv (and probably at any voltage) the two depths are identical within the errors of measurement. The distributions of x-ray luminosity with target depth for Ag $K\alpha$ from a thick target are calculated for six tube potentials from 50 kv to 175 kv from the intensity observations of Webster, Hansen and Duveneck. There is as yet no theory of these distribution functions. The characteristics of the curves obtained are shown to be capable of fairly simple mathematical description and to be in harmony with certain physical checks.

INTRODUCTION

WHEN x-rays are produced by normal incidence of electrons upon a thick target, radiation originates at all depths within a layer extending from the target surface to some heretofore undetermined maximum depth which depends upon the characteristics of the target material and the energy of the incident electrons. It is the purpose of this paper to discuss the distribution with depth of the *x-ray luminosity* of the target, that is, the energy (of a specified wave-length) radiated per second per unit volume of target per unit target current. This luminosity is a function of electron energy as well as of depth and wave-length and for any given value of these three independent variables it is presumably different for characteristic and general radiations. While the following discussion is partly of general application it relates more particularly to the $K\alpha$ luminosity of silver targets.

MEAN DEPTH OF PRODUCTION

The work of Ham,[1] of W. P. Davey[2] and of L. G. Davey[3] established the concept of a *mean depth of production* for the unresolved x-ray output of a thick target, and showed the possibility of measuring such a depth by observation of the relative intensities of total x-radiation emerging at different angles with the target face. Webster and Hennings,[4] in a study of the penetration of cathode rays in molybdenum, measured the mean depth of production of a particular wave-length (i.e., the wave-length of the absorption limit of the target) for a number of molybdenum continuous spectra. While the next step in the problem is the determination of the depth distribution of luminosity for a particular wave-length, this

[1] W. R. Ham, Phys. Rev. **30**, 1 (1910).
[2] W. P. Davey, J. Frank. Inst. **171**, 277 (1911).
[3] L. G. Davey, Phys. Rev. **4**, 217 (1914).
[4] D. L. Webster and A. E. Hennings, Phys. Rev. **21**, 301 (1923).

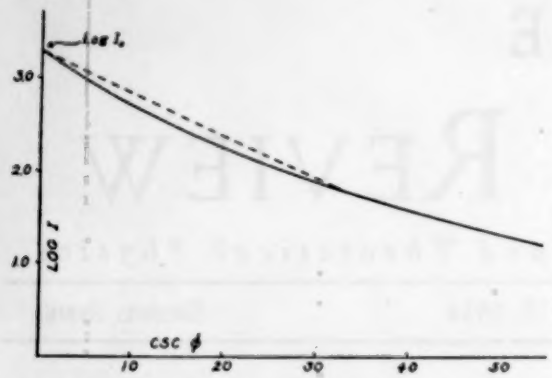

FIG. 1. Kulenkampff curve for determining mean depth of production and target absorption correction for monochromatic x-rays. (Ag $K\alpha$ at 100 kv.)

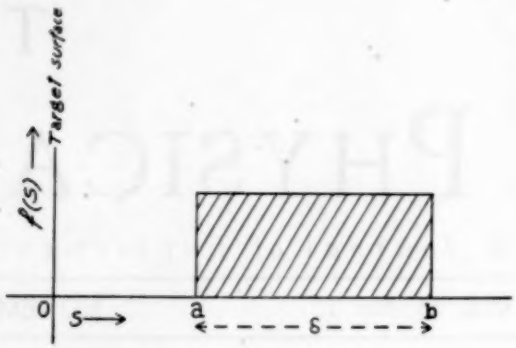

FIG 2. Assumed rectangular x-ray luminosity distribution.

matter is deferred until the next section, while we consider here an extension of the theory of the mean depth of production.

The only known method of measuring the mean depth of production of monochromatic radiation applicable to any chosen x-ray wave-length is the method of Ham[1] and the Daveys[2, 3] with the addition of an x-ray spectrometer for wave-length resolution. This is essentially the method used by Kulenkampff[5] to determine the attenuation of primary x-rays through absorption in the target, and since used by others for the same purpose and for the determination of mean depths of production. Following Kulenkampff, one sees that if all radiation (of some observed wave-length) were actually produced in a thin layer situated at a depth S below the target face, with I_0 representing the intensity *as emitted* then the intensity *as observed* would be similarly represented by $I=I_0e^{-\mu Sx}$, where μ is the x-ray absorption coefficient of the target and x the cosecant of the angle of observation measured from the target face. It follows that $\log I=\log I_0-\mu Sx$ and that both S and I_0 may be obtained graphically from a plot of $\log I$ *vs.* x. In particular

$$S=(-1/\mu)d(\log I)/dx. \tag{1}$$

Now although the equation above shows a linear relation between $\log I$ and x the real graph (Fig. 1) is not straight, for it results from a luminosity distribution which is quite different from the assumed concentrated layer, and with such a distribution the effective depth of production may be said to vary with x. When, as in real targets, luminosity is distributed over a range of depths the mean depth of production is best defined as that depth at which the entire luminosity could be concentrated without change in the externally observed intensity. We shall designate the depth so defined by $\bar{S}$ and call it hereafter the effective depth of production.

The graph of Fig. 1, which is typical of the many Kulenkampff curves which have been used in thick target studies, shows a marked upward concavity. That such curves must always possess this type of curvature unless the radiation all originates at the same depth may be shown by considering a rectangular luminosity distribution buried in a thick target as in Fig. 2, in which $f(s)$ measures the luminosity and s represents distance into the target. The emerging intensity is

$$I=\int_a^b f(s)e^{-\mu xs}ds=(-k/x\mu)[e^{-\mu bx}-e^{-\mu ax}].$$

If $y\equiv\log I$ this leads to

$$\frac{dy}{dx}=\frac{\mu\delta e^{-\mu x\delta}}{1-e^{-\mu x\delta}}-\mu a-\frac{1}{x}, \tag{2}$$

where, as in Fig. 2, $\delta=b-a$. Upon differentiating again it is found that the second derivative is positive, which insures the upward concavity for this special distribution. But any distribution whatever can be analyzed into rectangular elements and consequently any Kulenkampff curve may be regarded as the sum of the curves belonging to its constituent rectangular distributions. Since all the constituent curves are concave up-

[5] H. Kulenkampff, Ann. d. Physik **69**, 548 (1922).

ward their sum must be curved in the same sense.

We may now examine the variation of the effective depth of production with the angle of observation. By definition of $\bar{S}$ we have $I = I_0 e^{-\mu \bar{S} x}$ or

$$\bar{S} = (\log I_0 - \log I)/\mu x, \qquad (3)$$

which is $(1/\mu)$ times the absolute value of the slope of the chord drawn in Fig. 1, from the intercept on the log I axis to the point of the curve having the abscissa x. It is apparent from the graph that the effective depth of production varies with the angle of observation, being zero when $\phi = 0$ and increasing with ϕ, in a manner which depends upon the form of $f(s)$, to a maximum for normal observation of the target face ($\csc \phi = 1$).

Although the angle $\csc^{-1} 0$ is fictitious, it has useful properties in this analysis. Kulenkampff[5] shows that the extrapolation of the curve to $\csc \phi = 0$ furnishes an intercept (in the case of smooth targets) which measures I_0, the intensity which the radiation would have if the target were non-absorbing. We now show that the effective depth of production for this fictitious angle is the depth of the *center of gravity* of the luminosity distribution curve. As x approaches zero, Fig. 1 shows that the chord of the curve approaches the tangent, and at the limit we have by Eq. (1)

$$\bar{S}_{x=0} = \frac{-1}{\mu}\left(\frac{d \log I}{dx}\right)_{x=0}. \qquad (4)$$

To evaluate the derivative we first restrict ourselves to the conventional distribution of Fig. 2, whose derivative is given by Eq. (2). Rearranging Eq. (2) we have

$$\frac{dy}{dx} = \frac{-\frac{(\mu\delta)^2}{2!} - \frac{(\mu\delta)^3 x}{3!} - \frac{(\mu\delta)^4 x^2}{4!} - \cdots}{\mu\delta + \frac{x(\mu\delta)^2}{2!} + \frac{x^2(\mu\delta)^3}{3!} + \cdots} - \mu a,$$

from which it is apparent that

$$(dy/dx)_{x=0} = -\mu(a + \delta/2) = -\mu S_g, \qquad (5)$$

where S_g is the distance from the target surface to the *center of gravity* of the assumed distribution. From Eqs. (4) and (5) it follows that

$$\bar{S}_{x=0} = S_g.$$

Though the luminosity distribution assumed was a special one, more general conclusions may be drawn. Imagine two distinct (though permissibly contiguous) rectangular distributions in the same target, and suppose it to be possible to observe in various directions the radiation from either separately or from both together. In each of the three cases of observation suppose the Log I *vs.* x curve to be plotted and extrapolated to $x = 0$, where all the intensities and intensity derivatives used below are taken. Using subscripts 1, 2 and T to designate quantities related to the separate distributions and to their total, respectively, we have

$$I_T = I_1 + I_2 \quad \text{and} \quad (dI_T/dx) = dI_1/dx + dI_2/dx.$$

The depths to the centers of gravity of the separate distributions, as shown by Eq. (4), are

$$S_{g1} = (-1/\mu)(dy_1/dx) = (-dI_1/dx)/\mu I_1$$

and

$$S_{g2} = (-dI_2/dx)/\mu I_2.$$

From the equations of this paragraph we may obtain

$$dy_T/dx = (dI_T/dx)/I_T = -\mu \frac{S_{g1} I_1 + S_{g2} I_2}{I_1 + I_2} = -\mu S_T, \qquad (6)$$

where S_T is the depth of the center of gravity of the combination. Since any real distribution may be built up by the successive addition of properly chosen rectangular blocks it follows that in any case the depth of the center of gravity of a distribution is given by Eq. (4).

The center of gravity depth is greater than the effective depth of production, even when the latter is at its maximum ($\phi = 90°$), but it is obvious in Fig. 1 that the change in slope from $x = 0$ to $x = 1$ is very small, for any reasonable extrapolation, so the difference in these two depths must also be small in this fairly typical case. We refer to these depths again in a later section.

Method of Determining Luminosity Distributions

Webster, Hansen and Duveneck[6] have measured the intensity of the $K\alpha$ lines from a thick silver target upon whose plane face cathode rays were incident normally, making observations at several voltages up to 175 kv and at various angles ϕ between the direction of observation and the target face. With the symbols used above the observed intensity (in arbitrary units) at any given electron energy is

$$I(\phi)=\int_0^\infty f(s)e^{-\mu s\csc\phi}ds, \tag{7}$$

where $I(\phi)$ is known for a number of values of ϕ from experiment and $f(s)$ is the luminosity distribution function to be found. The history of this equation as recorded in the literature of mathematics does not encourage an attempt at an exact analytical solution, and it seems necessary to resort to methods of approximation. Physical considerations impose important conditions upon $f(s)$ which serve as guides in seeking solutions: the function is never negative or infinite, it is zero for all negative values of s and practically so for all positive values exceeding the foil range of cathode electrons. It is finite at $s=0$ and almost certainly goes to zero with zero slope.

Eq. (7) has appeared in physical problems before[7] and several possible methods of attack have been used or proposed. We have found most useful an as yet unpublished method suggested by Professor William V. Houston of California Institute of Technology. In this method it is assumed that the luminosity distribution is adequately representable by

$$f(s)=e^{-Hs}(a+bs+cs^2+\cdots), \tag{8}$$

an assumption which gives Eq. (7) the form

$$I(\phi)=\frac{a}{\mu x+H}+\frac{b}{(\mu x+H)^2}+\frac{2c}{(\mu x+H)^3}+\cdots.$$

Having a number of observations of I equal to the number of constants retained in $f(s)$ we can solve for these constants and thus determine the function. Since $f(s)$ must in reality be a smooth curve and since it is believed to decrease monotonically to zero at the maximum depth somewhat after the manner of an exponential, it seems certain that the assumed form will permit a satisfactory representation.

Our procedure has been to replot the data contained in Fig. 1 of reference 6 in such a way as to smooth out certain slight irregularities caused by the use of non-identical units of measurement for different angles of observation. This smoothing did nothing to correct for possible *systematic* variations of the unit of measurement with angle. If such variations existed they were probably worst at the largest grazing angles of observation, so we have not used Webster, Hansen and Duveneck's data for any angles above 8.05°, except for checking purposes. From the selected data the constants of Eq. (8) were obtained, through the method suggested by Houston, assisted by graphical devices and cut-and-try approximations which cannot be economically described.

The constant a in the expression for $f(s)$ represents the luminosity of the target surface, which should vary with voltage in approximately the same manner as does the intensity of the $K\alpha$ lines from a *thin* target of silver. The two cases differ in that the thick target surface emits a greater proportion of radiation produced by fluorescence and electron rediffusion, but both of these secondary effects show voltage variations which approximately parallel the variation in intensity of the directly produced radiation, so we have ignored the difference and imposed the condition that variations of a with voltage shall agree with the *thin* target intensity variations found by Webster, Hansen and Duveneck.[8]

The function assumed in Eq. (8) takes on small negative values for large values of s, since the constant c turns out to be negative. This physically impossible result emphasizes the arbitrary nature of the functional form assumed, and in this connection we must certainly disclaim any suggestion that the terms in the series represent separate physical processes of x-ray production. However, any method of luminosity analysis based upon the angular variation of external in-

[6] D. L. Webster, W. W. Hansen and F. B. Duveneck, Phys. Rev. **44**, 258 (1933).

[7] L. Silberstein, J. O. S. A. **22**, 265 (1932); Phil. Mag. **15**, 375 (1933); C. Eckart, Phys. Rev. **45**, 851 (1934).

[8] D. L. Webster, W. W. Hansen and F. B. Duveneck, Phys. Rev. **43**, 839 (1933).

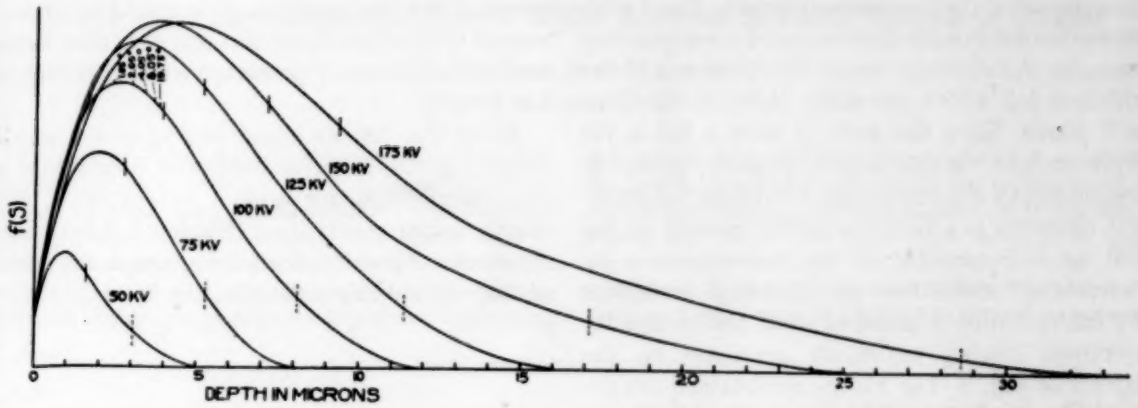

FIG. 3. Luminosity distributions of $K\alpha$ radiation from a thick silver target with cathode rays incident along normals to the plane target face. Solid vertical line segments intersecting the curves mark the positions of the centers of gravity of respective distributions. The relation of the center of gravity to the effective depths of production for various angles of observation is illustrated in the case of the 100 kv curve. For 90° (normal) observation the two depths are sensibly identical. Dotted lines crossing the curves indicate foil ranges of electrons at corresponding potentials. Ordinates are in arbitrary units which are the same for all curves.

tensity will give results which are less dependable the greater the depth, and the negative luminosities which we obtain are within the probable error of luminosity determination for the depths at which they occur, as is shown by the fact that the calculated external intensity from the integrated negative luminosity is within the error of intensity measurement. We have therefore discarded the negative part of the distribution curves and smoothed off the region of amputation in an arbitrary but, we believe, physically plausible manner.

RESULTS AND DISCUSSION

The distributions obtained are shown for a series of six cathode-ray energies in Fig. 3. The equation representing each curve contains four constants and has been derived from intensity observations at four values of the angle ϕ. Since the simultaneous solution of the four equations containing experimentally determined magnitudes was a very inexact process and since the obtained solutions have been arbitrarily adjusted in some particulars it is important to check the distributions obtained back against the original data. This is a much simpler operation than its inverse, and is in line with our view that the proof of the distribution is not in the rigor of its derivation but in its ability to recreate all the original intensity observations. The recheck was performed by plotting from each $f(s)$ in Fig. 3 a series of curves represented by $y=f(s)e^{-\mu\rho z}$ for five values of ϕ, including the four used in obtaining $f(s)$. The areas of the curves so obtained were found to be proportional to the corresponding original observations upon $I(\phi)$, as they should be, closely enough so that the two sets of values could be matched with an average discrepancy of between 1 and 2 percent and with a maximum under 5 percent. Uncertainties in the original data, make it useless to strive for a better fit. The distributions obtained are therefore as good as the observations permit.

It is difficult to evaluate the probable errors of the distributions in Fig. 3, or, indeed, to define a suitable measure of probable error. We find, however, that a distribution will fail to check back upon the data from which it came, causing discrepancies of 5 or 10 percent, if the maximum of the distribution be raised or lowered by as much as 10 percent relative to the ordinate at $s=0$, or if the extreme depth of the distribution be changed by 20 percent.

Present knowledge of electron scattering and stopping processes is probably not complete enough to permit a theoretical calculation of the luminosity distribution functions, and even with such knowledge the computation would be formidably complex. A partial check on the experimental distributions may be obtained, however,

by comparing the maximum depths in Fig. 3 with measured foil ranges of electrons of corresponding energies. A foil range means the thickness of the thickest foil which normally incident electrons will pierce. Since the path in such a foil is far from straight, the foil range is, in silver,[9] probably less than half the real range. Foil range for different elements is a function of the density of the foil, so it is possible to use measurements by Schonland[10] and others on aluminum to deduce by interpolation a series of *silver* foil ranges for electrons having potentials pertinent to the curves of Fig. 3. The ranges so obtained are denoted by vertical dotted lines crossing the distribution curves.

The relation of these ranges to the luminosity distributions was an afterthought and has not been injected in any way into the solutions themselves, so the agreement shown in the figure may be accepted as a useful confirmation. The existence of luminosity below the depth of the foil range is presumably caused by fluorescence.

The centers of gravity of these distributions all agree in depth with the values obtained by the graphical method (Eq. 4) within the limits of error of our determinations of the latter. Since both methods start from the same data, this is not exactly an independent check on the correctness of the distribution curves but is a demonstration that the same result can be had by two methods for computing the same quantity when one method depends heavily upon the correctness of the distributions.

Webster, Hansen and Duveneck,[6] after correcting their thick target silver $K\alpha$ intensities for target absorption by extrapolating the curve of log I *vs.* csc ϕ to csc $\phi=0$, found the corrected intensity $I_0(U)$ to vary with U, the ratio of tube voltage to K-ionizing voltage, according to the equation $I_0(U)=K(U-1)^{1.65}$ up to about $U=4$. Using for $I_0(U)$ the areas under the curves of Fig. 3 we find a similar relation to hold, over the same range of voltage, except that the exponent is 1.58. This difference does not seem too large to be accounted for by the combined non-systematic errors of the two methods so it would be unwarranted to conclude from this one case that either method is inherently prone to yield either high or low results.

Along the 100 kv curve of Fig. 3 are marks indicating the effective depths of production of this distribution for several values of ϕ. For ninety degree observation this depth differs from the center of gravity depth by less than the width of the vertical line indicating the latter.

Conclusion

Summarizing, the luminosity, $f(s)$, of silver $K\alpha$ radiation produced in a thick target by normal cathode rays when plotted against depth, s, in the target results in a distribution curve which starts with a finite $f(s)$ at $s=0$, rises to a maximum and falls away gradually to zero at a depth several times the depth of the maximum. This general character is possessed by all distributions investigated, from 50 kv to 175 kv. The depth of the maximum in microns is given approximately by $S_m=0.8\ (U-1)$. The depth to the center of gravity of the distribution, which is almost identically the effective depth of production for normally emerging rays, is given approximately by $S_g=1.45\ (U-1)$. The maximum depth limit is difficult to state since the curve has no sharp intersection with the s axis, but the depth at which the distribution has decreased to 1/10 of its value at the maximum may be stated approximately as $S_l=3.3\ (U-1)$, at least up to $U=5$, after which S_l seems to increase slightly faster with U. The height of the maximum of $f(s)$ varies from 2.5 times its value at the target surface in the case of the 50 kv curve to 6.5 times for the 175 kv curve. The height of the maximum increases with U less rapidly as U increases and attains a maximum between $U=6$ and $U=7$. The area under the curves, giving the total emitted energy, varies with U according to the formula found by Webster, Hansen and Duveneck in a different treatment of the same data.

It is a pleasure to acknowledge a number of helpful conversations with Professor Carl Eckart of the University of Chicago upon the solution of Eq. (7).

[9] E. J. Williams, Proc. Roy. Soc. **A130**, 310 (1931).
[10] B. F. J. Schonland, Proc. Roy. Soc. **A104**, 235 (1923); **108**, 187 (1925); C. E. Eddy, Proc. Camb. Phil. Soc. **25**, 50 (1929); R. W. Varder, Phil. Mag. **29**, 726 (1915).

Direct and Fluorescence Excitation of the *K*-Level in Thick Targets of Copper

K. B. STODDARD, *Stanford University*

(Received August 27, 1934)

The ratio P of the probability of exciting the K shell of copper by direct cathode-ray impact to the probability of exciting the same shell by fluorescence in a thick target, is measured with normally emergent rays over a range of voltages extending from 2 to 17.4 times the K excitation voltage. P is found to vary from 6.63 at $U=2$ to 7.2 at $U=17.4$, where U is the ratio of tube voltage to K excitation voltage. The ratio Q of the probability of a cathode ray ionizing the K shell directly to the probability of a cathode ray exciting a continuous quantum of frequency greater than the K-limit frequency is found to be very nearly constant at 3.5 for the same voltage range. The variation of P with Z is examined theoretically and compared with experiment showing a lack of good agreement.

INTRODUCTION

A NUMBER of measurements have been made of the relative probabilities of exciting the K shell of atoms in a thick target by direct cathode-ray impact and by fluorescence.[1-4] The more quantitative measurements have been made since 1928 and have indicated that for silver and palladium the ratio of the probabilities of exciting the K level by the two methods is practically constant, showing no significant variation with voltage.

The question immediately arises as to whether this ratio will be independent of voltage for other elements and further; what is the variation of this ratio with change in atomic number?

The first attempt to investigate the method of excitation of characteristic x-radiation was made by Beatty.[1] This investigation was made before the development of the Bragg spectrometer and hence the results can be accepted only as tentative. Making use of a copper target this experiment led to the conclusion that practically all the characteristic radiation resulted from direct cathode-ray impact. Beatty likewise examined the subject theoretically and announced that not over ten percent of the radiation could be accounted for by fluorescence.

It was thought expedient to determine the ratio P for Cu by the more accurate methods now available as a step in the more general problem of the variation of P with atomic number.

In the previous work on this subject a curious relationship between line and continuous spectra was found to persist.[4, 5] The ratio Q defined above was found to be practically constant over a wide range of voltages for the two elements silver and palladium. It is interesting to investigate this ratio further to see whether it will continue to be independent of voltage for other elements, in particular copper.

THEORY OF EXPERIMENT

In previous work recourse was had to a composite target of two elements of adjacent atomic number. The backing block or target proper was made of the one of higher atomic number and the other element was in the form of a foil of sufficient thickness to stop all cathode rays. This insured that all the characteristic radiation from the block was excited by fluorescence. The ratio P was calculated from certain expressions after the ratio of the intensities of the resulting two $K\alpha$ radiations was determined experimentally. This method is quite successful as long as the thickness of the foil necessary to stop the cathode rays is small and the α-line radiation from the block of sufficiently short wave-length. However, as the atomic numbers of the foil and block decrease, the thickness of the foil necessary to stop all cathode rays increases as does also the wave-length of the $K\alpha$ radiation; both factors tending to reduce the intensity of the characteristic x-radiation from the block. The effect of the increase of wave-length of the fluorescence rays from the block on foil absorption more than offsets the effect of the reduction in atomic number. Preliminary calculations showed that for copper such a scheme as outlined above would be impracticable, for the higher voltages at least, as the

[1] R. T. Beatty, Proc. Roy. Soc. **A87**, 511 (1912).
[2] Mark Balderston, Phys. Rev. **27**, 696 (1926).
[3] D. L. Webster, Proc. Nat. Acad. Sci. **13**, 445 (1927); **14**, 330 (1928).
[4] W. W. Hansen and K. B. Stoddard, Phys. Rev. **43**, 701 (1933).
[5] D. L. Webster, Proc. Nat. Acad. Sci. **14**, 339 (1928).

intensity of the block characteristic x-radiation would be reduced to a point where it could not be distinguished from the continuous background.

Another method, suggested by Beatty's original experiment, was therefore used. This method makes use of the comparison between the $K\alpha$-line intensity from a copper target and the $K\alpha$-line intensity from the same target covered with an aluminum foil sufficiently thick to stop all cathode rays. The ratio of these two intensities together with certain calculations to be outlined below will enable the determination of the ratio P. It should be noted, parenthetically, that this method using the aluminum foil while enabling one to carry the measurements to a higher voltage than the previously described method, nevertheless eventually is limited. The necessary foil thickness to stop cathode rays, reduces the characteristic x-radiation from the block by increasing both the absorption of the continuous rays going in and the α-line radiation coming out. There is evidently a limiting thickness beyond which no characteristic x-radiation will be observed. A method of overcoming this difficulty by obtaining P from a bare copper target will be discussed below.

Theoretical

In the following development all intensities are to be defined as energy per unit solid angle, per cathode electron.[3, 4]

The following symbols are defined as follows:

Let I = intensity of Cu $K\alpha$ lines (unresolved) from the bare copper target.
d = fraction of I excited directly.
i = fraction of I excited by fluorescence.
i_+ = part of i that is excited at depths greater than the mean depth of production of the continuous rays $\bar{x}$.
i_- = part of i excited at depths less than $\bar{x}$.
i_b = intensity of Cu $K\alpha$ lines from Cu target covered with Al foil.

The intensity from the bare copper target will be composed of both direct and fluorescence rays. $I=d+i$ and as $P=d/i$ by definition, $P+1=I/i$ where $i=i_++i_-$. The expressions for i_+, i_- and i_b are given immediately below. The reader is referred to Webster's[4] original paper for the development of the expressions for i_+ and i_-. The expression i_b is obtained in substantially the same way, taking into account the Al foil on the copper target.

$$i_+=R\exp(-\mu_{\alpha_2}\bar{x}_2)F(V,0);\qquad i_-=R\Phi(V,\bar{x}_2);\qquad i_b=R\exp(-\mu_{\alpha_1}x_1)f(V,x_1-\bar{x}_1)$$

where

$$F(V,0)=\int_{\nu_k}^{\nu_0}\frac{I(V,\nu)}{\nu}\frac{\mu_2}{\mu_{\alpha_2}}\log\left(1+\frac{\mu_{\alpha_2}}{\mu_2}\right)d\nu$$

$$\Phi(V,x)=\int_{\nu_k}^{\nu_0}\frac{I(V,\nu)}{\nu}\frac{\mu_2}{\mu_{\alpha_2}}\left\{\exp(-\mu_{\alpha_2}x)\left[Ei\{(\mu_{\alpha_2}-\mu_2)x\}-\log\left|\left(1-\frac{\mu_{\alpha_2}}{\mu_2}\right)\right|\right]-Ei(-\mu_2x)\right\}d\nu$$

$$f(V,x)=\int_{\nu_k}^{\nu_0}\frac{I(V,\nu)}{\nu}\frac{\mu_2}{\mu_{\alpha_2}}\left[\exp(a\mu_{\alpha_2}x)Ei\{-(a\mu_{\alpha_2}+\mu_1)x\}-Ei(-\mu_1x)\right]d\nu$$

$$R=\tfrac{1}{2}u_a\nu_a(\mu_k/\mu_2)$$

where $\mu_1=3.86\times10^{24}C^{2.55}\nu^{-2.55}$ cm^{-1} = absorption coeff. for Al[6]

$\mu_2=1.165\times10^{25.4}C^{2.5}\nu^{2.5}$ cm^{-1} = absorption coeff. for Cu[6]

$\mu_{\alpha_1}=133.7$ cm^{-1} = absorption coeff. of Al for Cu $K\alpha$ -rays

$\mu_{\alpha_2}=460$ cm^{-1} = absorption coeff. of Cu for Cu $K\alpha$ -rays

$a=\mu_1/\mu_2$

$\mu_k/\mu_2=0.88$ = ratio of K absorption to total absorption in Cu[6]

u_α = α-line fluorescence efficiency in Cu

ν_k = frequency of K discontinuity

ν_0 = high frequency limit

ν_α = α-line frequency

$\bar{x}_1$ and $\bar{x}_2$ are the mean depths of production of the continuous rays in Al and Cu, respectively

x_1 = thickness of Al foil.

[6] Martin and Lang, Proc. Roy. Soc. **A137**, 199 (1932).

$I(V, \nu)$, the intensity of the continuous radiation per unit frequency interval at the mean depth of production $\bar{x}$, is approximated as $I(V, \nu) \cong k(\nu_0 - \nu)$. This could be improved somewhat for voltages less than twice the excitation voltage for Cu $K\alpha$-rays but any better approximation for higher voltages is unknown at present, so this form is used in all the numerical calculations.

$P+1 = I/i$ can be found without the foil measurements, if u_a and k are known. u_a may be found from various data now available, but k is unknown for the present work. However, by making use of i_b

$$P+1 = \frac{I}{i} = \frac{I}{i_b}\left[\frac{\exp(-\mu_{a_1}x_1)f(V, x_1 - \bar{x}_1)}{\exp(-\mu_{a_2}\bar{x}_2)f(V, 0) + \Phi(V, \bar{x})}\right]$$

where I/i_b is the ratio of the intensity of the Cu α-lines without the foil to the intensity with the Al foil measured in the same units. This is accomplished by comparing each line intensity with the continuous intensity at the mean depth of production $\bar{x}$ for each case and then reducing these to the same intensity unit. The remainder of the expression for $P+1$ is readily calculated. The unknown or uncertain factors such as k and u_a appear in both numerator and denominator and are eliminated. The α-line intensity produced directly is a fraction $P/P+1$ of the total.

When this method fails the unknown factors in i may be obtained from values of P measured by the Al foil method at lower voltages; allowing the evaluation of P for higher voltages from the bare copper target measurements of the ratio of line ordinate to continuous ordinate.

$$P+1 = \epsilon I(V, \nu_a)/i = \gamma(\nu_0 - \nu_a)\delta/S,$$

where ϵ is the ratio of K line area to continuous ordinate at λ_a; γ is the ratio of line ordinate to continuous ordinate;

$$S = \tfrac{1}{2}\nu_a\nu_K[\exp(-\mu_{a_2}\bar{x}_2)F(V, 0) + \Phi(V, \bar{x}_2)];$$

and δ, a factor to be found from P measured by the Al foil method at lower voltages, the ratio of line area to line ordinate being constant.[3]

The ratio Q of the probability of a cathode ray ejecting a K electron directly to the probability of a cathode ray exciting a continuous quantum frequency greater than the K-limit frequency, as determined from a thick target, may be immediately evaluated from P with a small calculation.

$$Q = \mu_2 i P \exp(\mu_{a_2}\bar{x}_2) \Big/ \mu_k R \int_{\nu_k}^{\nu_0} \frac{I(V, \nu)}{\nu} d\nu.$$

The results of the calculations obtained by numerical integration, together with the measurements and values for P and Q are given in Table I. The results are shown graphically in Fig. 1.

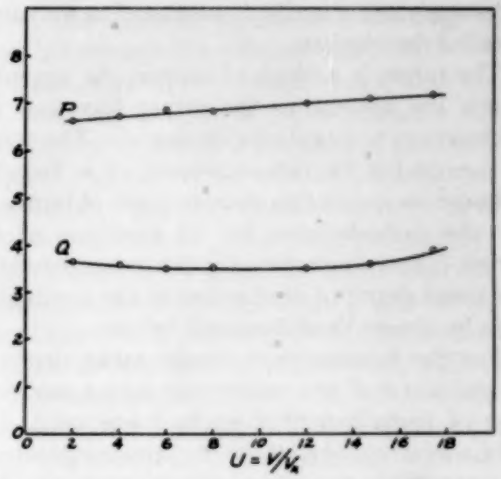

FIG. 1. P and Q are plotted as functions of U.

TABLE I. *Calculations and measurements leading to the values for P and Q.*

$U = V/V_k$	2	4	6	8	12	14.7	17.4
Calculated quantities							
i_b/D*	0.317	1.795	3.50	5.18	8.64	10.6	11.7
i_a/D	0.043	0.486	1.30	2.67	5.70	8.4	12.2
i/D	0.360	2.281	4.80	7.85	14.34	19.0	23.9
i_b/D	0.122	0.640	1.27	1.94	—	—	—
$\delta \times 10^{-18}$	1.01	0.97	1.00	1.06	1.15†	1.22†	1.28†
Measured quantities							
$\bar{x}_1 \cdot 10^4$ cm	0.59	2.14	3.95	5.85	—	—	—
$\bar{x}_2 \cdot 10^4$ cm	0.18	0.65	1.20	1.78	3.2	4.4	6.6
I/i_b	22.4	27.4	29.7	31.6	—	—	—
γ	49.2	117	146	161	178	181	183
Results							
P	6.63	6.71	6.87	6.83	7.0	7.1	7.2
$P/P+1$	0.869	0.870	0.873	0.872	0.875	0.877	0.878
Q	3.67	3.58	3.50	3.50	3.5	3.6	3.9

* $D = Rk\nu_k$; † extrapolated values.

EXPERIMENTAL

The type of tube used in this research is not sufficiently different from other tubes used in this

laboratory and described elsewhere[7] to warrant a detailed description.

The target is a block of copper; the angle between the normal to the target face and the cathode-ray stream being 60 degrees. The target is surrounded by the equivalent of a Faraday cylinder to insure this definite angle of incidence for the cathode rays for all positions of the target. This is important for the measurement of the mean depth of production of the continuous rays by the method discussed below.

For the measurement of the mean depth of production $\bar{x}$ of the continuous rays a modification of Kulenkampff's[8] method was used. The tube was arranged so that the cathode-ray stream was parallel to the slits of the spectrometer. The intensity of the continuous spectrum at some wave-length less than the K-limit wave-length was observed for a number of positions of the target; the target being rotated about the cathode-ray stream as an axis, to these positions. Then if φ is the angle of rotation about the axis measured from the position $\varphi=0$ illustrated in Fig. 2,

$$\log I_\varphi = \log I_{\bar{x}} - \bar{x} \sec 30^\circ \sec \varphi$$

provided all the continuous rays are assumed to originate at the depth $\bar{x}$.

If now $\log I_\varphi$ is plotted against $\sec \varphi$, $\bar{x}$ may be obtained from the slope of this curve at $\sec \varphi = 1$.

This method worked admirably with copper but when tried with aluminum, I_φ did not differ measurably from $I_{\varphi=0}$ except for φ very close to 90 degrees. φ could not be determined accurately enough for the rapid variation of $\sec \varphi$ in this region, so for aluminum this method was abandoned. The values for $\bar{x}$ were finally calculated from the Cu $\bar{x}$ measurements by assuming that $\bar{x}$ is approximately inversely proportional to the number of electrons per unit volume.[9] This extrapolation is decidedly uncertain but fortunately no great accuracy is needed as i_b for which $\bar{x}_1$ is needed changes very slowly with variation in $\bar{x}_1$.

In the calculations the assumption is made that not only the continuous rays for a given wave-length are all produced at a depth $\bar{x}$ but also that all wave-lengths from λ_k to λ_0 are also produced at this depth. A special investigation, rather rough to be sure, indicated no significant variation in $\bar{x}$ with λ except very near the quantum limit, substantiating to some extent the latter assumption.

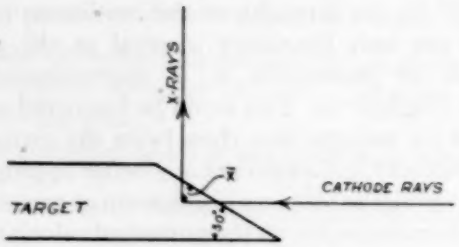

FIG. 2.

In measuring the ratio I/i_b the first step was to measure the ratio of the line ordinate to the continuous ordinate for the bare Cu target. The same ratio was obtained for the Cu target covered with the Al foil. Since the ratio I/i_b really is obtained by matching the continuous spectrum intensities in the two cases, it is essential that this be done at the mean depth of production in each case.

Therefore

$$I/i_b = \frac{I_a/I_{c_a} \exp\left(\mu_{a_1}\bar{x}_1 - \mu_{a_2}\bar{x}_2\right)}{i_a/i_{c_a}}.$$

In the measurement of γ, the ratio of the line ordinate to the continuous ordinate, the continuous spectrum intensity was corrected for second and higher order reflections from calcite by using Kirkpatrick's method. The continuous spectrum intensity at λ_a was obtained analytically by a Taylor series expansion about λ_a.

$$I(\lambda_a+\Delta\lambda) = I(\lambda_a) + C_1\Delta\lambda_a + C_2(\Delta\lambda_a)^2 + \cdots.$$

Terms involving the third and higher powers in $\Delta\lambda$ were neglected. $I(\lambda_a+\Delta\lambda)$ was measured for at least three different $\Delta\lambda$'s.

The thickness x_1 of the aluminum foil necessary to stop all cathode rays was calculated from Williams's[8] expression for cathode-ray retardation in the form

$$x = \frac{V_k^{1.36}(U^{1.36}-1)A}{7.65\times 10^4 Z\rho},$$

[7] D. L. Webster, W. W. Hansen and F. B. Duveneck, Rev. Sci. Inst. 3, 729 (1932).
[8] H. Kulenkampff, Ann. d. Physik 69, 548 (1922).
[9] H. M. Terrill, Phys. Rev. 21, 476 (1923); 22, 107 (1923).

where x is the penetration in cm measured along the path of cathode ray, A the atomic weight, Z the atomic number, ρ the density, V_k the excitation voltage for Cu $K\alpha$-rays, and $U=V/V_k$. Since the direct range is the important thing here rather than the total range Williams's[10] estimate $x_{direct}/x=1/1.37$ for Al obtained from Schonland's[11] work, is used. Parenthetically it might be pointed out that $\bar{x}$ as measured by target absorption methods is roughly 1/10 of x calculated from Williams's formula. This relation holds more accurately for the measurements of $\bar{x}$ in palladium[4] than for copper. In connection with any use of this expression it should be remembered that $\bar{x}$ is measured in a direction perpendicular to the target face, which is inclined 60° to the cathode-ray stream.

Discussion of Results

The first topic to be discussed in this section is the important one of limit of error. The random error in the determination of I/i_b is about 2 percent. It is practically impossible to determine the overall error in P beyond a rough estimate because of the numerous assumptions involved in the calculation of the fluorescence intensity. It is thought, however, that P and Q are determined with a probable overall error less than 20 percent. For the three highest voltages the error is probably somewhat greater due to the uncertainty in determining δ by extrapolation from the lower voltage values. The error in $P/P+1$, the fraction of the total α-line radiation that is directly produced, is of course very much less than 20 percent.

The results tabulated in Table I are in general accord with other determinations[3, 4] of P and Q, (except that of Wisshak[12]) in that both P and Q show little variation with voltage. It is interesting to note at this point that Beatty's original estimate of the indirectly produced x-radiation in copper is exceptionally good considering the necessarily rough nature of his experiment. It should be remembered that he estimated that not more than 10 percent of the characteristic radiation in copper could be accounted for by fluorescence; the present experiment showing that about 13 percent is produced indirectly.

In palladium it was found that Q was about 0.9, showing that it is more probable for a cathode ray to excite a continuous quantum of frequency greater than the K-limit frequency than for it to eject a K electron directly. It is to be observed that for copper the probability of direct ionization is about 3.5 times that of its continuous spectrum equivalent. A general variation of this type is to be expected from the change of characteristic and continuous thick target intensities with atomic number. As to the value of Q to be expected beyond the limits of the voltage range examined here, the reader is referred to the discussion of this point elsewhere.[4]

Variation of P with Z

Now that quantitative measurements of P are available for at least three atomic numbers it will be of interest to investigate the variation of P with Z. In order to do this one examines separately the variation of d and of i with Z.

The $K\alpha$-line intensity produced directly from a thick target may be obtained as follows:

$$d=\exp(-\mu_\alpha \bar{x}_d)\int_0^{U_0} i(U)(ds/dU)dU,$$

where $i(U)$ is the α-line intensity per unit solid angle, per unit cathode-ray path, and per cathode ray of energy U; U_0 is the initial energy of the cathode ray; dU/ds, the cathode-ray retardation expressed as a function of U.

In the above expression all electrons are assumed to possess an energy U after traversing a distance s in the target; also the number of cathode rays losing a large amount of energy in any one interaction producing either characteristic or continuous x-radiation is small compared to the total number. Rediffusion effects are neglected. Correction for target absorption is made by the insertion of the attenuation factor $\exp(-\mu_\alpha \bar{x}_d)$ on the assumption that the average depth of production of the directly produced α-line x-rays is $\bar{x}_d$. The approximate expression, $U_s^n=U_s^n-as$ is used for cathode-ray retardation, in which $n=2$ for the Thomson-Widdington law and about 1.6 to agree with the more recent work of Williams[10] and Webster, Hansen and

[10] E. J. Williams, Proc. Roy. Soc. **A130**, 310 (1931).
[11] B. F. J. Schonland, Proc. Roy. Soc. **A108**, 187 (1925).
[12] F. Wisshak, Ann. d. Physik **5**, 507 (1930).

Duveneck.[13] $i(U)$ is obtained from Bethe's[14] expression for the ionization cross section for K electrons, although the exact dependence on U is not essential here.

$$i(U)=\frac{c_1 u_a \nu_a b}{Z^4 U}\log\frac{4U}{B}\sim\frac{c_2 u_a b}{Z^2}f(U),$$

in which quantities not previously defined are the constants c_1 and c_2; b, a factor changing very slowly with Z, and $B\leqq 1$ except for very low atomic numbers.

Integration then gives

$$d\sim\text{const. } u_a b \exp(-\mu_a \bar{x}_d)Z^{0.2}F_d(U_0),$$

assuming $n=1.6$.

This expression for d together with i from the section on theory expressed in a more suitable fashion

$$i\sim\text{const. } \mu_k Z^5 \exp(-\mu_a \bar{x}_i)F_i(U_0)/\mu$$

gives $P\sim A\beta Z^{-4.8}\Psi(U_0)$. Here A is a constant, β is a factor including a number of factors such as μ_k/μ, rediffusion,[15] etc., that show such small variations with Z that this dependence may be neglected in this rough consideration. The assumption is also made that the mean depth of production of the directly produced rays $\bar{x}_d$ is equal to the mean depth of the fluorescence rays $\bar{x}_i$, which is sufficiently good for the purpose here.

The comparison of P for different elements keeping U constant (assuming the form of $\Psi(U_0)$ remains the same), should show a direct variation roughly as $Z^{-4.8}$. Referring to Table II it is seen that this is not confirmed experimentally, in fact the experimental dependence insofar as it can be estimated from the experimental data at hand is about $Z^{-2.6}$.

The estimated error in both the palladium and copper P measurements is not in excess of 20 percent. Assuming that the error is 20 percent and of opposite sign in the two experiments, which seems exceedingly improbable, the dependence of P on Z would be about $Z^{-3.3}$, still leaving a factor of $Z^{-1.5}$ to be accounted for if the theoretical prediction is correct. Of course a number of simplifying assumptions were made in the theoretical expression for the variation of P with Z but all of them together do not seem to be of sufficient importance to account for the divergence of the theoretical and experimental results. In fact any improvement in the theory such as taking into account rediffusion, etc., seems to make the divergence slightly greater.

In spite of the fact that the theory does not predict the variation of P with Z quantitatively it shows several qualitative facts quite clearly. First, it predicts a rapid decrease in P with increasing Z; and second, it shows the increasing relative importance of the fluorescence method of excitation over the direct excitation with increasing Z. The directly produced x-rays increasing with Z to a positive power less than 1 and the fluorescence rays increasing very much faster, about as Z^5.

The variation of Q with Z theoretically as predicted by a line of reasoning similar to that used for P is the same as for P, namely, an inverse variation with $Z^{4.8}$. The experimental variation is the same as for P so the same discrepancy between prediction and observation is observed for Q as for P.

TABLE II. *Comparison of P for different elements keeping U constant. The ratio varies more nearly as $Z^{-2.6}$ than as $Z^{-4.8}$.*

U	$\frac{P_{Cu}}{P_{Pd}}$	$\frac{P_{Cu}}{P_{Ag}}$	U	$\frac{P_{Cu}}{P_{Pd}}$	$\frac{P_{Cu}}{P_{Ag}}$
1.5		3.57	4.0	3.24	
2.0	3.37	3.51	6.0	3.26	
2.5	3.34	3.46	Ave.	3.30	3.49
3.0	3.31	3.41	$(Z_{Cu}/Z_{Pd})^{-4.8}$	9.10	10.06
			$(Z_{Cu}/Z_{Ag})^{-2.6}$	3.31	3.50

[13] Webster, Hansen and Duveneck, Phys. Rev. **44**, 258 (1933).

[14] H. Bethe, Ann. d. Physik **5**, 325 (1930).

[15] A special calculation showed that rediffusion effects would introduce a multiplication factor of 1.08 into the comparison of the P's for palladium and copper. The variation of μ_k/μ for the same comparison is negligible.

The Widths of the *L*-Series Lines and of the Energy Levels of Au(79)

F. K. RICHTMYER,* S. W. BARNES AND E. RAMBERG, *Cornell University*

(Received September 1, 1934)

Following a résumé of the Weisskopf-Wigner theory of the shape of spectral lines, and, making certain simplifying assumptions, an expression is derived for the shape of an x-ray absorption discontinuity for the case where absorption is due to the ejection of electrons from inner orbits to the continuum of unoccupied Fermi-Sommerfeld levels. If these levels be assumed equally distributed, the curve (μ *vs.* λ) is a simple arctangent, from which the width of the associated energy level (K, $L\cdots$), corresponding to the full width of half-maximum of a radiated line, may be read directly. A more complicated expression results if the Fermi-Sommerfeld levels be not equally distributed. It is shown that the predicted shape of an absorption limit agrees reasonably well with the observed shape of the L_{III} limit of Au(79), the width of which was found to be 4.4 volts. Data are presented on the widths of some 23 lines in the *L*-series of Au(79), obtained by a two-crystal spectrometer. These widths, corrected for effect of the crystals, vary from 7.6 to 20.8 volts. Making use of the conclusion of Weisskopf and Wigner, that the width of a line may be interpreted as the sum of the widths of the energy states involved, and starting from the value 4.4 volts for the width of the L_{III} state, the widths of the several *L*, *M*, *N* and *O* states of Au(79) are computed. For a given total quantum number n, the width decreases with increasing orbital quantum number l. States having the same value of n, l have nearly the same width. For any given l, the *L* states are narrowest.

I. INTRODUCTION

THE advent of the two-crystal spectrometer has given impetus to the study of the shapes of x-ray lines; several comprehensive investigations have been recently reported. For example Williams[1] studied the widths of twelve of the *L*-series lines of U(92), using the Ehrenberg-Mark-Schwarzschild[2] equation

$$W_T=(W_O^2-W_R^2)^{\frac{1}{2}} \tag{1}$$

to obtain the true full width W_T at half-maximum intensity from W_O, the observed width with the crystals in the (1, +1) position, and W_R, that of the (1, −1) rocking curve. It is now known that this equation is in general not applicable, since neither the (1, −1) nor the (1, +1) rocking curves follow the Gauss law of errors upon which the equation is based. More recently Williams[3] has reported measurements on the lines $L\alpha_1$, $L\beta_1$, $L\beta_2$ and $L\gamma_1$ for seven elements from W(74) to Bi(83), no correction being made for the finite resolving power of the crystals on account of the uncertainty of the correct relation that exists among W_T, W_O and W_R.

In a recent paper[4] on the widths of the diagram lines in the *K*-series of W(74) the authors have shown that for those lines and spectral regions where *true* line shapes and (1, −1) rocking curves are given by the Hoyt[5] equation

$$y=a/[1+(x/b)^2] \tag{2}$$

(a is the maximum ordinate; b, the half-width at half-maximum) one may use, to correct for the effect of the crystals, the equation

$$W_T=W_O-W_R. \tag{3}$$

As will be seen from the present work, there is good reason to believe that, in accordance with the theory of Weisskopf and Wigner,[6] discussed below, an equation of the form of (2) represents with surprising accuracy the shape of an x-ray line. Wherever Eq. (2) applies, it and Eq. (3)—or, as will be shown below, an empirical modification of the latter—provide the tools for determining the true widths of x-ray lines from observed data.

Now, all theory aside, one might confidently expect that the width of a given spectral line would be determined by the width—or some quantity analogous thereto—of each of the energy states connected with the emission of the

* The senior author wishes to express his indebtedness to the Heckscher Research Council of Cornell University for a grant in aid of this research.

[1] J. H. Williams, Phys. Rev. **37**, 1431 (1931).

[2] W. Ehrenberg and H. Mark, Zeits. f. Physik **42**, 807 (1927); M. M. Schwarzschild, Phys. Rev. **32**, 162 (1928).

[3] J. H. Williams, Phys. Rev. **45**, 71 (1934).

[4] F. K. Richtmyer and S. W. Barnes, Phys. Rev. **46**, 252 (1934).

[5] Archer Hoyt, Phys. Rev. **40**, 477 (1932).

[6] V. Weisskopf and E. Wigner, Zeits. f. Physik **63**, 54 (1930); V. Weisskopf, Phys. Zeits. **34**, 1 (1933).

line. If so, a systematic study of the widths of as many as possible of the lines in each of the x-ray series, K, L, M . . . , for a given element should shed some light on the widths of the corresponding energy states. Accordingly, the present paper reports measurements on some twenty-three of the L-series lines and on the L_{I}, L_{II} and L_{III} absorption limits of Au(79); and also gives preliminary estimates of the widths of the several L, M . . . energy states of that element. It is hoped that similar data for the K- and the M-series lines of Au(79) will be reported from this laboratory later. As a by-product there are also reported: (1) relative intensities of the lines in each of several groups and (2) new values of the wave-lengths of several lines not heretofore completely resolved.

II. Theory of the Shapes of Lines and Absorption Limits

As Weisskopf[6] has pointed out, three factors serve to broaden out, and to determine the shape of, a spectral line. These are, in classical language, the radiation damping of the emitting atom, its heat motion, and the effects of neighboring atoms. Since the frequency width due to the first factor increases in proportion to the square of the frequency (Eq. (5)), while the effect of the remaining factors is proportional to the first or lower powers of the same, the effect of radiation damping predominates in the case of x-rays of short wave-length: Therefore the observed shape of an x-ray line, suitably corrected for the finite resolving power of the spectrometer used, is usually defined as the *true* line shape and very closely approximates the "natural line shape" of the spectral line in question.[7]

Classical theory treated the radiating atom as a damped harmonic oscillator with a displacement $A(t)$ given by

$$A(t)=A_0e^{-\pi\Gamma t}\cos(2\pi\nu_0 t+\varphi). \tag{4}$$

Here A_0 is the initial amplitude of the oscillator, ν_0 its undamped frequency, and φ a phase constant. The rate at which the oscillator loses energy, and hence the damping coefficient $2\pi\Gamma$, are determined by the frequency of the oscillation:

$$\Gamma=(4\pi/3)(e^2\nu_0^2/mc^3). \tag{5}$$

For not too heavily damped vibration, that is, for $\Gamma\ll\nu_0$, the spectral distribution of the radiation from such an oscillator is:[8]

$$J(\nu)d\nu=\frac{\Gamma}{2\pi}\frac{d\nu}{(\nu_0-\nu)^2+(\Gamma/2)^2}, \tag{6}$$

so that on a frequency scale Γ is simply the full width at half-maximum of the line emitted. On a wave-length scale this width, corresponding to (5), becomes 0.12 X.U., independent of frequency.[8] A. H. Compton,[9] in 1922, was able to show that observed x-ray line widths were much greater than this.

The mean life τ of an atom in its excited state (represented classically by the oscillator with its initial amplitude) is, by definition,[10] equal to the reciprocal of the damping factor:

$$\tau=1/2\pi\Gamma. \tag{7}$$

A quantum-mechanical treatment based on Dirac's radiation theory[11] led to a formula similar to Eq. (6) for the natural shape of a spectral line, but with a changed meaning for Γ. If we denote the initial state by A, the final state by B, we have according to Weisskopf and Wigner[12] for the distribution of energy

$$J_{AB}(\nu)d\nu=\frac{\Gamma_A+\Gamma_B}{2\pi}\frac{d\nu}{(\nu_{AB}-\nu)^2+((\Gamma_A+\Gamma_B)/2)^2}, \tag{8}$$

where

$$\nu_{AB}=\nu_A-\nu_B=(E_A-E_B)/h \tag{8a}$$

and

$$\Gamma_A=1/2\pi\tau_A=\sum_{E_C\leq E_A}{}'(C)\gamma_{AC};\qquad \Gamma_B=1/2\pi\tau_B=\sum_{E_D\leq E_B}{}'(D)\gamma_{BD}. \tag{8b}$$

[7] "Natural," because it is an intrinsic property of the atom, unaffected by its momentary motion or position relative to other atoms. It must be mentioned, on the other hand, that, due to the close linkage, the effect of neighboring atoms in solids is not altogether negligible, as has been shown by the work of L. G. Parratt, Phys. Rev. **45**, 364 (1934) on the widths of x-ray lines from alloys.

[8] G. E. M. Jauncey, Phys. Rev. **19**, 64 (1922).

[9] A. H. Compton, Phys. Rev. **19**, 68 (1922).

[10] "Mean life" is here defined as the time in which the square of the amplitude is reduced to a fraction $1/e$ (e = Napierian base) of its initial value.

[11] V. Weisskopf and E. Wigner, Zeits. f. Physik **63**, 54 (1930); see also L. Landau, Zeits. f. Physik **45**, 430 (1927). J. C. Slater, Phys. Rev. **25**, 395 (1925), obtained similar formulas on the basis of a modification of the old quantum theory.

[12] Excluding the possibility of the successive emission of two quanta of equal frequency by the same atom.

Here ν_{AB}, the frequency corresponding to the center of gravity of the line, is equal to the difference in the term values ν_A and ν_B of the initial and the final state, and this in turn is equal to the difference of the atomic energies E_A and E_B of the same states divided by Planck's constant, h; $2\pi\gamma_{AC}$ is the probability that, in unit time, a transition takes place spontaneously from state A to any other state C, necessarily of lower or equal[13] energy. The sum of the quantities $2\pi\gamma_{AC}$ for all such states C is hence the probability that, in unit time, an atom originally in state A leaves this state changing over to any other. If there are altogether N atoms in state A the most probable decrease in this number in time dt becomes, by (8b): $dN=-2\pi\Gamma_A N dt$, which, integrated, leads to the relation $N=N_0e^{-2\pi\Gamma_A t}$, N_0 being the number of atoms in state A at $t=0$. $2\pi\Gamma_A$ is thus the reciprocal mean life of the state A and, similarly, $2\pi\Gamma_B$ the reciprocal mean life of the state B.

According to Eq. (8) the width of any line depends on the life of both the initial and the final state of the emitting atom. If, making use of a picture given in an early paper by Schrödinger,[14] we were to regard the emission of radiation as associated with "beats" between the characteristic oscillations of the atom in the initial and final state, the time-decay of *each* of these states would contribute to the "fading," and hence to the spectral breadth, of the wave train emitted.

The form of the frequency distribution given in Eq. (8) immediately suggests as an alternative point of view the concept of unsharp levels with exact fulfillment of Bohr's frequency condition in every emission or absorption process.[15] Thus if the initial state A has the width Γ_A and frequency distribution

$$J_A(\nu)d\nu=\frac{\Gamma_A}{2\pi}\frac{d\nu}{(\nu_A-\nu)^2+(\Gamma_A/2)^2} \tag{9}$$

and analogously for the final state B, the frequency distribution for the transition $A\rightarrow B$ will be

$$J_{AB}(\nu)d\nu=\int_{\nu'=0}^{\infty}J_A(\nu')J_B(\nu'-\nu)d\nu'd\nu, \tag{10}$$

which, on performing the integration, yields Eq. (8). *The width of the line is thus equal to the sum of the widths of the initial and the final state.* That is

$$W_T=\Gamma_A+\Gamma_B, \tag{11}$$

where W_T is the true width of the line emitted in transition from state A to state B. Both Eq. (8) and the concept of unsharp levels lead to incorrect results if quanta of like frequency may be emitted by the atom in successive stages.

The theory of Weisskopf and Wigner applies to line shapes in absorption as well as in emission. It is therefore possible, by making a suitable series of assumptions, to predict the shape of an absorption limit as *experimentally measured*. Let us, for example, consider an atom in which an electron has been transferred from a specified inner shell to the exterior. Subject to the selection rules for the excitation process, the resulting system may occupy any one of a close sequence (or continuum) of states E of energy greater than, or equal to, E_0, the state in which the ejected electron is in the lowest level (virtual orbit or conduction level) which is normally unoccupied. If we apply the theory of Weisskopf and Wigner to the problem of the absorption of radiation by atoms in the normal state (A), restricting our attention to processes involving the removal of an electron from the specified inner shell, we find for the corresponding partial absorption coefficient $K(\nu)$ in the neighborhood of the absorption limit:[16]

$$K(\nu)=\sum_{\nu_{EA}=\nu_{E_0A}}^{\nu_{EA}=\infty}C(E)\gamma_{EA}\left(\frac{\Gamma_E/2\pi}{(\nu_{EA}-\nu)^2+(\Gamma_E/2)^2}\right). \tag{12}$$

Here C is a constant. $2\pi\Gamma_A$, the reciprocal life of the normal state in the presence of the radiation, is extremely small compared to $2\pi\Gamma_E$, that of the excited state, and has been neglected in comparison with the latter in setting up the formula. Furthermore $2\pi\Gamma_{EA}$, the transition probability from state E to the normal state, is for a given

[13] Thus including the probabilities of radiation-less transitions (Auger jumps) in our consideration; see G. Wentzel, Handbuch der Physik **24**, Part 1, 768 (1933).
[14] E. Schrödinger, Ann. d. Physik **79**, 361 (1926).
[15] See, e.g., R. Becker, Zeits. f. Physik **27**, 173 (1924).
[16] A discussion of the derivation and the assumptions underlying this formula is to be found in the appendix.

sequence of energy levels[17] practically constant for intervals large compared with the width of the excited states.[18] Finally, Γ_E can be taken to be the same for all states E, since the most probable processes that reduce the life of the given excited state E are such as involve the filling of the vacancy in the specified inner shell by electrons from shells nearest to it; and these processes are practically independent of the condition of the ejected electron. For example, if the specified inner shell is the L_{III} shell of a heavy atom, we are justified in calling the corresponding Γ_E simply the width of the "L_{III} state" (i.e., the state of an atom lacking one L_{III} electron). This width Γ_E is at the same time the full width at half-maximum of the line which would be emitted if the atoms which have been excited to state E would return directly to the normal state.

We thus see that the form of the absorption curve in the neighborhood of a limit depends on (1), Eqs. (8) and (2) the distribution of free levels at the periphery of the internally ionized atom (the states beyond the "Fermi limit" of occupied states in the case of a metal). If now, in the absence of adequate information on this point, we make the simplest assumption possible, that is, that the distribution of these peripheral levels is uniform on an energy scale, we can replace the summation over the states E in Eq. (12) by an integration with respect to their term values. Replacing γ_{EA} by a constant[19] and recalling that $\nu_{EA}=\nu_E-\nu_A$ we find for the partial absorption coefficient $K(\nu)$:

$$K(\nu)=C'\int_{\nu_{E_0A}}^{\infty}\frac{(\Gamma_E/2\pi)d\nu_{EA}}{(\nu_{EA}-\nu)^2+(\Gamma_E/2)^2}$$

$$=C'\left\{\frac{1}{2}-\frac{1}{\pi}\arctan\left(\frac{\nu_{E_0A}-\nu}{\Gamma_E/2}\right)\right\}. \quad (13)$$

Here C' is a new constant.

The general principles involved in the derivation of Eq. (13) may be made clearer by Fig. 1 in which we have represented the absorption coefficient $K(\nu)$, as given by Eq. (13), as a function of the frequency ν of the absorbed radiation, on the assumption that the excited levels E of the atom have a width $\Gamma_E=5$ electron volts and form an evenly spaced, close, sequence from E_0 toward higher energies. The curve $ABCDE$ (solid line) for the absorption coefficient results from the superposition of the evenly spaced, identical absorption lines corresponding to the several atomic states E. The horizontal separation of the two points B and D, where the curve reaches $\frac{1}{4}$ and $\frac{3}{4}$, respectively, of its asymptotic ordinate C' for high frequencies, is defined as the width of the limit, which is seen to be identical with the full width at half-maximum, Γ_E, of any one of the absorption lines, *in exact correspondence to the full width at half-maximum of a radiated line.*[20] The even distribution of energy levels is represented below the curve by the horizontal line GH which is cut off sharply on the low frequency side at $\nu_E=\nu_{E_0}$.

If, on the other hand, considering the absorption by a metal, we suppose the distribution of levels E to correspond to that of a Fermi gas of free electrons,[21] we must multiply the integrand in Eq. (13) by a weight factor $g(\nu_E)$:

$$g(\nu_E)=\text{const.}\cdot(\nu_i+\nu_E-\nu_{E_0})^{\frac{1}{2}},$$

since the density of the levels on a frequency scale increases with the square root of the (kinetic) energy of the electrons. Here, ν_i measures the difference between the mean potential energy of an electron within the crystal lattice and the total energy of an electron occupying a state corresponding to the Fermi limit. In the case of gold the value of ν_i corresponds to about 10 electron volts.[22] Carrying out the integration

[17] That is, a succession of energy levels having the same angular quantum numbers.

[18] A. Sommerfeld and H. Bethe, Handb. d. Physik **24**, Part 2, 462 (1933).

[19] This is legitimate if we restrict our considerations to the immediate neighborhood of the absorption limit, since then the integrand is appreciable for only a small range in ν_{EA} on either side of ν_{E_0A}.

[20] The method of determining the width used by P. A. Ross, Phys. Rev. **44**, 977 (1933) would give $\pi\Gamma_E/2$ for the width of the limit.

[21] A. Sommerfeld and H. Bethe, Handb. d. Physik **24**, Part 2, 336 (1933). The calculations of J. C. Slater, Phys. Rev. **45**, 794 (1934), on sodium indicate that this assumption is reasonable in the case of the alkalis and, hence, perhaps also in the case of the noble metals. However, it should be emphasized that an internally ionized atom is effectively a foreign ion in the crystal lattice, as pointed out below. We disregard fine structure effects for the moment.

[22] R. deL. Kronig, Handb. d. Physik **24**, Part 2, 302 and 320 (1933). The mean potential energy of an electron in the interior of a crystal referred to that in free space is determined by electron diffraction experiments; and the electron energy corresponding to the Fermi limit, by the

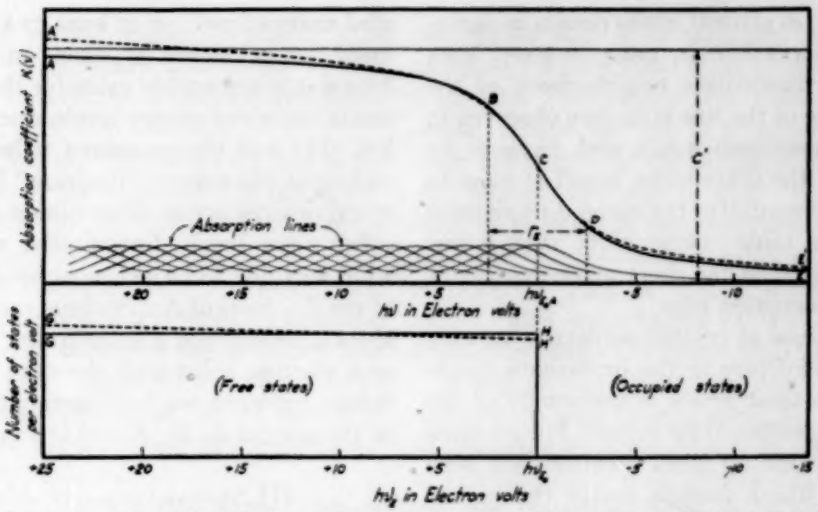

FIG. 1. Plot of Eq. (13), full line $ABCDE$ and Eq. (14), dotted line $A'CE'$. The individual absorption lines whose summation gives the predicted shape of the absorption limit, are shown below, for the case of equal distribution of levels (Eq. (13)).

for this case we obtain for $K(\nu)$

$$K(\nu)=C''\left\{A\left[\arctan\frac{B}{(2\nu_i)^{\frac{1}{2}}-A}+\arctan\frac{B}{(2\nu_i)^{\frac{1}{2}}+A}\right]+\frac{1}{2}B\log_e\left(\frac{\nu_i+D+(2\nu_i)^{\frac{1}{2}}A}{\nu_i+D-(2\nu_i)^{\frac{1}{2}}A}\right)\right\}, \quad (14)$$

where
$$A=(D+[\nu_i+\nu-\nu_{E_0A}])^{\frac{1}{2}},$$
$$B=(D-[\nu_i+\nu-\nu_{E_0A}])^{\frac{1}{2}},$$
$$D=([\nu_i+\nu-\nu_{E_0A}]^2+[\Gamma_E/2]^2)^{\frac{1}{2}},$$
$$0\leq\arctan[B/((2\nu_i)^{\frac{1}{2}}\pm A)]\leq\pi,$$
$$C''=\text{constant}.$$

Eq. (14) predicts an asymmetrical absorption limit: it is steeper on the long wave-length side. The width corresponding to an absorption line cannot be determined as readily as from Eq. (13). In Fig. 1 the absorption coefficient $K(\nu)$, as given by Eq. (14) for $\Gamma=5$ electron volts and $\nu_i=100$ electron volts, is represented by the broken curve $A'CE'$, the constant C'' having been adjusted so as to have the same ordinate $(C'/2)$ at the center of the limit as the full curve corresponding to Eq. (13). In the case of curve $A'CE'$, corresponding to Eq. (14), the distribution of levels is not quite uniform, and is indicated by the dotted curve $G'H'$ below: the individual absorption lines, from whose superposition the absorption curve may be constructed, lie progressively closer together toward higher frequencies.

We shall discuss in Section V below the agreement between Eqs. (13) and (14) and the experimental data on absorption limits.

Approaching finally the question of the fine structure superposed on the absorption curve in the neighborhood of the limit, we have to consider primarily two effects: (1) In a crystal, the existence of forbidden energy bands for electrons moving in a given direction, to which Kronig first called attention;[23] (2) In a monatomic vapor, the existence of discrete, unoccupied levels, which Kossel has pointed out as source of fine structure of x-ray absorption limits.[24] Effects of both types may have to be considered in interpreting the structures of the absorption edges of matter in still different form, e.g., polyatomic gases.[25] The secondary structure predicted by Kronig for the absorption edge of a crystal consists in oscillations of the absorption index covering a range of some hundred volts on the short wave-length side of the edge. His method of calculating the location of the maxima and

threshold value for the photoelectric effect. It is reasonable to regard the Fermi limit as sharp, as its width, in the cases here considered, is of the order of 1/100 of that of the absorption limit. See Sommerfeld and Bethe, reference 18, p. 466.

[23] R. de L. Kronig, Zeits. f. Physik **70**, 317 (1931); **75**, 191 (1932).
[24] W. Kossel, Zeits. f. Physik **1**, 119 (1920).
[25] J. D. Hanawalt, Phys. Rev. **37**, 715 (1931); R. deL. Kronig, Zeits. f. Physik **75**, 468 (1932).

minima, which, in general, gives results in agreement with observation, is, unfortunately, least reliable in the immediate neighborhood of the edge. The range of the fine structure observed in the case of monatomic gases and foreseen by Kossel[24] is, on the other hand, equal at most to the ionization potential of the succeeding element in the periodic table—never more than a few volts. It is located on the short wave-length side of the main absorption edge.

Even in the case of crystalline matter we may expect a fine structure in the immediate neighborhood of the limit which is essentially of the nature of that predicted by Kossel. For an atom or ion from which an inner electron has been removed acts like a foreign ion in the crystal lattice: the internal ionization changes a gold atom into a form resembling an atom of mercury which has lost one valence electron. It may be expected that the lowest free states of this "mercury ion" will not be perturbed sufficiently by the neighboring gold atoms to be drawn out into wide bands of energy states, since they may lie some 10 electron volts[24] below the corresponding states for the gold atom; due to the increased effective nuclear charge the outer orbits of the "mercury ion" shrink sufficiently so that a number of free orbits can be accommodated in the space normally filled by the occupied orbits of the gold atom. We may thus expect a fine structure of the absorption limit of metallic gold covering a range of about 10 volts qualitatively similar to the structure of the absorption edge of gold vapor. This should, in view of the selection rules, be practically the same (in frequency measure) for the K and L_{I} edges on the one hand, and the L_{II} and L_{III} edges on the other.

It is evident from the above that a close relationship exists between the widths and shapes of x-ray lines and absorption limits; at the same time, it is clear that the determination of level widths from the shapes of absorption limits is a more difficult and less certain process than the determination of line widths.

Nevertheless, from the observed shape of an absorption discontinuity, one can, by adopting the theory outlined above, make an estimate of the approximate value of the width of the associated energy level; or at least can set upper and lower limits thereto. If, then, one can obtain a reasonably acceptable value for the width of any one of the x-ray energy levels, one can, by use of Eq. (11) and the measured values of the true widths of the several "diagram" lines of the respective x-ray series, determine the widths of the other x-ray levels. Specifically, we have made what we think to be a close estimate of the width of the L_{III} level of Au(79) from measurements on the L_{III} absorption discontinuity, and from that as a starting point with the data on line widths herein reported we have estimated the widths of the several L, M, N and O levels.

III. Apparatus and Method

The two-crystal spectrometer used has been described elsewhere.[27] During the greater part of the investigations it was fitted with our pair of ground and etched calcite crystals $3A+3B$.[27] However, as was ascertained later, the crystals were not in adjustment for highest resolution during the major part of the work. Curve A of Fig. 2 gives the width of the $(1, -1)$ rocking curves, as a function of wave-length, for the crystals as actually used. Curve B gives similar data after the crystals had been carefully adjusted for verticality. Curve C, drawn through the lower point, is the width obtained for a pair

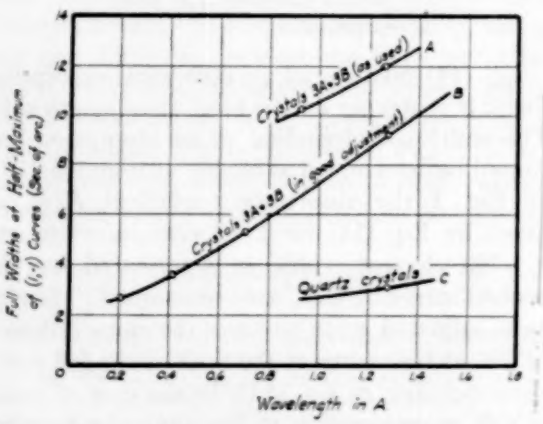

Fig. 2. Rocking-curve widths, as function of wave-length, of the crystals used, in the $(1, -1)$ position. A, for calcite crystals $3A+3B$ as used; B, for same crystals in better adjustment; C, for a quartz crystal.

[24] The first ionization potential of mercury (10.4 volts).

[27] F. K. Richtmyer and S. W. Barnes, Rev. Sci. Inst. 5, 351 (1934).

of ground and etched quartz crystals, $11\bar{2}0$ planes, which were kindly loaned by R. M. Bozorth and F. E. Haworth of the Bell Telephone Laboratories.

The slits limiting the vertical divergence of the x-ray beam were 1 cm high and 126 cm apart. This corresponds to an angle of maximum vertical divergence of 0.016 radian.

The ionization chamber, 3 cm in diameter and 8 cm long, is connected by a tube to a glass flask having 60 times the volume of the chamber. The chamber and flask were filled with methyl bromide to a pressure of 74 cm of mercury. There was practically no change in pressure over a period of several months.

The x-ray tube, which was fitted with a removable anode and cathode, was built with a thin glass window for transmission of the longer wave-lengths. Because mercury diffusion pumps gave trouble on account of the condensation of mercury on the gold anode,[28] the tube was evacuated by (metal) diffusion pumps using apiezon oil.

During the work on lines the tube was run at 50 kv and 20 to 25 m.a. For the study of limits it was run at 40 kv and 100 m.a.

Ionization currents were measured with a DuBridge[29] type of two tube bridge circuit, the sensitivity used being from 1000 to 10,000 mm per volt.

IV. Results

Line widths

Figs. 3(A), (B) and (C) show a "panorama" of the x-ray spectrum of Au(79) through the wave-length range comprising the L-series lines with the exception of Ll ($\lambda = 1457$ X.U.). It is important that the background due to the continuous spectrum be located with some care in order that values of half-maximum of intensity of the several lines may be accurately determined. As may be seen from the figures, a line, or particularly a partially resolved group of lines, may extend over a considerable wave-length region; so that it is necessary to go to some distance on each side of the group to locate the base line. Fortunately, the base line is nearly linear except for the discontinuities resulting from absorption in the target at the L_{I}, L_{II} and L_{III} absorption limits of gold and from the K-limit of bromine in the ionization chamber. The gold limits were located by observing the absorption in gold of x-rays from a platinum target. The wave-length of the K absorption limit of bromine was taken from Siegbahn.

It will be noted that very few of these lines, with the possible exception of $L\beta_1$, are separated far enough from other lines so that the full width at half-maximum may be read directly from the data as plotted in Figs. 3. To determine the "observed" width W_o (see Eq. (3)) of a line we must have the "observed" shape of the line apart from all other lines; that is, we must analyze Figs. 3 into the several component lines. As was pointed out by the authors,[4] if an equation of the Hoyt type, Eq. (2), gives the true shape of a line and also of the $(1, -1)$ rocking curve of the crystals used, then an equation of exactly the same form gives the shape of the line *as observed* by crystals in the $(1, +1)$ position.[30] However, as is pointed out below, in the wave-length range herein studied, the $(1, -1)$ rocking curves of the crystals depart considerably from Hoyt curves; accordingly, the *observed* line shape should not, mathematically, be Hoyt curves. Actually, however, the widths of the $(1, -1)$ curves for our calcites $3A+3B$ are only 10 or 15 percent of the widths of the lines as observed in the $(1, +1)$ position. And hence the observed shapes should not depart noticeably from Hoyt curves.

To test this conclusion observations on $L\beta_1$ were used. In Fig. 4, the observations (open circles) are compared with the Hoyt Eq. (2), the values of a and b for the latter being taken from the *observed* curve. The agreement is seen to be excellent.

---

[28] In the first search for β_7 and β_7' one quite intense line was found which proved to be Hg β_1. Even after the mercury pumps had been replaced by the oil pumps and the system thoroughly cleaned some evidence of this line remained, though greatly reduced in intensity. It can be seen as the peak between Au β_7 and β_7' on Fig. 3(B).

[29] L. A. DuBridge, Phys. Rev. **37**, 392 (1931).

[30] Strictly speaking Eq. (2) represents the shape of a line plotted to a frequency scale. On a wave-length plot the equation becomes (see Richtmyer and Barnes[4])

$$\mathfrak{y}_\lambda = a[1+((\lambda_0/\lambda)\cdot(x/b))^2]^{-1},$$

where λ_0 is the wave-length of the maximum ordinate. Although x-ray lines are relatively broad compared to optical lines, yet for any given line no errors greater than those of observation will be made if $(\lambda_0/\lambda)^2$ be set equal to unity.

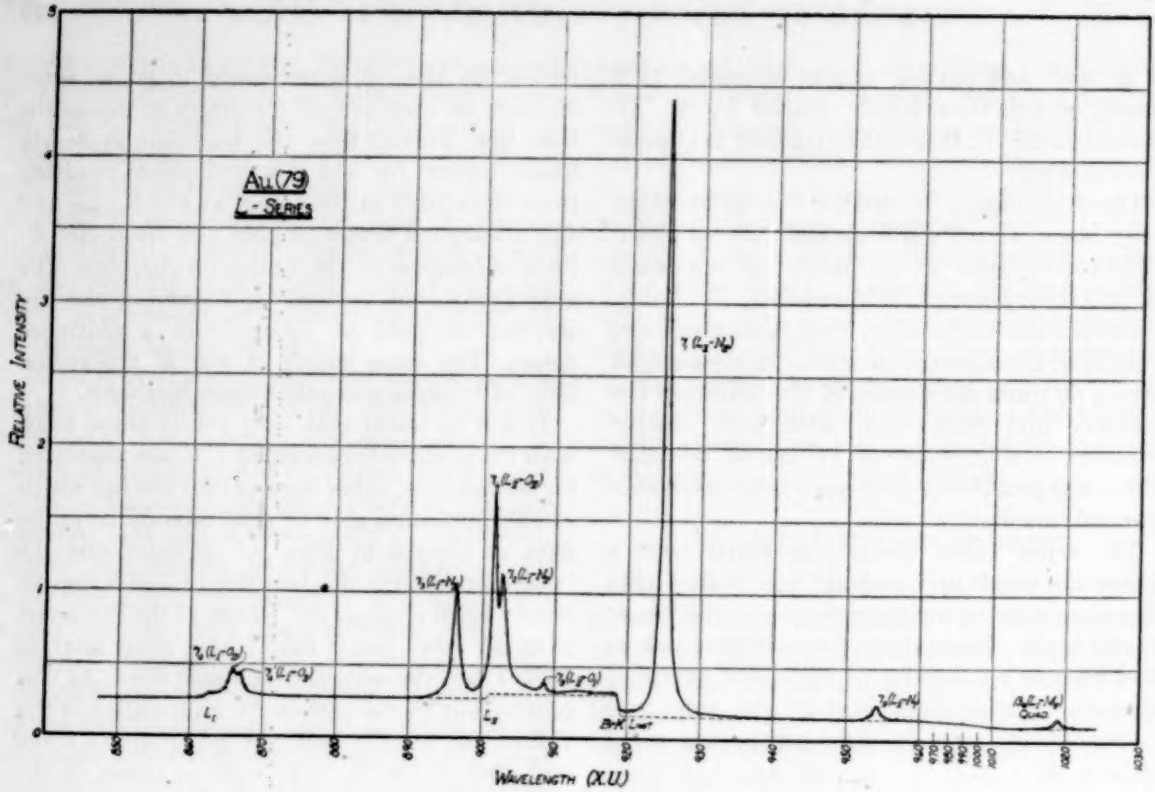
Au (79)
L - Series
Relative Intensity
Wavelength (X.U)

FIG. 3A.

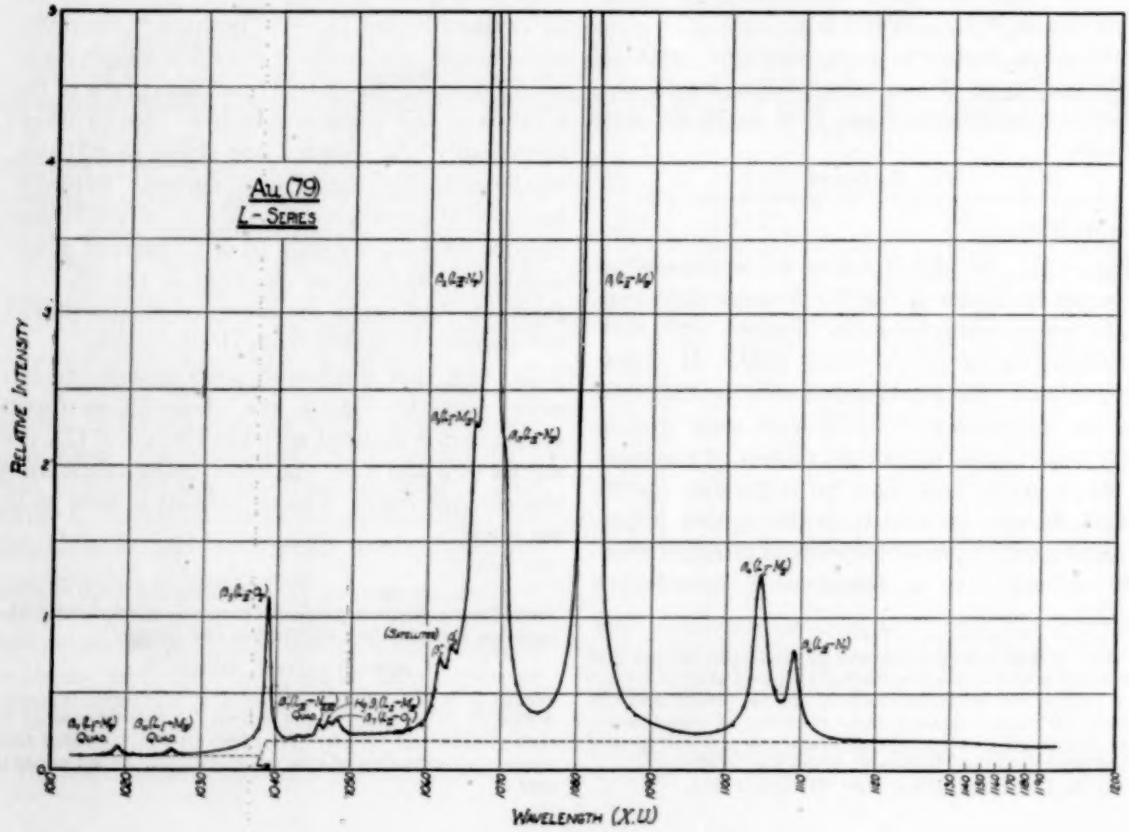
Au (79)
L - Series
Relative Intensity
Wavelength (X.U)

FIG. 3B.

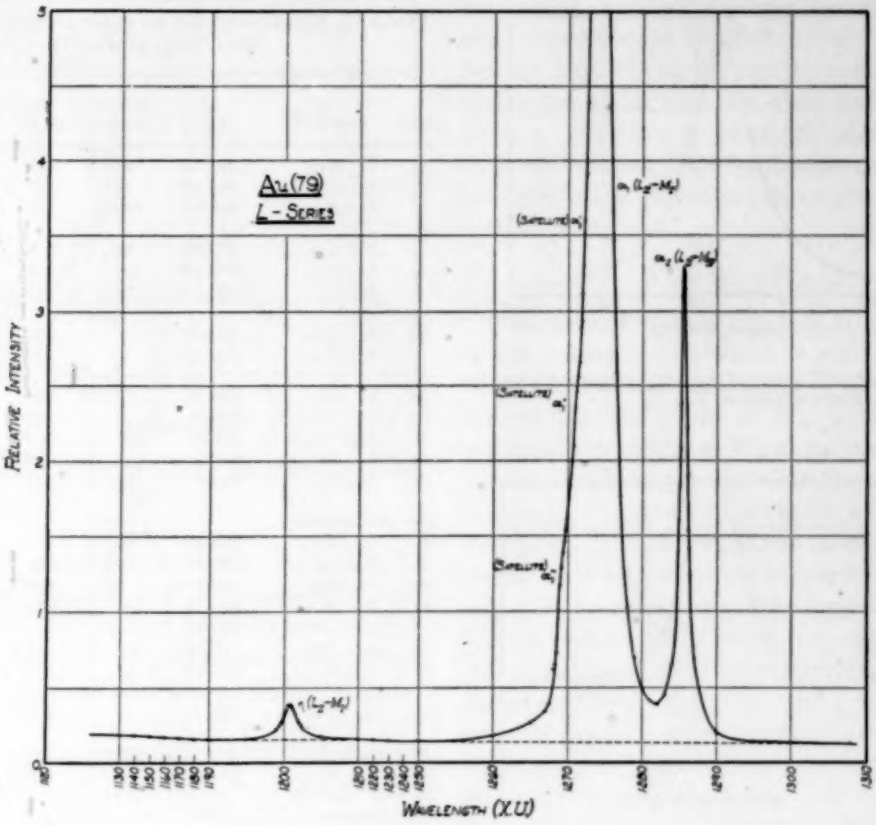

FIG. 3C.

FIG. 3. "Panorama" of the *L*-series of Au(79)[1] (A), short wave-length range; (B), middle range; (C), long wave-length range. The broken horizontal line gives the continuous spectrum.

TABLE I. *Test of the several methods of correcting the observed width of a spectral line for the effect of the crystals.*

Gauss:	$W_T=(W_O^2-W_R^2)^{\frac{1}{2}}$	Eq. (1)
Hoyt:	$W_T=W_O-W_R$	Eq. (3)
Empirical:	$W_T=W_O-W_R/2$	Eq. (15)

W_R = rocking curve widths (1, −1) position
W_O = observed line widths (1, 1) position
W_T = true widths

Crystals: calcite except as indicated.

Line	Observers	Crystal	W_R (sec.)	W_O (X.U.)	W_T (X.U.) by Eq. (1)	Eq. (3)	Eq. (15)
$L\alpha_1$	R & B	Quartz[1]	3.0″	1.08	1.078	1.035	1.058
	W	III*A*, III*B*	8.8″	1.13	1.125	1.005	1.068
	R & B	3*A*+3*B*	12.2″	1.15	1.135	0.976	1.063
$L\beta_1$	W	III*A*, III*B*	7.7″	0.785	0.779	0.675	0.730
	R & B	3*A*+3*B*[2]	7.8″	0.80	0.790	0.69	0.745
	R & B	3*A*+3*B*	11.2″	0.81	0.794	0.65	0.730
$L\gamma_1$	W	III*A*, III*B*	6.7″	0.791	0.784	0.695	0.743
	R & B	3*A*+3*B*	10.2″	0.806	0.806	0.673	0.747

W = Williams, reference 3. R & B = Richtmyer and Barnes.
[1] Etched Quartz crystals, 1120 planes.
[2] Carefully adjusted for minimum width.

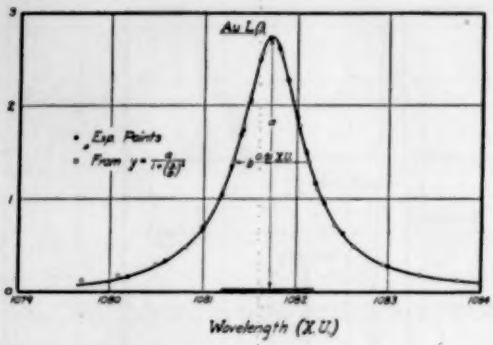

FIG. 4. The "observed" shape of Au $L\beta_1$, compared with the Hoyt equation, Eq. (2).

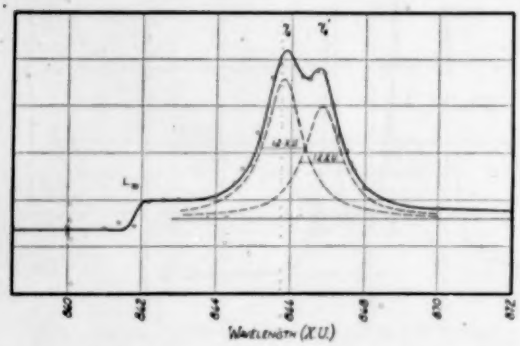

FIG. 5. Showing the method of separating the partially resolved lines γ_4 and γ_4' into the respective components, by use of Hoyt curves. The full line is the envelope of the two Hoyt curves. The circles give the observed points.

TABLE II. *The observed and the natural widths of the lines of the L-series of Au(79).*

Line	Transition	λ (X.U.)	Relative intensity	W_O (X.U.)	W_T (X.U.)	$\bar{W}_T$ (volts)
γ_4	$L_I\ O_{III}$	865.10[1]	21	1.20	1.13	18.6
γ_4'	$L_I\ O_{II}$	866.15[1]	14	1.20	1.13	18.6
γ_3	$L_I\ N_{III}$	895.81	100	1.06	0.99	15.2
γ_8	$L_{II}\ O_{IV}$	901.00	82	0.60	0.53	8.05
γ_2	$L_I\ N_{II}$	902.20[1]	100	1.20	1.13	17.2
γ_6	$L_{II}\ O_I$	907.9 [1]	3	0.70	0.63	9.5
γ_1	$L_{II}\ N_{IV}$	924.61		0.82	0.75	10.8
γ_5	$L_{II}\ N_I$	953.60		1.20	1.12	15.2
β_9	$L_I\ M_V$	1018.8	15	1.10	1.02	12.1
β_{10}	$L_I\ M_{IV}$	1026.0 *	8	1.20	1.12	13.1
β_6	$L_{III}\ O_{IV,V}$	1038.0	100	0.74	0.67	7.6
β_7'	$L_{III}\ N_{VI,VII}$	1045.2	9	0.95	0.87	9.8
β_7	$L_{III}\ O_I$	1047.8	15.5	1.25	1.17	13.1
$(\beta_3'+\beta_3'')$ satellites			2.5			
β_3	$L_I\ M_{III}$	1065.83[1]	16.5	2.00	1.92	20.8
β_2	$L_{III}\ N_V$	1068.01	45.5	1.04	0.96	10.3
β_{15}	$L_{III}\ N_{IV}$	1069.7 [1]	5.5	1.10	1.02	11.0
β_1	$L_{II}\ M_{IV}$	1081.28	100	0.81	0.73	7.75
β_4	$L_I\ M_{II}$	1104.22	100	2.00	1.92	19.4
β_6	$L_{III}\ N_I$	1108.63	35.5	1.70	1.62	16.3
η	$L_{II}\ M_I$	1200.3		2.35	2.27	19.3
α_2	$L_{III}\ M_V$	1273.77	100.0	1.15	1.06	8.1
α_1	$L_{III}\ M_{IV}$	1285.02	11.3	1.22	1.13	8.5
$(\alpha_1'+\alpha_1''+\alpha_1'''+\ldots)$ satellites			5.0			
l	$L_{III}\ M_I$	1456.9		3.50	3.41	19.8

[1] New values. See Table III. Remainder from Siegbahn.

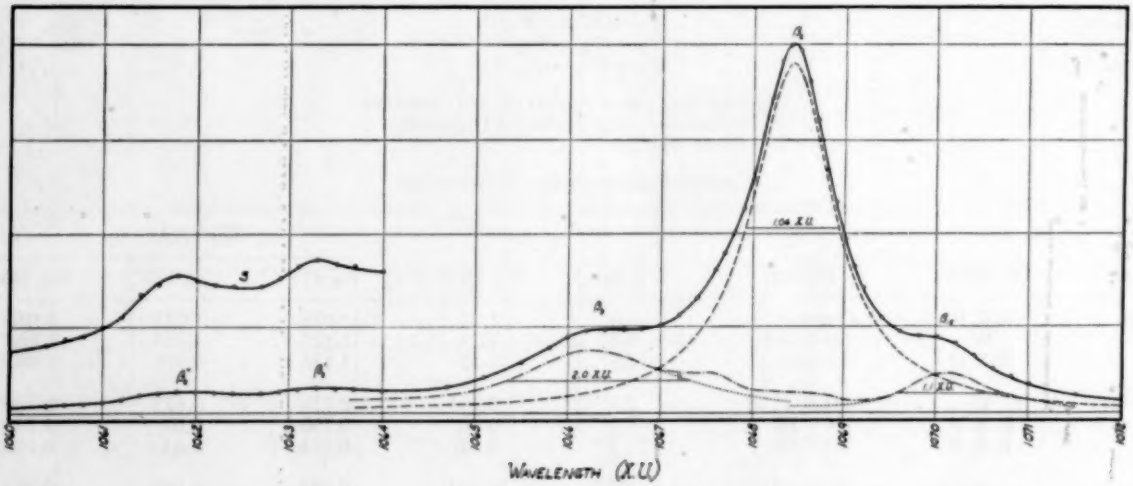

FIG. 6. The dotted lines show the Hoyt curves for the components of the group β_3, β_2 and β_{15}. (Note the residuals which have been neglected.) The satellites $L\beta_3'$ and $L\beta_3''$ are shown at the left; the line marked "S" being the satellite structure plotted to a 5×ordinate scale.

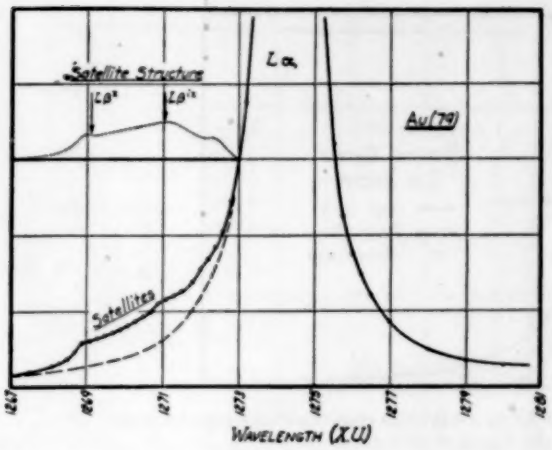

FIG. 7. The "foot" of $L\alpha_1$ of Au(79), showing the satellite structure.

Accordingly we felt justified in using Eq. (2) in analyzing Figs. 3 into the respective component lines. The method is illustrated in Figs. 5 and 6. In Fig. 5 the circles represent the observations on the close doublet γ_4, $\gamma_4'(L_1 \rightarrow O_{II, III})$. By "trial and error" two Hoyt curves were plotted with such intensity, width and position that their envelope, the solid line, gave the best fit with the experimental points. Fig. 6 shows the way in which the group β_3, β_2, β_{15}, with the satellites accompanying β_2, was analyzed. In this case there were certain "residuals" which we neglected. The curve "S" shows the satellite structure $L\beta_2'$ and $L\beta_2''$ plotted to an open ordinate scale. Fig. 7 shows the "foot" of $L\alpha_1$, revealing the satellite structure, which is seen to consist of at least four components. Photographic methods[31] reveal only two components.

The observed widths W_O of the several lines expressed in X.U. are shown in column 5 of Table II.

Correction for the effect of the crystals

Only if the (1, −1) rocking curves of the crystals as well as the true shape of a line obey either the Gauss error curves or the Hoyt curve can Eqs. (1) or (3), respectively, be used to obtain the true width of W_T of a line from the observed widths, W_O. Fig. 8 shows that the actual rocking curve for our calcite crystals $3A$ and $3B$ at $\lambda = 0.925$A obeys neither the Gauss error curve nor the Hoyt equation. Consequently neither Eqs. (1) or (3) can be used, the former giving too small, and the latter too large, a correction. We observe that the observations lie midway between the two theoretical curves and we were led, rather naively, to propose the correction formula

$$W_T = W_O - W_R/2. \qquad (15)$$

One obvious test of Eq. (15) is the constancy of the values of W_T which it yields for a given line which has been measured by pairs of crystals having different values of W_R. Table I shows in column 5 the widths of W_O of Au $L\alpha_1$ as observed by three different pairs of crystals, the widths of the (1, −1) rocking curves for which are given in column 4. The last three columns show the values of W_T as obtained by use of Eqs. (1), (3) and (15), respectively. The superiority of Eq. (15) is evident. This point is brought out more clearly by Fig. 9. The remainder of Table I shows similar data for $L\beta_1$ and $L\gamma_1$. The superiority of Eq. (15) is perhaps not so marked as in the case of α_1; but it does give somewhat more consistent results than Eqs. (1) and (3). Since these three lines, α_1, β_1 and γ_1, lie, respectively, near the long wave-length, the center and the short wave-length region of the wave-length range covered, we felt justified in using Eq. (15) for all the lines in the L-series.

The final values of the natural width W_T of the several lines of the L-series of Au(79), obtained by use of Eq. (15), are shown in Table II in X.U. and in volts, the values of W_R being taken from curve A of Fig. 2. The true widths vary from 7.6 volts for β_5 to 20.8 volts for β_3. The components of doublets have nearly identical widths, the long wave-length component usually being wider by an amount that is not much, if any, outside experimental error.

Wave-lengths

The careful analysis of the several groups of lines into Hoyt components, as illustrated in Figs. 5 and 6, makes possible[32] a redetermination

[31] F. K. Richtmyer and S. Kaufman, Phys. Rev. **44**, 605 (1933).

[32] Our spectrometer is not calibrated to give absolute values of wave-lengths with high precision. It does, however, give wave-length differences over small range of wave-lengths with great accuracy.

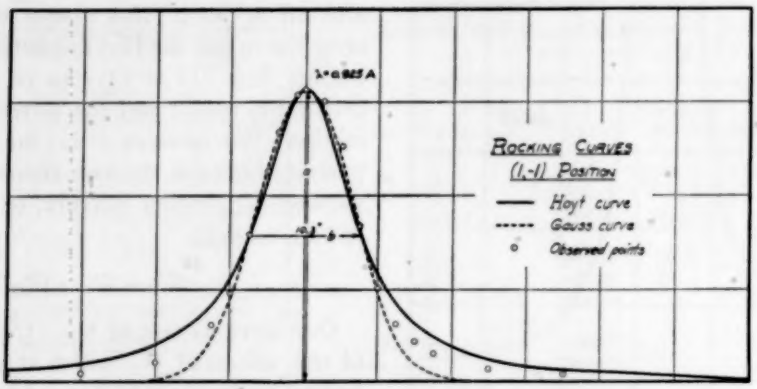

FIG. 8. The (1, −1) rocking curve of crystals $3A+3B$ at $\lambda=0.925$A showing disagreement with both the Hoyt curve and the Gauss error curve.

of the wave-lengths of the weaker components referred to Siegbahn's values for the stronger components, the "wave-length of a line" being taken to mean the wave-length of the maximum ordinate. Table III shows the new values so determined for the wave-lengths of β_3, β_{15}, γ_2, γ_8, γ_4 and γ_4'. These values are to be compared with similar data by Williams[3] for β_3 and β_{15}.

By an inspection of Fig. 3(A) it is seen that the wave-length of the center of the L_I absorption limit can be determined with reference to the γ_4 doublet. In the neighborhood of the L_{II} and the L_{III} edges, however, there are strong lines overlapping the edge, and it was impossible to determine the wave-length of either edge from the emission spectrum of gold. Accordingly a platinum target was substituted for the gold target and the L_{II} and L_{III} limits of Au(79) were measured by use of absorbing screens. The values so obtained (center of the limit) are included in Table III referred to Siegbahn's values of the wave-length of γ_8 and β_5, respectively. The wave-lengths of L_I and of γ_4 and γ_4' are determined by reference to Siegbahn's value of the wave-length of the γ_4 doublet, which value is assumed to be that of the weighted mean of the unresolved doublet.

Intensities

It has been shown by Hoyt[5] that the intensity of a line whose energy distribution is represented by Eq. (2) is $\pi a b_\nu$, where b_ν is the natural (half) width in frequency units. If line width be expressed in wave-length units, b_λ, the ratio R of the intensities of two lines of wave-length λ_1, and λ_2, respectively, is[4]

$$R=(\lambda_2/\lambda_1)^2\cdot(ab_\lambda)_1/(ab_\lambda)_2. \qquad (16)$$

An accurate comparison of the relative intensities of two lines necessitates the introduction into

TABLE III. *New values of the wave-lengths of several lines and of the absorption limits in the L-series of Au(79).*

Line	β_2 [1]	β_5	β_{15}	γ_8 [1]	γ_2	γ_8	L_{II}
Drum reading	1068.42	1066.24	1070.10	901.6	902.8	908.5	900.9
Correction	−0.41	−0.41	−0.41	−0.6	−0.6	−0.6	−0.6
	1068.01	1065.83	1069.69	901.0	902.2	907.9	900.3
Siegbahn	1068.01	1065.50	1069.90	901.0	902.48	907.9	900.9

Line	(γ_4, γ_4')	γ_4	γ_4'	L_I	β_5 [1]	L_{III}
Drum reading	866.2	865.8	866.85	862.0	1038.76	1038.46
Correction	−0.7	−0.7	−0.7	−0.7	−0.76	−0.76
	865.5	865.1	866.15	861.3	1038.00	1037.7
Siegbahn	865.5			862.2	1038.00	1038.2

[1] Siegbahn's value (*Spektroskopie der Roentgenstrahlen*) taken as standard of reference.

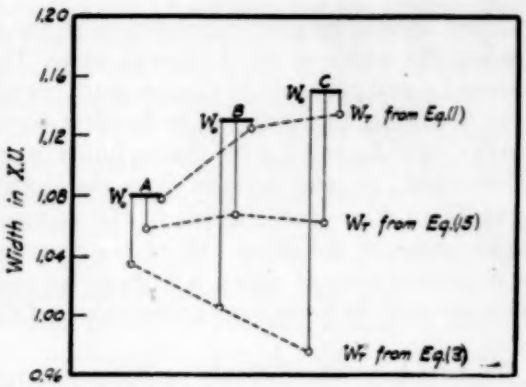

FIG. 9. Showing graphically the superiority of the empirical Eq. (15) as a method of correcting for the crystals.

Eq. (16) of rather elaborate corrections,[33] unless the two lines do not differ greatly in wave-length. We have not felt justified in departing far enough from the main object of this investigation to make measurements for and to determine these corrections. However, for lines that do not differ greatly in wave-length Eq. (16) may be used as a first approximation. Accordingly, using Eq. (16) we have computed the relative intensities of the lines in each of several arbitrarily selected groups, the lines in any group being close enough together so that we have neglected the corrections referred to above. The intensity of the strongest line in each group is arbitrarily set at 100. Values of a are taken from Figs. 3; of b_λ from column 5 of Table II ($2b_\lambda = W_O$). The various values of R are given in Table II, column 4.

We have also recorded the intensities of the satellites of $L\alpha_1$ and $L\beta_2$. The $L\alpha$ satellites have an intensity of 5 percent of that of the parent line; the corresponding value for the $L\beta_2$ satellites is 5.5 percent.

V. The Widths of Absorption Limits and Energy Levels

One test of the relation between the widths of lines and energy levels given by Eq. (11) is afforded by the data in Table II. Two lines which have a common final level but different initial levels should differ in width by the difference between the widths of the initial levels. For example, for the respective widths of the lines α_2 and β_1 Eq. (11) predicts

$$W_{\alpha_2} = \Gamma_{L_{III}} + \Gamma_{M_{IV}}; \quad W_{\beta_1} = \Gamma_{L_{II}} + \Gamma_{M_{IV}}.$$

Therefore $W_{\alpha_2} - W_{\beta_1} = \Gamma_{L_{III}} - \Gamma_{L_{II}}$. The several pairs of lines which give the difference in width between L_{III} and L_{II}, and the differences so predicted, are given in the upper half of Table IV.

TABLE IV. *Differences in width between the L energy levels of Au(79).*

Lines	$l-\eta$	$\alpha_2-\beta_1$	$\beta_6-\gamma_1$	$\beta_{10}-\gamma_1$	$\beta_7-\gamma_5$
Width V (volts)	19.8−19.3	8.5−7.75	16.3−15.2	11.0−10.8	13.1−9.5
ΔV for $L_{III}-L_{II}$ (volts)	0.5	0.75	1.1	0.2	3.6

Lines	$\beta_9-\alpha_1$	$\beta_{10}-\alpha_1$
Width V (volts)	12.1−8.1	13.1−8.5
ΔV for L_I-L_{III} (volts)	4.0	4.6

Considering the difficulty in determining the widths of β_{15}, β_7 and γ_5 (see Figs. 3 and 6) not too much dependence should be put on the last two values. It is believed therefore that the table shows no significant variation from constant value for the difference $L_{III}-L_{II}$. The values given for the widths of α_2 and β_1 are probably more accurate than are those of the other lines; hence 0.75 volt is thought to be the best value for the difference in width of the states L_{III} and L_{II} of Au(79).

The lower half of Table IV contains two values for the difference L_I-L_{II}, the mean of which may be taken as 4.3 volts. Combining this with the value 0.75 for the difference $L_{III}-L_{II}$ we obtain 5.1 volts for the difference L_I-L_{II}.

The data in Table IV are thus in substantial agreement with Eq. (11). Although absolute values for the widths of the several L energy states are not obtainable from these data, it is to be noted that L_I is several volts wider than either L_{II} or L_{III}; and that these latter differ from each other in width by less than a volt, a conclusion in agreement with the authors' observation[4] that the $K\alpha$ lines of W(74) differ from each other in width by less than a volt.

As pointed out above, if the width of one energy state can be determined from an analysis of the observed shape of an absorption limit, one can, by use of Eq. (11) and the values of W_T for the L lines as given in Table II, determine the

[33] J. H. Williams, Phys. Rev. **44**, 146 (1933).

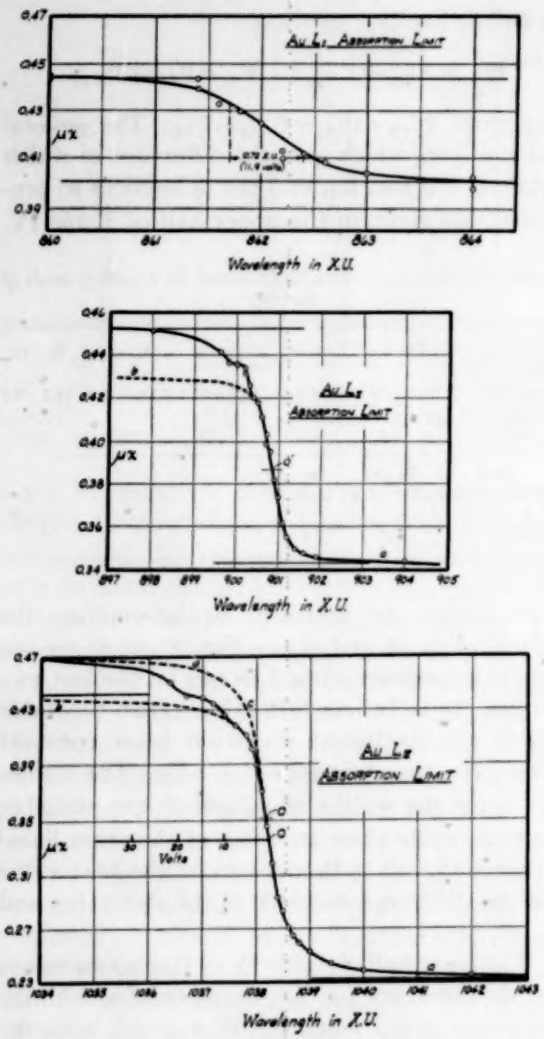

FIG. 10. (a) The L_I absorption discontinuity of Au(79).
(b) The L_{II} absorption discontinuity of Au(79). The circles are observed points. The smooth curve a $O'b$ is an arctangent curve adjusted to fit the main absorption edge with center at O'.
(c) The L_{III} absorption discontinuity of Au(79). The circles are the observed points. The dotted line $aO'b$ is an arctangent curve fitted to the main absorption edge with center at O'. The dotted curve Ocd is the "reversed mirror image" of the lower half of the observed curve, plotted from O as a center, point O being halfway between the upper and lower asymptotic values.

widths of the several L, M, N and O levels. Accordingly, by use of a platinum-target tube, careful measurements were made of the L_I, the L_{II} and the L_{III} limits of gold. The observations are shown graphically by the circles in Figs. 10(a), (b) and (c). The data[34] on L_I should be regarded as only roughly quantitative, so far as yielding the width of the L_I energy state. The data on L_{II} and particularly L_{III} are much better. Even neglecting the "humps" on the short wave-length side of L_{II} and L_{III} the discontinuity is not symmetrical, as may be seen from the dotted curve bc in Fig. 10(c), which is the reversed mirror image of the lower half of the observed curve plotted from O, which is halfway between the upper and the lower asymptotic values of the curve.

We now have the difficult problem of interpreting these data so as to determine therefrom the value of Γ, the energy level width. There are at least two possibilities: (1) We may regard the L_{III} discontinuity (L_{II} or L_{III} as shown in Fig. 10(b) and (c)) as made up of a "main" discontinuity, upon the short wave-length side of which are two secondary discontinuities, the origin of which is not explained and which cause the "humps," separated some 10 and 20 volts, respectively, from the center of the main edge. If we further adopt the assumptions upon which Eq. (13) is based (equal distribution of energy levels at the periphery of the atom) this main edge should follow an arctangent curve. Such a curve $aO'b$ plotted from O' as a center is fitted to this main edge. The agreement with the observations is seen to be excellent particularly on the long wave-length side of the edge. The "observed" width of the L_{III} energy level (see explanation following Eq. (13)) as obtained from this arctangent curve is 6.5 volts for the L_{II} level and 5.1 volts for the L_{III} level. These values must be corrected for the effect of the crystals.

Since as explained above (Fig. 1) the arctangent curve is the envelope of a series of overlapping, equal and equally spaced absorption lines, the width of each such line is 6.5 volts for L_{II} and 5.1 volts for L_{III}. After correcting for the $(1, -1)$ rocking curve of the crystals by use of Eq. (15) just as correction is similarly made for an emission line, we have for the *true* width Γ of the L_{II} level 5.8 volts; and for the L_{III} level 4.4 volts. According to these directly observed values, the L_{II} level should be wider than the L_{III} level by about 1.4 volts; whereas from the

[34] The values of μ(μ = absorption coefficient) are not corrected for higher orders of radiation present in the incident beam. This correction if made would change the absolute magnitude of μ but not the *form* of the curves in Figs. 10.

data in Table IV we saw that the reverse should be true: that the L_{III} level should be wider by about 0.7 volt. We think that this discrepancy between the difference in widths obtained from line data and from the direct observations on limits is outside experimental error; but we are unable to explain the cause thereof.

Since the L_{III} data are the more precise, we think that the value for it—4.4 volts—is more reliable. Accordingly we take that value as a starting point and proceed, by use of Eq. (11) and the line-width data of Table II, to determine the widths of the several L, M, N and O states. The results are shown in Table V. (The emission line the width of which is combined with that of the appropriate L level to give the width in question, is given in brackets.)

TABLE V. *The widths of the x-ray energy levels of Au(79).*

Level	Quantum numbers		Level width computed from	Level width (volts)
K	$n=1, l=0$		[1]	40
L_I	2	0	See Table IV	8.7
L_{II}	2	1	See Table IV	3.7
L_{III}	2	1	[1]	4.4
M_I	3	0	$\eta-L_{II}$, $l-L_{III}$	15.6, 15.4
M_{II}	3	1	β_4-L_I	10.7
M_{III}	3	1	β_2-L_I	12.1
M_{IV}	3	2	β_1-L_{II}, α_2-L_{III}, $\beta_{10}-L_I$	4.0, 4.1, 4.4
M_V	3	2	α_1-L_{III}, β_9-L_I	3.7, 3.4
N_I	4	0	γ_8-L_{II}, β_6-L_{III}	11.5, 11.9
N_{II}	4	1	γ_2-L_I	8.5
N_{III}	4	1	γ_3-L_I	6.5
N_{IV}	4	2	γ_1-L_{II}, $\beta_{15}-L_{III}$	7.1, 6.6
N_V	4	2	β_2-L_{III}	5.9
$N_{VI, VII}$	4	3	$\beta_7'-L_{III}$	5.4
O_I	5	0	β_7-L_{III}, γ_8-L_{II}	8.7, 5.8
O_{II}	5	1	γ_4-L_I	9.9
O_{III}	5	1	$\gamma_4'-L_I$	9.9
O_{IV}	5	2	γ_6-L_{II}	4.4
O_V	5	2	β_5-L_{III}	3.2

[1] Determined from observation on L_{III} absorption limit and taken as a starting point for computing the other levels.

However, the assumptions upon which Eq. (14) are based (Fermi-Sommerfeld distribution of energy levels in a metal) should be more applicable to gold than are the assumptions underlying Eq. (13). As was mentioned above, Eq. (14) predicts an asymmetrical limit, the curvature being less on the short wave-length side. An inspection of the data shown in Figs. 10(b) and 10(c) shows that, except for the humps, both L_{II} and the L_{III} limits have exactly this type of asymmetry. To test Eq. (14) the necessary constants were chosen by trial and error so as to get the best fit between the equation and experiment. The results are shown in Figs. 11 and 12 for the L_{II} and the L_{III} limits, respectively. For the L_{II} limit, the width Γ of the L_{II} level was assumed to be 7.0 volts, which corrected for the crystals, becomes 6.3 volts. For the L_{III} limit the corresponding assumed width was 5.3 volts, corrected to 4.6 volts. However, to make the curves fit, it was necessary to assume a value for ν_i (see page 846) of 100 volts, instead of 10 volts normally to be expected for the gold lattice. The source of this discrepancy is not obvious.

Again we assume that the greater accuracy of the L_{III} data gives preference to the value of 4.6 volts for the width of the L_{III} energy level, as a starting point for the determination of the remaining levels. This value is within experimental error equal to that obtained from the arctangent curve—4.4 volts. Hence Eq. (14) predicts substantially the same set of energy levels as does Eq. (13).

Only a rough estimate of the width of the L_I limit can be obtained from Fig. 10(a); but the curve seems to give a somewhat greater width for the L_I level than predicted in Table V.

Some significant regularities in the values obtained for the widths of these energy states are to be noted. (1) In any given series of levels—L, M . . . —the width decreases with increasing value of the orbital quantum number l. Exceptions to this rule, found in the N and the O levels, may be due to experimental error. (2) Energy states having the same total quantum number n

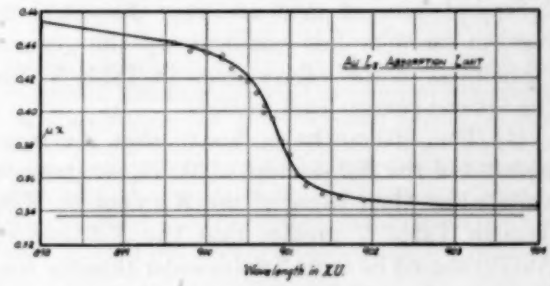

FIG. 11. The L_{II} absorption discontinuity of Au(79). The circles are observed data. The curve is a plot of Eq. (14) for $\nu_i=100$ volts and $\Gamma=7.0$ volts.

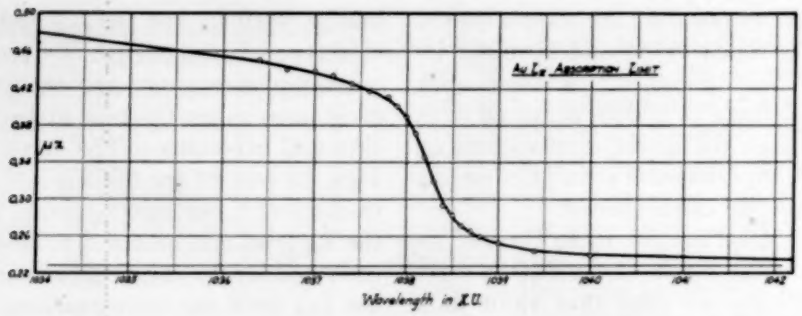

FIG. 12. The L_{III} absorption discontinuity of Au(79). The circles are observed data. The curve is a plot of Eq. (14) for $\nu_i = 100$ volts and $\Gamma = 5.3$ volts.

and orbital quantum number l have nearly the same width. This is in agreement with the authors' observations[4] that the components of any given K doublet of W(74) have nearly identical widths. (3) Except for the L_I level, the widths of levels for which $l=0$ decrease in width with increasing value of n. The K level ($n, l=1$, 0) may be included in this statement. We have no accurate direct measurements on the width of the K-limit of Au(79) but we may make a reasonable estimate of it. The authors have reported[4] that the width of the lines $K\alpha_{1,2}$ of W(74) is about 43 volts; and of the $K\beta$ lines about 48 volts. Making the reasonable assumption that the widths of $L_{II, III}$ and of the $M_{II, III}$ levels of W(74) are not very different from those of Au(79), we conclude that the width of the K level Au(79) should be of the order of 40 volts.

Within any given series, these regularities are in agreement with the rule proposed by Coster[35] that energy levels are sharper the smaller the value of n/k, where n is the total quantum number and $k(=l+1)$ is the azimuthal quantum number. From one series to another, however, Coster's rule does not seem to apply.

Several bits of evidence may be cited to confirm more or less qualitatively the general correctness of the values given in Table V, for the several energy-level widths.

(1) The authors have shown[4] that the components of the $K\beta$ doublet of W(74) are some 6 volts wider than those of the $K\alpha$ doublet. The data in Table V predict that the $K\beta$ lines of Au(79) should be some 7 volts wider than for $K\alpha$. However, from Table V one would also predict that the $K\gamma$ lines of gold should be wider than the $K\alpha$ lines. The opposite was found to be the case for W(74). This discrepancy may mean either that the underlying theory of the relation of the widths of lines and energy levels is incomplete; or that the width assumed for the L_{III} level is incorrect.

(2) Siegbahn[36] gives the widths of several of the M lines of Au(79) based on measurements by Molin. Although uncorrected for the error due to the crystals used, these values cannot be far from the true widths. They are given in column 3 of Table VI. The values predicted for these same line widths by use of the level widths given in Table V (column 4) are given in the last column of Table VI. The agreement is seen to be reasonably good.

TABLE VI.

		Full width at half-maximum	
Line	Transition	Siegbahn	Computed from Table V, column 4
$M\alpha_1$	$M_V \rightarrow N_{VII}$	5.0 volts	9.0 volts
$M\gamma$	$M_{III} \rightarrow N_V$	17.0	18.0
—	$M_{III} \rightarrow N_I$	20.0	23.8

APPENDIX

DERIVATION OF EQ. (12) OF TEXT

According to Eq. (12) the total probability of absorption of a quantum $h\nu$ is given by the sum of the probabilities of such an absorption involving the change of state of the atom from the normal state (A) to a particular state E. In

[35] D. Coster, Zeits. f. Physik **45**, 797 (1927).

[36] *Spektroskopie der Roentgenstrahlen*, 2d Ed., p. 367.

other words, supposing that the energy levels E are discrete (due to the introduction of a fictitious high potential wall surrounding the atom or crystal which we are considering), Eq. (12) tells us that the absorption curve for the limit results from the additive superposition of the absorption lines corresponding to the individual states E. Now Weisskopf and Wigner[37] have demonstrated by examples that transition probabilities (and hence, in particular, absorption probabilities) from the same initial state to a group of other (excited) states are simply additive under the condition that the final state of the atom and the radiation field[38] is necessarily different for every one of the excited states. Normally this is not so, even if the excited states have different energy. For if they lie very closely together, differing, e.g., in term value by less than the width of the absorption line corresponding to excitation to a single level, it is perfectly possible that the atom may pass from the normal state back to the normal state by way of different excited states with the absorption and emission of an identical group of photons (due to the overlapping of the several absorption and emission lines). In the following we shall try to show that, in the case we are considering, we can eliminate this possibility by slightly altering the problem through the introduction of certain artificial assumptions. To the modified problem we can then adapt Weisskopf and Wigner's calculations and, for it, derive formula (12) of the text.

Consider an atom initially in the normal state in a radiation field of given density and spectral distribution,[39] $\Sigma_n n_n h\nu_n$. Let the probability that the system (atom plus field) is in this condition be given by $|a_A|^2$, a_A being the so-called probability amplitude of the initial state. As time goes on, a probability develops that the atom has absorbed a quantum $h\nu_\beta$ from the radiation field, leaving the atom in the excited state E; let the probability amplitude for this latter condition be a_E^β. Simultaneously, probabilities for the existence of other states arise, corresponding to the emission of fluorescent radiation.[40]

To make the treatment as simple as possible without losing sight of the characteristic features of the problem, let us suppose that the return of the atom to the normal state from state E takes place in three stages, $E \to B \to C \to A$, with the emission of the photons $h\nu_\sigma$, $h\nu_\tau$ and $h\nu_\omega$, such that $\nu_\sigma \gg \nu_\tau \gg \nu_\omega$, in this succession. Let the first two steps involve a readjustment of the inner shells only and the last the return of the ejected electron to the residual vacancy, which can be assumed to be in one of the outermost occupied shells of the atom. We will also consider a second probability, i.e., that the atom is excited by absorption of radiation of frequency ν_β' to the state immediately above E in the sequence of energy levels, E',[41] and returns to the normal state by way of the states B' and C' with the emission of radiation of frequency ν_σ', ν_τ' and ν_ω'. Again we suppose the ejected electron not to alter its quantum state before the atom, by the transitions involving the emission of the photons $h\nu_\sigma'$ and $h\nu_\tau'$, has transferred most of its energy to the radiation field.[42] The two series of transitions are represented in Fig. 13. With the above assumptions we can be certain that the term separation $|\nu_C' - \nu_C|$ is at least of the same order of magnitude as $|\nu_E' - \nu_E|$. On the other hand, we know that, since the atomic state C corresponds to a vacancy in one of the outermost shells of the atom, the widths of the state C and C' (Γ_C and $\Gamma_{C'}$) are extremely small (approaching those for optical levels) compared with those of the states E and E' ($\Gamma_E \gtrsim \Gamma_{E'}$). To be able to apply the calculations of Weisskopf and Wigner (reference 6, p. 67) directly to our problem we now make use of the following device: We adjust the dimensions of our fictitious shell of high potential around the atom until the separations between the successive levels E, E', etc., satisfy the following relation: $\Gamma_E \gg |\nu_{E'} - \nu_E| \gg \Gamma_C$ and therefore also $|\nu_C' - \nu_C| \gg \Gamma_C$. As the probability of emission of a quantum of frequency ν_ω is appreciable only when ν_ω differs from $(\nu_C - \nu_A)$ by a quantity not materially greater than Γ_C, this means that the ranges for which the probabilities of emission of $h\nu_\omega$ and $h\nu_\omega'$ are other than negligible, are well separated. On the other hand, in view of the smallness of Γ_C referred to the resolving power of the spectrometer, the introduction of the high potential wall of the required dimensions may be assumed not to alter the structure of the absorption limit to an observable extent. The introduction of this fictitious shell of perfectly definite dimensions and the exclusion of a number of possible transitions of low probability constitute the artificial changes which we have to make in the real problem in order to make Weisskopf and Wigner's calculations applicable and hence to derive our formula for the absorption coefficient.

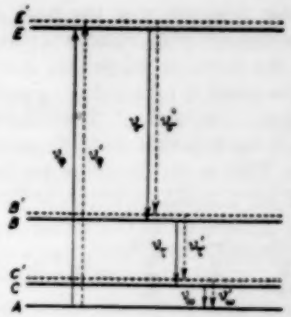

FIG. 13. Schematic diagram of transitions involved in the excitation of an atom by absorption of a photon and its subsequent return to the normal state.

[37] V. Weisskopf and E. Wigner, Zeits. f. Physik **63**, 67 (1930).

[38] In our case this is the normal state of the atom and the initial state of the radiation field minus the photons absorbed in the process of excitation and plus those emitted during the return of the atom to the normal state.

[39] We think of the atom, including the high potential wall, and the radiation field as enclosed in a large box with perfectly reflecting walls. It is then possible to describe any radiation field in the interior in terms of a discrete set of standing waves of frequency ν_n and energy $n_n h\nu_n$, where n_n is an integer. See, e.g., E. Fermi, Rev. Mod. Phys. **4**, 87 (1932).

[40] The change with time in the several probability amplitudes is due to the interaction of the atom and the radiation field and governed by the time-dependent Schrödinger equation (Weisskopf and Wigner, Zeits. f. Physik **63**, 54 (1930), Eq. (12)). The purpose of the present considerations is to show that certain solutions of this equation found by Weisskopf and Wigner for particular cases can be applied directly to the problem of x-ray absorption in the neighborhood of a limit if certain simplifications are introduced.

[41] For the present we consider only a single sequence of terms, i.e. terms corresponding to a single set of angular quantum numbers.

[42] This excludes the possibility that the states B and C may be identical with B' or C'.

We have now achieved that the final state with the probability amplitude[43] $a^{\rho}{}_{A\sigma\tau\omega}$ can be reached by one path only, i.e., by the series of transitions $A\to E\to B\to C\to A$, even though the possible values of ν_ρ, ν_σ and ν_τ may overlap with those of ν_ρ', ν_σ' and ν_τ'. The same is true for any other final state, such as that with the probability amplitude $a^{\rho}{}_{As'\tau'\omega'}$. This is the condition for the application of Weisskopf and Wigner's calculation to the problem of finding the value of the relative probability that, after a long time has elapsed,[44] the atom has absorbed radiation of frequency between ν_ρ and $\nu_\rho+d\nu_\rho$, and emitted radiation quanta of frequency between ν_σ and $\nu_\sigma+d\nu_\sigma$, ν_τ and $\nu_\tau+d\nu_\tau$, and ν_ω and $\nu_\omega+d\nu_\omega$. This is equal to:[45]

$$\lim_{t\to\infty}\sum_{\nu_\rho}^{(\nu_\rho+d\nu_\rho)}\sum_{\nu_\sigma}^{(\nu_\sigma+d\nu_\sigma)}\sum_{\nu_\tau}^{(\nu_\tau+d\nu_\tau)}\sum_{\nu_\omega}^{(\nu_\omega+d\nu_\omega)}|a^{\rho}{}_{A\sigma\tau\omega}|^2=J(\nu_\rho,\nu_\sigma,\nu_\tau,\nu_\omega)d\nu_\rho d\nu_\sigma d\nu_\tau d\nu_\omega$$

$$=\frac{\nu_\rho}{\nu_{EA}}\frac{\nu_\sigma}{\nu_{EB}}\frac{\nu_\tau}{\nu_{BC}}\frac{\nu_\omega}{\nu_{CA}}\frac{(1/\nu_\rho)f(\nu_\rho)(\gamma_{EA}/2\pi)d\nu_\rho}{(\Gamma_{A/2})^2+(\nu_\rho-\nu_\sigma-\nu_\tau-\nu_\omega)^2}$$

$$\frac{(\gamma_{EB}/2\pi)d\nu_\sigma}{(\Gamma_{E/2})^2+(\nu_{EA}-\nu_\sigma-\nu_\tau-\nu_\omega)^2}\frac{(\gamma_{BC}/2\pi)d\nu_\tau}{(\Gamma_{B/2})^2+(\nu_{BA}-\nu_\tau-\nu_\omega)^2}\frac{(\gamma_{CA}/2\pi)d\nu_\omega}{(\Gamma_{C/2})^2+(\nu_{CA}-\nu_\omega)^2}.$$

Finally we obtain for the total probability that a quantum of frequency between ν_ρ and $\nu_\rho+d\nu_\rho$ has been absorbed, summing over all states E,

$$J(\nu_\rho)d\nu_\rho=\sum_{\nu_E=\nu_{E_0}}^{\nu_E=\infty}(E)\int_{\nu_{EB}-\Delta\nu_\sigma}^{\nu_{EB}+\Delta\nu_\sigma}d\nu_\sigma\int_{\nu_{BC}-\Delta\nu_\tau}^{\nu_{BC}+\Delta\nu_\tau}d\nu_\tau\int_{\nu_{CA}-\Delta\nu_\omega}^{\nu_{CA}+\Delta\nu_\omega}d\nu_\omega\,J(\nu_\rho,\nu_\sigma,\nu_\tau,\nu_\omega)d\nu_\rho$$

$$=\sum_{\nu=\nu_{E_0}}^{\nu_E=\infty}(E)\frac{f(\nu_\rho)}{\nu_{EA}}\frac{\gamma_{EA}}{\Gamma_A}\frac{\gamma_{EB}}{\Gamma_E}\frac{\gamma_{BC}}{\Gamma_B}\frac{\gamma_{CA}}{\Gamma_C}\frac{(\Gamma_A+\Gamma_E/2\pi)d\nu_\rho}{((\Gamma_A+\Gamma_E)/2)^2+(\nu_{EA}-\nu_\rho)^2}.$$

Here $f(\nu_\rho)$ gives the spectral distribution of intensity of the incident beam.[46]

Here $\Delta\nu_\sigma$, $\Delta\nu_\tau$, $\Delta\nu_\omega$ are frequency intervals large compared with Γ_E, Γ_B, Γ_C, respectively, so that the range of integration covers the region where the integrand is not negligible. Furthermore an inspection of the calculation of Weisskopf and Wigner shows that if we would take into consideration all the possible cascaded transitions from state E to the normal state[47] the factor $(\gamma_{EB}/\Gamma_E)(\gamma_{BC}/\Gamma_B)(\gamma_{CA}/\Gamma_C)$ would have to be replaced by unity. This is of course evident if the only possible transitions from the states E, B and C are just $E\to B$, $B\to C$ and $C\to A$, respectively. Furthermore, we may, without causing an appreciable error, replace ν_{EA} in the multiplying factor by ν_ρ. If we finally consider the fact that the life of the normal state in the radiation field is extremely long compared with that of an excited state E, i.e., $\Gamma_A\ll\Gamma_E$, and also that the absorption coefficient is given by the product of the probability of absorption of a quantum from a beam of unit intensity and of the energy of the quantum, we arrive at our Eq. (12) for the partial absorption coefficient $K(\nu)$:

$$K(\nu)=C\sum_{\nu_{EA}=\nu_{E_0A}}^{\nu_{EA}=\infty}(E)\,\gamma_{EA}\left(\frac{\Gamma_{E/2\pi}}{(\nu_{EA}-\nu)^2+(\Gamma_{E/2})^2}\right).$$

We must still discuss the effect of the existence of several sequences of energy levels, corresponding to different angular quantum numbers. Wentzel[48] has shown that the degeneracy resulting from the existence of different magnetic states of equal energy produces no difficulties as long as we confine ourselves to dipole absorption; then the transition probabilities of the several degenerate states simply add up. We know that with x-rays of about 1A wave-length the quadrupole absorption is not negligible, but yet far less than the dipole absorption, so that the effect of the former on the shape of the absorption limit can be at most very slight. We cannot dispose as easily of the case that there are coincident states E with different j-values and azimuthal quantum numbers. In this case, however, the different selection and intensity rules make it extremely likely that the return to the normal state will take place by different routes (with the emission of quanta of different frequency). Under these circumstances we can apply the method of Weisskopf and Wigner as before.

[43] We indicate by the upper index the absorbed quantum, by the lower indices the state of the atom and the emitted quanta. We exclude from consideration the possibility of repeated absorption by the same atom as this is very improbable during the short period of excitation and cannot change the results if it takes place after the atom has returned to the normal state.

[44] The time should be long compared to the mean lives of the atomic states involved.

[45] V. Weisskopf and E. Wigner, reference 11, Eq. (29a).

[46] G. Wentzel, Handb. d. Physik **24**, Part 1, 756 (1933).

[47] The exclusion of certain of these, such as the direct transition $E\to A$, to make the method applicable, plays a minor rôle, as their relative probability is small.

[48] G. Wentzel, reference 46, p. 757.

The Secondary Structure of X-Ray Absorption Edges from Elements in Certain Cubic Crystals

G. P. BREWINGTON, *University of Michigan*

(Received August 4, 1934)

The K x-ray absorption spectra of potassium, chlorine, calcium and sulfur in several different cubic crystals have been photographed. The absorption spectrum was obtained for potassium from filters prepared with KF, KCl, KBr and KI, and the chlorine spectrum from LiCl, NaCl, KCl, RbCl. The calcium and sulfur absorption spectra were obtained from powdered calcium sulfide. A secondary structure was found on the short wave-length side of the K edge of each of these elements. The following results are not in accord with the demands of the Kronig theory for secondary structure:—The absorption spectra of two elements in the same crystal are not similar. The product of the separation of each of the secondary structure components in volts and the square of the lattice space is not a constant for the crystals studied. Some of the structure previously reported for the sulfur edge is shown to be due to the sulfur contained in goldbeater's skin which had been used to cover the slit of the x-ray tube.

A SECONDARY structure[1] has been observed close to the K and L absorption edges of a large number of elements.[1, 2] Kronig,[3] from wave mechanical considerations, suggested that the separation in the secondary structure should be inversely proportional to the square of the lattice constant of the crystal used as absorbing material. This dependence has been confirmed by Coster and Veldkamp[4, 5] for certain metal crystals. Lindsay and Barton[6, 7] find the relations suggested by the theory are not easily satisfied by the observed separations in the K absorption spectrum of several elements in polar crystals. Coster and Klamer[8] have shown that the secondary structures of two elements in the same crystal are not similar.

The alkali halides crystallize in the simple cubic system and it seemed desirable to obtain the secondary structure of the K edges of potassium and chlorine in their various combinations in this crystal system. Calcium sulfide was studied because it is also of the same type.

Experimental Procedure

A Siegbahn vacuum spectrograph of 180.6 mm radius was used to obtain the absorption photographs. The metal x-ray tube was separated from the main chamber of the spectrometer by windows of goldbeater's skin or films of pyroxalin or collodion.[9] The targets of the x-ray tube were made of silver, copper, molybdenum or tungsten and were so chosen that no emission lines appeared in the region of secondary structure. The filament consisted of a flat spiral of chromel wire coated with barium oxide. The tube was run at currents up to 30 milliamperes.

Screens of the alkali halides may easily be prepared by saturating a very thin paper with a water solution of the salt and drying rapidly over a hot plate. A variation of this procedure was necessary in the case of lithium chloride, which is hygroscopic. The paper was placed in position in the path of the x-ray beam and saturated with a water solution of lithium chloride. A dish of phosphorous pentoxide was then placed in the chamber of the spectrometer and the pumps turned on. This was also successfully tried with some of the other water soluble salts. The calcium sulfide was ground in a mortar containing a small quantity of amyl acetate. The finely divided particles remained in suspension long enough to be transferred to an amyl acetate solution of collodion or pyroxalin. This solution was then thoroughly mixed and spread on a glass plate to

[1] J. D. Hanawalt, J. Frank. Inst. **214**, 569 (1932). This article contains references to early work.
[2] B. J. Kievit and G. A. Lindsay, Phys. Rev. **36**, 648 (1930); P. A. Ross, Phys. Rev. **44**, 977 (1933); A. H. Barnes, Phys. Rev. **44**, 141 (1933).
[3] R. de L. Kronig, Zeits. f. Physik **70**, 317 (1931); **75**, 191 (1932); **75**, 468 (1932); H. J. Groenewold, Zeits. f. Physik **76**, 766 (1932); H. Peterson, Zeits. f. Physik **76**, 768 (1932).
[4] D. Coster and J. Veldkamp, Zeits. f. Physik **70**, 306 (1931); **74**, 191 (1932).
[5] J. Veldkamp, Zeits. f. Physik **77**, 250 (1932).
[6] G. A. Lindsay, Zeits. f. Physik **71**, 735 (1931).
[7] G. A. Lindsay and V. P. Barton, Phys. Rev. **41**, 391 (1932); **46**, 362 (1934).
[8] D. Coster and G. H. Klamer, Physica **1**, 145 (1934).
[9] L. Harris and E. A. Johnson, Rev. Sci. Inst. **4**, 455 (1933).

TABLE I. *Separation of secondary structure of absorption edges.*

		A	*α*	*B*	*β*	*C*	*γ*	*D*	*δ*	*E*	*ε*
Potassium absorption											
	ν	1.76	6.12	10.2	17.0	23.0	30.2	36.9			
KF	x.u.	1.68	5.85	9.2	16.3	22.0	28.9	35.2			
	ν·a²	50	176	290	483	653	863	1000			
	ν	1.44	3.12	4.73	6.16	8.20	12.8	18.7	23.6	28.7	
KCl	x.u.	1.00	2.98	4.54	5.90	7.85	12.2	17.2	22.6	27.4	
	ν·a²	39	123	186	243	324	505	710	893	1080	
	ν	1.11	2.90	4.33	6.20	9.54	12.1	16.5	22.0	27.1	
KBr	x.u.	1.06	2.77	4.14	5.92	9.10	11.5	15.8	21.1	25.9	
	ν·a²	45	125	187	268	411	522	712	949	1170	
	ν	1.01	2.27	3.30	5.54	6.67	10.1	14.1	18.3	23.2	29.4
KI	x.u.	.97	2.17	3.15	5.29	6.38	9.7	13.5	17.6	22.2	28.7
	ν·a²	50	112	164	275	332	502	702	910	1152	1490
Chlorine absorption											
	ν	1.51	3.35	5.50	9.94						
LiCl	x.u.	2.34	5.21	8.57	15.5						
	ν·a²	40	89	145	267						
	ν	1.83	6.07	8.20	10.5	12.8	15.2	16.6			
NaCl	x.u.	2.84	9.45	12.8	16.4	19.9	22.6	25.8			
	ν·a²	58	193	260	334	405	483	527			
	ν	1.84	3.41	5.40	6.59	7.56	9.54	11.6			
KCl	x.u.	2.85	5.32	8.41	10.3	11.8	14.9	18.1			
	ν·a²	53	136	213	260	299	376	460			
	ν	.97	2.94	5.02	8.67	10.8	14.6	17.2			
RbCl	x.u.	1.52	4.54	7.80	13.5	16.9	22.6	26.7			
	ν·a²	42	127	216	537	468	627	740			
Calcium absorption											
	ν	3.45	5.62	7.20	13.0	18.7	25.5	37.5	46.6	59.8	
CaS	x.u.	2.35	4.27	5.47	9.9	14.2	19.4	28.5	35.4	45.4	
	ν·a²	111	181	232	422	604	824	1210	1502	1930	
Sulfur absorption											
	ν	1.67	4.39	6.3	8.8	10.6	12.4	16.8			
CaS	x.u.	3.41	8.94	12.9	17.9	21.9	25.3	34.1			
	ν·a²	54	142	210	285	342	402	543			

dry. The films could be stripped off and were ready for use as screens.

The screens were placed between the reflecting crystal and the photographic plate. A very thin pyroxalin film, blackened by holding it over burning camphor was placed in front of the plate. The screen and the blackened film thus assist in reducing the amount of scattered and fluorescent radiation that may be present. Using these precautions, plates have been obtained which show almost no blackening except that due to the reflected beam.

The separations between the *K* absorption edge and the center of each dark line and each absorption line, respectively, on the short wavelength side of the edge were measured and reduced to electron volts and x units and are shown in Table I. The Greek letters refer to the minimum of absorption (black lines on the plate) and the Latin letters to the maximum of absorption. On several of the plates some of the dark lines appeared to contain a further structure but this structure was so faint that it could not be satisfactorily measured. The dispersion was scarcely sufficient to resolve the secondary structure accompanying the *K* edges of rubidium, bromine and iodine.

DISCUSSION OF RESULTS

Several theories have been proposed to explain the secondary structure of x-ray absorption edges. A brief review of the several suggestions

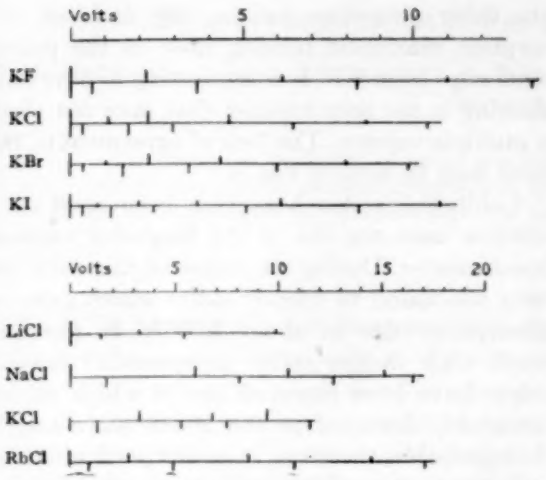

FIG. 1. Structure of potassium and chlorine edges in terms of the electron volt separations of the secondary structure from the absorption edge. The minima of absorption (black lines on the plate) are represented by vertical lines rising above the horizontal. The maxima of absorption (white lines on the plate) are represented by vertical lines extending down from the horizontal.

has been published by Hanawalt.[1] By means of wave mechanics Kronig has developed a theory of secondary absorption. The absorbing crystal was considered by Kronig as a periodic array of potential walls corresponding to the ions in the lattice. The ejected electron, resulting from the ionization of the K level, can enter into only certain energy bands resulting from the crystal lattice structure. The transition of an electron from a K level of an atom to the lowest of these energy bands accounts for the absorption edge. Absorption lines in the secondary structure of the edge correspond to energies an electron may possess after being ejected from the K shell. The values of these energies are given by

$$W_n = n^2h^2/8ma^2,$$

where $n=1, 2, 3, \cdots$, m is the mass of the electron, a the lattice constant and h Planck's constant. The correctness of this formula has been experimentally verified by the work of Coster and Veldkamp,[4, 5] who obtained the K absorption spectra of a number of metallic elements of similar crystal structure.

Kronig's formula suggests several tests that may be applied to the data. These are:

a. The secondary structure of the absorption edges of two or more elements in the same

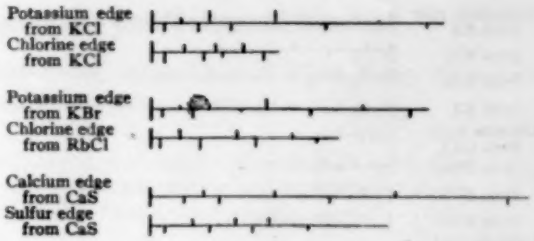
Potassium edge from KCl
Chlorine edge from KCl
Potassium edge from KBr
Chlorine edge from RbCl
Calcium edge from CaS
Sulfur edge from CaS

FIG. 2. Comparison of two elements in the same crystal.

crystal should be identical unless very near the edge. A comparison of the x-ray absorption spectrum of potassium and chlorine (Fig. 2) obtained from a KCl screen and the absorption spectrum of calcium and sulfur from CaS, shows that this is not true. Coster and Klamer[8] arrive at the same conclusion. They photographed the potassium and chlorine absorption spectra using a KCl filter with an instrument having a smaller radius than that reported here. The secondary structure reported in this paper is much closer to the absorption edge; however, the two sets of measurements are not inconsistent as the line farthest from the edge measured by the author coincides with the line nearest the edge as reported by Coster and Klamer. Stephenson[10] obtained the absorption spectrum of bromine near the K edge by using a KBr crystal in a double crystal spectrometer. A comparison of the the bromine spectrum with that of potassium shows them to be quite dissimilar.

b. If the structure of the absorption spectrum is determined by the lattice constant of a crystal, the spectra of elements in different crystals having the same lattice constant should be identical. Two of the alkali halides have approximately the same lattice constant; KBr and RbCl. A comparison of the absorption spectra of potassium in the KBr and that of chlorine in the RbCl shows little similarity (Fig. 2).

c. In a series of crystals of the same structure, the product of the separation of the lines in the secondary structure, expressed in volts, and the square of the lattice dimension should be a constant for corresponding lines, since $W \cdot a^2 = n^2h^2/8m = kn^2$. Lindsay[6] reported only an approximate agreement for potassium from KCl, KBr, and KI. This same approximate agreement

[10] S. T. Stephenson, Phys. Rev. **44**, 349 (1933).

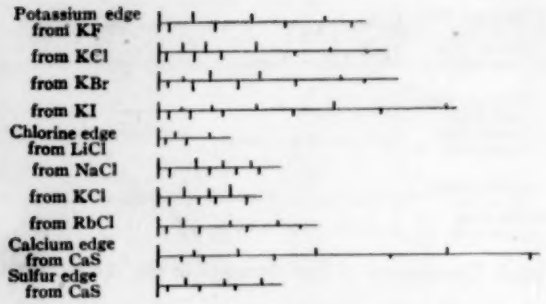

FIG. 3. Comparison of potassium, chlorine, calcium and sulfur edges showing lack of agreement of the data. The scale is in arbitrary units. Volts$\times a^2$.

was found in the present work for potassium but it will be noted that there is no such regularity in the secondary structures of the chlorine edges. When the absorption spectrum of potassium from KF is compared with the potassium from the other potassium halides, one finds an absorption maximum missing close to the potassium edge from KF. It is interesting to note that fluorine is the only halogen that does not show a multiple valence. The lack of agreement of the data may be seen in Fig. 3.

Goldbeater's skin has often been used as a window over the slit of the Siegbahn vacuum spectrometer. During the course of this work the skin was found to contain sulfur which gave an absorption edge at about 4.990A. In previous work with various sulfur compounds,[11] several edges have been reported one of which almost invariably occurred at the above wave-length. It is probable, therefore, that this particular edge was due to the goldbeater's skin, rather than to the compound in the filter. A photometer trace of this absorption will be found in Fig. 4.

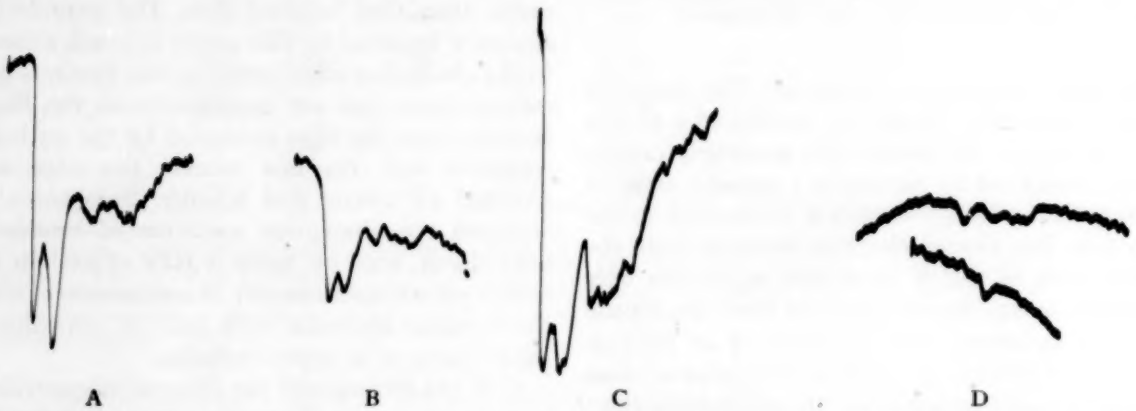

FIG. 4. Representative photometer traces of plates. (A) Potassium absorption edge from KF; (B) chlorine absorption edge from RbCl; (C) chlorine absorption from KCl; (D) sulfur absorption edge from CaS, photographed through goldbeater's skin (upper), sulfur absorption edge in goldbeater's skin (lower).

It would appear, from the data obtained, that Kronig's theory is not, in its present form, capable of explaining completely the secondary structure of x-ray absorption edges of elements existing in crystals with polar binding.

The writer wishes to take this opportunity to express his appreciation to Professor G. A. Lindsay, who suggested the problem and greatly assisted in its completion with many helpful criticisms; also to Professor H. M. Randall for the privilege of working in the laboratory.

[11] M. Siegbahn, *Spektroskopie der Röntgenstrahlen*, p. 284, 1931.

Measurement of the X-Ray Absorption Coefficient of Xenon*

T. N. WHITE, *Office of Cancer Investigations, U. S. Public Health Service, Harvard Medical School, Boston, Massachusetts*

(Received August 2, 1934)

The absorption coefficient of xenon was measured over a wave-length range 0.18 to 1.5A. The formula obtained for the mass-absorption coefficient was $655\lambda^{2.98}+0.7$ below, and $92.8\lambda^{2.79}+0.7$ above the K discontinuity, giving values somewhat below Jönsson's "universal absorption curve."

XENON, because of its stability and high absorption, is undoubtedly the ideal gas for an ionization chamber. In order to make comparisons of intensities of x-rays of different wave-lengths, a knowledge of its absorption coefficient is necessary. As such comparisons are needed in certain biophysical experiments at this laboratory, a series of measurements was made to determine this variable over a suitable wave-length range. In addition, the absorption coefficient of xenon was considered to be of interest, apart from its use in connection with ionization chambers, since Jönsson's "universal absorption curve"[1] does not yield very accurate values, and the only certain knowledge of the absorption of a material is obtainable only by careful absorption measurements on the material itself. It is hoped, at some future time, to measure the energy required to form a pair of xenon ions, and thus render the xenon ionization chamber capable of measuring absolute x-ray intensities.

The xenon was collected by the Air Reduction Sales Corporation with a stated purity of 99.9 percent. The experimental arrangement was standard, and involved as x-ray source a Müller autoprotective tube, cooled with forced circulation of kerosene, filament on storage batteries, and with kenotron-rectified, capacity-smoothed high voltage from a three-phase supply. The ripples in the high voltage were less than 1 percent. A specially constructed xenon ionization chamber was mounted on a Gaertner spectrometer, and connected to a Compton electrometer, across which 3×10^{10} ohms was shunted in measuring large currents. In order to obtain strong ionization, two Soller collimators[2] were used, and reflection took place on the 5×10 cm face of a fine calcite crystal. The angle between the most divergent rays through the slits was such as to permit reflection of wave-lengths through a range ($\Delta\lambda$) of about 0.040A for a given setting of the crystal. Soller[3] has indicated that the intensity curve for these wave-lengths falls off linearly and symmetrically to zero from the central wave-length, provided, of course, that the wave-lengths were of equal intensity before entering the apparatus. Assuming, in addition, that $\Delta\lambda \ll \lambda$, it can be shown, by integrating the absorption ratios for all λ in the range $\Delta\lambda$, that the correction factor to be applied to the observed absorption ratio, in order to obtain the true value for the central wave-length, is approximately $[1-(x\Delta\mu)^2/48]$ where $\Delta\mu$ corresponds to $\Delta\lambda$ and x is the path in gas at normal pressure. This correction is exceedingly small, but unfortunately Soller's finding is not correct in all cases,[2] nor is it always possible to adjust the operating conditions of the tube so that its spectrum is flat at the wave-length at which a particular measurement is being made. Calculation of the correction factor in the case where all wave-lengths shorter than the central wave-length are eliminated gives $[1+x\Delta\mu/6]$ as a first approximation. This is of the order of magnitude of the experimental error in the following results for wave-lengths just greater than the critical absorption edge of xenon, but since there is no reason to expect such complete asymmetry, the effect of the divergence of the beam may be

* Presented at the Boston meeting of the American Physical Society, 1933.

[1] Handb. d. exp. Physik **24**, 1, 250; Siegbahn, *Spektroskopie der Röntgenstrahlen*, 2nd ed., p. 470, Table 228a. It might be noted that the values presented in this table have not been entirely "smoothed out," since there are discontinuities in the progress of the differences.

[2] Described R. S. I. **4**, 591 (1933).

[3] Soller, Phys. Rev. **24**, 158 (1924). Strictly speaking, Soller used a single wave-length and varied the spectrometer setting, while we consider the fate of various wave-lengths which pass through at a given setting, but this does not alter the argument.

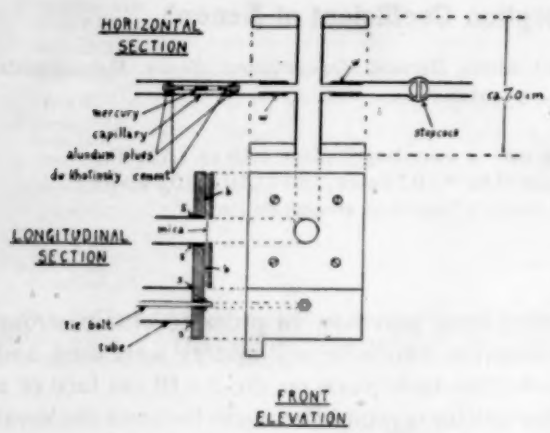

FIG. 1. Diagram of absorption vessel. *s*, solder joint; *w*, white wax; *b*, beeswax.

neglected, provided still that $\Delta\lambda \ll \lambda$. This is, of course, hardly true for wave-lengths less than the critical absorption wave-length of xenon, and the formula obtained for the absorption coefficient in this region is probably not so reliable as the formula for longer wave-lengths. It was determined because needed for intensity comparisons with the apparatus just described, and is presented for what it is worth.

Two absorption vessels were used, one of Pyrex with waxed-on metal flanges to carry the windows and support it, and another all of metal, the construction of which is detailed in Fig. 1. The legs were provided to fix its lateral position on the spectrometer bench. Mica windows were used in each case and determination of their absorption gave a very satisfactory check on the recent measurement of J. H. Williams.[4] The vessels were filled by means of a gas-transfer apparatus, and the pressure was measured by balancing against a barometer through the device shown under Horizontal Section, Fig. 1. The plugs were cut from an alundum filter: they begin to pass mercury at about 2 atmospheres pressure difference. Two pressures were used—about 1/5 atmosphere for the longer wave-lengths, and a little less than an atmosphere for the shorter. The density of xenon was taken as 5.86 g/l at 0°C and 760 mm of mercury.

The first series of measurements was made with the Pyrex vessel placed immediately in front of the ionization chamber, and over the range 0.4 to 1.0A. This was during the summer when the electrometer was not working very well. The vessel eventually broke, and the all-metal one was constructed, with which the second series of measurements was made. This vessel was placed between the crystal and the second Soller collimator on which stops were so placed that no radiation from the walls of the vessel could enter the chamber.

From 20 to 50 readings were taken at each wave-length from 0.18 to 1.5A and the statistical weight of the mean ratio of the intensities with and without the vessel in the beam was estimated in each case, according to the consistency of the individual ratios. Correction was made for the background of scattered radiation in the spectrum, and the short wave-length limit was adjusted to avoid second order reflection except in the case of the longest wave-length, where the W $L\alpha$ line was used, and the neighboring spectral intensity subtracted.

Table I gives the values of the mass-absorption coefficient from the second series of measurements.

TABLE I. *Mass-absorption coefficients of xenon.*

λ (A)	μ/ρ (cm²/g)	λ (A)	μ/ρ (cm²/g)
0.176	5.18	0.634	27.17
.209	7.65	.708	34.9
.247	11.79	.794	48.4
.282	17.55	.891	71.6
.317	24.10	1.000	92.7
.423	8.93	1.096	116.6
.528	16.60	1.473	276.5

In accordance with Jönsson,[1] 0.7 was taken as a suitable value for the mass scattering coefficient. Fig. 2 shows the weighted root-mean-square straight lines through the logarithm of the mass photoelectric absorption coefficient from the data of the second series. The resulting equation for the mass-absorption coefficient is:

$$\mu/\rho = 655\lambda^{2.90} + 0.70 \qquad 0.18 < \lambda < \lambda_K$$
$$= 92.8\lambda^{2.79} + 0.70, \qquad \lambda_K < \lambda < 1.5$$
$$\lambda_K = 0.358\text{A}$$

with mean errors of 1.3 percent and 2.2 percent estimated from the departures of the points from the straight line. The corresponding line for the first series is not shown, as it differs by an amount

[4] J. H. Williams, Phys. Rev. **44**, 146 (1933).

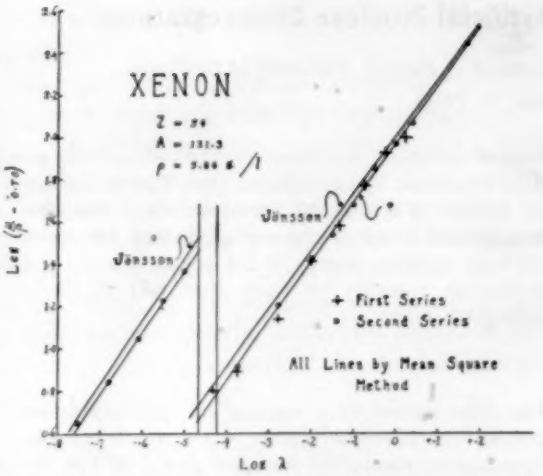

FIG. 2. X-ray absorption coefficient of xenon as a function of wave-length.

less than the mean error 6.4 percent of the first series. The pressure changes were made at about $\log \lambda = -0.20$. Measurements within 0.02A of the K absorption edge of xenon have no value, due to the divergence of the beam. This region is isolated by the vertical lines on Fig. 2.

The jump ratio, 6.29, at the K edge from these data agrees within experimental error with the ratio, 6.34, of the frequencies of the K to L_I absorption edges. The lines marked "Jönsson" are root-mean-square straight lines through values taken from his "universal absorption curve." In general the disagreement, which reaches 16 percent near the K discontinuity, is greater than what would be expected from the 5 percent accuracy claimed for his curve. At the longest wave-length, however, the difference is only about 4 percent and at the shortest, the value of $Z\lambda$ is less than 9, and his values are not claimed to be reliable in this region.

It may be noted that the recent measurements of Hahn[5] at short wave-lengths show in certain cases a trend toward somewhat lower values than those of Richtmyer and Allen which were presumably used by Jönsson in drawing up his table, while Carr[6] records for bismuth even greater deficiencies in the wave-length range from 0.5 to 1.2A than are reported here for xenon.

An inspection of Fig. 2 will quickly show that where the difference is greatest, a wave-length displacement of more than half the whole range of wave-lengths permitted by the divergence of the beam would be required to bring the observed line into agreement with the Jönsson line. The difference, therefore, cannot be blamed on inhomogeneity, and careful check on length of absorption vessel, pressure of xenon, window correction, scattering in the spectrum, and natural leak of ionization chamber have failed to reveal any source of systematic error which would give so large a difference. The pressure in the absorption vessel was the same at the end of the measurements as at the time of filling. In order to check on the purity of the xenon, a small specimen of gas from the same supply bulb was filled into a carefully baked electrodeless discharge tube which was then sealed off and excited by means of a leak-testing sparker. The resulting spectrogram[7] showed no impurity except mercury vapor (pressure 2×10^{-3} mm of mercury) from the gas transfer apparatus. A previous attempt to obtain the spectrum, by using a discharge tube with aluminum electrodes, failed, because of copious liberation of hydrogen from the electrodes by the electric discharge in the xenon, though the tube was carefully prepared, and due to disappearance of the xenon during discharge.[8] Both of these phenomena have been noted by earlier workers. In view of the consistency of the results, and thorough consideration of possible sources of systematic error, it is felt that the formula given above is closer than Jönsson's "universal curve" to the absorption coefficient of xenon.

[5] T. M. Hahn, Phys. Rev. **46**, 149 (1934).

[6] L. H. Carr, Phys. Rev. **46**, 92 (1934).

[7] Thanks are due to Dr. Egon Lorenz for obtaining the emission spectrum.

[8] Tubes with aluminum electrodes for xenon have been made to work by others; our experience indicates that the electrodeless tube is more easily prepared, but the xenon does disappear, though perhaps more slowly.

Some Gamma-Rays Accompanying Artificial Nuclear Disintegrations[1]

EDWIN MCMILLAN,* *Radiation Laboratory, Department of Physics, University of California*

(Received September 24, 1934)

Gamma-rays have been observed from the bombardment of F, Li, and possibly B and Be by 1.15 m.e.v. protons, and gamma-rays and neutrons in varying proportions from the bombardment of Be, C, Li, B, and possibly F, Li, Mg and Al by 2.3 m.e.v. deutons. Studies have been made of the excitation function and of the absorption of some of these radiations, and also of the absorption of the "annihilation radiation" accompanying the radioactivity stimulated in carbon. The gamma-ray from fluorine bombarded by protons is of especial interest, since it furnishes an experimental check of the pair-production absorption at the high quantum energy of 5.4 m.e.v., where the pair-production accounts for more than half of the total absorption in lead.

IN many artificial nuclear disintegrations gamma-rays are emitted, and a knowledge of these is necessary for a complete understanding of the nuclear reactions involved. Also, the artificial gamma-rays offer the possibility of investigating the variation of absorption coefficients over a hitherto unavailable range of energies. This aspect of the problem is of particular interest at present, because of its bearing on the recently developed theory of γ-ray absorption by the production of pairs of positive and negative electrons. Bethe and Heitler[2] have worked out the consequences of the theory, giving values of the absorption to be expected. Their paper also gives references to previous theoretical work, and discusses the existing experimental checks, including absorption measurements with 2.6 m.e.v. γ-rays, where the pair production accounts for about 20 percent of the absorption in lead.

Gamma-rays are absorbed in traversing matter according to the equation $I=I_0e^{-\mu x}$, the "absorption coefficient" μ depending on the quantum energy of the radiation and the nature of the absorber. Three processes contribute to μ:

(1) The photoelectric effect. This of important magnitude only for energies of 2 m.e.v. or less, and can be calculated from the empirical formula of Gray.

(2) The Compton effect. This gives an absorption proportional to the number of electrons present. It decreases monotonically with increasing quantum energy, and can be calculated from the theoretical Klein-Nishina formula.

(3) The pair-production. This occurs at energies above 1 m.e.v., becoming appreciable at 2 m.e.v. and increasing to a large fraction of the total absorption at higher energies. The cross section of a nucleus for pair-production by gamma-rays increases rapidly with atomic number Z. Approximate theoretical formulae give a Z^2 law for the energy range important to us. This law is rigorously valid only for small Z, but may hold approximately for all elements. Following this law, the absorption *per electron in the absorber* increases directly with the atomic number.

The different dependence of the Compton absorption and the pair production absorption on Z furnishes a method for distinguishing them experimentally. For if (after subtracting the photoelectric absorption) one plots the absorption coefficients *per electron* for different materials against Z, a straight line should be obtained, whose intercept at $Z=0$ gives the Compton part and whose slope gives the pair-production part of the absorption.

EXPERIMENTAL

Protons or deutons were brought to high velocity by successive accelerations in a magnetic field, in an apparatus developed by Lawrence,

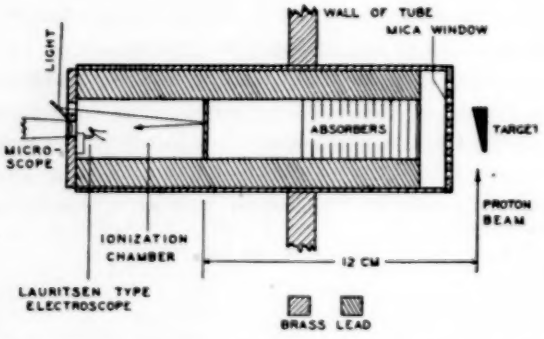

FIG. 1. Arrangement of ionization chamber and absorbers. The electroscope consists of a sputtered quartz fiber supported at one end on a light wire frame. A short cross-hair attached to the free end of the fiber is observed against a scale in the microscope eyepiece.

* National Research Fellow.

[1] A preliminary report of this work was given at the Berkeley meeting of the American Physical Society in June; abstract in Phys. Rev. **46**, 325 (1934).

[2] Bethe and Heitler, Proc. Roy. Soc. **A146**, 83 (1934).

whose construction and operation are described elsewhere.[3]

The gamma-radiation was observed by means of a small ionization chamber containing a quartz fiber electroscope of the type devised by Lauritsen. Fig. 1 shows the ionization chamber in place. The heavy lead tube which forms the wall of the chamber slides into a brass tube set into the side of the magnetic acceleration apparatus. The ion beam, travelling as shown by the arrow, strikes a target in front of the ionization chamber. Absorbers of various materials can be put into the end of the lead tube.

Calibration of ionization chamber

The sensitivity of the electroscope, calculated from its voltage sensitivity and estimated capacity, is about 2×10^8 ion pairs per scale division. Its gamma-ray sensitivity was determined by observing the leak produced by a milligram of radium placed in the position of the target, with 3 cm of lead filter in place. This amount of lead practically stops all but the hard components (1.8 and 2.2 million volts) of the radium gamma-radiation; we thus get a calibration of the chamber for gamma-rays of this energy. The result is that one division on the electroscope scale corresponds to 1.2×10^8 quanta emitted from the target, for 2 million volt gamma-rays. When measuring gamma-rays of other energies, it is assumed that the ionization per quantum is proportional to μ_a (part of the absorption coefficient due to absorption of energy) in lead multiplied by the quantum energy. The natural leak of the electroscope is 0.001 divisions/sec.; this is always subtracted from the ionization readings.

Absorption measurements. Calibration

Absorbers of Al, Cu, Sn, and Pb were used. The first three were in the form of solid cylinders 2.5 cm in diameter and 5.1 cm long. The lead was in the form of disks 0.33 cm thick; with these more complete absorption curves could be made, to test the homogeneity of the radiation. A water absorber contained in a thin-walled metal cell 6.6 cm long was also used in some of the experiments.

All measurements of gamma-ray absorption coefficients are subject to an error due to radiation scattered by the absorber into the ionization chamber. This has the result of giving too small a value for the absorption. The magnitude of the scattering error was found empirically by determining the apparent absorption coefficient of the gamma-radiation from a source consisting of a milligram of radium screened with 2.6 cm of lead. The following values were obtained for absorbers of different materials:

Al	0.112 cm^{-1}	Sn	0.293 cm^{-1}
Cu	0.364	Pb	0.525

It was found that an additive correction of 6 percent makes these fit the calculated values very well, as shown in the upper curve of Fig. 2. Here they are plotted as absorptions per electron, after subtracting the photoelectric part (from Gray's formula) and adding 6 percent. The calculated Klein-Nishina coefficients for the two hard radium gamma-rays are indicated by short horizontal lines at 1.53 and 1.37×10^{-25}. The slight rise with Z is partly due to pair production, and possibly partly due to an underestimation of the photoelectric absorption.

This correction of +6 percent is applied to all the values given in the following part of the paper. Although it is not strictly justifiable to use the same correction for the different frequencies and absorbers, the variation will not be large

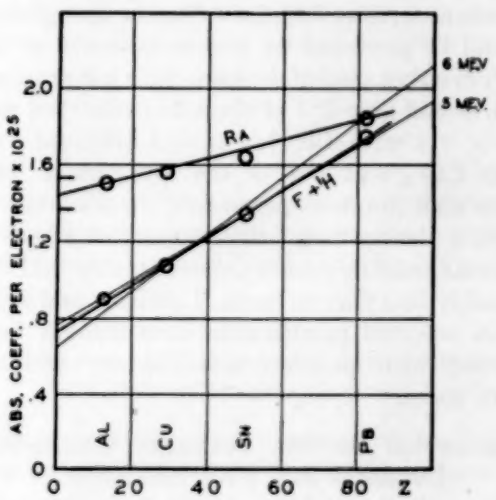

FIG. 2. Absorption coefficients of filtered radium γ-rays (for calibration) and of the radiation from fluorine bombarded by protons, in the materials indicated. The theoretical predictions for 5 and 6 million volt γ-rays are shown.

[3] Lawrence and Livingston, Phys. Rev. **45**, 608 (1934).

and will not affect the validity of the results even if it is of the order of the whole correction.

Results with Proton Bombardment

A beam of about 1 microampere of 1.15 m.e.v. protons (in form of H_2^+ ions) was used. With targets of Pt, Mg, Al, Si, C, and $Ca(OH)_2$ an ionization of 0.06–0.10 divisions per hundred seconds per microampere of protons was observed. The same effect was found when the beam was not striking any target, and is a background of stray radiation coming from all parts of the apparatus. It is subtracted from the values given below; in making absorption measurements, the background was also determined with each absorber in place. With other targets the observed ionizations were, in the same units,

B_2O_3	0.19	LiOH	0.40
Be	0.38	CaF_2	1.83

A paraffin lining in the ionization chamber reduced all these affects to about 1/2; this indicates that they are caused by gamma-rays rather than by neutrons.

The possibility that some of these effects might be caused by deuton contamination of the ion beam must not be overlooked. An upper limit to the possible amount of contamination can be set by comparison with the results obtained using a deuton beam. The closest limit is set by the ionization observed when a carbon target is bombarded; this effect, including the background, would be produced by a contamination of one part in a thousand of deutons. Such a contamination would give 1/2 of the effect observed with B_2O_3, 3/4 with Be, 1/4 with LiOH and 1/60 with CaF_2, and most of the background. Thus even with the most pessimistic supposition concerning the contamination, the proton effects on fluorine and lithium are unquestionably real, and possibly also that on boron. Lauritsen and Crane have reported gamma-rays from lithium[4] bombarded with protons, and did not find any with boron.[5]

Absorption of the Fluorine Gamma-Ray. Evidence for Pair Production

Absorption measurements were made on the radiation from CaF_2. Fig. 3 is a logarithmic plot

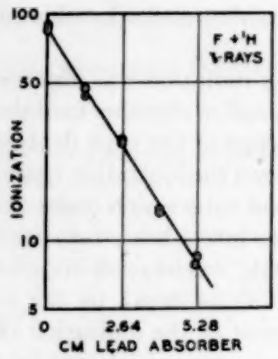

Fig. 3. Absorption of the fluorine+proton γ-rays in lead, plotted logarithmically.

of their absorption in lead. It is seen to be linear over a factor of 10 in intensity. The absorption coefficient 0.49 cm^{-1} in lead, if interpreted as being due entirely to the Compton effect, leads to an energy of about 2 million volts for the γ-ray. Such a γ-ray is not reconcilable with observations of the α-particles emitted during the bombardment of fluorine by protons.[6] For if the γ-ray arises from the same process that gives the observed α-particles, no reasonable mass for the fluorine atom will give an energy balance; while if it is associated with a shorter-range α-particle, the computed range of this particle is such that it should have been found. This difficulty caused Professor Oppenheimer to suggest that the radiation might be much harder, the phenomenon of pair production accounting for the large absorption.

Following this suggestion, the absorption in some other materials was determined. The coefficients were found to be 0.073 in Al, 0.27 in Cu, and 0.24 in Sn. When the corresponding absorptions per electron were plotted against Z (lower curve in Fig. 2) a very sloping line was found, as is to be expected from a large pair-production effect. The intercept at $Z=0$, giving the Compton part of the absorption, leads to an energy of 5.4 m.e.v. At that time (in May) there were no good published values of the pair-production at this energy, but the calculation was made by Oppenheimer and Furry. Their values for 5 and 6 m.e.v. give the fine lines shown on Fig. 2. The experimental values fit extremely well, confirming

[4] Lauritsen and Crane, Phys. Rev. **45**, 63 (1934).
[5] Lauritsen and Crane, Phys. Rev. **45**, 493 (1934).
[6] Henderson, Livingston and Lawrence, Phys. Rev. **46**, 38 (1934).

the theory at an energy twice as high as had been investigated before by absorption (Th C″ γ-ray). The linearity with Z shows that the deviations from the law given by the approximate theory are not important, even at high atomic numbers. The observed excess absorption per electron in lead is 1.03×10^{-25}; Oppenheimer and Furry give, for 5.4 m.e.v., 1.10×10^{-25}. Bethe and Heitler give a somewhat lower value, 0.96×10^{-25}. The disagreement between the calculated values arises from the use of different modes of numerical approximation; the observed value fits well within the errors of the experiment and the computations.[7] The measured intensity of this radiation corresponds to a yield of 130 quanta per 10^9 protons.

Origin of the Fluorine Radiation

The disintegration of fluorine by protons has been carefully studied by Henderson, Livingston and Lawrence.[6] They observe the emission of 6.7 cm α-particles corresponding to the reaction

$$^1H+{}^{19}F\rightarrow{}^{16}O+{}^4He+8.1 \text{ m.e.v.}$$

The number of these particles at 1.15 m.e.v. bombarding energy is 10 per 10^9 protons. It is apparent that the γ-rays cannot be associated with the 6.7 cm α-particles, because of the large difference in yield and because such an assumption would lead to an impossibly large value for the mass of fluorine. But we can suppose that another process occurs, in which a short range α-particle is emitted and the resulting ^{16}O nucleus is left in an excited state, emitting the γ-quantum on returning to its normal state.[8] The range of the α-particle is too short for it to have been observed by H., L. and L.

Another support for this mechanism is given by a study of the excitation curve of the γ-rays. Gamow's theory of nuclear disintegration by the penetration of potential barriers predicts that the form of this curve will depend on the energy of the emitted α-particle, being steeper for the process giving the short range particle. Reducing the energy of the incident protons by placing foils in the beam, the curve shown in Fig. 4 (open circles) was obtained. On the same diagram is plotted the yield of long range α-particles (from H., L. and L.) multiplied by 13, and also the yield predicted by Gamow's theory (using the equation given by H., L. and L.) for the short range α particles multiplied by an arbitrary constant. The fit with the theoretical curve is not precise, but the deviation from the long range α-particle curve is clearly shown, and is in the right direction.

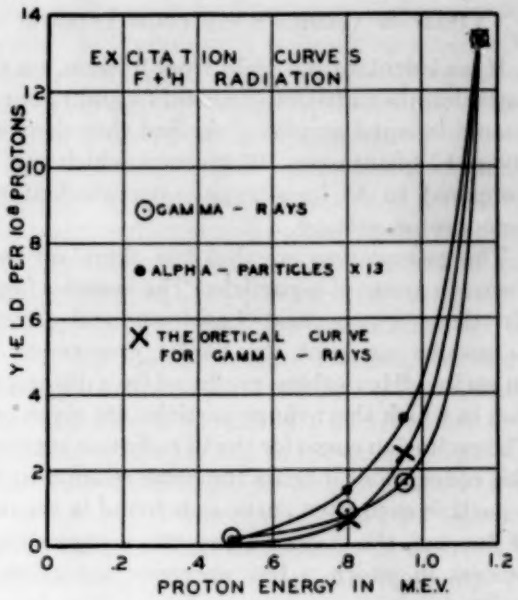

FIG. 4. Excitation curves of the radiations from fluorine bombarded by protons. The theoretical curve is from Gamow's formula.

Search for a Resonance Absorption in Oxygen

Since the fluorine γ-ray most probably arises from an excited level in ^{16}O, one might hope to find a resonance scattering of this radiation by oxygen. Such an effect was looked for, using a water absorber; it was not found, and one can conclude that the nuclear cross-section for this process is not more than 10^{-25} cm^2.

---

[7] Crane, Delsasso, Fowler and Lauritsen (Phys. Rev. **46**, 531 (1934)) have recently made cloud chamber observations of the curvature in a magnetic field of the secondary electrons produced by this radiation, finding its energy to be 5.4 m.e.v. and also showing that it produces a large number of positive electrons in lead, and has the predicted absorption in lead and copper. In the same letter they report that the radiation from Li bombarded with protons consists of 4 and 12 m.e.v. quanta in about equal numbers.

[8] It is interesting to note that the very similar nucleus ^{12}C also has an excited level at about 5 m.e.v., as reported by Becker and Bothe, Zeits. f. Physik **76**, 421 (1932).

Yield of Gamma-Rays from Lithium

If we calculate the yield from lithium, on the basis that the radiation consists of 4 and 12 m.e.v. quanta in equal numbers,[7] we find that there are about 12 quanta per 10^9 protons, which can be compared to 53 long-range α-particles[9] at the same proton voltage.

The gamma-rays are thus less abundant than the main group of α-particles. The energies found for these γ-rays lead Lauritsen and Crane[8] to ascribe at least the harder component to an excited ^{4}He nucleus, produced by a disintegration in which short-range particles are given out. The excitation curve for the Li radiation supports this conception; it bears the same relation to the α-particle excitation curve as is found in the case of fluorine, the steeper γ-ray curve suggesting a process in which a less energetic α-particle is emitted.

Results with Deuton Bombardment

The beam of about 1/2 microampere of deutons had an energy of 2.3 m.e.v., twice that of the protons which were accelerated as molecular ions in the same magnetic field. The effects observed were enormously larger than those with protons, but the background radiation from the accelerating apparatus was larger in comparison with the target effects. This made it difficult to get good absorption curves over a large range of intensities, since the background is only slightly weakened by the absorbers. Carbon contamination from the oil vapor vacuum pumps, deposited throughout the interior of the apparatus where it is hit by stray deutons, probably accounts for the background.

The ionizations observed, in terms of divisions per hundred seconds for 1 microampere deuton current, were:

Background (Pt target or no target)			48
Targets with background subtracted:			
$Ca(OH)_2$	17	B_2O_3	90
Al	23	LiOH	120
Mg	30	C	120
Si	30	Be	290
CaF_2	36		

The effects from the first five targets are small in comparison with the background, and may arise from carbon contamination on the target surfaces, but it is probable that they are real, with the exception of that from $Ca(OH)_2$. When a paraffin lining was put into the chamber, the ionization from the background, $Ca(OH)_2$, Al, Mg, Si, and C was reduced to about 1/2, indicating a preponderance of γ-radiation; that from LiOH was doubled, showing that here neutrons are the chief component of the radiation; and for Be and B_2O_3 the ratios paraffin/Pb were 0.9 and 0.8, showing a mixture of γ-rays and neutrons.

Lauritsen and Crane have reported γ-rays from C,[10] neutrons alone from Li,[11] and γ-rays and neutrons in equal numbers from Be[12] and B.[13] It is known that carbon also gives some neutrons as is in fact indicated by the absorption measurements discussed later, but they are not present in sufficient number to be shown by the rough criterion afforded by the relative ionizations in the lead and paraffin chambers.

Study of the Carbon Radiation

Because of the large background, it was impossible to obtain absorption data of high precision for this radiation, and the interpretation of the data is rendered difficult by the presence of neutrons. The absorption curve in lead is linear over a factor of five, and then flattens out slightly; when the curve was taken using a paraffin lining in the ionization chamber the flattening occurred with a smaller thickness of absorber, which may be an indication of the occurrence of neutrons. The values found for the initial absorption coefficients, using the lead chamber, were:

H_2O, 0.041 cm^{-1}; Al, 0.07; Cu, 0.22; Sn, 0.21; Pb, 0.39 cm^{-1}.

These are converted to absorptions per electron and plotted against atomic numbers in Fig. 5, curve marked O. The curves marked 0.1 and 0.2 were obtained by correcting for a supposed admixture of 10 and 20 percent of neutrons, which were assumed to be absorbed according to the results of Dunning.[14] It is seen that none of these curves fits well with any of the theoretical lines.

[8] Lauritsen and Crane, Phys. Rev. **46**, 537 (1934).
[9] Henderson, Phys. Rev. **43**, 98 (1933).
[10] Lauritsen and Crane, Phys. Rev. **45**, 345 (1934).
[11] Lauritsen and Crane, Phys. Rev. **45**, 550 (1934).
[12] Crane and Lauritsen, Phys. Rev. **45**, 226 (1934).
[13] Lauritsen and Crane, Phys. Rev. **45**, 493 (1934).
[14] Dunning, Phys. Rev. **45**, 586 (1934).

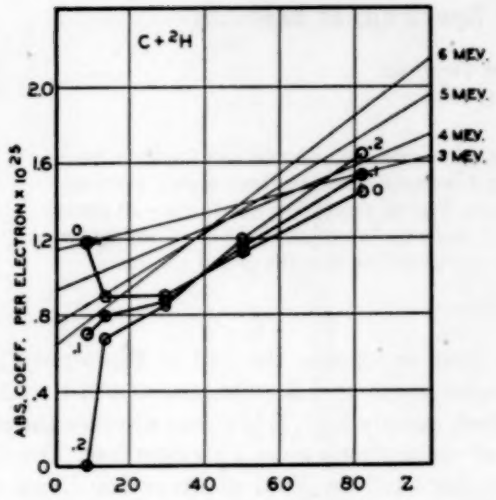

FIG. 5. The curve marked 0 shows the absorption coefficients in various materials of the radiation from carbon bombarded by deutons. The curves marked 0.1 and 0.2 are the γ-ray absorption values obtained after correcting for the presence of 10 and 20 percent of neutron ionization.

The nearest approach to a straight line is given by the assumption that 10 percent of the ionization is caused by neutrons; then the absorption in lead (this value is experimentally more trustworthy than the others) corresponds to an energy of 3 m.e.v. for the γ-ray, the slope of the line to 5 m.e.v., and the intercept to 6 m.e.v. Considering the doubtful applicability of Dunning's neutron absorption values in this case, the above analysis of the data cannot be given much weight, and the apparent discrepancies must not be taken as evidence against the validity of the γ-ray absorption theory.

The probable nuclear reactions when deutons strike carbon are:

$$^2H+^{12}C\rightarrow{}^{13}C+{}^1H+5.1 \text{ m.e.v.}, \quad (1)$$

$$^2H+^{12}C\rightarrow{}^{13}N+n\rightarrow{}^{13}C+e^+ +n+4.8 \text{ m.e.v.} \quad (2)$$

The reaction energies are calculated from the masses, 1.007 being used for the neutron mass. Lauritsen and Crane[10] have pointed out that a γ-ray of 3.1 m.e.v. must accompany the 18 cm protons observed by Lawrence, Livingston and Lewis,[15] and presumably arising from process (1), in order to secure an energy balance. If we assume that these are the γ-rays observed, the yield is 18 quanta per 10^6 incident deutons.

The second reaction involves a radioactive substance with a ten-minute decay period.[16, 17] The positive electrons given out during the decay are "annihilated" with the production of two quanta of 0.51 m.e.v. γ-radiation for each positive electron, and this radiation was studied by observing the ionization after stopping bombardment of a carbon target. Its intensity immediately after exposure to a beam of 1 microampere for a time long in comparison to the decay period was found to be 0.5 division per second, corresponding to 10 quanta, or 5 activations, per 10^6 deutons. (This radiation was not present in appreciable amount when the radiation accompanying the bombardment was studied, since the exposures were too short to obtain good activation.)

It was possible to make very good measurements of the absorption of the annihilation radiation. The radioactive background effect from carbon contamination in the apparatus was small (about 1/100 of the total ionization), stray soft rays being largely excluded by the walls of the ionization chamber.

An accurately logarithmic absorption in lead over a factor of 100 was found; the absorption coefficient was 1.72 cm^{-1}. That calculated for 0.51 m.e.v. γ-rays is 1.70.

In conclusion, the author wishes to thank Professor Lawrence and Professor Oppenheimer for their assistance and advice in this work, and Commander T. Lucci for his help in taking the measurements. The financial support of the Research Corporation and the Chemical Foundation is acknowledged with great appreciation.

[15] Lawrence, Livingston and Lewis, Phys. Rev. **44**, 56 (1933).
[16] Henderson, Livingston and Lawrence, Phys. Rev. **45**, 428 (1934).
[17] Crane and Lauritsen, Phys. Rev. **45**, 430 (1934).

High Series Terms in the Arc Spectrum of Mercury

I. WALERSTEIN, *Purdue University*

(Received August 1, 1934)

The spectrum of luminous mercury vapor drawn into a low pressure chamber was found to have the series lines developed to high members. Wave-length measurements of these higher members in the singlet and triplet diffuse and sharp series were made. The $^3S_1$ terms developed to $m=20$ show that this series follows a Ritz formula accurately. The $^1S_0$ series and especially the ^{1} and ^3D series also follow a Ritz formula with definite indications of slight perturbations near the end of the series.

ON the basis of the perturbation theory of wave mechanics R. M. Langer[1] deduced an equation to represent the series of optical terms for atoms containing more than one optical electron. The equation of the form

$$\nu_n = R/[n+\sum_0^\infty p_{in}/(\nu_i-\nu_n)]^2 = R(n^*)^2, \quad (1)$$

where p_{in} is a function of the probability of transition between ν_n and the observable spectroscopic terms ν_i, reduces to a simple Ritz formula

$$\nu_n = R/(n+\mu+\alpha\nu_n)^2 = R/(n^*)^2, \quad (2)$$

when the effect of the perturbing ν_i terms becomes negligible.

For cases where the atom has two optical electrons, an electron configuration may arise which does not belong to the particular series considered, but which has an energy value nearly equivalent with one of the terms of the series. In that case a perturbation effect will be observed and the equation for the terms will be given by

$$\nu_n = R/(n+\mu+\alpha\nu_n+\beta/(\nu_i-\nu_n))^2 = R/(n^*)^2. \quad (3)$$

Such an equation has been used by Shenstone and Russell[2] for the study of the series in Ca I, Ba I, Al II, Cu I and Hg I. In the last named element the $^1P_1^0$ series is perturbed by a term around 5368 and can fairly well be represented by the last equation. The $^3P^0$ terms also show some perturbation especially in the case of $^3P_2^0$. The authors leave open the question as to whether the ^3S and ^3D series of Hg I will fit a simple Ritz formula or whether these are affected by some term near the end of the series. The simplest method of determining whether a series follows exactly Eq. (2) is to see whether the plot of n^*-n against ν gives a straight line. This line can also yield the limit of the series. Using the values of the wave-lengths of the ^3S and ^3D series measured by Dingle[3] and Buisson[4] and the values of the limits of these series as given by Fowler,[5] Shenstone and Russell find that the plot of the ^3S and ^3D terms departs from a straight line near the end of the series. Such a departure may sometimes not be indicative of a true perturbation, but rather of inaccuracies either in the limit assignment or in the measurements of the higher members of the series. The term values of these higher members are below 500 cm^{-1} and the value of n^*-n is changed by about 0.015 for an error of 1 cm^{-1}. Some attempts to change the value of the limit were made by the author with slight success. However, it was felt that the measurement of the wave-lengths of the lines which was dependent on a comparison spectrum of iron placed below the spectrum of mercury may be slightly in error. In the region of 2500A an error of 0.06A introduces an error of 1 cm^{-1} in the term value.

At the suggestion of Professor Shenstone, I undertook to extend the ^3S and ^3D series to still higher members and to improve the accuracy of the measured wave-lengths.

APPARATUS

It was shown by Lord Rayleigh[6] that the higher members of the diffuse series of mercury are broadened by the Stark effect produced on

[1] R. M. Langer, Phys. Rev. **35**, 649 (1930).
[2] A. G. Shenstone and H. N. Russell, Phys. Rev. **39**, 415 (1932).
[3] H. Dingle, Proc. Roy. Soc. **A100**, 167 (1921).
[4] H. Buisson, C. R. **178**, 1270 (1924).
[5] A. Fowler, *Report on Series in Line Spectra*, 1922.
[6] Rayleigh, Proc. Roy. Soc. **A112**, 14 (1926).

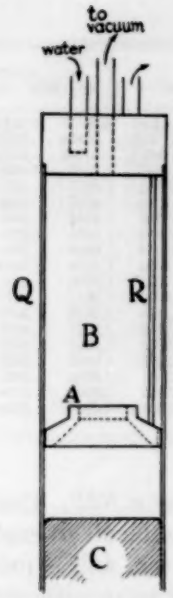

FIG. 1. Diagram of apparatus.

the excited atoms by the electric fields of neighboring ions. This broadening makes it difficult to see many members of the series in the light from an ordinary arc, and only by leading the luminous vapor into a more highly evacuated field free space are the higher series members observable.

The apparatus used (shown in Fig. 1) makes use of this fact. A quartz tube Q was sealed at the top by a water-cooled steel plug which was attached with picein. A steel rod R, 10 cm long, was attached to the rod and carried at its lower end the steel anode A. This anode fitting closely to the quartz tube had a conical hollow below and a slit 1.5 cm long, 3 mm wide and 4 mm deep. Liquid mercury collecting over the anode could flow down through a groove cut in its edge. The cathode was a column of mercury C, whose level was a few cm below the anode and was held in place by barometric pressure. Luminous vapor from the mercury arc between A and C diffused through the slit in A into the low pressure chamber which was connected to a Cenco pump attached to the tube in the plug. In this region the luminous vapor showed the series line of the arc spectrum developed to very high members. The P. D. across the arc was about 30 volts and the current used about 10–12 amp. The light from the luminous vapor which formed a vertical column about 5 mm wide and 2 cm deep was examined with a Hilger E 1 quartz spectrograph. The slit of the spectrograph was about 6 inches from the edge of the column and the light from the full depth of the column at its lower end was utilized. The angle subtended at the slit by the source was large enough to fill the collimating lens completely with light. Photographs were taken on Eastman Process Plates and exposures lasted 15 to 30 hours. A check was kept on the temperature of the room and only those plates were used which were taken during a period of comparative constancy of the barometric pressure, a precaution necessary for long exposures. Plates sensitized with Eastman ultraviolet sensitizer were sometimes used in the region of 2200A but it was found that although they intensified many of the strong lines they were not an improvement over the Process plates for the weak members at the end of the series.

The determination of wave-lengths from a comparison spectrum placed alongside the observed one has received some critical consideration lately. The moving of a Hartman diaphragm over the slit of a spectrograph has been known at times to produce a shift of the lines. Moreover it would be difficult to place an iron arc exactly in the position which the mercury vapor occupied and any displacement from this position causes a shift of the lines as was brought out by Stockbarger and Burns.[7] It was therefore attempted to introduce at least some of the comparison lines into the luminous column itself. Attempts to get iron lines were made by spraying colloidal iron into the beam or arc and by using an electrolytically prepared mercury-iron amalgam as cathode but although in the arc itself the iron spectrum was fully developed none of the iron lines were present in the light of the luminous vapor in B. Greater success was attained with copper. A copper mercury amalgam was floated on top of the mercury column and almost all the lines of the arc spectrum of copper were registered in the light from the vapor column in the time required to bring out the higher series members in the mercury spectrum. (In the space between A and C both the arc and spark lines of copper appeared.) A diaphragm was placed in front of the spectroscope slit. It was mounted on a

[7] D. C. Stockbarger and L. Burns, J. Opt. Soc. 23, 379 (1933).

TABLE I.

m	$2^3P_2^0-m^3S_1$ λ	ν	m^3S_1	$2^3P_1^0-m^3S_1$ λ	ν	m^3S_1	$2^3P_0^0-m^3S_1$ λ	ν	m^3S_1	Ave. m^3S_1	n^*-n	$\alpha\nu$	$\mu-\alpha\nu=(n^*-n)_{calc.}$	$\nu_{calc.}$	$\nu_{obs.}-\nu_{calc.}$
2	5460.740 C	18307.5	21833.6	4358.342 C	22938.1	21833.6	4046.563 C	24705.4	21833.6	21833.6	0.24189	0.06030	0.24432	21783.9	49.7
3	3341.478 C	29918.3	10222.8	2893.596 C	34548.9	10222.8	2752.775 C	36316.2	10222.8	10222.8	.27636	.02824	.27639	10222.6	.2
4	2925.406 C	34173.4	5967.7	2576.290 C	38803.9	5967.8	2464.059 C	40571.2	5967.8	5967.8	.28814	.01648	.28814	5967.8	0
5	2759.704 C	36225.3	3915.8	2446.899 C	40855.7	3916.0	2345.43	42623.0	3916.0	3915.9	.2937	.0108	.2938	3915.7	.2
6	2674.99 S	37372.5	2768.6	2380.08	42003.6	2768.1	2283.91	43771.1	2767.9	2768.2	.2961	.0077	.2970	2767.4	.8
7	2625.24 S	38080.7	2060.4	2340.55	42711.9	2059.8	2247.56	44478.8	2060.2	2060.1	.2982	.0057	.2989	2059.7	.4
8	2593.41 S	38548.0	1593.1	2315.21	43179.3	1592.4	2224.19	44946.2	1592.8	1592.8	.3003	.0044	.3002	1592.8	0
9	2571.76	38872.2	1268.9	2297.97	43503.3	1268.4	2208.24	45270.8	1268.2	1268.5	.3010	.0035	.3011	1268.5	0
10	2556.35	39106.3	1034.8	2285.66	43737.6	1034.1	2196.86	45505.2	1033.8	1034.2	.3010	.0029	.3018	1034.0	.2
11	2544.94	39281.8	859.3	2276.54	43912.7	859.0	2188.46	45679.9	859.1	859.1	.3020	.0024	.3023	859.0	.1
12				2269.61	44046.8	724.9	2182.06 *	45813.8	725.2	725.1	.3021	.0020	.3026	725.0	.1
13	2539.53	39521.1	618.0	2264.21	44151.8	619.9	2177.08 *	45918.6	620.4	620.1	.3029	.0017	.3029	620.1	0
14	2534.20	39604.5	536.6	2259.93	44235.5	536.2	2173.05 *	46003.8	535.2	536 2	.3059	.0015	.3031	536.4	− .2
15	2519.91	39672.1	469.0	2256.46 *	44303.4	468.3				468.7	.3013	.0013	.3033	468.6	.1
16	2516.37	39727.9	413.2	2253.62 *	44359.3	412.4				412.8	.3055	.0011	.3035	412.8	0
17	2513.43 *	39774.2	366.9	2251.27 *	44405.6	366.1				366.5	.3038	.0010	.3036	366.5	0
18	2510.97 *	39813.3	327.8	2249.28 *	44444.9	326.8				327.5	.3051	.0009	.3037	327.5	0
19	2508.86 *	39846.7	294.4							294.4	.3066	.0008	.3038	294.5	− .1
20	2507.08 *	39875.0	266.1							266.1	.3074	.0007	.3039	266.2	− .1

separate support and was not in contact with the slit. In this manner the mercury and copper spectra were exposed to the whole slit except for a narrow strip across the middle. Over this region a subsequent exposure was taken of the light from an arc using an iron anode and copper cathode. This arc was aligned as accurately as possible.

Measurements of the wave-lengths were carried out by using an interpolation formula with the constants and corrections determined from Burns' values of the wave numbers of the copper lines, and by using a linear interpolation between iron lines. Any shift between the mercury and iron lines could be determined by observing the position of the copper lines appearing in the two spectra. The wave-lengths so obtained are probably correct to within 0.01 or 0.02A for lines at 2500A or lower. The accuracy is not as high for the series around 3400A where the dispersion is less.

RESULTS

To determine the term values of the states $6sms^3S$ the three sharp series were measured and the average of the term values was obtained. The wave-lengths and wave numbers of the lines are given in Table I.

The term values can be calculated by subtracting from the limits $2^3P_2^0$, $2^3P_1^0$ and $2^3P_0^0$. If one uses the limits given by Fowler and calculates from a Rydberg table the value of n^*-n for each of the terms one obtains the curve A for the plot of n^*-n against ν which reaches a value of 0.415 for the term 20^3S_1. This departure from a straight line is difficult to explain on the basis of a perturbing term and is more probably due to an error in the value assigned to the limit. It was found that if the values of $2^3P^0_{0,1,2}$ were increased by 2.8 cm^{-1} the plot for the $^3S_1$ terms is a straight line with variations no greater than the experimental error except for the first term. The same effect was found for the diffuse series. If Fowler's value of $2^3P_2^0$ were used the values of n^*-n rose from -0.047 at 6^3D_3 to $+0.23$ at 26^3D_3, whereas if the limit was increased by 2.8 the terms more nearly followed a Ritz formula.

In the following tables therefore the values of the 2^3P^0 terms are set at

$$2^3P_2^0=40141.1,\ 2^3P_1^0=44771.7,\ 2^3P_0^0=46539.0.$$

Table I contains the terms m^3S_1 calculated from these limits. In column 11 is given the values of n^*-n obtained from a Rydberg table prepared by Miss J. MacInnes at Princeton. The next three columns are steps used in calculating the term value that would exactly fit a Ritz formula taken for two of the terms. The values of the slope of the line α and the intercept μ were calculated for the best straight line through the plotted points. The last column gives the difference between the observed and calculated term values.

The wave-lengths of the first few lines in each series are taken from Cardaun's[8] or Stiles'[9] measurements and are marked C or S. The other lines

[8] L. Cardaun, Zeits. f. Wiss. Phot. **14**, 56, 89 (1914).
[9] H. Stiles, Astrophys. J. **30**, 48 (1909).

TABLE II.

m	$2^3P_2^0-m^3D_1$ λ	ν	m^3D_1	$2^3P_1^0-m^3D_1$ λ	ν	m^3D_1	$2^3P_0^0-m^3D_1$ λ	ν	m^3D_1	Ave. m^3D_1	Calc. m^3D_1	$\nu_{obs.}-\nu_{calc.}$
3	3662.878 C	27293.2	12847.9	3131.546 C	31923.9	12847.8	2967.278 C	33691.1	12847.9	12847.9	12837.9	10.0
4	3025.617 S	33041.5	7099.6	2653.681 C	37672.3	7099.4	2534.771 C	39439.4	7099.6	7099.5	7099.1	.4
5	2805.33	35636.0	4505.1	2482.721 C	40266.2	4505.5	2378.31	42033.8	4505.2	4505.3	4505.3	0
6	2699.81 *	37028.7	3112.4	2399.76	41658.2	3113.5	2302.06	43426.0	3113.0	3113.1	3113.0	.1
7	2640.65 *	37858.2	2282.9	2352.65 *	42492.2	2279.5	2258.71	44259.4	2279.6	2279.6	2279.4	.2
8	2603.42 *	38399.6	1741.5	2323.21 *	43030.6	1741.1	2231.55	44797.9	1741.1	1741.1	1741.1	0
9							2213.36	45166.1	1372.9	1372.9	1373.1	− .2
10							2200.58	45428.3	1110.7	1110.7	1110.7	0
11							2191.25	45621.8	917.2	917.2	916.9	.4
12							2184.21	45768.8	770.2	770.2	769.7	.5
13							2178.75	45883.4	655.6	655.6	655.3	.3
14							2174.49	45973.4	565.6	565.6	564.7	.9
15							2170.98 *	46047.6	491.4	491.4	491.6	− .2
16							2168.12 *	46108.4	430.6	430.6	431.8	− 1.2
17							2165.80 *	46157.8	381.2	381.2	381.9	− .7
18							2163.87 *	46198.9	340.1	340.1	340.9	− .6
19							2162.23 *	46234.0	305.0	305.0	305.9	− .9

TABLE III.

m	$2^3P_2^0-m^3D_2$ λ	ν	m^3D_2	$2^3P_1^0-m^3D_2$ λ	ν	m^3D_2	$2^1P_1-m^3D_2$ λ	ν	m^3D_2	Ave. m^3D_2	Calc. m^3D_2	$\nu_{obs.}-\nu_{calc.}$
3	3654.833 C	27353.3	12787.8	3125.663 C	31984.0	12787.7	5769.60 C	17327.4	12787.8	12787.8	12772.8	15.0
4	3023.470 C	33065.0	7076.1	2652.042 C	37695.6	7076.1	4339.233 C	23039.1	7076.1	7076.1	7075.4	.7
5	2804.44	35647.2	4493.9	2482.008 C	40277.8	4493.9	3901.899 C	25621.4	4493.8	4493.9	4493.9	0
6	2699.36	37035.0	3106.1	2399.35	41665.3	3106.4	3701.46	27008.7	3106.5	3106.3	3106.7	− .4
7	2640.15 *	37865.5	2275.6	2352.41	42496.5	2275.2	3591.01	27839.4	2275.8	2275.4	2275.4	0
8	2603.20 *	38402.9	1738.2	2323.03	43033.9	1737.8	3523.02	28376.6	1738.6	1738.2	1738.3	− .1
9	2578.59 *	38769.3	1371.8	2303.43	43400.1	1371.6	3478.04	28743.7	1371.5	1371.6	1371.3	.3
10	2561.33 *	39030.6	1110.5	2289.62	43661.9	1109.8	3446.64 *	29005.5	1109.7	1109.9	1109.3	.6
11				2279.51	43855.5	916.2				916.2	915.7	.5
12				2271.90	44002.4	769.3				769.3	768.9	.4
13				2266.02	44116.5	655.2				655.2	654.7	.5
14				2261.36	44207.5	564.2				564.2	564.2	0
15				2257.63 *	44280.4	491.3				491.3	491.2	.1
16				2254.59 *	44340.2	431.5				431.5	431.5	0
17				2252.05 *	44390.2	381.5				381.5	382.1	− .6
18				2249.94 *	44431.9	339.8				339.8	340.7	− .9
19				2248.16 *	44466.9	304.8				304.8	305.7	− .9
20				2246.62 *	44497.4	274.3				274.3	275.8	− 1.5
21				2245.35 *	44522.6	249.1				249.1	250.1	− 1.0
22				2244.28 *	44543.8	227.9				227.9	227.8	.1
23				2243.29 *	44563.6	208.1				208.1	208.4	− .3

are newly measured and those marked with an asterisk have not previously been reported in the literature.

The plot of the weighted average of the term values of the $^3S_1$ series against their values of n^*-n is shown in the graph. The points are on a straight line showing that the series follows a Ritz formula within the limits of the experimental error. This Ritz equation for the $^3S_1$ terms is

$$\nu = R/[n+0.3046-2.762\times10^{-6}\nu]^2$$

and as is often found the residual $\nu_{obs.}-\nu_{calc.}$ is large for the first term.

The measurements of the diffuse series cannot be carried out with as great an accuracy as the sharp series due to the diffuse character of the higher series lines.

The $^3D_1$ series was determined to $m=19$ from the $2^3P_0^0-m^3D_1$ lines although some of the first few terms were also obtained from the lines in the $2^3P_1^0-m^3D_1$ and the $2^3P_2^0-m^3D_1$ series. Table II gives the wave-lengths, wave numbers and term values for the $^3D_1$ series. The last two columns give the calculated values on the basis of a Ritz formula and the difference between the observed and calculated term values. The constants of the Ritz equation $\nu=R/(n+\mu+\alpha\nu)^2$ were $\mu=-0.0585$ and $\alpha=-1.390\times10^{-6}$.

The $^3D_2$ series has been extended by nine new terms to $m=23$. The terms up to $m=10$ were determined also with the aid of $2^3P_2^0-m^3D_2$ lines and measurement of the $2^1P_1-m^3D_2$ series, the 2^1P_1 term being also corrected by 2.8 cm^{-1} and set at 30,115.2 cm^{-1}. These are given in Table III and the constants used for the cal-

TABLE IV.

m	$2^3P_2^0-m^3D_3$ λ	ν	m^3D_3	Calc. m^3D_3	$\nu_{obs.}-\nu_{calc.}$
3	3650.146 C	27388.4	12752.7	12744.6	8.1
4	3021.499 C	33086.5	7054.6	7054.6	0
5	2803.48	35659.5	4481.6	4481.5	.1
6	2698.83	37042.2	3098.9	3098.9	0
7	2639.80	37870.4	2270.7	2270.4	.3
8	2602.97	38406.2	1734.9	1735.3	− .4
9	2578.39	38772.3	1368.8	1368.8	0
10	2561.15	39033.3	1107.8	1107.4	.4
11	2548.53	39226.6	914.5	914.3	.2
12	2539.07	39372.7	768.4	767.8	− .4
13	2531.72	39486.9	654.2	654.8	− .6
14	2525.94	39577.3	563.8	563.5	.3
15	2521.27	39650.6	490.5	490.7	− .2
16	2517.49	39710.1	431.0	431.1	− .1
17	2514.37	39759.4	381.7	381.7	0
18	2511.76	39800.6	340.5	340.4	.1
19	2509.54	39836.0	305.1	305.4	− .3
20	2507.64	39866.2	274.9	275.6	− .7
21	2506.08	39890.9	250.2	249.9	.3
22	2504.71 *	39912.7	228.4	227.7	.7
23	2503.46 *	39932.6	208.5	208.3	.2
24	2502.35 *	39950.4	190.7	191.2	− .5
25	2501.47 *	39964.4	176.7	176.2	.5
26	2500.57 *	39978.8	162.3	162.9	− .6

culated term value are $\mu=-0.0529$ and $\alpha=-1.247\times10^{-6}$.

Table IV gives the series m^3D_3 to $m=26$, the constants of the Ritz equation being $\mu=-0.0440$ and $\alpha=-1.695\times10^{-6}$.

The plots of the term values against n^*-n for the $^3D_{1,\,2,\,3}$ series are shown in Fig. 2. The points for the high terms are seen to fall off the straight line representing the Ritz equation more often than in the case of $^3S_1$ series. The decreased accuracy in the wave-lengths of the diffuse lines is not sufficient, however, to account for these deviations. At about 800 cm^{-1} there is a dip in the curve with a subsequent rise at about 500 cm^{-1}. The reality of these small deviations is confirmed by the fact that the separate series are calculated from lines in quite different parts of the spectrum. The deviations are small and they occur in each of the component ^3D series at about the same place. There is no obvious cause for such a perturbation.

Measurements were also carried out on the $2^1P_1-m^1S_0$ and the $2^3P_1^0-m^1S_0$ series. The wave-lengths, wave numbers and term values are collected in Table V which also contains the calculated term values on the basis of a Ritz formula. The small difference between observed and

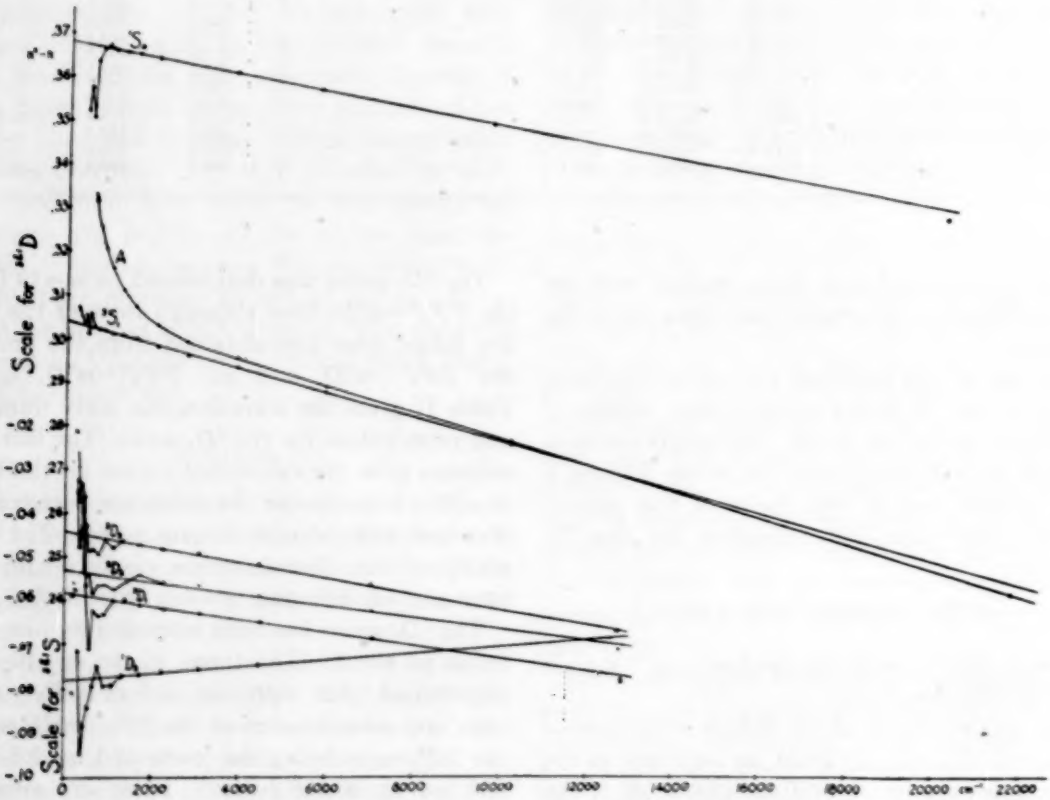

FIG. 2. Plot of n^*-n for the terms of the S and D series.

TABLE V.

m	$2^1P_1-m^1S_0$ λ	ν	m^1S_0	$2^3P_1^0-m^1S_0$ λ	ν	m^1S_0	Ave. m^1S_0	Calc. m^1S_0	$\nu_{obs.}-\nu_{calc.}$
2	10139.75	9859.5	20255.7	4077.828 C	24516.0	20255.7	20255.7	20201.4	54.3
3	4916.036 C	20335.9	9779.3	2856.938 C	34992.3	9779.4	9779.3	9778.8	.5
4	4108.082 C	24335.4	5779.8	2563.88	38991.8	5779.9	5779.8	5779.8	0
5	3801.665 S	26296.8	3818.4	2441.10	40952.6	3819.1	3819.1	3819.5	− .4
6				2376.77 *	42061.0	2710.7	2710.7	2710.3	.4
7	3558.73 *	28091.9	2023.3	2338.55 *	42748.5	2023.2	2023.3	2023.3	0
8	3502.00 *	28547.0	1568.2	2313.88 *	43204.1	1567.6	1567.9	1568.2	− .3
9	3463.52 *	28864.1	1251.1	2297.03 *	43521.0	1250.7	1250.9	1250.9	0
10	3436.15 *	29094.0	1021.2				1021.2	1021.2	0
11	3415.98 *	29265.9	849.3				849.3	849.3	0
12	3400.68 *	29397.5	717.7				717.7	717.7	0
13	3388.78 *	29500.7	614.5				614.5	614.2	.3
14	3379.44 *	29582.3	532.9				532.9	531.6	1.3
15	3371.73 *	29649.9	465.3				465.3	464.7	.6
16	3365.49 *	29704.8	410.4				410.4	409.7	.7

TABLE VI.

m	$2^1P_1-m^1D_2$ λ	ν	m^1D_2	$2^3P_2^0-m^1D_2$ λ	ν	m^1D_2	$2^3P_1^0-m^1D_2$ λ	ν	m^1D_2	Ave. m^1D_2	Calc. m^1D_2	$\nu_{obs.}-\nu_{calc.}$
3	5790.66 C	17264.4	12850.8	3663.276 C	27290.2	12850.9	3131.837 C	31920.9	12850.8	12850.8	12763.8	87.0
4	4347.500 C	22995.3	7119.9	3027.483 C	33021.2	7119.9	2655.127 C	37651.8	7119.9	7119.9	7114.0	5.9
5	3906.399 C	25591.9	4523.3	2806.74	35618.0	4523.1	2483.829 C	40248.4	4523.3	4523.2	4523.2	0
6	3704.217 C	26988.6	3126.6	2700.80	37015.1	3126.0	2400.51	41645.1	3126.6	3126.4	3126.5	− .1
7	3592.74	27826.0	2289.2	2641.08	37852.0	2289.1	2353.18 *	42482.7	2289.0	2289.1	2289.1	0
8	3524.27	28366.6	1748.6	2603.82	38393.7	1747.4	2323.56 *	43024.1	1747.6	1747.9	1747.9	0
9	3478.91	28736.4	1378.8	2579.01	38763.0	1378.1	2303.78 *	43393.6	1378.1	1378.3	1378.3	0
10	3447.27	29000.1	1115.1	2561.61 *	39026.3	1114.8	2289.88 *	43656.9	1114.8	1114.9	1114.4	.5
11	3424.26 *	29195.0	920.2							920.2	919.8	.4
12	3406.99 *	29343.0	772.2							772.2	772.0	.2
13	3393.71 *	29457.8	657.4							657.4	657.2	.2
14	3383.30 *	29548.5	566.7							566.7	566.1	.6
15	3374.93 *	29621.8	493.4							493.4	492.8	.6
16	3368.15 *	29681.4	433.8							433.8	432.9	.9
17	3362.71 *	29729.4	385.8							385.8	383.2	2.6
18	3357.69 *	29773.8	341.4							341.4	341.6	− .2

calculated values, as well as the plot shown in Fig. 2, indicates that the $^1S_0$ terms can well be represented by a Ritz formula. The constants are $\mu=0.3679$ and $\alpha=-1.835\times10^{-6}$.

The $^1D_2$ terms were obtained by measuring the $2^1P_1-m^1D_2$, $2^3P_2^0-m^1D_2$ and $2^3P_1^0-m^1D_2$ series. These are collected in Table VI. The attempt to fit these values to a Ritz equation again showed deviations of the order of those found in the ^3D series. The straight line through the $^1D_2$ terms has a positive slope and misses the first term by a considerable amount. It is difficult to put the line through the second term without getting the other points all off. The Ritz equation which best fits the set of terms has constants $\mu=0.9218$ and $\alpha=8.071\times10^{-7}$.

The list below contains a number of lines, not belonging to the sharp or diffuse series, which were measured in the course of the work. Some of these lines have not been identified and in every case the intensity of the line was weak.

2478.64	40332.5	$2^3P_1^0-5^3F_2^0$
2402.48	41610.9	
2401.19	41633.3	
2397.80	41692.1	$2^3P_1^0-6^3F_2^0$
2384.92	41917.4	
2380.72	41991.2	
2376.20	42071.2	
2375.29	42087.2	
2374.62	42099.2	$2^3P_0^0-5^3F_2^0$
2351.56	42512.0	$2^3P_1^0-7^3F_2^0$
2322.52	43043.5	$2^3P_1^0-8^3F_2^0$
2300.30	43459.2	$2^3P_0^0-6^3F_2^0$
2230.94	44810.2	$2^3P_0^0-8^3F_2^0$

It is a pleasure to acknowledge the constant interest shown in this work by Professor A. G. Shenstone who first suggested the investigation and who continued with his advice while the work was being done at Purdue University.

The Arc Spectrum of Selenium[1, 2]

J. E. RUEDY[3] AND R. C. GIBBS, *Cornell University*

(Received August 16, 1934)

The arc spectrum of selenium, as excited by means of a positive column discharge in helium, has been photographed over the wave-length range 300–11,000A. Four different grating spectrographs were used having dispersions of from 11 to 2.5A per mm. A total of 510 lines has been measured as belonging to the arc spectrum and of these 391 have been classified. Seven series built on the ^4S state of the ion have been carried to five or more members and the absolute term values are determined to within 0.2 cm^{-1}. All the $4p^4$, $4p^3(^2D)\,5s$, $4p^3(^2P)\,5s$, and $4p^3(^2D)\,5p$ terms have been located and also some of the $4p^3(^2D)\,4d$ terms. Perturbation effects are frequently evident and are illustrated by plots of the various series.

A HOLLOW cathode discharge tube, described in a recent paper,[4] was first used for the production of the selenium spectrum, but difficulty in maintaining the glow within the cathode when selenium vapor was condensing upon it (as was also previously experienced when using sulfur) made a different method of excitation desirable. A positive column tube with water cooled electrodes functioned more satisfactorily in nearly all respects. The discharge occurring in a tube of $\frac{3}{4}$ inch diameter and 1 foot length was photographed endwise, circulated helium being used to maintain the discharge. The selenium was vaporized as desired from a small side tube. By increasing the density of selenium vapor, spark lines were decreased in intensity while arc lines were increased, and if carried sufficiently far, strong bands were produced from 2600–6000A, with arc lines very prominent and spark lines almost absent. With the one known exception of mercury, all impurity lines were also decreased in intensity by this same procedure. In each spectral region two exposures were made on the same plate, one with a low and the other with a high density of selenium vapor. The tube was generally run at 0.8 ampere d.c. supplied by an a.c. rectifier set.

The region from 300–2550A was photographed with a 1.5 meter grating in a vacuum spectrograph giving a dispension of 11A per mm, from 2550–6550A with a 21-foot grating in a Wads. worth mounting giving a dispersion of 2.5 per mm, and from 6550–10,400A with a 7-foot grating in a Rowland mounting giving a dispersion of 8.3A per mm. Two lines were also observed at still longer wave-lengths using a Zeiss triple prism spectrograph which gave a dispersion of about 125A per mm in that region. Schumann plates were used for the vacuum wave-lengths and Eastman plates of suitable sensitizations over the rest of the range. The vacuum wave-lengths have a maximum error of 0.07A, which corresponds to about 3 cm^{-1}. The stronger lines from 1890–2420A were measured in the second order of the 21 foot grating and their accuracy is believed to be within 0.01A, which gives a wave number accuracy of about 0.2 cm^{-1} for some transitions involving the deepest terms. The wave-length accuracy from 2550 to 10,400A varies, but the wave number errors are always within 0.2 cm^{-1}.

Previous work has been done by several investigators[5, 6, 7, 8, 9] leading to a partial analysis of the selenium arc spectrum. The data, however, were quite incomplete and as shown by the present work some of the term assignments were incorrect. The more complete data yield 103 classified lines for the vacuum region and 288 for the longer wave-lengths. From these a total of 130 terms are established, of which 100 are new. All the stronger lines have been classified,

[1] This research was supported by a grant from the Heckscher Foundation for the Advancement of Research, established at Cornell University by August Heckscher.

[2] A report on the subject matter in this paper was read at a meeting of the American Physical Society, April, 1934. Phys. Rev. **45**, 747 (1934).

[3] Heckscher Research Assistant in Physics.

[4] J. E. Ruedy, Phys. Rev. **44**, 757 (1933).

[5] C. Runge and F. Paschen, Ann. d. Physik **61**, 641 (1897).

[6] J. C. McLennan, A. B. McLay and J. H. McLeod, Phil. Mag. **4**, 486 (1927).

[7] J. C. McLennan and M. F. Crawford, Nature **124**, 874 (1929).

[8] R. C. Gibbs and J. E. Ruedy, Phys. Rev. **40**, 204 (1932).

[9] K. R. Rao and S. G. T. Murti, Proc. Roy. Soc. **A145**, 681 (1934).

TABLE I. *Lines of Se I.*

Int.	λ(air)	ν(vac)	Transition
2	10652.7	9387.3	$(^3D)5s\ ^1D_2 - (^3D)5p\ ^1P_1$
1	10533.4	9493.6	$(^4S)4d\ ^3D_2 - (^3D)5p\ ^1P_1$
10	10386.28	9625.45	$(^4S)5s\ ^3S_1 - (^4S)5p\ ^3P_1$
12	10327.19	9680.52	$(^4S)5s\ ^3S_1 - (^4S)5p\ ^3P_2$
8	10307.39	9699.11	$(^4S)5s\ ^3S_1 - (^4S)5p\ ^3P_0$
6	10217.26	9784.68	$(^3D)5s\ ^1D_2 - (^3D)5p\ ^1F_3$
1	10132.40	9866.62	$(^4S)4d\ ^3D_3 - (^3D)5p\ ^3F_4$
2	10107.52	9890.91	$(^4S)4d\ ^3D_2 - (^3D)5p\ ^1F_3$
1	10086.45	9911.58	
4	9969.73	10027.62	$(^3D)5s\ ^3D_3 - (^3D)5p\ ^3D_1$
1	9938.09	10059.54	
6	9825.51	10174.80	$(^3D)5s\ ^3D_1 - (^3D)5p\ ^3D_1$
2	9816.63	10184.00	
1	9754.19	10249.20	$(^4S)4d\ ^3D_3 - (^4S)7f\ ^3F$
1	9716.00	10289.48	$(^4S)4d\ ^3D_1 - (^4S)7f\ ^3F$
1	9695.76	10310.96	$(^4S)4d\ ^3D_2 - (^4S)7f\ ^3F$
1	9603.34	10410.19	$(^4S)5p\ ^3P_0 - (^4S)5d\ ^3D_1$
2	9595.41	10418.79	$(^4S)5p\ ^3P_2 - (^4S)5d\ ^3D_2$
7	9549.40	10468.99	$(^3D)5s\ ^3D_3 - (^3D)5p\ ^3F_3$
3	9544.96	10473.86	$(^4S)5p\ ^3P_1 - (^4S)5d\ ^3D_2$
5	9541.64	10477.50	$(^4S)5p\ ^3P_2 - (^4S)5d\ ^3D_3$
1	9535.83	10483.88	$(^4S)5p\ ^3P_1 - (^4S)5d\ ^3D_1$
1	9517.91	10503.63	
10	9432.43	10598.81	$(^3D)5s\ ^3D_2 - (^3D)5p\ ^3D_2$
0	9427.43	10604.44	$(^3D)5s\ ^1D_2 - (^3D)5p\ ^3P_1$
0	9419.85	10612.97	$(^3D)5s\ ^1D_2 - (^3D)5p\ ^3P_2$
1	9329.83	10715.37	
1	9329.15	10716.15	
2	9303.15	10746.10	$(^3D)5s\ ^3D_1 - (^3D)5p\ ^3D_2$
6	9271.02	10783.35	$(^3D)5s\ ^3D_3 - (^3D)5p\ ^3D_3$
1	9265.41	10789.87	$(^3D)5s\ ^3D_2 - (^3D)5p\ ^3F_3$
2	9252.40	10805.04	$(^3D)5s\ ^3D_3 - (^4S)7p\ ^3P_2$
1	9228.03	10833.58	
2	9218.30	10845.01	$(^4S)4d\ ^3D_2 - (^4S)6f\ ^3F$
0	9216.81	10846.76	$(^3D)5s\ ^3D_3 - (^4S)7p\ ^3P_2$
1	9214.28	10849.74	$(^4S)4d\ ^3D_1 - (^4S)6f\ ^3F$
1	9212.77	10851.52	$(^4S)4d\ ^3D_0 - (^4S)6f\ ^3F$
1	9211.04	10853.56	$(^3D)5s\ ^3D_3 - (^4S)7p\ ^3P_2$
2	9206.14	10859.33	$(^4S)4d\ ^3D_3 - (^4S)6f\ ^3F$
3	9203.58	10862.36	$(^4S)4d\ ^3D_4 - (^4S)6f\ ^3F$
6	9181.80	10888.12	$(^3D)5s\ ^3D_2 - (^3D)5p\ ^3F_2$
8	9140.79	10936.98	$(^3D)5s\ ^3D_1 - (^3D)5p\ ^3F_2$
0	9090.26	10997.77	$(^4S)5p\ ^3P_2 - (^4S)5d\ ^3D_2$
12	9088.70	10999.66	$(^4S)5p\ ^3P_2 - (^4S)5d\ ^3D_3$
6	9088.14	11000.34	$(^4S)5p\ ^3P_2 - (^4S)5d\ ^3D_2$
8	9083.05	11006.50	$(^3D)5s\ ^3D_3 - (^3D)5p\ ^3F_4$
0	9074.86	11016.43	$(^3D)5s\ ^3D_2 - (^3D)5p\ ^1F_3$
20	9038.56	11060.67	$(^4S)5s\ ^3S_1 - (^4S)5p\ ^3P_1$
0	9035.05	11064.97	$(^4S)4d\ ^3D_3 - (^4S)8f\ ^3F$
3	9005.99	11100.66	$(^4S)5p\ ^3P_2 - (^4S)5d\ ^3D_1$
7	9005.58	11101.17	$(^4S)5p\ ^3P_2 - (^4S)5d\ ^3D_2$
8	9003.44	11103.82	$(^4S)5p\ ^3P_2 - (^4S)5d\ ^3D_3$
20	9001.93	11105.68	$(^4S)5s\ ^3S_1 - (^4S)5p\ ^3P_2$
10	8969.63	11145.68	$(^4S)5p\ ^3P_1 - (^4S)5d\ ^3D_1$
8	8969.23	11146.17	$(^4S)5p\ ^3P_1 - (^4S)5d\ ^3D_2$
9	8938.14	11184.94	$(^3D)5s\ ^3D_1 - (^3D)5p\ ^1P_1$
1	8930.67	11194.30	$(^4S)5p\ ^3P_0 - (^4S)7s\ ^3S_1$
3	8924.19	11202.42	$(^3D)5s\ ^3D_2 - (^3D)5p\ ^3D_3$
30	8918.80	11209.19	$(^4S)5s\ ^3S_1 - (^4S)5p\ ^3P_2$
4	8915.88	11212.86	$(^4S)5p\ ^3P_2 - (^4S)7s\ ^3S_1$
4	8914.58	11214.50	$(^3D)5s\ ^3D_2 - (^4S)7p\ ^3P_1$
1	8882.72	11254.72	$(^3D)5s\ ^3D_2 - (^4S)7p\ ^3P_1$
3	8872.26	11268.11	$(^4S)5p\ ^3P_1 - (^4S)7s\ ^3S_1$
0	8868.51	11272.75	$(^3D)5s\ ^3D_2 - (^4S)7p\ ^3P_2$
3	8799.79	11360.78	$(^3D)5s\ ^3D_1 - (^4S)7p\ ^3P_2$
1	8791.73	11372.49	
15	8742.29	11435.51	$(^3D)5s\ ^3D_2 - (^3D)5p\ ^1F_3$
0	8666.30	11535.78	
0	8663.11	11540.03	
0	8654.77	11515.15	
1	8651.54	11555.47	
2	8568.39	11670.33	
1	8495.97	11767.06	
1	8491.35	11773.46	
15	8450.47	11830.41	$(^3D)5s\ ^1D_2 - (^3D)5p\ ^1D_2$
15	8440.55	11844.31	$(^3D)5s\ ^3D_3 - (^3D)5p\ ^3P_2$
1	8425.16	11865.96	
1	8423.76	11867.93	
8	8375.31	11936.58	$(^4S)4d\ ^3D_3 - (^3D)5p\ ^1D_2$
1	8368.57	11946.19	$(^4S)5p\ ^3P_1 - (^3P)5s\ ^1P_1$
1	8368.25	11946.65	
0	8367.44	11947.80	
0	8356.26	11963.78	
2	8350.60	11971.89	
1d	8341.64	11984.75	$(^3D)5s\ ^3D_3 - (^4S)6f\ ^3F$
4	8340.03	11987.06	$(^3D)5s\ ^1D_2 - (^4S)6f\ ^3F$
0	8335.14	11994.10	
1	8309.52	12031.09	
0	8304.66	12038.13	
1	8282.40	12070.47	
1	8274.55	12081.92	
2	8272.45	12085.00	
0	8265.34	12095.39	
1	8258.24	12105.79	
2	8256.74	12107.99	$(^3D)5s\ ^1D_2 - (^4S)7f\ ^3F$
0d	8255.78	12109.40	
0	8253.04	12113.42	
1	8217.53	12165.76	
12	8194.61	12199.79	$(^4S)4d\ ^3D_3 - (^4S)7f\ ^3F$
8	8191.43	12204.53	$(^4S)4d\ ^3D_1 - (^4S)7f\ ^3F$
4	8190.13	12206.47	$(^4S)4d\ ^3D_2 - (^4S)7f\ ^3F$
10	8185.00	12214.11	$(^4S)4d\ ^3D_3 - (^4S)7f\ ^3F$
15	8182.93	12217.20	$(^4S)4d\ ^3D_4 - (^4S)7f\ ^3F$
0	8172.00	12233.54	
18	8163.08	12246.92	$(^4S)5p\ ^3P_2 - (^4S)7s\ ^3S_1$, $(^3P)5s\ ^3P_2$
20	8157.73	12254.95	$(^3D)5s\ ^3D_3 - (^3D)5p\ ^3P_1$
3	8155.69	12258.01	
15	8152.02	12263.53	$(^3D)5s\ ^3D_3 - (^3D)5p\ ^3P_2$
18	8149.28	12267.65	$(^4S)5p\ ^3P_2 - (^3P)5s\ ^3P_2$, $(^4S)7s\ ^5S_2$
1	8147.09	12270.95	
0	8140.17	12281.38	
2	8098.51	12344.57	
15	8094.69	12350.39	$(^4S)5p\ ^3P_2 - (^4S)7s\ ^4S_2$, $(^3P)5s\ ^3P_2$
15	8093.19	12352.68	$(^3D)5s\ ^3D_1 - (^3D)5p\ ^3P_0$
2	8087.77	12360.95	
12	8081.14	12371.09	$(^4S)5p\ ^3P_2 - (^3P)5s\ ^3P_2$, $(^4S)7s\ ^5S_2$
12	8065.31	12395.37	$(^4S)5p\ ^3P_1 - (^4S)7s\ ^4S_2$, $(^3P)5s\ ^3P_2$
12	8060.91	12402.15	$(^3D)5s\ ^3D_1 - (^3D)5p\ ^3P_1$
1	8058.60	12405.70	
4	8058.37	12406.06	$(^3D)5s\ ^3D_2 - (^4S)6f\ ^3F$
1	8055.29	12410.80	$(^3D)5s\ ^3D_1 - (^3D)5p\ ^3P_2$
10	8051.81	12416.16	$(^4S)5p\ ^3P_1 - (^3P)5s\ ^3P_2$, $(^4S)7s\ ^5S_2$
1d	8043.62	12428.80	
20	8036.35	12440.04	$(^4S)5s\ ^5S_2 - (^4S)5p\ ^3P_1$
1	8029.14	12451.21	
1	8024.18	12458.90	
1	8020.62	12464.45	
1	8018.42	12467.86	
30	8000.96	12495.06	$(^4S)5s\ ^5S_2 - (^4S)5p\ ^3P_1$
0	7979.51	12528.66	
3	7963.89	12553.23	$(^3D)5s\ ^3D_1 - (^4S)6f\ ^3F$
0	7960.67	12558.30	
0d	7958.20	12562.20	
0	7934.70	12599.41	
1	7932.83	12602.38	$(^4S)5p\ ^5P_3 - (^4S)7s\ ^5S_2$
3	7929.48	12607.70	
0d	7924.16	12616.16	
0d	7916.20	12628.85	
0	7904.59	12647.39	$(^4S)5p\ ^3P_1 - (^4S)7s\ ^5S_2$
0d	7902.07	12651.42	
1	7796.15	12823.32	
1	7771.60	12863.82	$(^4S)5p\ ^3P_2 - (^4S)6d\ ^3D_2$
0	7770.26	12866.04	$(^4S)5p\ ^3P_2 - (^4S)6d\ ^3D_1$
2	7767.87	12870.00	$(^4S)5p\ ^3P_2 - (^4S)6d\ ^3D_3$; $4p^4\ ^1D_2 - 4p^4\ ^1S_0$
0	7766.88	12871.64	
0	7756.53	12888.81	
1	7754.51	12892.16	
5	7750.41	12899.00	$(^1D)5s\ ^3D_3 - (^4S)8p\ ^3P_2$
0	7737.00	12921.35	$(^4S)5p\ ^3P_1 - (^4S)6d\ ^3D_1$
0d	7735.16	12924.42	$(^3D)5s\ ^1D_2 - (^4S)8f\ ^3F$
1	7724.04	12943.02	
6	7680.61	13016.22	$(^4S)4d\ ^3D_3 - (^4S)8f\ ^3F$
3	7677.83	13020.94	$(^4S)4d\ ^3D_1 - (^4S)8f\ ^3F$
1	7676.69	13022.87	$(^4S)4d\ ^3D_2 - (^4S)8f\ ^3F$
1	7674.82	13026.04	
1	7672.39	13030.00	
4	7672.17	13030.54	$(^4S)4d\ ^3D_2 - (^4S)8f\ ^3F$
8	7670.33	13033.66	$(^4S)4d\ ^3D_4 - (^4S)8f\ ^3F$
8	7653.59	13062.18	$(^3D)5s\ ^3D_3 - (^3D)5p\ ^1D_2$
12	7606.81	13142.50	$(^4S)5p\ ^3P_1 - (^4S)6d\ ^3D_2$
15	7592.19	13167.81	$(^4S)5p\ ^3P_0 - (^4S)6d\ ^3D_1$
0	7587.16	13176.53	
25	7583.37	13183.12	$(^4S)5p\ ^3P_2 - (^4S)6d\ ^3D_3$
1	7581.47	13186.42	$(^4S)5p\ ^3P_2 - (^4S)6d\ ^3D_1$
20	7575.08	13197.56	$(^4S)5p\ ^3P_1 - (^4S)6d\ ^3D_2$
10	7549.97	13241.44	$(^4S)5p\ ^3P_1 - (^4S)6d\ ^3D_1$
10	7508.97	13313.74	$(^1D)5s\ ^3D_2 - (^4S)8p\ ^3P_1$
5	7506.44	13318.22	$(^1D)5s\ ^3D_2 - (^4S)8p\ ^3P_2$
0	7494.39	13339.65	$(^1D)5s\ ^3D_2 - (^4S)7f\ ^3F$
3	7493.47	13341.28	$(^1D)5s\ ^3D_2 - (^4S)7f\ ^3F$
0	7430.72	13453.95	$(^1D)5s\ ^1D_2 - (^4S)9f\ ^3F$
8	7429.27	13456.58	$(^1D)5s\ ^3D_1 - (^4S)8p\ ^3P_0$
7	7426.81	13461.03	$(^1D)5s\ ^3D_1 - (^4S)8p\ ^3P_1$
0	7424.39	13465.42	$(^1D)5s\ ^3D_1 - (^4S)8p\ ^3P_2$
1	7415.58	13481.41	$(^1D)5s\ ^3D_2 - (^1D)5p\ ^1D_2$
2	7414.02	13484.25	$(^4S)5p\ ^3P_2 - (^1D)4d\ 1_2$, $(^4S)8s\ ^5S_2$
6	7383.88	13539.27	$(^4S)5p\ ^3P_1 - (^1D)4d\ 1_2$, $(^4S)8s\ ^5S_2$
5	7380.34	13545.79	$(^4S)4d\ ^3D_3 - (^4S)9f\ ^3F$
3	7377.77	13550.50	$(^4S)4d\ ^3D_1 - (^4S)9f\ ^3F$
1	7376.75	13552.38	$(^4S)4d\ ^3D_2 - (^4S)9f\ ^3F$
4	7372.54	13560.11	$(^4S)4d\ ^3D_2 - (^4S)9f\ ^3F$
6	7370.82	13563.28	$(^4S)4d\ ^3D_3 - (^4S)9f\ ^3F$
0	7357.53	13587.79	$(^4S)5p\ ^3P_1 - (^4S)8s\ ^5S_2$, $(^3D)4d\ 1_2$

TABLE I.—*Continued.*

Int.	λ(air)	ν(vac)	Transition
4	7338.96	13622.16	$(^4S)5p\ ^3P_0 - (^4S)8s\ ^5S_1$
1	7335.51	13628.56	$(^2D)5s\ ^3D_1 - (^2D)5p\ ^1D_2$
10	7328.97	13640.72	$(^4S)5p\ ^3P_2 - (^4S)8s\ ^5S_1$
0	7319.18	13658.96	
8	7299.51	13695.78	$(^4S)5p\ ^3P_1 - (^4S)8s\ ^5S_1$
0	7287.53	13718.29	
0	7266.13	13758.70	$(^2D)5s\ ^3D_2 - (^4S)7f\ ^5F$
3	7265.31	13760.25	$(^2D)5s\ ^3D_2 - (^4S)7f\ ^3F$
0d	7256.48	13776.99	
4	7210.04	13865.72	$(^2D)5s\ ^3D_3 - (^4S)9p\ ^3P_2$
2	7188.31	13907.64	$(^2D)5s\ ^3D_1 - (^4S)7f\ ^3F$
2	7187.86	13908.52	$(^4S)4d\ ^5D_3 - (^4S)10f\ ^5F$
1	7185.46	13913.16	$(^4S)4d\ ^5D_1 - (^4S)10f\ ^5F$
1	7180.49	13922.79	$(^4S)4d\ ^5D_2 - (^4S)10f\ ^5F$
3	7178.84	13925.99	$(^4S)4d\ ^5D_4 - (^4S)10f\ ^5F$
1	7099.70	14081.21	
0	7069.59	14141.21	
1	7062.49	14155.42	
30	7062.06	14156.28	$(^4S)5p\ ^3P_2 - (^4S)6d\ ^5D_{3,4}$
1	7061.56	14157.29	$(^2D)5s\ ^3D_3 - (^4S)8f\ ^3F$
1	7056.27	14167.88	$(^4S)4d\ ^5D_3 - (^4S)11f\ ^5F$
1	7049.15	14182.20	$(^4S)4d\ ^5D_2 - (^4S)11f\ ^5F$
1	7047.55	14185.42	$(^4S)4d\ ^5D_4 - (^4S)11f\ ^5F$
1	7043.15	14194.28	
1	7024.30	14232.36	
15	7013.85	14253.54	$(^4S)5p\ ^3P_2 - (^4S)6d\ ^5D_2$
8	7012.75	14255.82	$(^4S)5p\ ^3P_2 - (^4S)6d\ ^5D_1$
20	7010.82	14259.78	$(^4S)5p\ ^3P_2 - (^4S)6d\ ^5D_3$
2	7002.84	14275.99	$(^2D)5s\ ^3D_2 - (^4S)9p\ ^3P_1$
1	6998.47	14284.90	$(^2D)5s\ ^3D_2 - (^4S)9p\ ^3P_2$
10	6991.77	14298.58	$(^4S)5p\ ^3P_1 - (^4S)6d\ ^5D_2$
12	6990.65	14300.87	$(^4S)5p\ ^3P_1 - (^4S)6d\ ^5D_1$
0	6973.33	14336.40	
2	6931.32	14423.29	$(^2D)5s\ ^3D_1 - (^4S)9p\ ^3P_1$
1	6925.63	14435.13	
1	6905.76	14476.68	$(^4S)5p\ ^3P_2 - (^4S)7d\ ^5D_1,\ (^2D)4d\ 2_1$
1	6899.91	14488.95	
2	6879.52	14531.88	$(^4S)5p\ ^3P_1 - (^4S)7d\ ^5D_1,\ (^2D)4d\ 2_1$
2	6865.09	14562.44	$(^4S)5p\ ^3P_0 - (^2D)4d\ 2_1,\ (^4S)7d\ ^5D_1$
1	6860.17	14572.88	$(^4S)5p\ ^3P_2 - (^4S)6d\ ^5D_3$
1	6858.47	14576.49	$(^2D)5s\ ^3D_2 - (^4S)8f\ ^3F$
1	6858.14	14577.19	$(^4S)5p\ ^3P_1 - (^4S)6d\ ^5D_0$
1	6856.29	14581.12	$(^4S)5p\ ^3P_2 - (^2D)4d\ 2_1,\ (^4S)7d\ ^5D_1$
15	6831.27	14634.54	$(^4S)5p\ ^3P_2 - (^4S)7d\ ^5D_2$
6	6830.89	14635.35	$(^4S)5p\ ^3P_2 - (^4S)7d\ ^5D_2$
2	6830.56	14636.06	$(^4S)5p\ ^3P_1 - (^2D)4d\ 2_1,\ (^4S)7d\ ^5D_1$
5	6815.28	14668.86	$(^4S)5p\ ^3P_0 - (^4S)7d\ ^5D_1$
8	6805.24	14690.50	$(^4S)5p\ ^3P_1 - (^4S)7d\ ^5D_2$
0	6796.23	14709.97	
0	6789.93	14723.63	$(^2D)5s\ ^3D_1 - (^4S)8f\ ^3F$
3	6781.22	14742.54	$(^4S)5p\ ^3P_1 - (^4S)7d\ ^3D_1$
6	6768.50	14770.24	$(^4S)5p\ ^3P_2 - (^2D)4d\ 1_2,\ (^4S)8s\ ^5S_2$
1	6757.12	14795.13	
0	6755.42	14798.85	
1	6748.73	14813.52	
8	6746.43	14818.56	$(^4S)5p\ ^3P_2 - (^4S)8s\ ^5S_2,\ (^2D)4d\ 1_2$
1	6743.57	14824.85	
1	6737.46	14838.29	
5	6721.37	14873.80	$(^4S)5p\ ^3P_2 - (^2D)4d\ 1_2,\ (^4S)8s\ ^5S_2$
0d	6708.45	14902.46	
0	6704.74	14910.70	
3	6701.04	14918.93	$(^4S)5p\ ^3P_1 - (^2D)4d\ 1_2,\ (^4S)8s\ ^5S_2$
7	6699.56	14922.23	$(^4S)5p\ ^3P_2 - (^4S)8s\ ^5S_2,\ (^2D)4d\ 1_2$
1	6690.67	14942.07	$(^4S)5p\ ^3P_0 - (^4S)9s\ ^5S_2$
2	6682.36	14960.65	$(^4S)5p\ ^3P_2 - (^4S)9s\ ^5S_2$
5	6679.43	14967.21	$(^4S)5p\ ^3P_1 - (^4S)8s\ ^5S_2,\ (^2D)4d\ 1_2$
1	6666.69	14995.80	
2	6657.83	15015.75	$(^4S)5p\ ^3P_1 - (^4S)9s\ ^3S_1$
1	6544.85	15274.98	
1	6512.69	15350.40	
5	6470.15	15451.32	$(^4S)5p\ ^3P_2 - (^4S)8d\ ^3D_3,\ (^2D)4d\ 4_3$
1	6456.43	15484.17	$(^4S)5p\ ^3P_2 - (^4S)8d\ ^3D_2$
3	6441.43	15520.22	$(^4S)5p\ ^3P_0 - (^4S)8d\ ^3D_1$
1	6420.32	15571.25	$(^4S)5p\ ^3P_2 - (^4S)8d\ ^3D_2$
2	6410.99	15593.90	$(^4S)5p\ ^3P_1 - (^4S)8d\ ^3D_1$
4	6497.69	15626.30	$(^4S)5p\ ^3P_1 - (^4S)8d\ ^3D_2$
2	6358.37	15722.95	$(^4S)5p\ ^3P_2 - (^2D)4d\ 4_2,\ (^4S)8d\ ^3D_3$
1	6344.31	15757.82	$(^4S)5p\ ^3P_2 - (^4S)10s\ ^3S_1$
0	6332.32	15787.63	
20	6325.57	15804.50	$(^4S)5p\ ^3P_2 - (^4S)7d\ ^5D_{3,4}$
3	6325.11	15805.65	$(^4S)5p\ ^3P_2 - (^4S)7d\ ^5D_2$
1	6322.21	15812.89	$(^4S)5p\ ^3P_1 - (^4S)10s\ ^5S_1$
4	6300.99	15866.15	$(^4S)5p\ ^3P_2 - (^4S)7d\ ^5D_1,\ (^2D)4d\ 2_1$
0	6295.32	15880.42	
10	6284.47	15907.86	$(^4S)5p\ ^3P_2 - (^4S)7d\ ^5D_3$
9	6283.96	15909.14	$(^4S)5p\ ^3P_2 - (^4S)7d\ ^5D_3$
8	6283.16	15911.16	$(^4S)5p\ ^3P_1 - (^4S)7d\ ^5D_1,\ (^2D)4d\ 2_1$
6	6269.15	15946.73	
8	6266.23	15954.14	$(^4S)5p\ ^3P_1 - (^4S)7d\ ^5D_2$
4	6259.81	15970.52	$(^4S)5p\ ^3P_2 - (^2D)4d\ 2_1,\ (^4S)7d\ ^5D_1$
6	6242.21	16015.53	$(^4S)5p\ ^3P_1 - (^2D)4d\ 2_1,\ (^4S)7d\ ^5D_1$
1	6220.86	16070.50	$(^4S)5p\ ^3P_0 - (^4S)9d\ ^5D_1$
1	6216.57	16081.61	$(^4S)5p\ ^3P_1 - (^4S)9d\ ^3D_1$
1	6207.78	16104.36	$(^4S)5p\ ^3P_2 - (^4S)9d\ ^3D_2$
3	6207.20	16105.88	$(^4S)5p\ ^3P_2 - (^4S)9d\ ^3D_3$
1	6203.27	16116.07	
1	6192.45	16144.24	$(^4S)5p\ ^3P_1 - (^4S)9d\ ^5D_1$
1	6188.23	16155.25	$(^4S)5p\ ^3P_1 - (^4S)9d\ ^3D_1$
2	6186.60	16159.51	$(^4S)5p\ ^3P_1 - (^4S)9d\ ^3D_2$
6	6177.71	16182.76	$(^4S)5p\ ^3P_2 - (^4S)9s\ ^5S_2$
5	6138.46	16286.23	$(^4S)5p\ ^3P_2 - (^4S)9s\ ^3S_2$
4	6121.54	16331.24	$(^4S)5p\ ^3P_1 - (^4S)9s\ ^5S_2$
8	5962.01	16768.23	$(^4S)5p\ ^3P_2 - (^4S)8d\ ^3D_4$
1	5961.71	16769.07	$(^4S)5p\ ^3P_2 - (^4S)8d\ ^3D_2$
5	5961.32	16770.17	$(^4S)5p\ ^3P_2 - (^4S)8d\ ^3D_3$
2	5936.32	16840.81	$(^4S)5p\ ^3P_2 - (^4S)8d\ ^3D_3,\ (^2D)4d\ 4_3$
5	5925.15	16872.54	$(^4S)5p\ ^3P_2 - (^4S)8d\ ^5D_2$
1	5924.98	16873.03	$(^4S)5p\ ^3P_2 - (^4S)8d\ ^3D_1$
6	5924.76	16873.67	$(^4S)5p\ ^3P_2 - (^4S)8d\ ^5D_3$
4	5909.38	16917.58	$(^4S)5p\ ^3P_1 - (^4S)8d\ ^5D_2$
5	5909.20	16918.08	$(^4S)5p\ ^3P_1 - (^4S)8d\ ^3D_1$
3	5907.08	16924.16	
3	5878.70	17005.86	$(^4S)5p\ ^3P_2 - (^4S)10s\ ^5S_2$
2	5843.14	17109.36	$(^4S)5p\ ^3P_2 - (^4S)10s\ ^3S_2$
2	5827.80	17154.38	$(^4S)5p\ ^3P_1 - (^4S)10s\ ^3S_2$
4	5753.32	17376.46	$(^4S)5p\ ^3P_2 - (^4S)9d\ ^5D_4$
2	5752.03	17380.37	$(^4S)5p\ ^3P_2 - (^4S)9d\ ^5D_2$
3	5738.29	17421.99	
1	5719.68	17478.65	$(^4S)5p\ ^3P_2 - (^4S)9d\ ^3D_1$
2	5718.43	17482.49	$(^4S)5p\ ^3P_2 - (^4S)9d\ ^5D_2$
3	5717.99	17483.82	$(^4S)5p\ ^3P_2 - (^4S)9d\ ^3D_2$
2	5704.98	17523.71	$(^4S)5p\ ^3P_1 - (^4S)9d\ ^3D_1$
3	5703.73	17527.53	$(^4S)5p\ ^3P_1 - (^4S)9d\ ^5D_2$
1	5703.11	17529.44	
2	5702.44	17531.50	
2	5701.37	17534.78	$(^4S)5p\ ^3P_1 - (^4S)\ 9d\ ^3D_1$
2	5700.24	17538.28	$(^4S)5p\ ^3P_2 - (^4S)11s\ ^5S_2$
1	5666.80	17641.76	$(^4S)5p\ ^3P_2 - (^4S)11s\ ^3S_2$
1	5652.36	17686.82	$(^4S)5p\ ^3P_1 - (^4S)11s\ ^3S_1$
1	5618.92	17792.09	$(^4S)5p\ ^3P_2 - (^4S)10d\ ^3D_2$
3	5617.87	17795.41	$(^4S)5p\ ^3P_2 - (^4S)10d\ ^5D_4$
2	5586.43	17895.58	$(^4S)5p\ ^3P_2 - (^4S)10d\ ^5D_3$
1	5586.34	17895.87	$(^4S)5p\ ^3P_2 - (^4S)10d\ ^3D_2$
1	5572.31	17940.92	$(^4S)5p\ ^3P_1 - (^4S)10d\ ^5D_2$
1	5572.22	17941.21	$(^4S)5p\ ^3P_1 - (^4S)10d\ ^3D_1$
1	5530.28	18082.28	$(^4S)5p\ ^3P_2 - (^4S)11d\ ^3D_2$
2	5530.12	18082.80	$(^4S)5p\ ^3P_2 - (^4S)11d\ ^5D_4$
1d	5499.48	18183.55	$(^4S)5p\ ^3P_2 - (^4S)11d\ ^5D_{1,2}$
2	5498.78	18185.83	$(^4S)5p\ ^3P_2 - (^4S)11d\ ^3D_2$
11	5374.14	18602.46	$(^4S)5s\ ^3S_1 - (^4S)6p\ ^5P_1$
12	5369.91	18617.14	$(^4S)5s\ ^3S_1 - (^4S)6p\ ^3P_2$
10	5365.47	18632.54	$(^4S)5s\ ^3S_1 - (^4S)6p\ ^3P_0$
6	4886.99	20456.78	$4p^4\ ^3P_1 - 4p^4\ ^1S_0$
3	4792.73	20859.11	$(^4S)5s\ ^3S_1 - (^2D)5p\ ^3D_1$
30	4742.25	21081.16	$(^4S)5s\ ^3S_2 - (^4S)6p\ ^5P_1$
40	4739.03	21095.49	$(^4S)5s\ ^3S_2 - (^4S)6p\ ^5P_2$
50	4730.78	21132.29	$(^4S)5s\ ^3S_2 - (^4S)6p\ ^3P_2$
6	4667.80	21417.41	$(^4S)5s\ ^3S_2 - (^4S)6p\ ^3P_1$
8	4664.98	21430.36	$(^4S)5s\ ^3S_1 - (^2D)5p\ ^3D_2$
10	4664.20	21431.99	$(^4S)5s\ ^3S_2 - (^4S)6p\ ^3P_2$
8	4623.77	21621.35	$(^4S)5s\ ^3S_1 - (^2D)5p\ ^3F_2$
1	4571.36	21869.24	$(^4S)5s\ ^3S_1 - (^2D)5p\ ^1P_1$
1	4534.89	22045.08	$(^4S)5s\ ^3S_1 - (^4S)7p\ ^5P_0$
2	4534.68	22046.11	$(^4S)5s\ ^3S_1 - (^4S)7p\ ^3P_1$
3	4532.74	22055.55	$(^4S)5s\ ^3S_1 - (^4S)7p\ ^3P_2$
8	4339.59	23037.22	$(^4S)5s\ ^3S_1 - (^2D)5p\ ^3P_0$
10	4330.28	23086.73	$(^4S)5s\ ^3S_1 - (^2D)5p\ ^3P_1$
12	4328.70	23095.17	$(^4S)5s\ ^3S_1 - (^2D)5p\ ^3P_2$
2	4184.08	23893.40	
2	4141.17	24140.97	$(^4S)5s\ ^3S_1 - (^4S)8p\ ^5P_0$
3	4140.40	24145.44	$(^4S)5s\ ^3S_1 - (^4S)8p\ ^3P_1$
4	4139.66	24149.82	$(^4S)5s\ ^3S_1 - (^4S)8p\ ^3P_2$
2	4111.88	24312.93	$(^4S)5s\ ^3S_1 - (^2D)5p\ ^1D_2$
4	4023.23	24848.68	$(^4S)5s\ ^5S_2 - (^2D)5p\ ^3D_3$
3	4021.26	24860.85	$(^4S)5s\ ^5S_2 - (^4S)7p\ ^3P_1$
4	4019.72	24870.33	$(^4S)5s\ ^5S_2 - (^4S)7p\ ^3P_2$
6	4014.77	24901.04	$(^4S)5s\ ^5S_2 - (^4S)7p\ ^5P_1$
8	4012.96	24912.27	$(^4S)5s\ ^5S_2 - (^4S)7p\ ^3P_2$
10	4011.88	24918.98	$(^4S)5s\ ^5S_2 - (^4S)7p\ ^3P_2$
1	3985.83	25081.79	$(^4S)5s\ ^5S_2 - (^2D)5p\ ^1F_3$
1	3981.74	25107.55	$(^4S)5s\ ^3S_1 - (^4S)9p\ ^3P_1$
1	3980.34	25116.38	$(^4S)5s\ ^3S_1 - (^4S)9p\ ^3P_2$
1	3735.02	26766.04	$(^4S)5s\ ^5S_2 - (^4S)8p\ ^5P_1$
2	3734.50	26769.73	$(^4S)5s\ ^5S_2 - (^4S)8p\ ^3P_1$
3	3733.34	26778.11	$(^4S)5s\ ^5S_2 - (^4S)8p\ ^3P_2$
1	3592.01	27831.74	$(^4S)5s\ ^3S_1 - (^4S)9p\ ^5P_1$
1	3591.66	27834.45	$(^4S)5s\ ^3S_1 - (^4S)9p\ ^3P_2$
2	3591.03	27839.33	$(^4S)5s\ ^5S_2 - (^4S)9p\ ^5P_2$
5	3501.52	28550.90	$4p^4\ ^1S_0 - (^4S)5s\ ^3S_1$
30	2547.98	39235.1	$4p^4\ ^1S_0 - (^2D)5s\ ^3D_1$
4	2442.07	40936.5	$4p^4\ ^1S_0 - (^4S)4d\ ^3D_1$
60	2413.517	41420.71	$4p^4\ ^1D_2 - (^4S)5s\ ^3S_1$
15	2332.81	42853.7	$4p^4\ ^1S_0 - (^4S)4d\ ^3D_1$
50	2164.160	46192.75	$4p^4\ ^3P_1 - (^4S)5s\ ^5S_2$

TABLE I.—*Continued.*

Int.	λ(air)	ν(vac)	Transition
6	2147.19	46557.8	
8	2081.08	48036.5	
50	2074.793	48182.14	$4p^4\ ^3P_2 - (^4S)5s\ ^5S_2$
40	2062.788	48462.50	$4p^4\ ^3P_0 - (^4S)5s\ ^5S_2$
4	2054.36	48661.3	$4p^4\ ^1S_0 - (^4S)5d\ ^3D_1$
6	2050.43	48754.6	$4p^4\ ^1S_0 - (^3P)5s\ ^3P_1$
50	2039.851	49007.38	$4p^4\ ^3P_1 - (^4S)5s\ ^5S_2$
4	2021.80	49445.0	$4p^4\ ^1S_0 - (^4S)7s\ ^5S_2$
15	1994.47	50122.5	$4p^4\ ^1S_0 - (^3P)5s\ ^1P_1$
50	1960.257	50996.97	$4p^4\ ^3P_2 - (^4S)5s\ ^5S_2$
30	1918.552	52105.32	$4p^4\ ^1D_2 - (^3D)5s\ ^3D_1$
35	1913.151	52252.39	$4p^4\ ^1D_2 - (^3D)5s\ ^3D_2$
40	1897.921	52671.64	$4p^4\ ^1D_2 - (^3D)5s\ ^3D_3$

Int.	λ(vac)	ν(vac)	Transition
6	1893.50	52812.3	$4p^4\ ^1S_0 - (^3D)4d\ 2_1$, $(^4S)7d\ ^3D_1$
5	1859.69	53772.4	
25	1858.84	53797.0	$4p^4\ ^1D_2 - (^4S)4d\ ^3D_3$
30	1855.20	53902.5	$4p^4\ ^1D_2 - (^3D)5s\ ^1D_2$
3	1852.02	53995.1	
3	1850.51	54039.2	
4	1849.55	54067.2	
4	1830.41	54632.6	
3	1828.65	54685.2	
8	1822.15	54880.2	
6	1796.04	55678.0	
30	1795.28	55701.6	$4p^4\ ^1D_2 - (^4S)4d\ ^3D_2$
5	1794.55	55724.3	$4p^4\ ^1D_2 - (^4S)4d\ ^3D_1$
25	1793.29	55763.4	$4p^4\ ^1D_2 - (^4S)4d\ ^3D_3$
3	1790.48	55850.9	
5	1772.64	56413.0	$4p^4\ ^1D_2 - (^4S)6s\ ^5S_2$
8	1759.24	56842.7	
6	1752.94	57047.0	$4p^4\ ^1D_2 - (^4S)6s\ ^3S_1$
3	1751.88	57081.5	
6	1750.89	57113.8	
3	1745.30	57296.7	
4	1742.75	57380.6	
3	1708.04	58546.6	
2	1706.70	58592.6	
4	1699.90	58827.0	
25	1690.70	59147.1	$4p^4\ ^3P_0 - (^3D)5s\ ^3D_1$
3	1688.79	59214.0	
25	1675.27	59691.9	$4p^4\ ^3P_1 - (^3D)5s\ ^3D_1$
25	1671.15	59839.0	$4p^4\ ^3P_1 - (^3D)5s\ ^3D_2$
15	1643.39	60849.8	$4p^4\ ^3P_0 - (^4S)4d\ ^3D_1$
1	1635.80	61132.2	
6	1629.06	61385.1	$4p^4\ ^3P_1 - (^4S)4d\ ^3D_2$
8	1628.85	61393.0	$4p^4\ ^3P_1 - (^4S)4d\ ^3D_{2,1}$
12	1626.25	61491.2	$4p^4\ ^3P_1 - (^4S)5s\ ^1D_2$
6	1625.45	61521.4	$4p^4\ ^1D_2 - (^4S)5d\ ^3D_1$
7	1625.19	61531.3	$4p^4\ ^1D_2 - (^4S)5d\ ^3D_2$
5	1623.90	61580.1	$4p^4\ ^1D_2 - (^4S)5d\ ^3D_3$
10	1622.73	61624.5	$4p^4\ ^1D_2 - (^3P)5s\ ^3P_1$
15	1621.21	61682.3	$4p^4\ ^3P_2 - (^3D)5s\ ^3D_1$
20	1617.35	61829.5	$4p^4\ ^3P_2 - (^3D)5s\ ^3D_2$
10	1611.26	62063.2	$4p^4\ ^1D_2 - (^4S)7s\ ^5S_2$, $(^3P)5s\ ^3P_2$
10	1610.72	62084.0	$4p^4\ ^1D_2 - (^3P)5s\ ^3P_2$, $(^4S)7s\ ^5S_2$
25	1606.46	62248.7	$4p^4\ ^3P_2 - (^3D)5s\ ^3D_3$
4	1604.70	62316.9	$4p^4\ ^1D_2 - (^4S)7s\ ^3S_1$
15	1593.19	62767.2	$4p^4\ ^3P_0 - (^4S)4d\ ^3D_1$
15	1587.46	62993.7	$4p^4\ ^1D_2 - (^3P)5s\ ^1P_1$
20	1580.04	63289.5	$4p^4\ ^3P_1 - (^4S)4d\ ^3D_2$
15	1579.49	63311.6	$4p^4\ ^3P_1 - (^4S)4d\ ^3D_1$
15	1577.90	63375.4	$4p^4\ ^3P_2 - (^4S)4d\ ^3D_2$
15	1577.61	63387.0	$4p^4\ ^3P_2 - (^4S)4d\ ^3D_{1,3}$
15	1575.26	63481.6	$4p^4\ ^3P_2 - (^3D)5s\ ^1D_2$
2	1563.28	63968.1	$4p^4\ ^1D_2 - (^4S)6d\ ^3D_{1,2,3}$
2	1562.50	64000.0	$4p^4\ ^3P_1 - (^4S)6s\ ^5S_2$
12	1560.28	64091.1	$4p^4\ ^3P_0 - (^4S)6s\ ^3S_1$
1	1556.54	64245.1	$4p^4\ ^1D_2 - (^4S)6d\ ^3D_2$
4	1555.55	64285.9	$4p^4\ ^1D_2 - (^4S)6d\ ^3D_{1,3}$
8	1548.29	64587.4	$4p^4\ ^1D_2 - (^3D)4d\ 1_2$, $(^4S)8s\ ^5S_2$

Int.	λ(vac)	ν(vac)	Transition
12	1547.12	64636.2	$4p^4\ ^3P_1 - (^4S)6s\ ^5S_2$
20	1531.84	65281.0	$4p^4\ ^3P_2 - (^4S)4d\ ^5D_2$
15	1531.33	65302.7	$4p^4\ ^3P_2 - (^4S)4d\ ^5D_1$
25	1530.39	65342.8	$4p^4\ ^3P_2 - (^4S)4d\ ^5D_3$
6	1524.88	65578.9	$4p^4\ ^1D_2 - (^4S)7d\ ^3D_1$, $(^3D)4d\ 2_1$
6	1522.45	65683.6	$4p^4\ ^1D_2 - (^3D)4d\ 2_1$, $(^4S)7d\ ^3D_1$
3	1521.20	65737.6	$4p^4\ ^1D_2 - (^4S)7d\ ^3D_{3,2}$
4	1519.99	65789.9	$4p^4\ ^1D_2 - (^4S)7d\ ^3D_1$
8	1515.33	65992.2	$4p^4\ ^3P_1 - (^4S)6s\ ^3S_2$
2	1511.27	66169.5	
3	1506.09	66397.1	$4p^4\ ^1D_2 - (^3D)4d\ 3_2$
2	1502.57	66552.6	$4p^4\ ^1D_2 - (^4S)8d\ ^3D_2$, $(^3D)4d\ 4_2$
15	1500.91	66626.2	$4p^4\ ^3P_1 - (^4S)6s\ ^5S_2$
3	1496.44	66825.3	$4p^4\ ^1D_2 - (^3D)4d\ 4_2$, $(^4S)8d\ ^3D_2$
6	1461.99	68399.9	$4p^4\ ^3P_1 - (^4S)5d\ ^3D_{1,2}$
8	1458.29	68573.5	$4p^4\ ^3P_0 - (^4S)5d\ ^3D_1$
12	1456.31	68666.7	$4p^4\ ^3P_0 - (^3P)5s\ ^3P_1$
15	1449.16	69005.5	$4p^4\ ^3P_1 - (^3P)5s\ ^3P_0$
10	1446.98	69109.5	$4p^4\ ^3P_1 - (^4S)5d\ ^3D_2$
10	1446.78	69119.0	$4p^4\ ^3P_1 - (^4S)5d\ ^3D_1$
10	1444.85	69211.3	$4p^4\ ^3P_1 - (^3P)5s\ ^3P_1$
5	1441.81	69357.3	$4p^4\ ^3P_0 - (^4S)7s\ ^3S_1$
12	1435.75	69650.0	$4p^4\ ^3P_1 - (^4S)7s\ ^3S_2$, $(^3P)5s\ ^3P_2$
12	1435.28	69672.8	$4p^4\ ^3P_1 - (^3P)5s\ ^3P_0$, $(^4S)7s\ ^3S_2$
6	1430.58	69901.7	$4p^4\ ^3P_1 - (^4S)7s\ ^3S_1$
6	1427.87	70034.4	$4p^4\ ^3P_0 - (^3P)5s\ ^1P_1$
5	1426.68	70092.8	
8	1420.64	70390.8	$4p^4\ ^3P_2 - (^4S)5d\ ^3D_{1,2,3}$
8	1416.84	70579.6	$4p^4\ ^3P_1 - (^3P)5s\ ^1P_1$
3	1414.26	70708.4	
10	1406.60	71093.4	$4p^4\ ^3P_2 - (^4S)5d\ ^3D_2$
10	1406.37	71105.0	$4p^4\ ^3P_2 - (^4S)5d\ ^3D_1$
10	1405.37	71155.6	$4p^4\ ^3P_2 - (^4S)5d\ ^3D_3$
8	1404.45	71202.2	$4p^4\ ^3P_2 - (^3P)5s\ ^3P_1$
1	1402.63	71294.6	
4	1401.92	71330.7	$4p^4\ ^3P_0 - (^4S)6d\ ^3D_1$
2	1397.49	71556.9	$4p^4\ ^3P_2 - (^4S)6d\ ^3D_{1,2}$
10	1395.88	71639.4	$4p^4\ ^3P_2 - (^4S)7s\ ^3S_2$, $(^3P)5s\ ^3P_2$
10	1395.43	71662.5	$4p^4\ ^3P_2 - (^3P)5s\ ^3P_2$, $(^4S)7s\ ^3S_2$
4	1392.97	71789.1	$4p^4\ ^3P_0 - (^4S)8s\ ^3S_1$
5	1392.13	71832.4	$4p^4\ ^3P_1 - (^4S)6d\ ^3D_2$
4	1391.27	71876.8	$4p^4\ ^3P_1 - (^4S)6d\ ^3D_{1,2}$
6	1390.99	71891.2	$4p^4\ ^3P_2 - (^4S)7s\ ^3S_1$
8	1385.54	72174.0	$4p^4\ ^3P_1 - (^3D)4d\ 1_2$, $(^4S)8s\ ^3S_2$
2	1384.63	72221.5	$4p^4\ ^3P_1 - (^4S)8s\ ^3S_2$, $(^2D)4d\ 1_2$
3	1382.56	72329.6	$4p^4\ ^3P_1 - (^4S)8s\ ^3S_1$
0	1379.50	72490.0	
10	1377.98	72570.0	$4p^4\ ^3P_1 - (^3P)5s\ ^1P_1$
2	1377.04	72619.5	$4p^4\ ^3P_0 - (^4S)7d\ ^3D_1$, $(^3D)4d\ 2_1$
2	1375.03	72725.7	$4p^4\ ^3P_0 - (^3D)4d\ 2_1$, $(^4S)7d\ ^3D_1$
2	1373.03	72831.6	$4p^4\ ^3P_0 - (^4S)7d\ ^3D_1$
0	1367.91	73104.2	$4p^4\ ^3P_0 - (^4S)9s\ ^3S_1$
1	1366.78	73164.7	$4p^4\ ^3P_1 - (^4S)7d\ ^3D_1$, $(^3D)4d\ 2_1$
3	1364.83	73269.2	$4p^4\ ^3P_1 - (^3D)4d\ 2_1$, $(^4S)7d\ ^3D_1$
1	1363.80	73324.5	$4p^4\ ^3P_1 - (^4S)7d\ ^3D_2$
3	1359.72	73544.6	$4p^4\ ^3P_1 - (^4S)6d\ ^3D_{1,2,3}$
0	1357.79	73649.1	$4p^4\ ^3P_1 - (^4S)9s\ ^3S_1$
5	1354.63	73820.9	$4p^4\ ^3P_2 - (^4S)6d\ ^3D_2$
7	1353.86	73862.9	$4p^4\ ^3P_2 - (^4S)6d\ ^3D_{1,3}$
7	1353.02	73908.7	
4	1351.62	73985.3	$4p^4\ ^1P_1 - (^3D)4d\ 3_2$
5	1348.40	74162.0	$4p^4\ ^3P_1 - (^3D)4d\ 1_2$, $(^4S)8s\ ^3S_2$
1	1347.50	74211.5	$4p^4\ ^3P_2 - (^4S)8s\ ^3S_2$, $(^2D)4d\ 1_2$
0	1346.58	74262.2	
4	1345.54	74319.6	$4p^4\ ^3P_2 - (^4S)8s\ ^3S_1$
4	1342.04	74513.4	
4	1330.55	75156.9	$4p^4\ ^3P_2 - (^4S)7d\ ^3D_1$, $(^3D)4d\ 2_1$
4	1328.75	75258.7	$4p^4\ ^3P_2 - (^3D)4d\ 2_1$, $(^4S)7d\ ^3D_1$
1	1327.80	75312.5	$4p^4\ ^3P_2 - (^4S)7d\ ^3D_{2,3}$
2	1326.83	75367.6	$4p^4\ ^3P_2 - (^4S)7d\ ^3D_1$
1	1322.06	75639.5	$4p^4\ ^3P_2 - (^4S)9s\ ^3S_1$
3	1316.26	75972.8	$4p^4\ ^3P_2 - (^3D)4d\ 3_2$
3	1313.53	76130.7	$4p^4\ ^3P_2 - (^4S)8d\ ^3D_2$, $(^2D)4d\ 4_2$

but there still remain 119 weak ones which have not been identified as impurities and for which no place has been found in the term scheme so far developed.

Table I lists all the observed wave-lengths, intensities (comparable only over short ranges), wave numbers and transition designations. In cases where one of the terms involved is the result of a recognized perturbation between two configurations, both designations are given, with the predominant one first. Some incompletely assigned terms are indicated by numbers with J subscripts as determined by their apparent combining properties. A d after the intensity number means the line was diffuse.

The transitions involving the five $4p^4$ terms

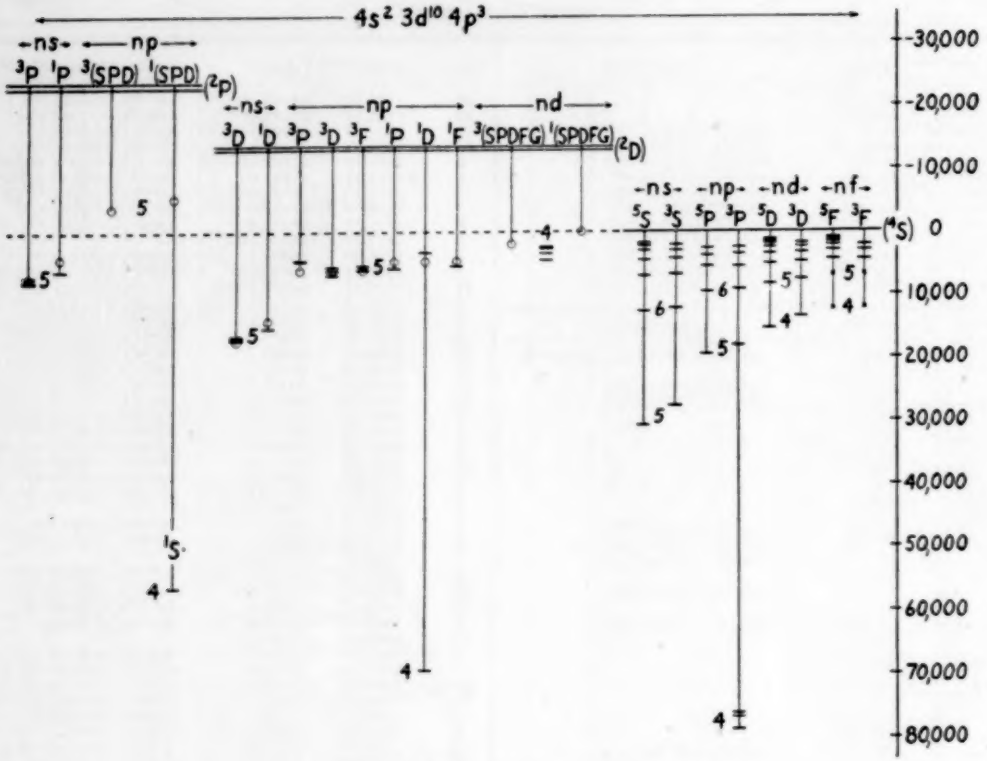

FIG. 1. Energy levels of Se I.

are open to almost no other interpretation. All are observed that would be expected due to combinations with $4p^3ns$ and $4p^3nd$ terms and no intense lines are left over. The 4*s* electron is not excited to any extent as the 2*s* and 3*s* electrons are in oxygen and sulfur. Long wavelength combinations and series relations serve to check most of the assignments, and analogies with oxygen and sulfur are well maintained in relative positions of terms. Intercombinations are quite strong and the L selection rule is commonly violated, which gives ample check on the choice of the $4p^4\ {}^1D_2$ and ${}^1S_0$ terms.

An analysis of Se II being carried out in this laboratory at the present time has established the relative positions of the low ${}^4S$, ${}^2D$, and ${}^2P$ terms which are the limits of the Se I series. The positions of the terms built on the doublet limits can be roughly predicted, as was done in the cases of oxygen[10] and sulfur,[4] by assuming that the energy of interaction of the excited electron and the atom core is independent of the state of the core. These positions are marked in Fig. 1 by the circles, and in every case where they lie below the ${}^4S$ limit, groups of terms are found having the appropriate combining properties. The atom would be expected to have such a short life in those states which lie above the ${}^4S$ limit (due to the auto-ionization effect[11]) that their combinations would not be observed. Fig. 1 indicates by short horizontal lines the known terms arranged in series. Crosses mark the approximate positions for the first and second members of the ${}^5F$ and ${}^3F$ series, which have not been located due to their unfavorable positions for observable combinations.

The two series $({}^4S)5p\ {}^5P_{123} - ({}^4S)ns\ {}^5S_2$ and $({}^4S)5p\ {}^5P_3 - ({}^4S)nd\ {}^5D_4$ were accurately measured to seven and nine members respectively and the limits obtained agree with each other and with those given by Runge and Paschen[5] within about one wave number. The method used for deter-

[10] R. Frerichs, Phys. Rev. **34**, 1239 (1929).

[11] A. G. Shenstone, Phys. Rev. **38**, 873 (1931).

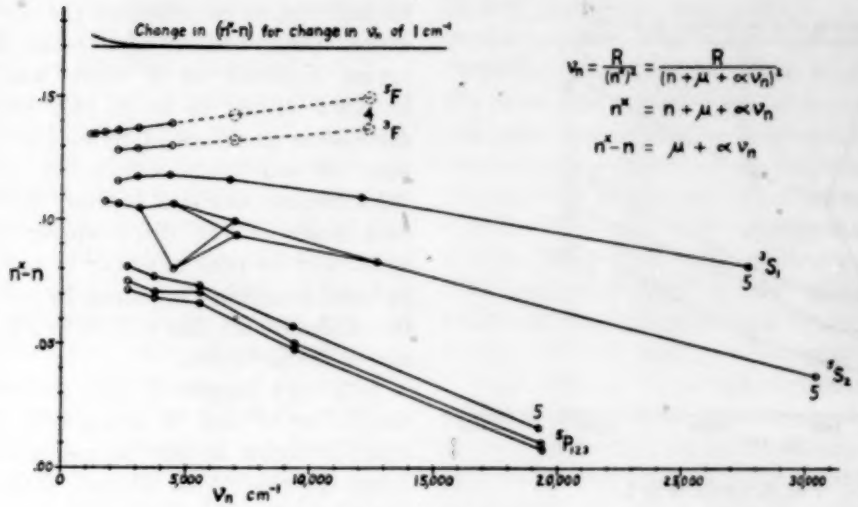

FIG. 2. Series in Se I.

mining limits was that recommended by Shenstone and Russell;[12] namely, plotting quantum defect against term value. The presence of perturbations is thus also clearly brought out, and these are found to be of quite frequent occurrence in selenium.

A new series of ^5F terms was obtained from the combination $(^4S)4d\ ^5D_{01234}-(^4S)nf\ ^5F$ for $n=6\cdots11$. The plot of this series (Fig. 2) shows no perturbations and it was possible to determine its limit within 0.2 cm^{-1}, as illustrated by the "sensitivity curve" at the top of the figure. Ample combinations were found with these accurately established terms to permit all the rest of the term scheme to be brought to the same absolute accuracy, excepting only five levels which are determined solely from the vacuum spectrograph measurements.

The plots of quantum defect *vs.* term value for all the series built on the (^4S) limit are shown in Figs. 2, 3 and 4. The quantity (n^*-n), which is plotted here, is actually the negative of the quantum defect. The point of origin on the ordinate scale is arbitrarily chosen and, in general, differs by different amounts from the true origin for each series. Within each of the multiplets $^5P_{123}$, $^3P_{012}$, and $^3D_{123}$, however, the origin is the same. The members of the $^5D_{1234}$ multiplet have been arbitrarily separated by amounts indicated by the darts. In a number of cases there are two terms which fit almost equally well as members of the series and both are plotted. In the $^5S_2$ series the perturbing terms for $n=7$ and 8 are $(^2P)5s\ ^3P_2$ and $(^2D)4d\ 1_2$. In the $^5D_1$ series the perturbing term for $n=7$ is $(^2D)4d\ 2_1$. In the $^3D_3$ series the perturbing term for $n=8$ is $(^2D)4d\ 4_2$. The $^3P_{012}$ series experiences a very strong perturbation due to the term $(^2D)5p\ ^3P_{012}$, which lies between members 7 and 8. The causes of the other series irregularities cannot be definitely fixed. The eighteen levels arising from the $(^2D)4d$ configuration should lie within a few thousand wave numbers of the (^4S) limit and others of these, besides the three just mentioned, may be producing disturbances of lesser extent.

Transitions between terms built on different states of the ion are "double electron jumps" and do not occur unless there is some form of coupling which makes possible such a simultaneous change. Such coupling is described as a mutual perturbation of two (or more) energy levels and can be accurately described only on the basis of wave mechanics.[13, 14, 15, 16] The necessary conditions for the occurrence of a perturbation

[12] A. G. Shenstone and H. N. Russell, Phys. Rev. **39**, 415 (1932).

[13] E. U. Condon, Phys. Rev. **36**, 1121 (1930).
[14] S. Goudsmit and L. Gropper, Phys. Rev. **38**, 225 (1931).
[15] N. G. Whitelaw, Phys. Rev. **44**, 544 (1933).
[16] J. H. Van Vleck and N. G. Whitelaw, Phys. Rev. **44**, 551 (1933).

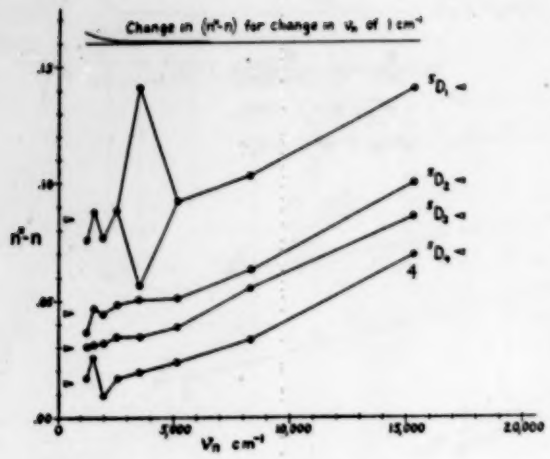

FIG. 3. Series in Se I.

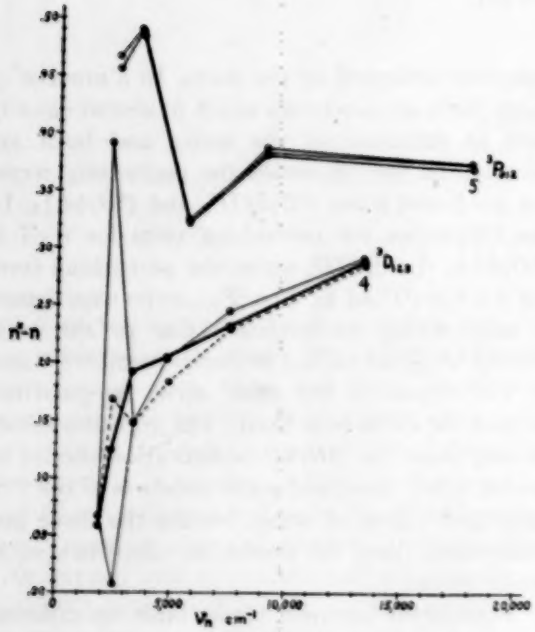

FIG. 4. Series in Se I.

between two terms in the case of LS coupling have been given by Shenstone and Russell[12] and are that they shall have parity (both odd or both even), the same J, the same L, and the same S, and generally the closer the terms the greater is the effect. However, it has been shown by Whitelaw[13] that closeness is not a necessary condition for a large effect. In selenium the coupling is not good LS and the perturbation conditions are relaxed in regard to equality of L's and S's.

In addition to the effect on the combining properties, perturbations also cause shifts in the terms involved as if there was a repulsion between them. It is to this effect that the anomalous positions of terms and partial inversions of multiplets, which are so common in selenium, are ascribed. In most cases the absolute magnitude of the displacement of a term is small and no near neighbor of the right type is at hand to accept the blame. In many cases there are undoubtedly more than two terms entering into a perturbation.

It is here suggested that the combination of the $(^4S)nf\ ^5F$ and ^3F terms with the $(^2D)5s\ ^3D$ and ^1D terms is due to perturbations of the latter by the $(^4S)4d\ ^5D$ and ^3D terms. The arc spectrum of sulfur exhibits the same peculiarities as that of selenium, and in particular the terms $(^4S)nf\ ^5F$ and ^3F were found to combine with the $(^2D)5s\ ^3D$ terms, as designated by Frerichs.[17] In a later paper on sulfur Meissner, Bartelt and Eckstein[18] objected to the $s\rightarrow f$ electron transition and interchanged the terms $(^2D)5s\ ^3D$ and $(^4S)4d\ ^3D$, although this gave the ^3D terms built on the single limit a considerably greater separation than those built on the double limit, and also seriously disturbed the agreement of the $(^2D)5s\ ^3D$ terms with their expected positions, as discussed by Ruedy.[4] We prefer the designations of Frerichs and the explanation involving perturbations, especially as the analogous alternative in selenium would lead to even greater discrepancies in separations and positions than it did in sulfur.

The terms due to the addition of the $5s$ electron to the (^2D) and (^2P) cores all combine strongly with the $4p^4$ levels. Each triplet has an outer separation somewhat smaller than its doublet limit separation and each singlet lies about the same distance above its corresponding triplet. The terms built on the (^2D) limit are also confirmed by other combinations. The $(^2P)5s\ ^3P_2$ term and the $(^4S)7s\ ^5S_2$ term perturb each other to such an extent as to make their individual designations nearly meaningless. The $(^2P)5s\ ^3P_{0,1}$ and $^1P_1$ terms show no other trustworthy com-

[17] R. Frerichs, Zeits. f. Physik **80**, 150 (1933).
[18] K. W. Meissner, O. Bartelt and E. Eckstein, Zeits. f. Physik **86**, 54 (1933).

binations but rely, for their identification, upon the considerations just stated and the fact that all the strong lines are thus accounted for.

Twelve levels are located in the neighborhood of the predicted positions for the $(^2D)5p$ terms, and their relative positions and combining properties, aided by certain of their perturbation effects, seem to justify the assignment of definite L and S values. Just three of these terms combine strongly with the $(^2D)5s\ ^1D_2$ and $(^4S)4d\ ^5D_2$ terms which are evidently perturbing one another. They are accordingly called the singlets, and the J selection rule permits but one possible designation for them. The three levels $(^2D)5p\ ^3P_{012}$ are unquestionably responsible for the great perturbation of the $(^4S)np\ ^3P_{012}$ series. It is not necessary that the levels with $J=1$ and 2 should be ^3P's but the term with $J=0$ is unique and otherwise to form a ^3P multiplet would spread it and the other multiplets in a much more erratic manner. Also the magnitude of the perturbations due to these three levels are nearly the same and are all much greater than any of the other perturbations observed. This is very reasonably explained on the basis that, although the equality of L's and S's of perturbing terms is not a necessity, such equality is conducive to a larger effect than would otherwise be the case. The level with $J=4$ is also unique, and the remaining triplet terms can be unambiguously designated from their combining intensities.

Four of the group of eighteen terms due to the configuration $(^2D)4d$ have been observed, and three of them show intimate sharing of their configurations with certain $(^4S)ns$ and nd terms. It is possible to assign only J values to these. Without such perturbations none of these terms would combine with any of those built on the

TABLE II. *Se I terms.*

$4s^2$ $3d^{10}$ $4p^3$	$4p$	$^3P_2$: 78658.22 $^3P_1$: 76668.73 $^3P_0$: 76123.87	$^1D_2$: 69082.14	$^1S_0$: 56212.19							
		Limit $^4S_{3/2}$: 0	Limit $^3D_{3/2}$: −13164 $^3D_{1/2}$: −13780	Limit $^2P_{1/2}$: −23032 $^2P_{3/2}$: −23890		Limit $^4S_{3/2}$: 0		Limit $^4S_{3/2}$: 0		Limit $^4S_{3/2}$: 0
	$5s$	$^5S_2$: 30476.03 $^3S_1$: 27661.29	$^3D_1$: 16976.91 $^3D_2$: 16829.70 $^3D_3$: 16410.60 $^1D_2$: 15178.91	$^3P_0$: 7663.2 $^3P_1$: 7458.6 $^3P_2$: 6999.20(1) $^1P_1$: 6089.66	$6s$	$^5S_2$: 12669.1 $^3S_1$: 12035.1	$8s$	$^5S_2$: 4448.16(2) $^3S_1$: 4340.02	$8d$	$^5D_4$: 2529.44(4) $^5D_3$: — $^5D_2$: 2498.61 $^5D_1$: 2497.77 $^5D_0$: 2497.27 $^3D_3$: 2496.63 $^3D_2$: 2441.94 $^3D_1$: 2409.53
	$5p$	$^5P_1$: 19415.34 $^5P_2$: 19370.31 $^5P_3$: 19266.84 $^3P_1$: 18035.85 $^3P_2$: 17980.76 $^3P_0$: 17962.15	$^5D_1$: 6802.13 $^5D_2$: 6230.91 $^3F_2$: 6039.93 $^3F_3$: 5941.60 $^3P_1$: 5792.01 $^3D_3$: 5627.29 $^3F_4$: 5404.12 $^1F_3$: 5394.19 $^3P_2$: 4624.16 $^3P_1$: 4574.65 $^3P_2$: 4566.12 $^1D_2$: 3348.34	—	$6p$	$^5P_1$: 9394.77 $^5P_2$: 9380.44 $^5P_3$: 9343.64 $^3P_1$: 9058.73 $^3P_2$: 9044.15 $^3P_0$: 9028.75	$6f$	$^3F_3$: 4425.75 $^3F_4$: 4423.64	$10s$	$^5S_2$: 2260.96 $^3S_1$: 2222.95
	$4d$	$^5D_4$: 15288.15 $^5D_3$: 15285.03 $^5D_2$: 15277.38 $^5D_1$: 15275.48 $^5D_0$: 15270.76 $^3D_3$: 13380.26 $^3D_2$: 13359.78 $^3D_1$: 13318.50	1_2: 4496.52(2) 2_1: 3399.73(3) 3_0: 2684.6 4_0: 2257.81(4) —	—	$5d$	$^5D_0$: — $^5D_1$: 8269.66 $^5D_2$: 8269.16 $^5D_3$: 8267.18 $^5D_4$: 8266.50 $^3D_1$: 7561.98 $^3D_2$: 7551.97 $^3D_3$: 7503.26	$8p$	$^5P_1$: 3709.99 $^5P_2$: 3706.30 $^5P_3$: 3697.92 $^3P_0$: 3520.33 $^3P_1$: 3515.90 $^3P_2$: 3511.51	$8f$	$^3F_3$: 2254.54 $^3F_4$: 2253.33
					$7s$	$^5S_2$: 7019.94(1) $^3S_1$: 6767.89	$7d$	$^5D_0$: — $^5D_1$: 3504.10(3) $^5D_2$: 3462.45 $^5D_3$: 3462.5 $^5D_4$: 3461.19 $^3D_1$: 3346.22 $^3D_2$: 3345.38 $^3D_3$: 3293.30	$9d$	$^5D_0$: — $^5D_1$: 1891.64 $^5D_2$: 1890.83 $^5D_3$: 1887.81 $^5D_4$: 1886.48 $^3D_1$: 1880.57 $^3D_2$: 1876.37 $^3D_3$: 1874.88
					$7p$	$^3P_0$: 5616.17 $^3P_1$: 5615.18 $^3P_2$: 5605.67 $^5P_1$: 5574.99 $^5P_2$: 5563.80 $^5P_3$: 5557.02	$9s$	$^5S_2$: 3084.08 $^3S_1$: 3020.10	$11s$	$^5S_2$: 1728.54
							$7f$	$^3F_3$: 3070.97 $^3F_4$: 3069.30	$9f$	$^3F_4$: 1724.97
					$6d$	$^5D_0$: — $^5D_1$: 5116.80 $^5D_2$: 5114.54 $^5D_3$: 5110.66 $^5D_4$: 5110.5 $^3D_2$: 4838.23 $^3D_3$: 4797.54 $^3D_1$: 4794.34	$9p$	$^5P_1$: 2644.29 $^5P_2$: 2641.58 $^5P_3$: 2636.70 $^5P_0$: — $^3P_1$: 2553.69 $^3P_2$: 2544.86	$10d$	$^5D_0$: — $^5D_1$: 1474.74 $^5D_2$: 1474.43 $^5D_3$: 1474.13 $^5D_4$: 1471.43
									$10f$	^4F: 1362.24
									$11d$	$^5D_0$: — $^5D_1$: 1186.7 $^5D_2$: 1184.52 $^5D_4$: 1184.04
									$11f$	^4F: 1102.81

(^4S) limit, and their possible combinations with other terms built on the same limit lie at too long wave-lengths to be photographed. The combinations that are observed are all relatively weak, and although some of the unclassified lines are probably due to other terms of this configuration, it is not possible to identify them at present.

Two lines are observed having wave numbers agreeing with the differences of certain $4p^4$ terms; namely, $^1D_2-{}^1S_0$ and $^3P_1-{}^1S_0$. The former of these fits equally well as a $(^4S)5p\,{}^3P_2-(^4S)6d\,{}^5D_3$ intercombination, several other lines of which are also found, and this seems to be the more reasonable assignment. The latter, however, has no other place in the present term scheme except as this transition.

Table II contains all the known Se I terms with their numerical values referred to the ^4S state of the ion as zero. Those terms which are known to perturb each other are listed under their predominating configurations and with a common number in the parentheses to show the sharing configuration of each.

NOVEMBER 15, 1934 PHYSICAL REVIEW VOLUME 46

The Paschen-Back Effect. II. *JJ*-Coupling (approx.)

J. B. GREEN AND R. A. LORING,* *Mendenhall Laboratory of Physics*

(Received September 24, 1934)

The Paschen-Back effect of four pairs of *mercury* lines, λλ5789–90, 3662–63, 3131-32 and 2967–68, have been measured. The results have been found to be in good agreement with Houston's theory, both as to position and intensities of components. *The red shift* of the central component of λ5790 was studied in greater detail at several field strengths and was found to be practically proportional to the square of the field strengths. *The Zeeman effect* of several other mercury lines was also measured, and the *g*-values calculated from them were slightly different from the normal *g*-values, but are in general accord with the values calculated from perturbation theory.

IN a previous communication,[1] the incomplete Paschen-Back effect of the Zn and Cd $^3P^3D$ multiplet was discussed. The agreement between Darwin's[2] calculations and experiment were very satisfactory. In Darwin's work, the effect of electrostatic interaction between the two electrons was neglected, so that the results could be expected to be satisfactory only for *LS*-coupling. The $sd\,{}^3D$ and $sd\,{}^1D$ terms of both Zn and Cd are sufficiently separated so that this approximation was valid. But in the case of Hg, the $6s4d\,{}^3D_1$ and $^1D_2$ are only 3 cm^{-1} apart, and in even moderately strong magnetic fields perturbing effects become quite large. Four groups of lines involving these two levels and the $6s6p\,{}^3P$ and ^1P levels, namely λλ5789–90, 3662–3, 3131–32, and 2967–68, were studied, with a view to comparing the experimental results with the theory of singlets and triplets developed by Houston.[3]

Houston has calculated the matrix elements of the interaction of two electrons (one an *s*-electorn) with an external magnetic field and has completed the calculations for weak fields, i.e., to first order terms. In our work we found that this method would not be sufficiently accurate even for our weakest fields, so that it was necessary to use the complete secular determinant of Houston and not to neglect the second and third order terms.

If $\psi=a_1\varphi_1+a_2\varphi_2+a_3\varphi_3+a_4\varphi_4$ be the zero-order approximation of the wave function where

* Assistant Professor of Physics, University of Louisville, Louisville, Ky.

[1] Green and Gray, Phys. Rev. **45**, 273 (1934).

[2] Darwin, Proc. Roy. Soc. **A115**, 1 (1927).

[3] Houston, Phys. Rev. **33**, 297 (1929).

$$\varphi_1 = A/\{2[(l-m)!][(l+m)!]\}\{P_l^m(2)+P_l^m(1)\}\{S_\alpha(1)S_\beta(2)-S_\beta(1)S_\alpha(2)\},$$
$$\varphi_2 = A/\{2[(l-m+1)!][(l+m-1)!]\}\{P_l^{m-1}(2)-P_l^{m-1}(1)\}S_\alpha(1)S_\alpha(2),$$
$$\varphi_3 = A/\{2[(l-m)!][(l+m)!]\}\{P_l^m(2)-P_l^m(1)\}\{S_\alpha(1)S_\beta(2)+S_\beta(1)S_\alpha(2)\},$$
$$\varphi_4 = A/\{2[(l-m-1)!][(l+m)!]\}\{P_l^{m+1}(2)-P_l^{m+1}(1)\}S_\beta(1)S_\beta(2),$$

the first part of the product being a function of the coordinates of the two electrons, and the second part a function of the spin. A is a function of l alone.

The secular equation then takes the form

$$\begin{vmatrix} X+\omega m-E & -2^{-\frac{1}{2}}[(l+m)(l-m+1)]^{\frac{1}{2}} & -m & 2^{-\frac{1}{2}}[(l-m)(l+m+1)]^{\frac{1}{2}} \\ -2^{-\frac{1}{2}}[(l+m)(l-m+1)]^{\frac{1}{2}} & \{\omega(m+1)+m-1-E\} & -2^{-\frac{1}{2}}[(l+m)(l-m+1)]^{\frac{1}{2}} & 0 \\ -m & -2^{-\frac{1}{2}}[(l+m)(l-m+1)]^{\frac{1}{2}} & \omega m-E & -2^{-\frac{1}{2}}[(l-m)(l+m+1)]^{\frac{1}{2}} \\ 2^{-\frac{1}{2}}[(l-m)(l+m+1)]^{\frac{1}{2}} & 0 & -2^{-\frac{1}{2}}[(l-m)(l+m+1)]^{\frac{1}{2}} & \{\omega(m-1)-m-1-E\} \end{vmatrix} = 0,$$

the four solutions (in general) of E giving the positions of the energy levels in the magnetic field. When $|m| = l+1$ the determinant reduces to a single diagonal element, for then only φ_2 has a meaning, and when $|m| = l$ to a third-order determinant, for then φ_4 has no meaning. The values of E put into the original equations then serve to determine the relations between the a's, from which the intensities of the transitions may be calculated.

If these computations are carried out, the intensities of the different transitions are

$l \to l-1, \quad m \to m-1$ (perpendicular polarization)

$$I \sim B\{a_{1,\,l,\,m}a_{1,\,l-1,\,m-1}[(l+m)!]^{\frac{1}{2}}/[(l+m-2)!]^{\frac{1}{2}} + a_{2,\,l,\,m}a_{2,\,l-1,\,m-1}[(l+m-1)!)]^{\frac{1}{2}}/[(l+m-3)!]^{\frac{1}{2}} + a_{3,\,l,\,m}a_{3,\,l-1,\,m-1}[(l+m)!]^{\frac{1}{2}}/[(l+m-2)!]^{\frac{1}{2}} + a_{4,\,l,\,m}a_{4,\,l-1,\,m-1}[(l+m+1)!]^{\frac{1}{2}}/[(l+m-1)!]^{\frac{1}{2}}\}^2,$$

$l \to l-1, \quad m \to m+1$ (perpendicular polarization)

$$I \sim B\{a_{1,\,l,\,m}a_{1,\,l-1,\,m+1}[(l-m)!]^{\frac{1}{2}}/[(l-m-2)!]^{\frac{1}{2}} + a_{2,\,l,\,m}a_{2,\,l-1,\,m+1}[(l-m+1)!]^{\frac{1}{2}}/[(l-m-1)!]^{\frac{1}{2}} + a_{3,\,l,\,m}a_{3,\,l-1,\,m+1}[(l-m)!]^{\frac{1}{2}}/[(l-m-2)!]^{\frac{1}{2}} + a_{4,\,l,\,m}a_{4,\,l-1,\,m+1}[(l-m-1)!]^{\frac{1}{2}}/[(l-m-3)!]^{\frac{1}{2}}\}^2,$$

$l \to l-1, \quad m \to m$ (parallel polarization)

$$I \sim 4B\{a_{1,\,l,\,m}a_{1,\,l-1,\,m}[(l+m)!]^{\frac{1}{2}}[(l-m)!]^{\frac{1}{2}}/[(l+m-1)!]^{\frac{1}{2}}[(l-m-1)!]^{\frac{1}{2}} + a_{2,\,l,\,m}a_{2,\,l-1,\,m}[(l+m-1)!]^{\frac{1}{2}}[(l-m+1)!]^{\frac{1}{2}}/[(l+m-2)!]^{\frac{1}{2}}[(l-m)!]^{\frac{1}{2}} + a_{3,\,l,\,m}a_{3,\,l-1,\,m}[(l+m)!]^{\frac{1}{2}}[(l-m)!]^{\frac{1}{2}}/[(l+m-1)!]^{\frac{1}{2}}[(l-m-1)!]^{\frac{1}{2}} + a_{4,\,l,\,m}a_{4,\,l-1,\,m}[(l+m+1)!]^{\frac{1}{2}}[(l-m-1)!]^{\frac{1}{2}}/[(l+m)!]^{\frac{1}{2}}[(l-m-2)!]^{\frac{1}{2}}\}^2,$$

B is a function of l alone and need not be used when considering relative intensities.

$\lambda\lambda$5789–90. This investigation was begun as a result of some correspondence with Professor Condon regarding the red shift of the central component of the 5790 line ($^1P_1 - {}^1D_2$). Previous workers[4, 5, 6] had found that this shift was proportional to the square of the magnetic field, and Gmelin[4] in an exhaustive investigation studied the behavior of the 5789 line ($^1P_1 - {}^3D_1$) also. Our measurements on these two lines soon showed that a second-order perturbation calculation was not sufficient to explain the anomalies observed in their behavior. Such a calculation leads one to expect a smaller effect for the perpendicular than for the parallel components of 5790, while actu-

[4] Gmelin, Phys. Zeits. **9**, 212 (1908); **11**, 1193 (1910).
[5] Zeeman, Proc. Amst. Acad. Sci. **10**, 351 (1907).
[6] Risco, Phys. Zeits. **13**, 137 (1912).

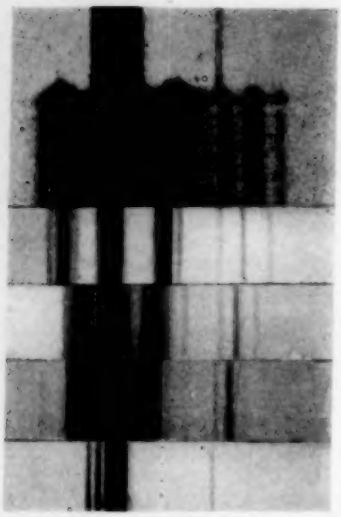

FIG. 1. λλ5789–90 at different field strengths. Hg 5789 +5790. (a) no field; (b) 34,700 gauss; (c) 29,800 gauss; (d) 21,670 gauss; (e) 16,860 gauss; (f) no field.*

ally the short-wave perpendicular component splits at about 18,000 gauss (see Fig. 1).

The behavior of these two lines in the magnetic field is very interesting, although one must be very careful in any investigation of the lines of mercury. All of these lines are contaminated by the presence of hyperfine structure, and care must be taken to avoid confusion of these components with Zeeman components of the even isotopes, which show no hyperfine structure. This can only be done by taking a sequence of photographs at varying field strength and noting the positions of the lines. The effect is shown clearly in Fig. 1. The two faint lines, one on each side of the long wave component, are clearly lines due to hyperfine structure. We are concerned here only with the even isotopes and their behavior.

Fig. 2 is a typical photograph of λλ5789–90 and shows the Zeeman effect at about 29,600 gauss. The lowest picture is a 7X enlargement of the second order (about 0.51 A/mm on the original negative), the middle picture the theoretical positions and intensities of the lines, and the top picture a microphotogram of the bottom picture, made by a Moll microphotometer.

If the classification of λ5790 were $^1P_1-{}^1D_2$ in strictly *LS*-coupling we should expect the pattern to be a normal triplet, but both the ^1P and ^1D levels are perturbed and the *g*-values are

FIG. 2. λλ5789–90, Field strength about 30,000 gauss.

different from unity, resulting in a splitting of each of the components into three, which is first manifested in the doubling of the component marked "*c*" in Fig. 2, beginning to be visible at about 20,000 gauss. This has not been noticed by other observers. Another evidence that ^1D has acquired some "triplet" character is shown by the fact that it exhibits a Paschen-Back effect. The central component "*b*" shifts toward the red with increasing field, while the parallel (usually forbidden component, for $\Delta J=0$, $m=0\rightarrow m=0$) component "*d*" of λ5789 shifts to the violet. The amount of this red shift of 5790 is shown graphi-

* In all figures, the wave-length increases from right to left.

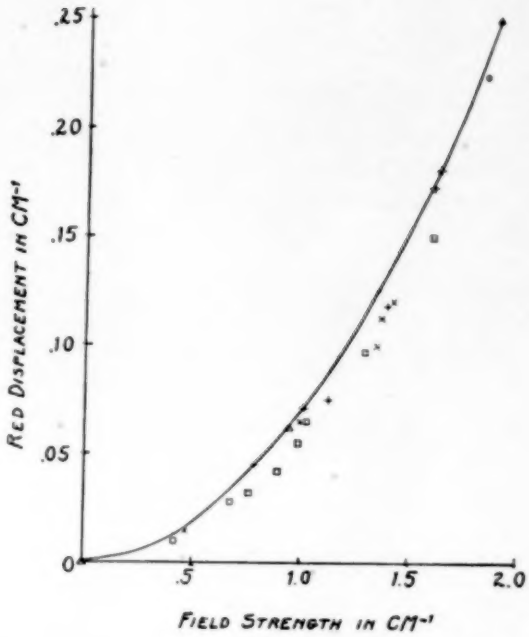

FIG. 3. Curve showing relation between red shift of central component of λ5790 and field strength. Triangle, theoretical points. The solid line is a theoretical curve. Plus, present experiment. Measured as displacement with respect to 5770. Circle, direct displacement measurement. Square, Gmelin's measurements. Cross, Risco's measurements. 1 cm^{-1} = 21,200 gauss.

cally in Fig. 3, together with the results of other observers. It was not possible to measure this shift directly by displacement from known iron lines, for the plate always seemed to be jarred when introducing comparison spectra. The shifts are therefore measured with reference to the central component of 5770, which did not seem to be disturbed. Gmelin and Rosco measured this displacement as half the dissymmetry of the pattern. Their results should therefore be lower than ours, because they were unable to resolve the short wave component, the outside edge of which behaves practically normally. The full curve is calculated theoretically from Eqs. (1) and (2) using the value $X = -\frac{1}{2}$ for the $^1D\,^3D$ electrostatic parameter. The results of all the observers are seen to be within experimental error, the largest observable shift being only 0.074A. The curve is practically parabolic, indicating a variation with H^2, although it eases off at the strongest field.

The line 5789 is represented by components *d*, *e*, *f* which are spaced at about half-normal distances. "*d*" is polarized parallel, "*f*" perpendicular, and "*e*" is unpolarized. This was interpreted by Gmelin as a new type of Zeeman pattern, and it is indeed confusing without the aid of the theory. The pattern should consist of two other lines disposed symmetrically about "*d*" as "*e*" and "*f*" are, but the calculated intensities of these

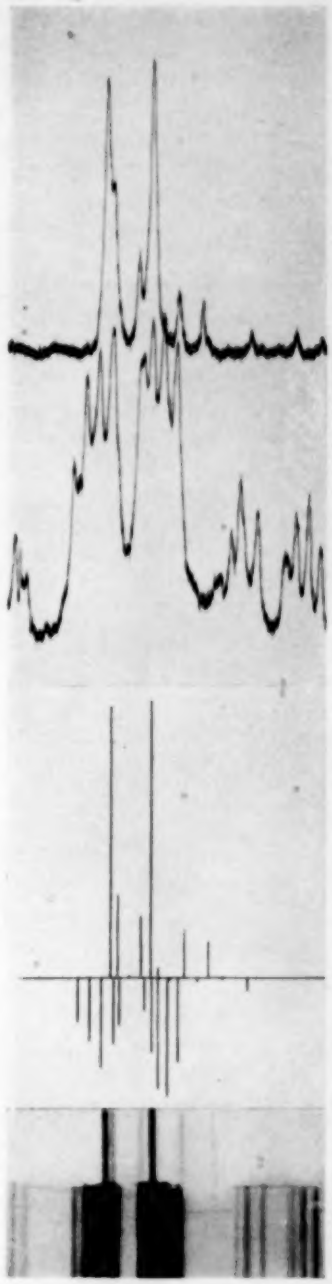

FIG. 4. λλ3662–63 at about 34,000 gauss.

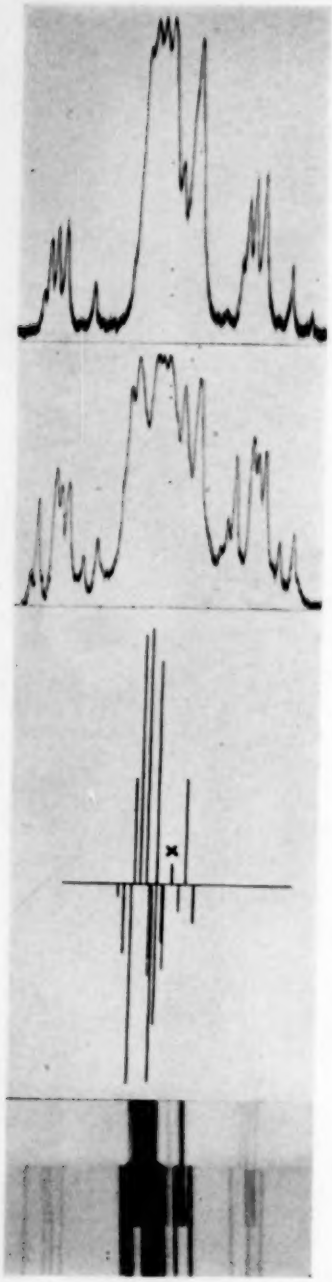

FIG. 5. λλ3131–32 at about 34,000 gauss.

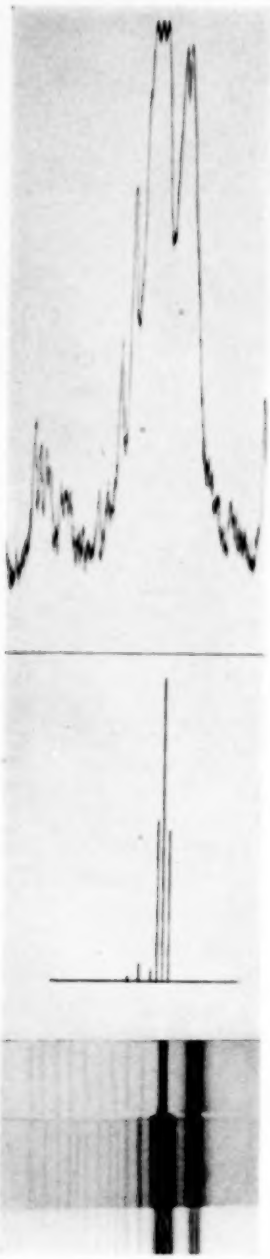

FIG. 6. λλ2967–68 at about 34,000 gauss.

lines are far below observable intensity. One of these lines is shown on the middle picture as a stub beside component "*c*." The agreement between theory and experiment is very satisfactory.

λλ3662–3 ($^3P_2-{}^3D_1$ and $^3P_2-{}^1D_2$)

The asymmetries introduced by the perturbations are clearly seen in Fig. 4. Here the polarizations have been separated, the parallel above and the perpendicular below, in all three pictures. The two lines are badly overlapped in the perpendicular components, only one line of λ3662 showing on the short wave side, and that is mixed in with the Rowland ghost of λ3663. Two components on the long wave side almost coincide with two components of λ3663 and show these components

as doublets, visible in the photograph but not so clear in the microphotogram. Here again, the agreement is quite satisfactory.

3131–32 ($^3P_1-^3D_1$ and $^3P_1-^1D_2$)

The polarizations here have been separated as in the previous figure. Fig. 5 shows very satisfactory agreement. The component marked "x" is a usually "forbidden" component ($\Delta J=0$, $m=0\rightarrow m=0$), but it appears here with quite appreciable intensity.

2967–68 ($^3P_0-^3D_1$ and $^3P_0-^1D_2$)

Fig. 6 shows the structure of these lines. λ2968 is a transition that is usually "forbidden" ($\Delta J=2$) but is quite strong in the figure. Two different degrees of contrast are shown, together with a reversed iron line which shows the behavior of the microphotometer. The agreement is very satisfactory.

Zeeman Effects of Other Hg Lines

The Zeeman effects of several other mercury lines were also measured. The apparatus used was essentially the same as previously described[7] except that the edge of the rotating disk was kept supplied with Hg by rolling through a trough containing Hg placed on the bottom of the vacuum chamber.

The lines measured were as follows:

5770	$^1P_1-^3D_2$	$(\bar{0})$ (0.094) —— —— $\overline{1.213}$
5461	$^3P_2-^3S_1$	$(\bar{0})$ (0.504) $\overline{0.999}$ 1.508 2.010
4358	$^3P_1-^3S_1$	(0.518) 1.481 2.001
3650	$^3P_2-^3D_3$	$(\bar{0})$ (0.170) (0.345) $\overline{1.001}$ 1.177 1.346 1.507
3654	$^3P_2-^3D_2$	(—) $(\overline{0.771})$ 0.718 $\overline{1.109}$ $\overline{1.494}$ 1.877
3125	$^3P_1-^3D_2$	$(\bar{0})$ (0.372) $\overline{0.729}$ 1.092 1.455
4916	$^1P_1-^1S_0$	(0) 1.013

yielding the following g-values.

					LS	Houston
$^3S_1$	2.000	2.007	Ave. = 2.003		2.000	2.000
$^1P_1$	1.025	1.013	Ave. = 1.019	Sum 2.498	1.000	1.018
$^3P_1$	1.482	1.473	Ave. = 1.479		1.500	1.482
$^3P_2$	1.512	1.495 1.503	Ave. = 1.503		1.500	1.500
$^3D_3$	1.342		Ave. = 1.342		1.333	1.333
$^3D_2$	1.109	1.119 1.101	Ave. = 1.109		1.167	1.091

If we calculate the g-values of $^1P_1$ and $^3P_1$ from Houston's formula we get $g(^1P_1)=1.018$ and $g(^3P_1)=1.482$ while the calculated g-values of $^1D_2$ and $^3D_2$ using $X=-\frac{1}{2}$ are $g(^1D_2)=1.076$ and $g(^3D_2)=1.091$.

The measuring of these lines were complicated, as mentioned, by the presence of hyperfine structure components, but in the case of lines above λ4000 these components were readily separable from the main lines, which were very much stronger. The ultraviolet lines were not so easily separated from their hyperfine structure and the results for these lines are consequently less accurate.

The measurements listed show an accuracy of 1/2 percent to 1 percent, and the authors believe, from much experience, that any attempt to list field-strength data based on Zeeman-effect measurements with a greater degree of accuracy than this is futile. Several authors have used the Zeeman effect of the mercury lines in the calculation of field strengths, especially the line λ4358, which, even well within the limits expressed above, shows a marked perturbation from the L–S pattern $\frac{(1)\ 3\ 4}{2}$.

[7] Green and Loring, Phys. Rev. **43**, 459 (1933).

The Relative Abundance of the Isotopes of Lithium, Potassium and Rubidium

A. KEITH BREWER AND P. D. KUECK, *Bureau of Chemistry and Soils, Washington, D. C.*

(Received September 20, 1934)

The abundance ratios of the isotopes of lithium, potassium and rubidium have been measured with a Dempster type mass spectrograph. Artificial aluminum silicates of these alkalis were used as the source of ions. An abundance ratio of 12.14 ± 0.4 was obtained for Li^7/Li^6. On the basis of this ratio the masses of the two isotopes are 7.016 ± 0.002 and 6.016 ± 0.002 and the packing fractions are 23 ± 3 and 26 ± 3, respectively. The observed abundance ratio for potassium is $K^{39}/K^{41}=13.88\pm0.4$. This value gives 38.96 ±0.003 and 40.96 ± 0.003 for the masses of the two isotopes, and -9.85 ± 0.9 and -9.37 ± 0.9 for their respective packing fractions. A ratio of $Rb^{85}/Rb^{87}=2.59\pm0.04$ was obtained for rubidium. On the basis of 85.44 for the atomic weight the masses of the isotopes come out to be 84.88 and 86.88 while the corresponding packing fractions are -14.1 ±0.7 and -13.8 ± 0.7. The values for the packing fractions given above fall fairly closely on the packing fraction *vs.* mass number curve given by Aston for lithium and potassium but are about 70 percent low for rubidium.

THE reports in the literature of the relative abundance of the isotopes of lithium and potassium differ widely, not only for various methods of measurement but between different investigators. In the case of lithium for mass-spectrographic measurements Harnwell and Bleakney[1] obtained a ratio for $Li^7/Li^6=8.4$, Bainbridge[2] gives 11.28 as the most probable value, Morand[3] found 14.9, while Dempster[4] obtained ratios ranging from 37.0 to 4.8 with an average value between 7 and 10. Using band spectra data, Wijkand and Koeveringe[5] found a ratio of 7.2 while Nakamura[6] obtained 8. Measurements of the abundance ratio of the potassium isotopes are limited. Dempster[4] observed a ratio of 18, while a published curve by Bainbridge[2] shows the ratio to be near 12.5. The best direct determination for rubidium is that of Aston[7, 8] who found $Rb^{85}/Rb^{87}=3$ as the most probable ratio.

The results for lithium, potassium and rubidium obtained with a Dempster type of mass-spectrograph are presented in the present paper.

APPARATUS

The spectrograph was made of brass with a 5 cm focusing radius. The analyzing chamber was designed for rapid evacuation. Various slit arrangements were tried, but the simple accelerating slit proved the most satisfactory. The slit openings were arranged to give flat topped peaks.

The resolved current was measured with an FP-54 Pliotron; the scale was checked for non-linearity by the application of known potentials after each series of runs.

In the case of lithium and potassium the filament aperature was a round hole, varying from time to time between 0.2 to 0.5 mm in diameter, located in the bottom center of a cup-shaped magnetic shield surrounding the filament. The slit in front of the Faraday cage was 1.5 mm wide and 5 mm long. The ion sources were artificially prepared aluminum silicates of the alkalies.[9] The filaments were of the short hairpin type with a straight section over the slit about 4 mm in length. The position of the filament was varied from 3 mm to 25 mm above the slit. Tests were made with and without a cylindrical shield 8 mm in diameter and 6.0 cm long surrounding the filament to concentrate the ion beam over the slit. When the shield was used the ion beam could be so focused that at 2.5 cm filament-slit separation the resolved current was one one-hundredth of the total ion current.

It was found necessary to change the slit arrangement slightly for a complete resolution of the rubidium isotopes. In this case the collector slit was 0.5 mm wide and 5 mm long, while the filament slit was 0.1 mm wide and 4 mm long. The filament, of the Hertz type, was a tungsten

[1] Harnwell and Bleakney, Phys. Rev. **45**, 117 (1934).
[2] K. T. Bainbridge, J. Frank. Inst. **212**, 317 (1931).
[3] Morand, Comptes rendus **182**, 460 (1926).
[4] Dempster, Phys. Rev. **18**, 415 (1921).
[5] Wijkand and Koeveringe, Proc. Roy. Soc. **A132**, 98 (1931).
[6] Nakamura, Nature **128**, 759 (1931).
[7] Aston, Proc. Roy. Soc. **A134**, 575 (1932).
[8] *Note:* For a general discussion see Aston, *Mass Spectra and Isotopes*, 1933 edition.
[9] Jones and Hendricks, Phys. Rev. **44**, 322 (1933).

hairpin on which a platinum disk 2 mm in diameter was spot-welded; the artificial rubidium aluminum silicate was coated on the disk.

The mass peaks were located by varying the field current of the magnet, the accelerating potential between the filament and slit being kept constant for each series of runs. Since the magnetic field could be varied through an appreciable range without changing the maximum of the resolved ion current the curves were all flat topped; values of these maximum currents therefore were taken as a measure of the relative abundance of the ions of the isotopes.

Results

A typical mass *vs.* abundance curve for lithium is shown in Fig. 1. The mass is plotted as a function of the magnetic field current.

It will be noted that the flat topped peaks eliminated the difficulty in setting on the maximum of the sharp pointed peaks generally obtained. The resolution, as shown by the curves, was sufficient for a complete separation of the peaks.

The deviations in the measurements for a single filament are shown in Table I. The results

Table I. *Abundance ratio Li^7/Li^6 obtained with a single filament.*

No. of run	Li^7/Li^6	Deviation
1	12.28	+0.07
2	12.24	+0.03
3	12.18	−0.03
4	12.14	−0.07
5	12.12	−0.09
Average	12.21	

in general do not show any trend with time. A set of runs on a given filament usually extended over a period of about an hour. Since slightly coated filaments were used the life of a filament for constant emissivity was not materially longer than this.

The ratios determined from four separate filaments are shown in Table II. *Va* is the accelerating potential, i_p the unresolved positive ion current, i_c the maximum resolved Li^7 currents to the collector, and n the number of tests made on each filament, average deviations are used in fixing the limit for the abundance ratio.

The data indicate a small trend towards higher

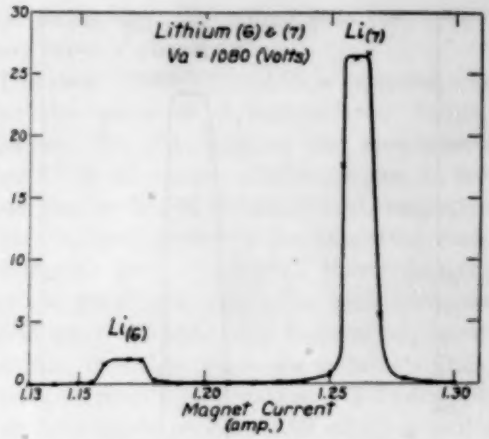

Fig. 1. Mass-spectrogram of lithium ions.

Table II. *Abundance ratio Li^7/Li^6 obtained with four different filaments.*

V_a (v.)	i_p (amp.)	i_c (amp.)	n	Li^7/Li^6
1080	5×10^{-8}	1.74×10^{-10}	5	12.21
1080	5×10^{-8}	1.7×10^{-10}	7	12.31
1080	3×10^{-8}	1.7×10^{-10}	7	11.36
1080	4.25×10^{-7}	9.0×10^{-10}	7	12.67
		Average		12.14±0.4

ratios for increasing positive ion currents but it is not felt that much significance can be placed on this trend.

A typical curve for the isotopes of potassium is shown in Fig. 2. In general the resolution was complete, the deflection returning close to zero between the peaks.

The average results from different filaments are shown in Table III. The third value was obtained from a special run made with a filament-slit separation of 3 mm and with no concentrating shield. The first two values were obtained with a separation of 2.5 cm The mass *vs.* abundance curves were identical in shape in both instances.

Table III. *Abundance ratio K^{39}/K^{41}.*

V_a (v.)	i_p (amp.)	n	K^{39}/K^{41}
450	1.1×10^{-8}	8	13.26
450	6.0×10^{-8}	9	14.16
540		1	14.22
		Average	13.88±0.4

A representative curve illustrating the separation of the isotopes of rubidium is shown in Fig. 3.

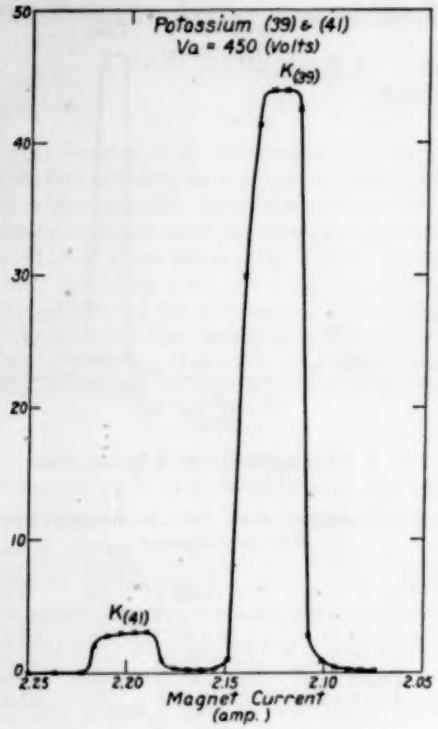

FIG. 2. Mass-spectrogram of potassium ions.

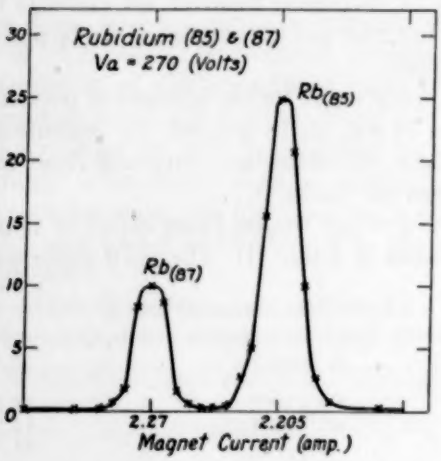

FIG. 3. Mass-spectrogram of rubidium ions.

The curves are flat topped for small changes in the magnetic current; the separation of the two isotopes is complete.

The results of a series of runs for several filaments are shown in Table IV. These values were taken with the position of the filament over the slit such that a maximum resolved current was obtained. The homogeneity of the primary ion beam was tested by measuring the isotope ratio when the filament was rotated to either side of the maximum; no change in the ratio was detected.

TABLE IV.

V_a (v.)	i_p (amp.)	i_e (amp.)	n	Rb^{85}/Rb^{87}
270	5×10^{-8}	1.85×10^{-10}	10	2.54 ± 0.04
"	"	2.31	4	$2.55\pm .02$
"	"	1.5	5	$2.65\pm .03$
"	"	1.5	5	$2.63\pm .03$
"	"	1.5	7	$2.59\pm .04$
			Average	2.59 ± 0.04

DISCUSSION OF RESULTS

An estimate of the abundance ratio from the ion emission ratio obtained in these experiments necessitates an understanding of the mechanism of diffusion of the alkali ions through the aluminum silicate. If perfect mixing takes place at the source, the movement of the alkali in the emitter will obey the laws of free diffusion; the ion ratio, therefore, must be corrected for the isotope effect in free evaporation by multiplying by the square root of the ratio of the heavy to the light isotope to give the abundance ratio. On the other hand, if the diffusion is of an electrolytic type in which the positive ions move step by step through a fixed negative ion lattice, the alkali ions in each underlying lattice layer moving up to take the place of those emitted, there will be no free diffusion effect and the ion ratio will represent the abundance ratio. It is impossible to state definitely which of the two mechanisms is correct, but the facts that the filaments were operated below the fusion temperature and that no change in the ion ratio could be detected throughout the entire life of the filament strongly support the latter alternative.

Assuming for lithium that the ion ratio represents the abundance ratio $Li^7/Li^6=12.14\pm0.4$ the mass of the isotopes on the basis of 6.94 for the atomic weight is $Li^7=7.016\pm0.002$ and $Li^6=6.016\pm0.002$. From these values the packing fraction expressed in parts per 10,000 is 26 ± 3 for Li^6 and 23 ± 3 for Li^7. Bainbridge,[10] measuring the mass of the isotopes directly, obtained

[10] K. T. Bainbridge, Phys. Rev. **44**, 56 (1933).

$Li^7 = 7.0146$ and $Li^6 = 6.0145$ on the basis of O^{16}. His values for the packing fraction, therefore, are $Li^7 = 20.85$ and $Li^6 = 24.2$. The two sets of data check each other fairly well, the agreement being within the experimental error in measuring the abundance ratio.

In the case of potassium the abundance ratio of 13.88 ± 0.4 is in fair agreement with 12.5 taken from the mass *vs.* abundance curve of Bainbridge, but is materially lower than the ratio of 18 found by Dempster and the value of 17.5 assumed by Aston (reference 8, p. 236). With 39.096 for the atomic weight of potassium this ratio gives 38.96 ± 0.003 and 40.96 ± 0.003 for the mass of the isotopes K^{39} and K^{41}, respectively, while the corresponding packing fractions come out to be 9.85 ± 0.9 and 9.37 ± 0.9. Since a small error in the abundance ratio necessarily makes a large error in the packing fraction it is significant that these values do not deviate from Aston's packing fraction-mass number curve (p. 167) by more than 20 percent; this is less than that found for many other elements.

The ratio $Rb^{85}/Rb^{87} = 2.59$ is materially lower than the value of 3 assigned by Aston for rubidium. On the basis of the atomic weight being 85.44 the masses of the isotopes 85 and 87 come out to be 84.88 and 86.88, respectively, while the corresponding packing fractions are -14.1 ± 0.7 and -13.8 ± 0.7. Aston has shown that the packing fractions for mass numbers 84 and 86 are -8.5 and -8.2, respectively; it seems probable, therefore, that the present values are in error. A packing fraction of -8.2 corresponds to an abundance ratio of 2.92 which is well outside the limits of experimental error in these experiments. While it does not seem possible to account for the discrepancy at this time, it is interesting to note that an abundance ratio of 2.59 ± 0.04 corresponds to an atomic weight for rubidium of 85.48 ± 0.005 in place of the accepted value of 85.44.

NOVEMBER 15, 1934 PHYSICAL REVIEW VOLUME 46

The Genesis of the Elements

GILBERT N. LEWIS, *Department of Chemistry, University of California*

(Received September 26, 1934)

The hypothesis is suggested that a great part of the matter in the universe is composed chiefly of iron and nickel, like the metallic meteors, and that such material, which is thermodynamically stable with respect to all spontaneous transmutations, except at extremely high temperatures, is superficially attacked by cosmic radiation to produce the material represented by the earth's crust and by the stony meteors. As a test of this hypothesis of the genesis of stony meteors from metallic meteors, a comparison is made of the relative abundance of the chief atomic species in the two types of meteors. The striking results of this comparison strongly indicate a genetic relationship. Three main disintegration processes to which the iron and nickel nuclei are subjected seem to be the splitting off of oxygen from these nuclei; the splitting of the nuclei into two identical parts; and the splitting of helium from the products of the preceding process.

IN spite of the extraordinarily interesting information regarding nuclear structure which is now coming week by week from experiments on atomic disintegration, it seemed to me that it might still be possible to extract useful information from the older data, especially those related to the relative abundance of the elements. It was Harkins[1] who first called attention to the striking connection between the atomic weights of the elements and their abundance, not only in the earth's crust, but in the meteors. For the latter he made use of analyses collected by Farrington[2] for hundreds of meteors of the stony and of the metallic type. These results, and Aston's[3] data concerning the relative abundance of isotopes, form the basis of this paper.

[1] Harkins, J. Am. Chem. Soc. **39**, 856 (1917).

[2] Farrington, Publications 120 and 151, Field Columbian Museum, Chicago.

[3] Aston, *Mass-Spectra and Isotopes*, Longmans, Green and Co., New York, 1933.

Important cosmological inferences have been drawn from the study of radioactivity. By such means it has been shown that some of our oldest terrestrial rocks have remained undisturbed for 3×10^9 years. However, if we assume that the solar system has remained in approximately its present state for one hundred times that period, the origin of radioactive materials becomes perplexing; for I once pointed out,[4] as I presume others have, that, even if at the beginning of such a period the whole solar system had been composed of pure uranium, there would now be not so much left as is known to exist in the earth's crust. In the same paper I pointed out that it is impossible to ascribe to the sun a high enough internal temperature to cause the reversal of the main radioactive processes and the synthesis of uranium. It does not help to assume that uranium is itself produced by the radioactive decomposition of some other element, because if it had a longer life it would now be present in greater amount than the uranium itself. It therefore appeared that the parent radioactive substances have been produced upon the earth, and presumably are now being produced, as fast as they are being consumed. I concluded therefore that radioactive substances are being produced in the earth's crust by some sort of radiation of extremely high energy and of extra-terrestrial origin.

It has long been a favorite theory among petrologists[5] that the interior of the earth is a metallic mass with a composition something like that of a nickel-steel. This hypothesis, first suggested perhaps by the earth's magnetic behavior, receives more support from the very high density of the earth and from the existence of metallic meteors, which, on the average, contain 90.6 percent of iron, 8.5 percent of nickel, 0.6 percent of cobalt, and only 0.3 percent of all other elements.

This composition of the metallic meteors is extremely suggestive when we examine the exact values of atomic weights obtained by the method of positive rays. It is well known that the departure of atomic weights from the integral relationship expressed in Prout's hypothesis may be used, as we use ordinary thermo-chemical data, to determine whether a process of transmutation is possible from the standpoint of energetics. The packing fractions of the elements given by Aston, incomplete though they are, show a definite minimum in the neighborhood of the iron group. Therefore if all processes of transmutation were rapid, and governed only by our simplest conservation rules, all other elements would be converted into a few elements of the iron group.

Let us imagine that the earth, and indeed all celestial bodies, except perhaps those which reach the very highest temperatures, are composed chiefly of the elements that we find in metallic meteors, but that each has a superficial crust caused by radiation, consisting of the known cosmic rays, and probably much harder rays which are only occasionally detected in the so-called "bursts." We may suppose that this radiation breaks the iron and nickel nuclei into fragments, some of which constitute the lighter elements, and some of which combine rarely to form the less abundant heavy elements.

So far we have a hypothesis which, plausible though it may be, is unsupported by any direct evidence. Recently it occurred to me that if the crust of the earth, and especially if the stony meteors, are representative of the material produced by the disintegration of the primal substance of the metallic meteors, then there should be discernible some immediate genetic relationship between the abundance of the main atomic species of the stony meteors and of the metallic meteors. Such a comparison leads at once to results of a most striking character. However, before presenting the data it should be pointed out that the earth's crust is constantly losing some of its volatile constituents. This is especially true of the stony meteors, which can hold no volatile substances except such as are occluded in the minerals.

According to the analyses of 318 iron meteors presented by Farrington, the two isotopes of iron and the two isotopes of nickel constitute over 99 percent (atomic percent). These four isotopes, using the modern symbols which show the atomic number at the lower left and the

---

[4] Lewis, *The Chemistry of the Stars and the Evolution of Radioactive Substances*, Publ. Astron. Soc. Pacific **34**, 309 (1922).

[5] See, for example, Goldschmidt, *The Distribution of Chemical Elements*, Nature **124**, 15 (1928).

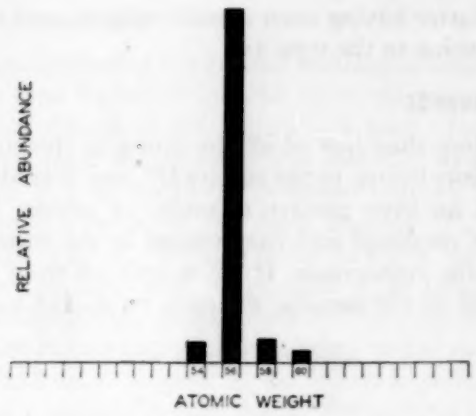

FIG. 1. Relative abundance of the major constituents of metallic meteors.

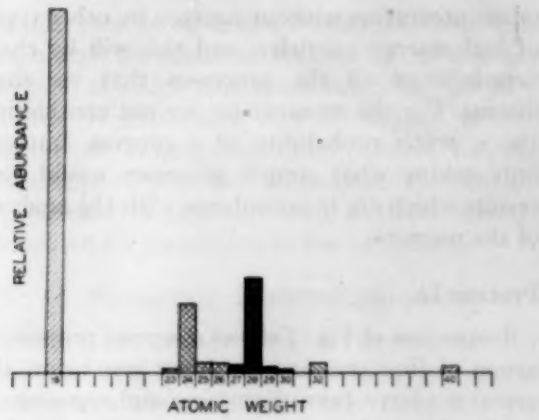

FIG. 2. Relative abundance of the major constituents of stony meteors.

atomic weight at the upper right, are $_{26}Fe^{54}$, $_{26}Fe^{56}$, $_{28}Ni^{58}$, $_{28}Ni^{60}$. Fig. 1 shows, in the average metallic meteors, the relative abundance of these four atomic species plotted against the atomic weight.

If these four atomic species are nearly equally affected by some one type of disintegration, we should expect similar groups of four atomic species to appear in the products of the disintegration. Such a process might split a nucleus of iron or nickel into one light and one heavy nucleus, or into two nearly equal nuclei. Let us consider first the symmetrical splitting into two nuclei having just one-half the charge and one-half the weight of the parent nucleus.

Process I

We thus have the four reactions

$$_{28}Ni^{60} = 2\ {}_{14}Si^{30},$$

$$_{28}Ni^{58} = 2\ {}_{14}Si^{29},$$

$$_{26}Fe^{56} = (2\ {}_{13}Al^{28}) = 2\ {}_{14}Si^{28} + 2\beta,$$

$$_{26}Fe^{54} = 2\ {}_{13}Al^{27}.$$

Three of the four immediate products of this splitting we recognize as known and important atomic species, but $_{13}Al^{28}$ does not conform to a rule which has been found universal in all elements beyond the eighth, namely, the rule that a stable isotope of odd atomic number does not have an even atomic weight. When such an isotope is formed in radioactive processes it has a short life and undergoes a beta-ray decomposition. I therefore assumed at the outset that $_{13}Al^{28}$ emits a beta-particle to give $_{14}Si^{28}$. That this assumption was correct has just been shown by Professor Lawrence and his collaborators, who have produced this very isotope and find that it is radioactive and emits negative electrons.

Except for about eleven percent of iron and nickel still remaining in the stony meteors, Fig. 2 shows the relative abundance of all the atomic species which are present in the stony meteors to a greater extent than 0.13 percent, and which, taken together, constitute over 99.5 percent of these bodies. In that figure the four products of Process I are shown in black and obviously constitute one of the most important groups in the stony meteors. Moreover, their relative abundance, with the possible exception of the last one (Al), is, within the limits of experimental knowledge, the same as that of their parent substances.

This group alone not only affords strong evidence of a genetic relationship between the species of nickel and iron and those of silicon and aluminum, but it offers some confirmation of our view as to the direction of the genesis. If, instead of the process we have assumed, the heavier elements had been built up from the lighter ones, we see no reason why $_{14}Si^{28}$ should not form $_{28}Ni^{56}$ rather than $_{26}Fe^{56}$.

The equations that we have written for Process I imply either disintegration by a photon

or disintegration without capture by other types of high energy particles, and this will be characteristic of all the processes that we shall discuss. For the moment we are not considering the *a priori* probability of a process, but are only asking what simple processes would give results which are in accordance with the analysis of the meteors.

Process IA

Inspection of Fig. 2 shows a second prominent group of four constituents lying just below the group we have been discussing and represented in the figure by cross hatching. The simplest interpretation of this group is that the four products of Process I are in turn disintegrated by cosmic radiation according to the following scheme.

$$_{14}Si^{30} = {}_{12}Mg^{26} + {}_{2}He^{4},$$

$$_{14}Si^{29} = {}_{12}Mg^{25} + {}_{2}He^{4},$$

$$_{14}Si^{28} = {}_{12}Mg^{24} + {}_{2}He^{4},$$

$$_{13}Al^{27} = {}_{11}Na^{23} + {}_{2}He^{4}.$$

Here also we see a rough quantitative relationship between the abundance of the members of this group, IA, and of corresponding members of group I. We could hardly expect more, since other processes will be considered which may also produce small amounts of both magnesium and silicon. The similarity that exists between the two groups, and the fact that they together constitute eight of the eleven major constituents of stony meteors, strongly suggests the sort of genetic connection that our equations assume. Nevertheless, we must inquire whether there may be some alternative explanation. The two most prominent constituents of the two groups, Si^{28} and Mg^{24}, both have nuclei of the type $4n$, and such nuclei are usually found to possess exceptional stability. It might be argued that their prominence is due solely to their stability. While it would be hard in this way to account for the importance of the other members of these groups, yet it must be admitted that the argument for a genetic relationship is not quite as convincing in this case as in the case of Process I. There we traced the connection between the four adjacent species of aluminum and silicon and the four species of iron and nickel, all of the latter having even atomic weights, and two belonging to the type $4n$.

Process II

More than half of all the atoms in the stony meteors belong to the species O^{16}, and it is likely that an even greater quantity of oxygen has been produced and has escaped in the form of volatile compounds. If O^{16} is split off from the nuclei of the metallic meteors, we should have:

$$_{28}Ni^{60} = {}_{8}O^{16} + {}_{20}Ca^{44},$$

$$_{28}Ni^{58} = {}_{8}O^{16} + {}_{20}Ca^{42},$$

$$_{26}Fe^{56} = {}_{8}O^{16} + {}_{18}A^{40},$$

$$_{26}Fe^{54} = {}_{8}O^{16} + {}_{18}A^{38}.$$

By this process from Fe^{56}, the most important constituent of the metallic meteors, we obtain the main isotope of oxygen and the main isotope of argon. Unfortunately we have no check on the validity of our assumed process because of the volatility of argon. The other three equations are less satisfactory since they yield the less common or unknown isotopes of calcium and argon. These unknown isotopes may be unstable and suffer spontaneous transmutation. While we cannot at present suggest the complete mechanism of its production, it seems highly probable that Ca^{40} is produced directly or indirectly by the same process as O^{16}.

An unstable nucleus may change to another nucleus of different atomic number by the emission of positive or negative electrons, alpha-particles, or protons. On the other hand it may change to an isotopic nucleus, either by the emission of neutrons, or by the emission of an alpha-particle, followed by two beta-particles. In what remains to be said in this paper we shall assume, rather arbitrarily, that the latter case is the more prevalent, and therefore that the various processes of disintegration of the metallic meteors are characterized primarily by the atomic numbers of the products. The fact is that most of the evidence in favor of the genetic connection between metallic and stony meteors has now been presented; but for the sake of completeness we shall consider all of the possible disintegrations of the iron and nickel nuclei which seem to possess *a priori* probability.

Other processes

On account of the general stability of nuclei of the type $4n$ let us consider all of the processes which consist in the splitting of each of these nuclei from the atoms of the metallic meteors. Thus in addition to the processes that we have already considered, we have Process III, the splitting off of $_2He^4$ from nickel and iron, leaving *iron* and *chromium*. Chromium is, in fact, the most important of the minor constituents of the stony meteors, in which it exists to the extent of 0.13 atom percent. If chromium is produced from iron, iron in turn should be produced from nickel, and we find, indeed, that the ratio of iron to nickel has changed from 11 : 1 in the metallic meteors to 20 : 1 in the stony meteors. Process IV would consist in the loss of $_6C^{12}$, leaving *titanium* and *calcium*. *Carbon* constitutes 0.12 atom percent of the stony meteors, and its ratio to titanium (0.005 percent) agrees approximately with that to be expected from this process, since the titanium comes only from the nickel and not from the iron. In Process V, $_{10}Ne^{20}$ would be split off, leaving *argon* and *sulfur*, and in Process VI, $_{12}Mg^{24}$, leaving *sulfur* and *silicon*.

The third most important minor constituent of the stony meteors is *potassium* (0.11 atom percent). This presumably does not come from the iron and nickel, but from that constituent of the metallic meteors which we have so far neglected, and which constitutes 0.6 percent of those bodies, namely, cobalt. Cobalt, by Process II, would produce potassium, as calcium and argon are produced from nickel and iron.

If we add this process to the others, which seem to comprise all possible processes of splitting that possess any high degree of *a priori* probability, we cannot help noticing a remarkable fact. There are fourteen elements involved in one or more of these processes. Of these, three are the volatile rare gases, ten are (together with iron and nickel) the commonest elements in the stony meteors, of which they constitute 99.87 percent. In order of abundance they are oxygen, silicon, magnesium, sulfur, aluminum, calcium, sodium, chromium, carbon, and potassium. The remaining element is titanium, and we have already accounted for its relatively low abundance.

Energetic Considerations

From the atomic weights determined by Aston, or from the curve for packing fractions in cases where the individual data have not yet been obtained, we may calculate the minimum energy required for the various processes which we have considered. Expressing these energy requirements in millions of electron volts, we obtain the following approximate figures for the several processes.

Process	I	II	III	IV	V	VI
Energy	18	26	6	27	32	32

Process III, which requires the least energy, is one which appears to occur only to a minor extent; although the analogous Process IA has been assumed to occur to a much greater extent. Process I, which requires the next smallest amount of energy, is also the second process in importance, but Process II, which is the most important of all, requires a much larger amount of energy.

I shall not attempt to discuss these relationships. It has been my purpose, not to erect any complete cosmological theory which would state the origin of the disintegrating rays, or where or when the material represented by the metallic meteors has been converted into the material represented by the stony meteors, but rather to present the very strong evidence for a genetic relationship between these two kinds of material, and to consider the various processes by which the genesis may have occurred.

The Constitution of the Atmospheres of the Giant Planets

ARTHUR ADEL AND V. M. SLIPHER, *Lowell Observatory and The University of Michigan*

(Received August 9, 1934)

An analysis is made of the absorption spectra of the major planets: Jupiter, Saturn, Uranus, Neptune. Approximately forty of the rotation-vibration bands are identified as due to absorption by the methane molecule, and are correlated in terms of the fundamental frequencies of vibration. It appears that methane is the major constituent of the atmospheres of these distant bodies, the quantity in the absorbing strata increasing markedly from Saturn to Neptune. The absence of any appreciable amount of other hydrocarbon material is demonstrated.

THE major planets: Jupiter, Saturn, Uranus and Neptune bear great resemblance to one another. They are strikingly different from the terrestrial planets: Mercury, Venus, Earth, and Mars. Fig. 1 shows to scale the relative diameters of these eight bodies, and to another scale shows their relative distances from the Sun. It is at once apparent that whereas the earth-like planets are very small and proximate to the sun, the major ones are colossal, and journey in the remote regions of the solar system. In contradistinction to the short years and long days of the minor planets, the giant planets rotate in from ten to fifteen hours and require exceedingly long times to traverse their orbits. Whereas, of the small planets Venus,[1] Earth, and Mars possess appreciable atmospheres, each of the large ones is surrounded by a vast one, as is evidenced by the high albedos and rich solar spectra of the major planets. Some photographs of these spectra,[2] taken at the Lowell Observatory, are shown in Fig. 2. A partial list[2] of the approximate positions of the bands is given in Table I which suffices to show how the absorptions are distributed through the spectra of the several planets.

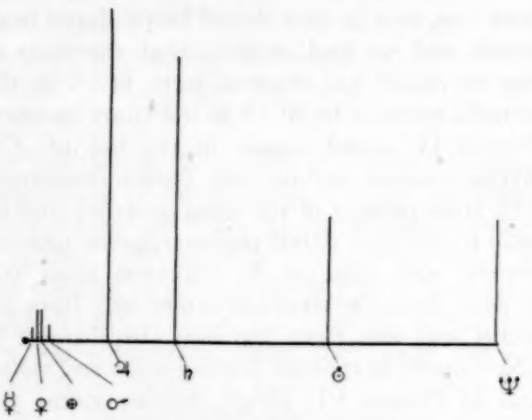

FIG. 1. The solar system.

During the course of the investigation which led to the analysis of these spectra, many gases were examined. This paper will, however, be confined to the methane molecule CH_4 which has

TABLE I. *Partial enumeration of the bands in the spectra of the major planets.*

Band ($\mu\mu$)	Planets J	S	U	N	Band ($\mu\mu$)	Planets J	S	U	N
441				*	647	*			
459				*	656			*	*
486			*	*	661			*	*
509			*	*	668	*	*	*	*
521				*	681			*	*
534				*	702	*	*	*	*
537			*	*	719	*	*		
543	*	*	*	*	726	*	*	*	*
576	*	*	*	*	782		*		
597			*	*	·	·	·	·	·
609			*	*	·	·	·	·	·
614		*	*	*	·	·	·	·	·
619	*	*	*	*	·	·	·	·	·

[1] Mercury. The small mass of this planet and the intense heating it receives from the sun have long since dissipated its atmosphere.

Venus. This planet has a very extensive atmosphere which appears to consist almost wholly of carbon dioxide. See Phys. Rev. **46**, 240L (1934).

Earth. The Earth possesses an atmospheric equivalent of five mile-atmospheres. The most abundant constituents are, of course, nitrogen and oxygen.

Mars. Mars has practically no oxygen and only a very small quantity of water vapour as compared with the earth. Astrophys. J. **79**, 308 (1934). The Martian atmosphere is rarer than the Earth's. Clouds have been noted in it at a height of fifteen miles, still the pressure at the surface is probably only a small fraction of that of the Earth.

[2] Lowell Observatory Bulletin No. 42; Monthly Notices of the Royal Astronomical Society **93**, No. 9 (1933).

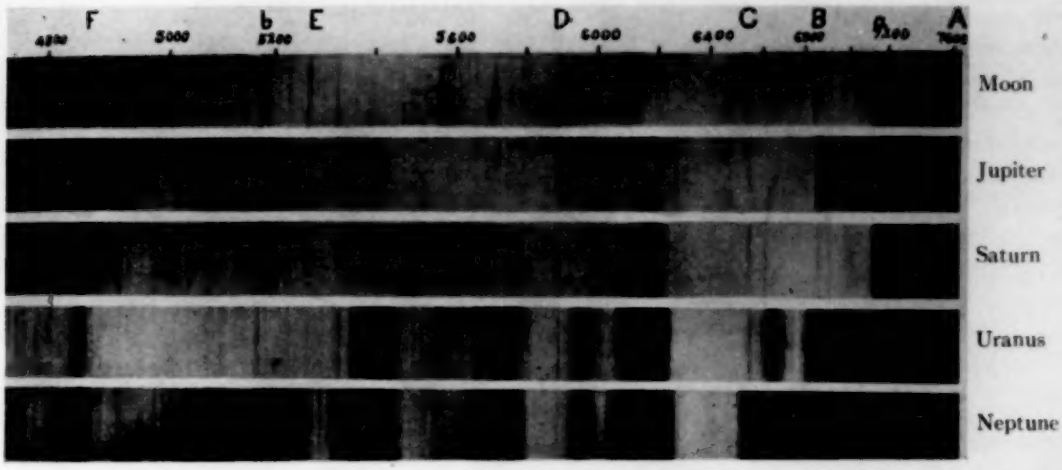

FIG. 2. The solar spectra of the major planets.

proved to be the major constituent of the giant planet atmospheres.[3]

DESCRIPTION OF APPARATUS

For the duplication of the spectra of the vast gaseous envelopes of the major planets recourse must be had to correspondingly long path-lengths in the laboratory. To meet the demands of this occasion a special absorption cell was constructed to withstand high pressures and provide a long normal path-length. A photograph of the apparatus is shown in Fig. 3.

Constructed from several sections of high pressure steam tubing, the absorption cell has a diameter of 5 cm and a length of 22.5 meters. Each of the windows, plateglass of two centimeter thickness, is separated from the cell end and the restraining cap by soft lead gaskets. The gas is passed into the evacuated cell directly from the high pressure cylinders by copper connecting coils. Pressures of about forty atmospheres have been maintained for weeks without appreciable loss. The radiation from a small incandescent source is condensed and guided down the tube by a large aperture spherical lens. At the remote extremity of the cell is situated a plane mirror with micrometer screw adjustment. The beam of radiation thus travels back down the tube creating a normal path-length of 45 meters and an aperture of approximately 1/1000. The parallel light leaves the gas chamber through a total reflecting prism, becomes incident upon a cylindrical lens, and is thrown as a sharp line upon the slit of the spectrograph. The latter is of the Littrow type. Its glass prism is especially

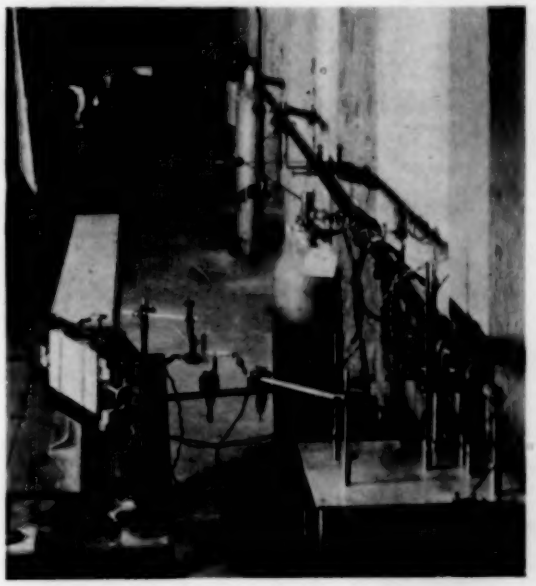

FIG. 3. The apparatus with which the planetary spectra were duplicated.

[3] Jupiter and Saturn contain small amounts of ammonia (NH_3) as was demonstrated by R. Wildt of Gottingen who compared the spectrum of this gas with the Lowell Observatory spectra of Jupiter and Saturn. He was also able to identify the bands at 5430A, 6190A and 7260A of the planets as due to methane, by means of a formula developed by Dennison and Ingram for the sequence $n\nu_2$ (see reference 4).

suitable because of its high dispersion in the less refrangible end of the spectrum. For a survey of the red and infrared regions, the Eastman plates 1–B, 1–N, 1–P, 1–Q were found especially convenient. The exposure times varied from a few seconds and few minutes for the 1–B and 1–N plates, respectively, to from one-half to several hours for the hypersensitized 1–P and 1–Q. The spectrum of neon served for comparison purposes.

The Infrared Spectrum of the CH_4 Molecule

Though the pentatomic molecule, methane, possesses nine degrees of internal freedom, it possesses but four distinct fundamental frequencies of vibration.[4] This is a consequence of the spherical symmetry of the molecule. The fundamental vibrations are diagrammed in Fig. 4.

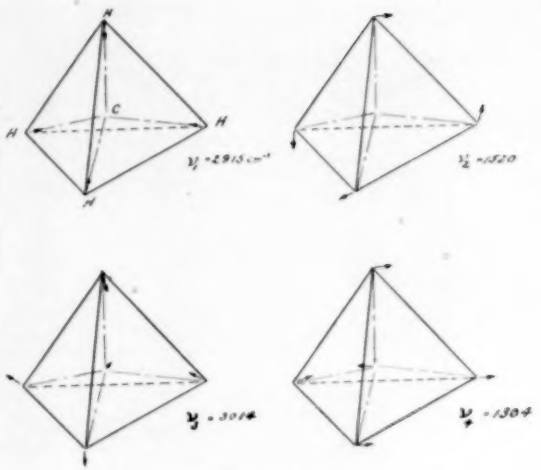

Fig. 4. The fundamental vibrations of the methane molecule.

The single vibration ν_1 consists of a symmetrical motion of the four hydrogen atoms toward the carbon atom which may be supposed to remain at rest. The H atoms retain their symmetrical positions at the corners of a regular tetrahedron all through the motion.

In the vibration ν_2 the carbon atom is again stationary, while the hydrogen atoms move in small ellipses on the surface of a sphere about the carbon as a center, but always keeping equidistant from the carbon atom. Since their motion is isotropic in two dimensions, this is a double vibration.

ν_3 is essentially a C−H vibration. The whole motion is isotropic in space. ν_3 is thus a triple vibration. The vibration ν_4 is a motion of the carbon atom relative to the frame of the four hydrogens. Again the motion is isotropic in space, and therefore has the weight three. ν_3 and ν_4 have the same symmetry character, but because of the nature of the forces involved ν_3 is greater than ν_4.

Of the four fundamentals, it is clear that only ν_3 and ν_4 will be active in infrared absorption, since the highly symmetrical oscillations ν_1 and ν_2 will involve no change in the electric moment of the molecule. The selection rules governing the appearance of the infrared spectrum consequently forbid the absorption of the frequencies $n\nu_1+m\nu_2$, where n and m may take all integral values including zero. The absence of this set of absorptions consitutes a great simplification in the appearance of the methane spectrum. If it were not for this fact, the planetary spectrum would be a much more difficult one to unravel.

The tetrahedral symmetry which is responsible for the simple distribution of the absorption centers throughout the spectrum, is at the same time the cause of the very complex fine-structure pattern inherent in each of the high harmonics and combination bands found in the planetary spectrum. An idea of the complexity of the fine structure may be gained from the following examination of the harmonics of ν_3. An analysis by Dennison and Ingram[5] based upon the three degrees of freedom of this mode taken in conjunction with the tetrahedral symmetry of the molecular force field has shown that the vibrational energy levels $n\nu_3$ are multiple, with a multiplet separation which is small in comparison with the fundamental frequency; in fact, of the same order of magnitude as the rotational structure. Thus, when n is the order of the harmonic, approximately $\frac{1}{4}(n+1)(n+2)$ bands superpose to form a single composite band $n\nu_3$. For example, such a band as the $7\nu_3$ one in the planets is actually a superposition of some eighteen bands. It is not surprising, therefore, that such a band should prove difficult of resolution.

[4] Astrophys. J. **62**, 84 (1925).

[5] Dennison and Ingram, Phys. Rev. **36**, 1451 (1930).

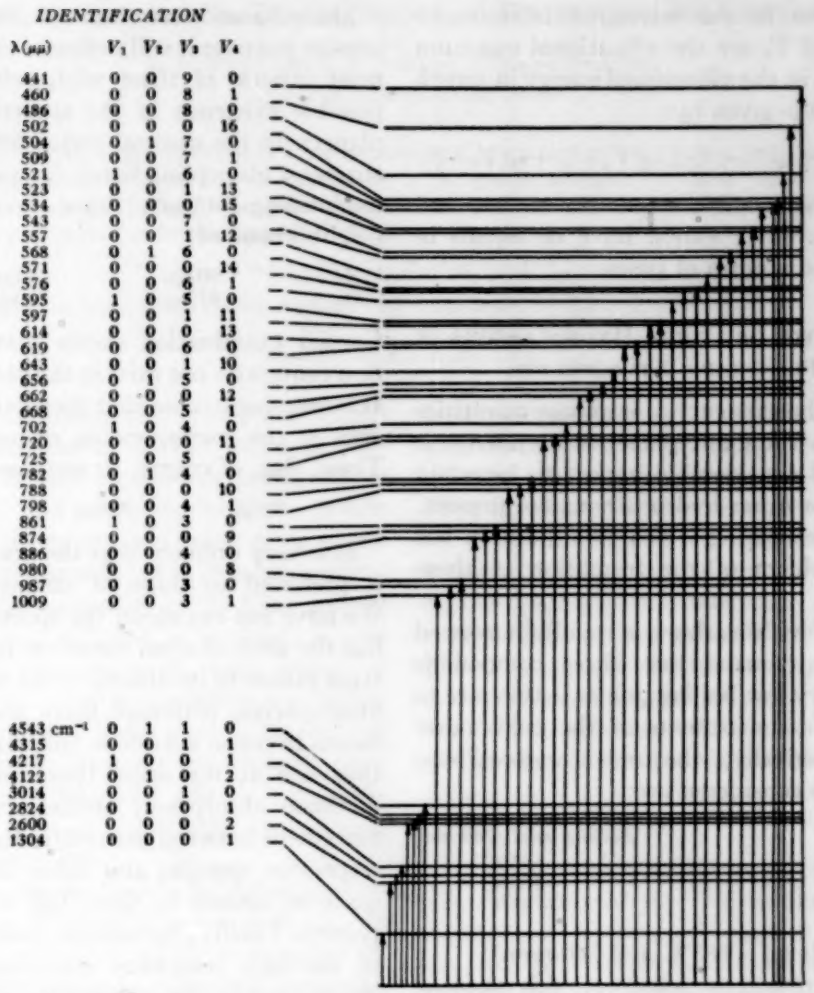

FIG. 5. The identification of the planetary bands and their correlation with the remote infrared spectrum of the methane molecule.

THE PLANETARY PROBLEM

By using gas pressures as high as 45 atmospheres, some twenty rotation-vibration bands have been photographed from 4500A to 10,000A. The laboratory spectra thus achieved are completely duplicated in the planetary ones. Not all of the methane bands showing in the spectra of the outer planets have as yet been detected in the laboratory, however, inasmuch as the absorption columns in Uranus and Neptune are much greater than the laboratory path-lengths described above. In conformity with expectation, the planetary bands which have been duplicated in the laboratory are the longer wave members of their respective groups. The present lack of complete duplication is, of course, no obstacle to the identification of the planetary bands. For, from those observed in the laboratory, the convergence constants of the several groups of bands may be determined; and with the aid of these coefficients the remaining planetary methane absorptions can be calculated. The absence of the frequencies $n\nu_1+m\nu_2$ means that there is a minimum of overlapping in the consequential spectral regions. The correlation is therefore rendered rather certain.

The identified planetary methane bands are indicated in Fig. 5 in their relation to the more remote infrared methane bands usually accessible

to the observer in the terrestrial laboratory.[6] V_1, V_2, V_3 and V_4 are the vibrational quantum numbers; that is, the vibrational energy in zeroth approximation is given by:

$$E=\nu_1(V_1+\tfrac{1}{2})+\nu_2(V_2+1)+\nu_3(V_3+\tfrac{3}{2})+\nu_4(V_4+\tfrac{3}{2}).$$

The most remarkable sequences are $n\nu_3$ and $m\nu_4$, which for sheer extent have no equals in terrestrial band spectra of gases.

The Possibility of Other Hydrocarbons in the Planetary Atmospheres

In view of the existence of immense quantities of methane in the giant planet atmospheres, it is a matter of considerable import to ascertain whether or not other hydrocarbons are present, because of the bearing which this question has upon the problem of the formation of these atmospheres.

The field of hydrocarbons is rapidly narrowed down by the demand that these compounds must have very low boiling points if they are to be *atmospheric* constituents of the cold, outer planets.[7] Practically, the only hydrocarbons which need be considered are:

Compound	*Boiling point (760 mm)*
Ethane (C_2H_6)	−95°C
Ethylene (C_2H_4)	−103°C
Acetylene (C_2H_2)	−85°C

(Methane boils at −165°C and 760 mm.)

In an effort to find the solution to this problem, the rotation-vibration spectra of ethane and ethylene were examined from the violet to the photographic infrared, employing a path length of gas the equivalent of more than a mile at atmospheric pressure (actually, a 45 meter path and a gas pressure of 40 atmospheres). Such a quantity of gas is roughly comparable with that in the absorption layers of Jupiter and Saturn, but of a lower order of magnitude than that in Uranus and Neptune.

Many bands were observed. However, for our present purpose it will suffice to examine only the most intense of these with reference to their possible existence in the spectra of the major planets. In the spectral region 6000A–9000A the strongest absorption bands (arranged in order of diminishing intensity) have their centers in the neighborhood of:

C_2H_6	902$\mu\mu$	742$\mu\mu$	632$\mu\mu$
C_2H_4	872$\mu\mu$	710$\mu\mu$	604$\mu\mu$

Careful examination shows that these absorption centers do not exist in the planetary spectra. It is amusing to note that they flank the strongest ones in the corresponding region of the latter. These, due, of course, to methane, lie at:

886$\mu\mu$ 725$\mu\mu$ 619$\mu\mu$.

It is very unlikely that the acetylene molecule is preferred to those of ethane and ethylene. We have not examined the spectrum of this gas, but the work of other observers on its band spectrum points to its absence from the major planet atmospheres. Although there are several agreements between acetylene and planetary spectra, they are at the same time coincidences with methane absorption; furthermore, there is no agreement between the relative intensities in the respective spectra; and other acetylene bands, quite as intense as these fail to appear in the planets. Finally, the simple, resolvable structure of the high frequency acetylene bands is decidedly unlike the complex, superimposed structure of the high frequency planetary (methane) bands.

We are thus led to the conclusion that the other hydrocarbons, if they are present at all in the atmospheres of the giant planets, must exist only in traces relative to the amount of methane present. Presumably, these hydrocarbons as well as many others exist below the atmospheres of the giant planets. The unanchored motion of Jupiter's Great Red Spot suggests that it is an island of solid hydrocarbon or ammonia floating in a vast hydrocarbon ocean as extensive as the planet's surface itself.

The authors wish to thank the Faculty Research Council of the University of Michigan for a grant-in-aid, and the American Academy of Arts and Sciences for a grant from its Permanent Science Fund.

[6] To this compilation of identified planetary bands should be added the following:

843$\mu\mu$	$7\nu_4+\nu_2$
942$\mu\mu$	$6\nu_4+\nu_2$,

thus bringing the total number of identified bands to thirty-six.

[7] The temperatures in the outer layers of the major planet atmospheres are below −150°C, as inferred from radiometric measures.

The Dependence of the Diamagnetism of Water upon Its Temperature

A. P. WILLS AND G. F. BOEKER, *Columbia University*

(Received September 24, 1934)

The anomalous results described in a previous communication are explained in part, and the results of recent experiments relating to the dependence of the specific susceptibility (χ) of water upon its temperature are given. For the temperature range from 20°C to 66°C these results are represented with fair approximation by the parabolic formula:

$$\chi/\chi_{20}=1+1.3\times10^{-4}(T-T_{20})-0.7\times10^{-6}(T-T_{20})^2.$$

A comparison is made of the results obtained with those found by previous observers.

IN a former communication[1] a new instrument for the measurement of the magnetic susceptibilities of liquids at different temperatures was described, and some preliminary results obtained in experiments on water were given. These results were anomalous in several respects, however, and the anomalies at the time seemed very puzzling and difficult to explain. It was suggested that the source of these anomalies might possibly be found in the differences in the thermal history of the water used in the various experiments, but subsequent experiments have shown that the anomalous effects previously observed were such as to preclude explanation on such an assumption.

Chief among the anomalies in question were the results of a susceptibility-temperature run on recently boiled water which incorrectly indicated decreasing diamagnetism with increasing temperature. In a recent paper[2] and in private communications H. Fahlenbrach has suggested a possible explanation of this anomaly based upon the assumption that the calibration of our instrument might have been at fault because of the possibly unwarranted reliance which we placed upon our method of calibration, which is fully described in our earlier paper. Although we are now certain that the explanation of Fahlenbrach is not tenable, the points which he raises are of sufficient importance to warrant mention. Our method of calibration depends upon the measurement of a magnetic field gradient by means of test aqueous nickel chloride solutions whose magnetic susceptibilities at a standard temperature are determined experimentally in terms of that of pure water at the same temperature as follows: A given test solution is prepared by first making up a magnetically neutral solution of nickel chloride in pure water at the standard temperature and then mixing with a mass m of this solution a mass μ of pure water. If χ_n and χ_{20} denote the specific susceptibilities of the test solution and of pure water at the standard temperature (20°C), we then make the assumption (Wiedemann's law) that:

$$\chi_n=[\mu/(\mu+m)]\chi_{20}.$$

It is the validity of this equation which is in effect questioned by Fahlenbrach, who has shown that the magnetic moment of the nickel ion of nickel chloride in solution may not have a determinate value, since it may depend upon the method of preparation of the solution and upon its concentration. Using our original apparatus, Mr. Donald Woodbridge has shown, however, that the method followed by us in the preparation of our test solutions is not subject to errors of the sort suggested by Fahlenbrach.

Eventually, we were led to the conclusion that our results indicating decreasing diamagnetism of water with increasing temperature could be explained only upon the assumption of an unsuspected leak of air into the vessel containing the helium gas against which the susceptibility of the water was to be measured; and that the anomalies in the results represented in Fig. 5 of our earlier paper might be accounted for likewise. Calculation shows that the effects in question could be thus explained.

[1] A. P. Wills and G. F. Boeker, Phys. Rev. **42**, 687, (1932).

[2] B. Cabrera and H. Fahlenbrach, Zeits. f. Physik **82**, 759 (1933).

Further experiments with our original apparatus showed that it could be modified advantageously in several details, and it was finally decided to construct an entirely new instrument upon the same basic principle[3] with which to continue our susceptibility-temperature investigations on water. In course of time this instrument was completed; it constitutes a manometric magnetic balance so simple and compact in design that we are confident it would prove a highly satisfactory instrument for physicists and chemists engaged in the study of the magnetic properties of liquids; it is proposed to give a detailed account of this instrument in a separate communication.

Results of Recent Experiments

Using the new balance, we have made further measurements of the magnetic susceptibility of water at different temperatures. The results for the specific susceptibility ratio χ/χ_{20}, where χ denotes the susceptibility at a temperature T and χ_{20} the susceptibility at 20°C (T_{20}), were furnished by nine individual susceptibility-temperature runs comprehended in the temperature interval from 20°C to 66°C. A typical run over this entire range is represented by a zigzag line in Fig. 1, constructed by joining consecutive experimental points by straight-line segments. By averaging curves of this sort for the nine runs the curve in Fig. 1 with the legend *average of runs* was obtained.

Our experimental results for the temperature interval specified above are on the whole fairly well represented by the parabolic formula:

$$\chi/\chi_{20}=1+1.3\times10^{-4}(T-T_{20})-0.7\times10^{-6}(T-T_{20})^2,$$

where χ, χ_{20} denote the specific susceptibilities of water at the temperatures T, T_{20}. The full-line curve in Fig. 1 is a graph of the parabola represented by this equation; 33 experimental values

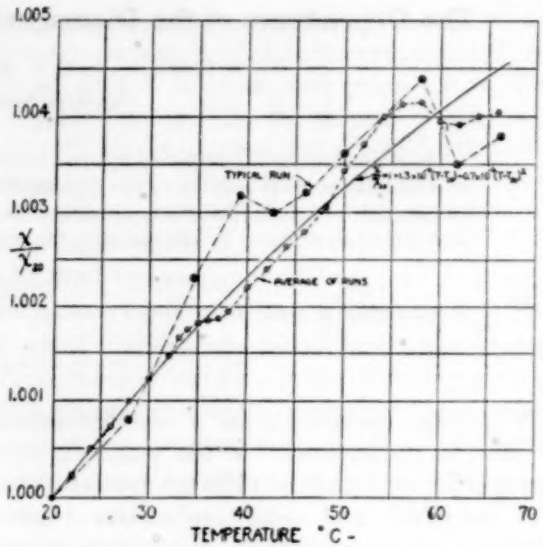

Fig. 1. Variation of susceptibility of water with temperature.

of the quantity χ/χ_{20} are represented by points which lie above this curve and 34 experimental values by points which lie below it. The average plus and minus deviations of these points from the curve and the corresponding maximum deviations, determined with the aid of a large-scale graph, are as follows:

average + deviation	+0.000365,
maximum + deviation	+0.00097,
average − deviation	−0.000365,
maximum − deviation	−0.00094.

Each individual run shows, however, a definite break in the slope of the susceptibility-temperature curve in the neighborhood of 35°C and another, more significant, in the neighborhood of 55°C; the average effects of these breaks is apparent from the curve in Fig. 1, representing the average of nine runs. It is possible that these breaks indicate significant changes in molecular arrangement or association of the water molecules.

The temperature coefficient at 20°C for the quantity χ/χ_{20} has been estimated with the aid of a large-scale graph of our experimental results to have the value 1.30×10^{-4}.

Our method is not subject, we believe, to many systematic errors, and those which must be most carefully guarded against have their origin in anomalous conditions which sometimes appear at the free surfaces of the liquids in the menisci

[3] The principle upon which our instrument operates depends upon balancing the force exerted by a magnetic field upon a standard liquid of known susceptibility, contained in a Pyrex tube of small diameter with its free surface (meniscus) at a fixed position in the field, by a corresponding force exerted by a second magnetic field upon the liquid whose susceptibility is to be measured and contained in a similar tube, balance being effected by moving the meniscus of this liquid to a determined position in the second field, whose gradient along the tube is known, such that the two forces equilibrate.

tubes and which manifest themselves by "sticking" or "drifting" of the menisci of the liquids; these conditions occasionally arise despite great care used in cleaning the menisci tubes and in the temperature control of the liquids themselves, particularly at the higher temperatures. As a result of long experience we now know that measurements made when there is any evidence of sticking or drifting are probably erroneous and should be rejected.

Comparison of Results of Different Observers

Comparison of the results obtained by different observers[4] for the magnetic susceptibility of water as a function of its temperature shows on the whole a not very satisfactory agreement. At room temperature, however, the agreement among the numbers found by a considerable number of observers for the temperature coefficient of the susceptibility ratio χ/χ_{20} is reasonably satisfactory, as is apparent from Table I.

Marke, Johner, and Cabrera and Fahlenbrach found the temperature coefficient for the quantity χ/χ_{20} to be independent of the temperature within the precision of their measurements.

In the temperature interval from 20°C to 65°C the results of Piccard and of Auer are in remarkably good agreement. For the same temperature interval our results indicate somewhat larger values for this quantity than those obtained by them, the greatest difference occurring at about 57°C, at which we find the value 1.0042 for the ratio χ/χ_{20} and Auer finds 1.0035; at this temperature, however, our value is in excellent agreement with those found by Marke and by Cabrera and Fahlenbrach.

For the temperature interval from 20°C to 0°C the values found by Piccard and by Auer for the quantity χ/χ_{20} diverge more and more as the temperature decreases, those of Piccard being notably higher. Because of difficulties connected with the condensation of water vapor on the colder of the meniscus tubes of our apparatus owing to the high humidity incident to summer weather we were forced to defer making measurements at temperatures below 20°C to a more favorable season.

Table I.

Observers	$\frac{1}{\chi_{20}}\frac{d\chi}{dT}\times 10^4$
Piccard (1913)	1.20
Marke (1916)	1.17
Piccard and Johner (1930)	1.3_1
Cabrera and Fahlenbrach (1933)	1.15
Auer (1933)	1.26
Wills and Boeker (1934)	1.30

[4] For a detailed comparison of the results obtained by Auer and by previous observers and for references the following paper may be consulted: H. Auer, Ann. d. Physik **410**, 593 (1933).

Thermal Conductivities of Bismuth Single Crystals as Influenced by a Magnetic Field

MILWARD T. RODINE, *Department of Physics, University of Wisconsin*
(Received August 20, 1934)

The thermal and electrical conductivities of two specimens of Bi single crystals were determined as a function of temperature and orientation of magnetic field relative to their crystallographic axes. These effects were observed at temperatures ranging from −170°C to −50°C. The first specimen was mounted with its trigonal axis $P\perp$ to H and $\|$ to heat or current flow. The second specimen was mounted with $P\perp$ to heat or current flow and $P\perp$ or $\|$ to H. In this specimen it was also known that the heat or current flow was $\perp$ to the traces in the (111) plane formed by the intersection of the (111) and the (11$\bar{1}$) planes. A magnetic field of 7800 gauss was used and the crystallographic orientation was determined by means of variations in electrical resistance as the field was rotated about the specimen. For the first specimen, $P\|$ to heat and current flow, the decrease in thermal and electrical conductivity with the field perpendicular to any one of the binary axes was greater than when the field was parallel to any one of them. For the second specimen, $P\perp$ to heat and current flow, the decrease in thermal conductivity with $H\perp P$ was greater than the corresponding decrease with $H\|P$, whereas the decrease in electrical conductivity for these two positions were less and greater, respectively.

I. PURPOSE

THE purpose of the following investigation was to determine the change in thermal conductivity of Bi single crystals at low temperatures as a function of magnetic field orientation relative to the crystallographic axes. A previous investigator[1] had completed similar work on multicrystal Bi and had designed part of the apparatus to be used in this investigation. Information on the thermal conductivities of metals furnishes an important test of the validity of any theory of the solid state. Inasmuch as any such theory usually assumes an orderly arrangement of the atoms in a space lattice, single crystals were used to satisfy this requirement. Thus with single crystals, unlike multicrystals, we have eliminated the complications resulting from random aggregations of small crystals held together by an intercrystalline layer of unknown structure and extent.

Two specimens were used in this investigation: one with its trigonal axis parallel to the length of the specimen and the other with its trigonal axis perpendicular to it. Each of these specimens were obtained through the courtesy of Professor Alexander Goetz of the California Institute of Technology. They were grown by an ingenious method known to yield very perfect single crystals.[2]

Other investigators[3, 4] have studied the effects of a magnetic field on the thermal conductivity of Bi single crystals but at higher temperatures. The results are in general agreement with those obtained in the present investigation.

II. EXPERIMENTAL METHOD

The specimen was mounted in a brass cylinder between the pole pieces of a magnet as shown in Fig. 1. On the upper end of the specimen was a small heater C. It consisted of a hollow copper cylinder (6 mm in diameter and 1 cm in length) closed at the lower end and having a double silk covered No. 40 nichrome wire coil wound around it. A strip of gold foil was wound around this coil in order to facilitate calculations on lateral radiation losses. The total mass of the heater was approximately 1 gram. The base of the heater made good thermal contact with the specimen by being soldered to it with Wood's metal and likewise the lower end of the specimen made good thermal contact with the copper rod E by means of a Wood's metal junction. The copper rod E was $\frac{1}{4}$ inch in diameter and was attached to a cylindrical copper base one inch in diameter. The initial purpose of this arrangement was to permit the cooling of the specimen by submerging D and only part of F in liquid air and thus permitting a minimum separation of the pole pieces.

[1] E. J. Knapp, University of Wisconsin, 1931.
[2] Alexander Goetz, Phys. Rev. **35**, 193 (1930).
[3] G. W. Kaye and W. F. Higgins, Phil. Mag. **8**, 1056 (1929).
[4] G. W. Kaye and J. K. Roberts, Proc. Roy. Soc. **A104**, 98 (1923).

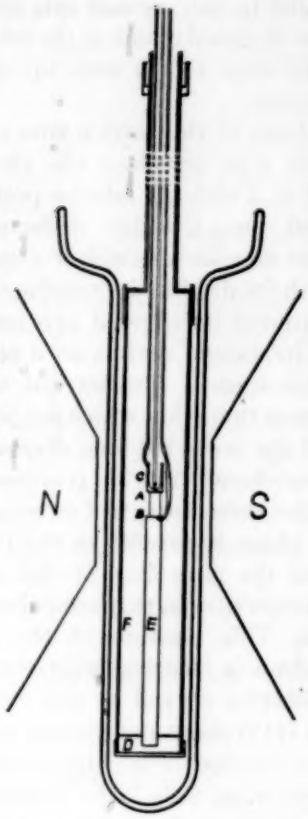

FIG. 1. Method of mounting the crystal specimen.

It was later found necessary to submerge the entire cylinder F in a Dewar flask filled with liquid air. The temperature gradient in the specimen was measured by means of two thermocouples located at A and B. Thermocouple A was soldered directly to the thin base of the copper heater while thermocouple B was inserted in a small hole drilled in the side of E and terminating near its upper surface. This couple was firmly held in this position by coating its junction with a bead of solder and thus also providing good thermal contact with the lower end of the specimen. The thermocouple elements used were platinum and palladium inasmuch as such a couple showed no change in thermoelectric power in the presence of a magnetic field. The magnet was a water-cooled type mounted so as to permit rotation of the field around the specimen. The specimen chamber F was kept evacuated to a pressure of 10^{-6} mm of Hg thus minimizing heat losses due to convection and gas conduction. To minimize conduction losses, the platinum and palladium leads were 0.08 mm in diameter and the leads to the heating coil were of No. 40 double silk covered copper wire.

III. Experimental Results

With a given crystal mounted according to the preceding arrangement, it became necessary to determine the orientation of its crystallographic axes relative to the magnetic field before proceeding with thermal conductivity measurements. For practical purposes, this was best accomplished by determining the change in electrical resistance as the field was rotated about the crystal. This method is well adapted to a study of Bi inasmuch as it is well known that this element shows a greater change in resistance in a magnetic field than any other metal.[5] It was used for both specimens but since each of these involve a slightly different problem, they will be discussed separately and in detail.

A. Orientation of crystal No. 1 ($P \perp H$ and $\parallel I$) as determined by the variation of electrical resistance with H

Bismuth belongs to the trigonal division of the hexagonal system and the principal cleavage planes are perpendicular to the trigonal axis, designated by P. The first specimen was mounted with its trigonal axis vertical[6] and the magnetic field rotated in a plane perpendicular to it. The two platinum members of the thermocouples were used as current leads through the specimen and the two palladium members were used as potential leads connecting to a potentiometer. With the specimen at liquid air temperatures, a current of about 10 milliamperes was sent through it and the potential drop across the specimen observed as a field of 7800 gauss was rotated about it. It is known from previous work[7] that the minimum change in electrical resistance occurs when the field is parallel to any one of the three binary axes of hexagonal symmetry and a maximum when along any line in the cleavage plane per-

[5] P. Kapitza, Proc. Roy. Soc. **A123**, 292 (1929).
[6] The principal cleavage planes were found to be inclined 4° 20′ from perpendicularity to the axis of the specimen.
[7] L. Schubnikow and W. J. de Haas, Communications from the Physical Laboratories of the University of Leyden. No. 210.

pendicular to any one of these axes. In the Bravais notation, these positions are, respectively, $H \perp 11\bar{2}$ plane and $H \parallel 10\bar{1}$ axis. These maxima and minima repeated themselves consistently and in accordance with the threefold symmetry about the trigonal axis.

B. Orientation of crystal No. 2 ($P \perp$ or $\parallel H$ and $\perp I$) as determined by the variation of electrical resistance with H

In this crystal the principal cleavage planes were parallel to the length of the vertically mounted specimen and the magnetic field was rotated around it as before. Fig. 2 shows the resulting changes in resistance[8] as the field was rotated around the specimen. It is known from other work[9] that a minimum change in resistance occurs at positions where the field is perpendicular to the trigonal axis ($H \perp P$) and that this change is greater when the field is parallel to it ($H \parallel P$). In Fig. 2 this minimum occurs at 65° and repeats itself in a period of 180°. These two minima then represent $H \perp P$ and rotating the field 90° to either side of these points give positions of increased resistance or $H \parallel P$. The two extreme positions are thus established by their periodicity but we may note that other maxima occur at 110° and 200° or 290° and 380°. Inasmuch as the rotation diagram for this orientation does not appear in literature it may be considered in some detail we may account for this symmetry by considering the rhombohedral structure of Bi. R. W. James[10] has shown that Bi crystallizes in the dihexagonal alternating class of the hexagonal system. The edges of the rhombohedron which meet in the trigonal axis are taken as the axes of the crystal. The angle between any two of these edges is 87° 34′ and the angle between the rhombohedral faces 100 : 010 is 92° 20′, the principal cleavage plane being parallel to the (111) planes and perpendicular to the trigonal axis. By means of x-ray analysis, it has been shown that the Bi atoms lie on two interpenetrating face-centered rhombohedral lattices.[10] Atoms of the second lattice are displaced in the same direction along diagonals parallel to the trigonal axis by a distance 0.052 of the diagonal of one of the small cells and therefore lie close to the unoccupied corners of the first lattice.

On the basis of this lattice structure, we can in a rough way correlate the characteristics shown in Fig. 2 with the relative positions of the atoms and magnetically deflected electron stream. Let us take a model of a unit rhombohedron with its displaced secondary lattice, and rotate it around its trigonal axis until the projection of its atomic centers on a plane parallel to this axis form a symmetrical arrangement about a line in that plane which is a perpendicular bisector of the projected long diagonal (trigonal axis) of the rhomb. In this position one of the traces of the three imperfect cleavage planes in the (111) plane is parallel to the plane of projection and the projection of this trace in the plane of projection is perpendicular to the trigonal axis. This position of the model unit rhombohedron is identical with the position of the experimental crystal as was determined by etching its (111) plane and thereby locating these traces. The method of locating these traces will be discussed more fully later. Now let the magnetic field be directed parallel to the trace in the (111) plane and perpendicular to the trigonal axis and a current flow through the specimen in a direction perpendicular to the plane of projection. The projected positions of the atoms with this orientation presents a configuration having a series of paths, unobstructed by atoms, parallel to the trigonal axis and in the direction of the magnetically deflected electrons. This position corresponds to a minimum change in resistance in Fig. 2 and we may identify it with the minimum at 65° which represents $H \perp P$. As previously mentioned, it is known that a minimum change in resistance occurs at $H \perp P$.[9] Rotating the field 45° from this position to 110° gives a maximum change in resistance and the appearance of the projection diagram also indicates a position where deflected electrons would experience a maximum number of atomic encounters. In a similar way the secondary minimum at 145° and the secondary maximum at 155° are suggested by the appearance of the projected crystal for these two orientations of the field. From this simple consideration of electron

[8] Fig. 2 shows variations in potential which in turn are proportional to resistance. The resistance of the specimen increased when placed in a magnetic field.

[9] P. Kapitza, Proc. Roy. Soc. **A119**, 358 (1928).

[10] R. W. James, Phil. Mag. **42**, 193 (1921).

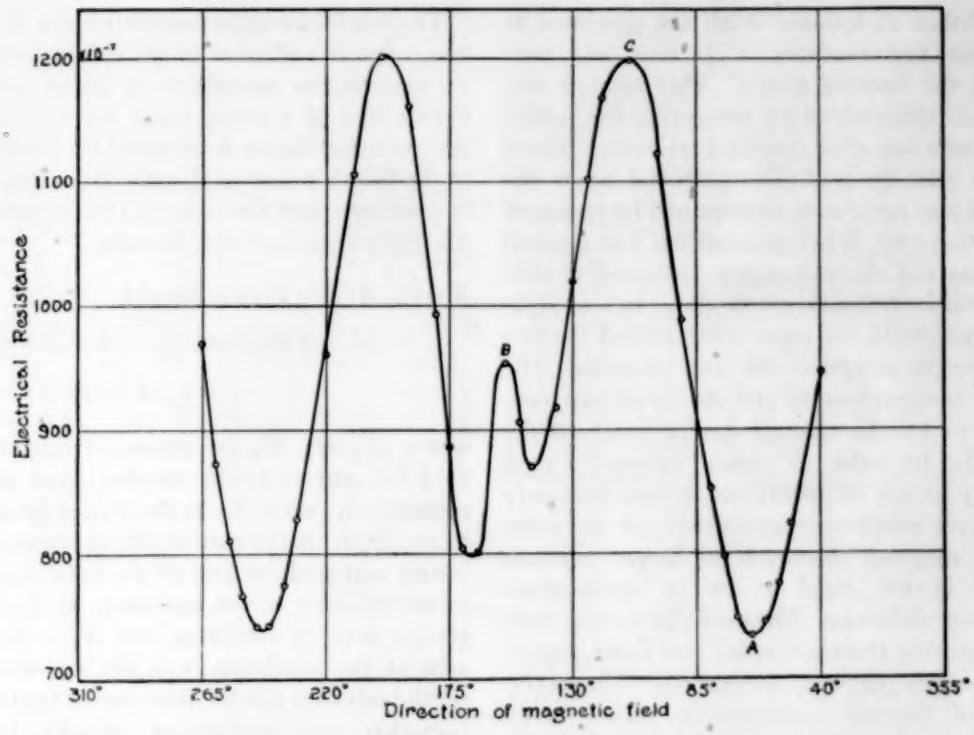

FIG. 2. Changes in resistance of bismuth crystal with orientation of the magnetic field. Position *A*, magnetic field perpendicular to trigonal axis; position *B*, magnetic field parallel to trigonal axis; position *C*, magnetic field along line 45° from *A* or *B*.

channels[11, 12, 13] the maxima and minima of Fig. 2 can be correlated with the symmetry of the crystal. This is of course but an elementary correlation between the symmetry of the crystal and its electrical resistance for these particular physical conditions. It is not, however, intended as an explanation of the more complex phenomena of electrical conduction.

In each of the preceding specimens, two further cases of orientation might have been considered wherein one of the traces of the three imperfect cleavage planes in the (111) plane was perpendicular or parallel to the direction of the current.[14, 15] Bismuth has three imperfect cleavage planes, symmetrical with respect to the trigonal axis, so that for any condition which is not symmetrical with respect to the trigonal axis it is important, as Stierstadt[14] has pointed out, to specify the position of the traces which these three planes make in the (111) plane. In this investigation it was impossible to alter the direction of the current relative to these traces by a mere rotation of the crystal. It is known, however, that in crystal No. 2 with $H \perp P$, one of these traces in the (111) plane was perpendicular to the current and parallel to the field. This was determined by etching the (111) plane by means of dilute nitric acid and observing the direction of the three sets of lines which were developed. It is known[15] that the lines which are developed in the (111) plane either by etching or, less perfectly, by mere cleavage, are parallel to the traces of the three imperfect cleavage planes in the (111) plane. With the orientation of the crystal thus determined we may consider the thermal conductivity measurements for these positions.

C. Thermal conductivity of crystal No. 1

Thermal conductivity in the absence of a magnetic field was first determined. This was

[11] J. J. Thomson, Rapports, Congrès Internat. Phys. **3**, 138 (1908).
[12] Ganz, Ann. d. Physik **20**, 310 (1906).
[13] Sommerfeld, Zeits. f. Physik **47**, 51 (1928).
[14] O. Stierstadt, Phys. Rev. **43**, 577 (1933).
[15] P. Kapitza, Proc. Roy. Soc. **A119**, 358, 412 (1928).

accomplished as follows: With the specimen at liquid air temperatures, a current was sent through the heating grid C. This current was accurately determined by measuring the potential across a one ohm standard resistance placed in series with the grid. The potential across the grid was also accurately determined by means of a potentiometer. When a condition was reached such that the thermocouples indicated a slow steady rise in temperature of about two to eight degrees per hour, the input wattage and the two thermocouple temperatures were recorded. The average temperature of the specimen was considered to be the average temperature of the two ends. In order to obtain values for conductivity at low temperatures, it was necessary to use very small heating currents of the order of 0.02 amperes inasmuch as larger currents resulted in too rapid a rise in temperature throughout this range. The resulting temperature gradients were therefore small and hence experimental errors played a serious rôle. The uncertainty of thermal conductivity values below -170°C is therefore evident. Inasmuch as equilibrium conditions were not fully attained, corrections must be made due to the changing temperatures of the various masses involved. The known specific heats[16] of these masses at their respective temperatures, as well as their different rates of rise in temperature, were used to make the necessary corrections.

In order to account for the energy losses of the heater due to its radiation as well as conduction along thermocouple and heater leads, the heater alone was suspended by these leads in the evacuated chamber F. A small current was then passed through the heater and the input wattage and temperature were recorded when it had reached a state of temperature equilibrium. By means of various current inputs, these equilibrium points were determined as a function of temperature until the necessary temperature range had been investigated. The combined losses due to radiation and conduction along leads could then be determined for any given temperature inasmuch as equilibrium meant an equivalence of the known energy input and the losses due to the above two factors.

[16] Landolt-Börnstein, Physikalisch-Chemische Tabellen, Vol. 2 (1931).

The last factor to be considered was the energy losses due to radiation of the specimen alone. If we assume the emissivity of Bi as being one-fourth that of a black body, we may calculate the radiation loss as determined by the difference of the fourth power of the absolute temperatures of specimen and the case F. Our complete conductivity equation then becomes

$$K=[L/A(T_2-T_1)][0.2389EI - (M_1S_1+M_2S_2)d\theta/dt_1-\tfrac{1}{2}M_3S_3d\theta/dt_2 - \eta-A'0.25\sigma(T_2'^4-T_1'^4)],$$

where M_1, M_2, M_3, are masses of copper heater, gold foil and nichrome winding, and specimen, respectively, while S_1, S_2 and S_3 are their specific heats. $d\theta/dt_1$ is the rate of rise in temperature of heater and gold foil and $d\theta/dt_2$ is the rate of rise in temperature of the specimen. A is the cross section area of specimen and A' is the lateral area of the specimen. σ is the emissivity of a black body and η is the heat loss of heater due to radiation and conduction through leads. T_2 = temperature of lower couple; T_1 = temperature of upper couple; T_2' = average temperature of specimen; T_1' = average temperature of case F. L = length of specimen; K = thermal conductivity in calories/sec., cm², cm length, 1°C temp. difference. The length of the specimen was 1.231 cm and the cross section was roughly triangular in shape with dimensions about 3 mm on a side.

TABLE I.[17] *Trigonal axis P parallel to length of specimen and P⊥H. Heat flow ||P and ⊥H.*

No Field		$H\|\|$ to binary axes		$H\perp$ to binary axes	
Temp.	K	Temp.	K	Temp.	K
160.9	0.0270	163.0	0.0212	156.1	0.0187
149.6	0.0246	153.8	0.0191	143.8	0.0164
139.9	0.0223	147.1	0.0184	131.8	0.0149
132.2	0.0210	135.7	0.0164	124.3	0.0138
130.6	0.0209	131.1	0.0158	116.9	0.0130
123.4	0.0198	126.9	0.0153	111.1	0.0124
117.3	0.0191	123.6	0.0147	100.5	0.0122
112.8	0.0183	120.6	0.0143	82.8	0.0115
106.7	0.0179	101.3	0.0128		
85.2	0.0164	86.7	0.0116		
77.4	0.0155	64.1	0.0114		
70.7	0.0148				
45.7	0.0138				

[17] In this table as well as in Table II, only a few representative points are tabulated due to the labor involved in computing the complete conductivity equation.

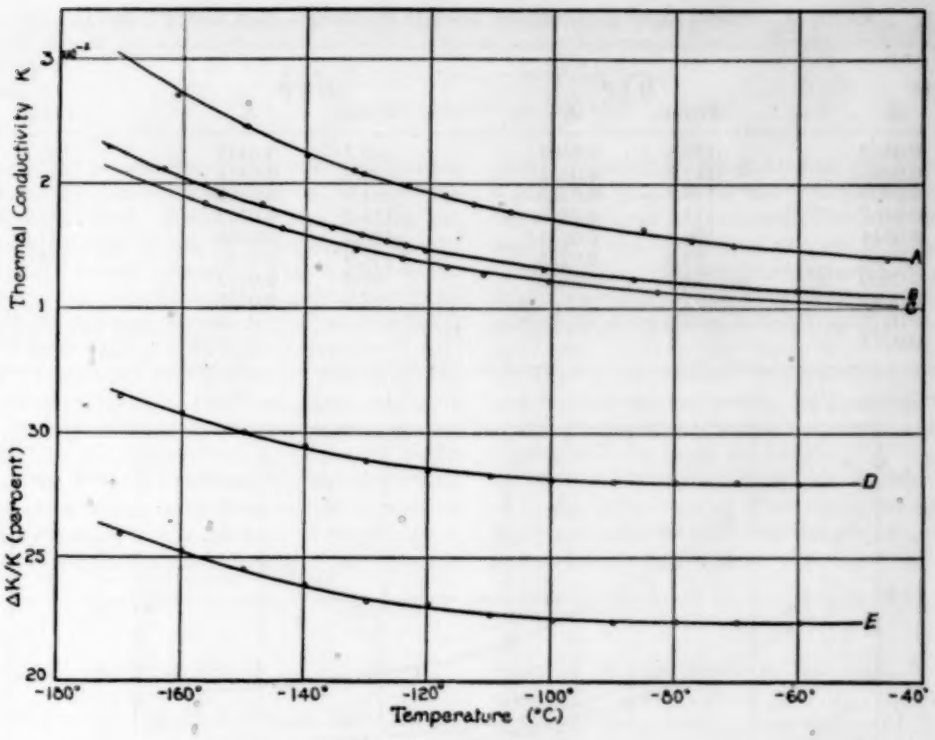

FIG. 3. Effect of magnetic field on thermal conductivity. Curve *A*, heat flow parallel to trigonal axis—no magnetic field; curve *B*, magnetic field parallel to one of binary axes; curve *C*, magnetic field perpendicular to one of binary axes; curve *D*, magnetic field perpendicular to one of binary axes; curve *E*, magnetic field parallel to one of binary axes.

Accurate determinations of cross-section area were made in terms of mass, density and length.

The same procedure was used in determining the thermal conductivity in a magnetic field. The field was directed as before, parallel or perpendicular to a given set of binary axes. The effect of the field was to reduce the conductivity of the specimen in each of the two positions. The results are indicated in Fig. 3, curves *B* and *C*. These results could be repeated very consistently from time to time as well as for different values of wattage input in the heating coil. Curves *D* and *E* show the percentage change in thermal conductivity due to a magnetic field as a function of temperature and orientation of the field. By using the preceding conductivity equation, the results are tabulated in Table I.

D. Thermal conductivity of crystal No. 2

This specimen was 1.3 cm in length and similar in form to No. 1. Thermal conductivity in the absence of a magnetic field was determined as before and the results are indicated in Table II and Fig. 4. From the preceding study of the lines in the etched (111) plane, it is known that for this specimen one set of traces of the imperfect cleavage planes in the (111) planes was $\perp$ to the direction of heat flow. The conductivities in the presence of a field were determined for three orientations of the field relative to the principal cleavage planes. When the field was perpendicular to the trigonal axis the values for thermal conductivity are indicated by curve *B*. For this position, one set of the previously mentioned traces in the (111) plane were $\perp$ to the direction of heat flow and $\parallel$ to *H*. With the field rotated 45° from this position the conductivity decreased relative to the previous position as indicated by curve *C*. With the field parallel to the trigonal axis, curve *D* indicates that the thermal conductivity increased and became greater than in either of the two former positions. In the case of electrical conductivity, the conductivity for

TABLE II. *Trigonal axis P perpendicular to length of specimen. Heat flow ⊥P and H.*

No Field		$H \perp P$		$H \parallel P$		H 45° from $H\perp$ and $H\parallel$	
Temp.	K	Temp.	K	Temp.	K	Temp.	K
168.5	0.0469	159.6	0.0309	165.2	0.0345	151.1	0.0280
163.9	0.0445	142.5	0.0273	158.9	0.0316	139.9	0.0266
156.1	0.0409	129.2	0.0252	144.8	0.0290	136.9	0.0261
141.4	0.0367	115.1	0.0236	135.8	0.0272	133.1	0.0257
131.7	0.0344	103.4	0.0231	126.3	0.0264	131.8	0.0250
120.7	0.0316	95.5	0.0225	114.9	0.0247	128.0	0.0246
113.2	0.0309	75.5	0.0218	99.0	0.0237		
100.6	0.0293			57.6	0.0227		
84.4	0.0278						
64.8	0.0272						

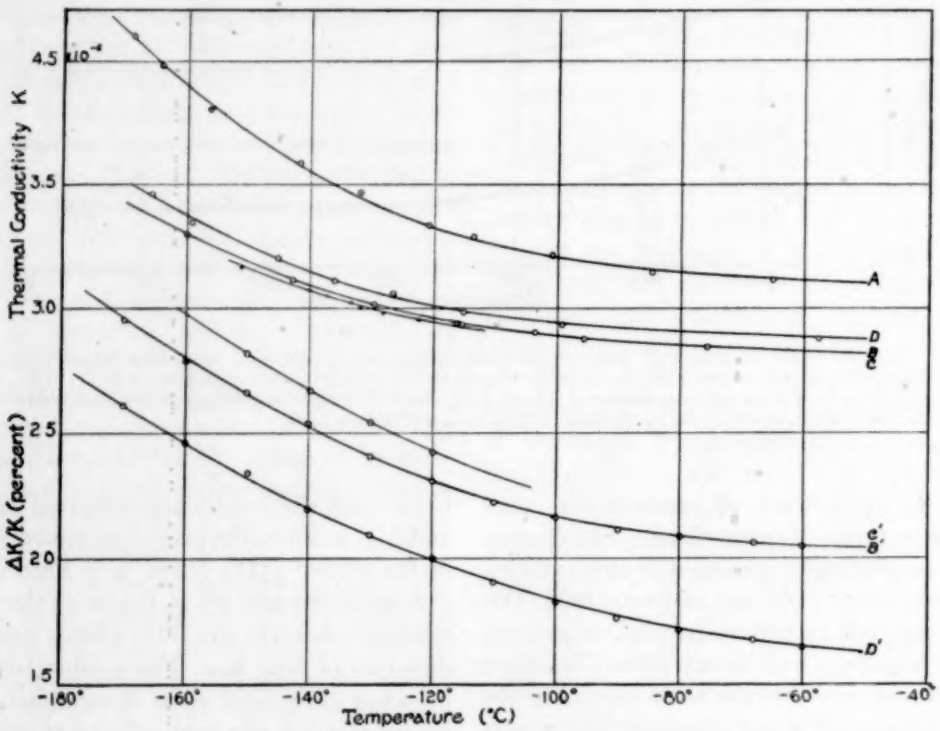

FIG. 4. Effect of magnetic field on thermal conductivity of bismuth crystal No. 2. Curve A, heat flow perpendicular to trigonal axis—no magnetic field; curve B, magnetic field perpendicular to trigonal axis; curve C, magnetic field along line 45° from A or B of Fig. 2; curve D, magnetic field parallel to trigonal axis. Corresponding curves of $\Delta K/K$ for these are, respectively, B', C', D'.

$H \perp P$ is indicated in Fig. 2A, and with the field rotated 45° from this position the conductivity decreased relative to the former position as indicated at C. With $H \parallel P$, Fig. 2B indicates that the conductivity increased relative to position C.

These results for thermal conductivity could be repeated consistently from time to time as well as for different values of wattage input in the heating coil and hence are evidently fixed characteristics for this crystal orientation.

In conclusion, I wish to express my appreciation to Dr. C. E. Mendenhall for his interest throughout this work.

Transport Phenomena in Einstein-Bose and Fermi-Dirac Gases. II

E. A. UEHLING, *University of California**

(Received September 24, 1934)

In this paper the general theory of transport phenomena in simple gases is concluded, and numerical values of the gas coefficients for heat conductivity and viscosity are obtained as a function of the temperature and density for the particular case of molecules acting as rigid elastic spheres. In the Introduction will be found a qualitative discussion of the principal results obtained and an interpretation of these results according to elementary considerations. In Section 1 the method of solution of the integral equations with which the formal theory of Part I was concluded is given together with the resulting general equations for the heat conductivity and viscosity coefficients. Since the integral equations can be solved only by a method of successive approximations, the expressions for the gas coefficients are in the form of infinite series the rapidity of convergence of which depends on a suitable choice of a complete set of auxiliary functions. In Section 2 all of the integrals appearing in the first two terms of the infinite series are evaluated. That only two terms are required is due to the fact that one is able to make an excellent choice of functions to represent the auxiliary set. In the evaluation of these integrals restriction is made in the application of the theory to small values of the degeneracy parameter A, since only terms in the zeroth and first power of A are retained. This restriction is only slightly greater than that imposed by the fundamental postulates of the general theory which restrict its applicability to moderately rare gases. In Section 3 the final equations for the gas coefficients are applied to gases consisting of molecules which interact quantum-mechanically as rigid elastic spheres of diameters and masses associated with the gases helium and hydrogen.

INTRODUCTION

IT has been shown in Part I[1] that the method of Lorentz, Hilbert and Enskog for the treatment of transport phenomena can be extended to take into account the modifications introduced by the quantum theory. In this paper the explicit solution of the integral equations will be obtained, and the general formulae for viscosity and heat conductivity will be developed. Numerical results for the case of the elastic sphere model will then be given. As already mentioned in Part I the quantum theory introduces two modifications into the classical kinetic theory of gases.

(a) The collision between two gas molecules which is the elementary process in all transport phenomena must be treated according to the quantum theory of collisions. Deviations from the classical theory may be expected, therefore, if the de Broglie wave-length corresponding to the mean temperature motion: $\lambda=\hbar/(mkT)^{\frac{1}{2}}$ is comparable to or larger than the diameter s of the molecule. Just as in the classical treatment, the mean free path l is inversely proportional to the density ρ, but the proportionality factor is now dependent on the temperature even for the case of elastic spheres. In fact $l\sim 1/\rho f(\lambda/s)$, where for small values of λ/s, f approaches the classical value. Thus, the temperature dependence of the gas coefficients will be different than in the classical treatment. For light gases like H_2 and He, λ/s is already as large as 0.1 at room temperatures, so that considerable deviations even at high temperatures may be expected. Massey and Mohr[2] have recently taken this effect into account by introducing the quantum theoretically determined differential cross-sectional area into the classical expressions of Chapman for the gas coefficients. The complete justification of this procedure for temperatures which are not *too* low will be given in this paper.

(b) For temperatures which are very low the second modification becomes important. This effect is a consequence of the change in the Stosz-zahlansatz, which is equivalent to a change in the equilibrium distribution function from the Maxwell-Boltzmann to the Einstein-Bose or Fermi-Dirac distribution law. Due to this modification the mean free path l, even for an ideal gas, will be no longer strictly inversely proportional to the density. Instead $l\sim 1/\rho(1+\alpha\rho\lambda^3)$, where α is a numerical factor, the sign of which depends on the statistics. Thus one

* National Research Fellow.

[1] E. A. Uehling and G. E. Uhlenbeck, Phys. Rev. **43**, 552 (1933).

[2] Massey and Mohr, Proc. Roy. Soc. **A141**, 434 (1933); **A144**, 188 (1934).

observes that the deviation from the inverse proportionality of l and ρ depends on the magnitude of λ/d where d is the mean distance between the molecules. In contrast with the first quantum effect the second will be small at ordinary temperatures, and will become important only at very low temperatures or very high densities. The ordinary reasoning, therefore, by which one shows in the classical kinetic theory the independence of the gas coefficients on the density is no longer strictly valid. At low temperatures the viscosity and heat conductivity coefficients become density dependent and the direction of the dependence is different for the two statistics.

That the latter effect depends on the magnitude of the parameter λ/d and therefore on the density as well as on the temperature requires that one consider also other possible contributions to the density dependence. Such an additional effect is the modification in the Stoszzahlansatz due to the extension of the molecules, a modification which again is equivalent to a departure from the strict inverse proportionality in the classical theory of l and ρ. Thus, even when considered classically, there will be a small density correction to the gas coefficients which becomes important for sufficiently high densities. In fact, one can write for the case of elastic spheres $l\sim 1/\rho(1+\beta\rho s^3)$, where β is a numerical factor, and s is the diameter of the molecule. This correction, which has been carefully estimated by Enskog,[3] will be used as a criterion for the estimation of the importance of the rare gas density correction of the quantum theory, and as a criterion, furthermore, for an estimate of the possibility of an experimental test of the statistics. Since the magnitude of the quantum correction depends on the parameter λ/d, and the correction due to the extension of the molecules depends on the parameter s/d which is temperature independent in the case of elastic spheres, there will exist a temperature sufficiently low for which the latter is negligible in comparison with the former at any density.

Applying the general formulae developed in this paper to the rigid elastic sphere model, one finds that only below about 15°A does the quantum theoretical density correction, which, depending on λ^3 varies as the inverse three-halves power of the temperature, have a magnitude greater than the classical density correction of the Enskog theory. In the case of helium, for example, one can expect at temperatures slightly greater than its critical temperature a correction of about $2\frac{1}{2}$ percent in the viscosity coefficient per atmosphere of pressure compared with the value of this coefficient in the limiting case of zero density, whereas the classical density correction due to the extension of the molecules should be about 0.5 percent. Assuming the Einstein-Bose statistics these corrections are of opposite sign. In this case the possibility of an experimental test of the statistics seems to be a favorable one. It is less favorable in the case of the heat conductivity coefficient for which the classical corrections are larger and the quantum corrections are smaller than for the viscosity coefficient. It is less favorable, also, in the case of other gases, hydrogen, for example, for which the range of temperatures and densities which lie well within the vapor phase are less suitable than in the case of helium for a test of this kind.

2. Solution of the Integral Equations

The formal theory of transport phenomena has given the following expressions for the heat conductivity and viscosity coefficients, κ and η

$$\kappa=\frac{3k}{2m}\frac{(mkT)^{\frac{1}{2}}}{s^2}\frac{2}{3}[\pi_i,\pi_i], \tag{43}$$

$$\eta=\frac{(mkT)^{\frac{1}{2}}}{s^2}\frac{3}{2}[\pi_{ij},\pi_{ij}], \tag{46}$$

where m is the mass of the molecule, s is a quantity having the dimensions of length, or in the case of elastic sphere molecules may be taken as representing the molecular diameter, and $\pi_i=\xi_i\chi_a(\tau)$ and $\pi_{ij}=(\xi_i\xi_j-\tau^2/3\delta_{ij})\chi_b(\tau)$ are solutions of the inhomogeneous integral equations:

$$\left.\begin{aligned}\frac{f^{(o)2}}{A^2e^{-\tau^2}}\xi_j\left(\tau^2-\frac{5}{2}\frac{p}{nkT}\right)&=J(\pi_j), \quad \text{a}\\ \frac{f^{(o)2}}{A^2e^{-\tau^2}}\left(\xi_i\xi_j-\frac{\tau^2}{3}\delta_{ij}\right)&=J(\pi_{ij}), \quad \text{b}\end{aligned}\right\} \tag{34}$$

[3] Kungl. Svenska Vetenskapsakademien Handlungar. 63, 5 (1921).

so determined that they fulfill the auxiliary conditions:

$$\int \psi_k f^{(o)}(1+\theta f^{(o)})\pi d\omega = 0 \quad (k=1, 2, \cdots 5), \quad (36)$$

$\psi_k = m$, $m\xi_1$, $m\xi_2$, $m\xi_3$ and mv^2 being the five solutions (spoken of henceforth as null solutions) of the homogeneous equation: $J(\psi)=0$ where, furthermore

$$J(F) = \frac{1}{s^2A^2}\int d\omega_1 \int d\Omega \cdot \gamma I(\vartheta\gamma) \cdot (F+F_1-F'-F_1') \cdot f^{(o)} f_1^{(o)} \times (1+\theta f^{(o)\prime}(1+\theta f_1^{(o)\prime}), \quad (32)$$

$$[F, G] = \int d\omega \cdot G J(F). \quad (32a)$$

For the remainder of the notation reference should be made to Part I.[4]

Eqs. (34a and b) will be solved by the Enskog method of successive approximations.[5] If one has a complete set of functions $h^{(r)}$ which fulfill the following conditions:

(a) $\int \psi_k f^{(o)}(1+\theta f^{(o)}) h^{(r)} d\omega = 0 \quad \begin{Bmatrix} k=1, 2, \cdots 5 \\ r=1, 2, \cdots \end{Bmatrix}$

(b) Linear independence,

(c) The integrals $[h^{(r)}, h^{(s)}]$ and $[h^{(r)}, \pi]$ have finite definite values,

a function $\pi^{(n)}$ may be constructed as a linear combination of the functions $h^{(r)}$ $(r=1, 2, \cdots n)$, and the n constants of $\pi^{(n)}$ may be so determined as to minimize the integral $[\pi-\pi^{(n)}, \pi-\pi^{(n)}]$. According to the fourth of the properties of this operator discussed in Part I:[6]

$[F, G]=[G, F]$,
$[F, G+H]=[F, G]+[F, H]$,
$[F, cG]=c[F, G]$, where c is independent of all
$[F, F]\geq 0$ variables of integration,

the integral $[\pi-\pi^{(n)}, \pi-\pi^{(n)}]$ can never be negative. Should one succeed in minimizing it to the value zero, the function $\pi^{(n)}$ for which this condition exists becomes the sought for solution. This result is a consequence of the fact that $\pi-\pi^{(n)}$ under this condition can be only a null solution. It satisfies, however, the auxiliary conditions since π as well as $\pi^{(n)}$ (which is only a linear combination of the $h^{(r)}$) separately satisfy these conditions. A function satisfying the auxiliary conditions, and which is itself a null solution can only be zero. Consequently $\pi=\pi^{(n)}$.

The values of the constants c_r in the function

$$\pi^{(n)} = \sum_{r=1}^{n} c_r h^{(r)} \quad (62)$$

are now determined by applying the condition for an extreme of $H^{(n)}=[\pi-\pi^{(n)}, \pi-\pi^{(n)}]$. This condition is

$$\partial H^{(n)}/\partial c_r = -2\left[h^{(r)}, \pi - \sum_{s=1}^{n} c_s h^{(s)}\right] = 0$$

or defining $a_{rs}=[h^{(r)}, h^{(s)}]$ and $\alpha_s=[h^{(s)}, \pi]$ the set of equations determining the extreme of $H^{(n)}$ is:[7]

[4] The operator previously designated as $I(F)$ is now written $J(F)$, and the primes attached to the operators $[F, G]$ and which were used to distinguish them from analogous operators which also appeared in the formal theory are here omitted since no confusion can arise. The differential cross-sectional area previously designated by $w(\vartheta\gamma)$ is now written as $I(\vartheta\gamma)$ to conform to the more usual notation.

[5] Dissertation, Uppsala, 1917, p. 43; Courant-Hilbert, *Methoden der Mathematischen Physik* I, chapter 3.

[6] That this operator has these properties becomes immediately obvious from the fact that $\int d\omega \cdot GJ(F)$ is unchanged if G is replaced by G_1, $-G'$, of G_1'. One may show also that the analogous operator

$$[F, G] = \int F(\xi_i) G(\xi_i) d\omega - \int\int F(\xi_i) G(\xi_i') K(\tau\tau'\epsilon) d\omega d\omega'$$

obtained from the homogeneous part of the integral equation in its more usual form

$$f(\xi_i) = \pi(\xi_i) - \int \pi(\xi_i') K(\tau\tau'\epsilon) d\omega'$$

into which form Eqs. (34a and b) may be put (Eq. (37), Part I) has these properties in general if the kernel is symmetrical and is positive definite with a first eigen value greater than or equal to unity. The kernel of Eqs. (34a and b) when the equations are written in the standard form has these properties.

[7] That the extreme of $H^{(n)}$ thus determined is actually a minimum and not a maximum is shown by obtaining the second differential quotients and developing $H^{(n)}$ for values of c_r slightly different than those determined by Eq. (63) in a Taylor series. One obtains, since $H^{(n)}$ is a quadratic function of the $h^{(r)}$

$$\frac{\partial^2 H^{(n)}}{\partial c_r \partial c_s} = 2[h^{(r)}, h^{(s)}], \qquad H^{(n)} = H_0^{(n)} + [\Sigma_r c_r' h^{(r)}, \Sigma_r c_r' h^{(r)}],$$

where $c_r' = c_r - c_{r0}$, the c_{r0} are the constants determined by Eqs. (63), and $H_0^{(n)}$ is the corresponding value of $H^{(n)}$. According to the fourth property of the square bracket operator the first variation of $H^{(n)}$ is positive. Furthermore, $H^{(n)}$ is equal to $H_0^{(n)}$ *only* when the c_r' are zero, since $\Sigma_r c_r' h^{(r)}$ cannot be a null solution consistently with the requirement that the $h^{(r)}$ be linearly independent and at the same time satisfy the auxiliary conditions.

$$\sum_{s=1}^{n} c_s a_{rs} - \alpha_r = 0 \qquad r = 1, 2, \cdots n. \quad (63)$$

From Eqs. (62) and (63) the nth approximation function $\pi^{(n)}$ then becomes

$$\pi^{(n)} = \sum_{s=1}^{n} (A_s^{(n)}/A^{(n)}) h^{(s)}, \quad (64)$$

where $A^{(n)}$ is the determinant $||a_{ij}||$ of n rows and columns, and $A_s^{(n)}$ is the determinant $A^{(n)}$ with the sth column a_{is} replaced by α_i. In order to make the character of the successive approximations of $\pi^{(n)}$ to the true solution π apparent in Eq. (64), this equation will be transformed so that the difference between $\pi^{(n)}$ and $\pi^{(n-1)}$ appears only in the last (the nth) term of $\pi^{(n)}$. Written in this manner Eq. (64) becomes

$$\pi^{(n)} = \sum_{s=1}^{n} [A_s^{(s)} D_s^{(s)}/(A^{(s-1)} A^{(s)})], \quad (65)$$

where $D_s^{(s)}$ is the determinant $A^{(s)}$ with the last (the sth) row a_{sj} replaced by $h^{(j)}$, or since the elements a_{ij} are symmetrical, $D_s^{(s)}$ is the determinant $A^{(s)}$ with the last column a_{is} replaced by $h^{(i)}$.

One can show now that the following relations exist:

$$\left.\begin{aligned} [h^{(r)}, D_s^{(s)}] &= A^{(s)} \qquad r = s \\ &= 0 \qquad r < s \end{aligned}\right\}, \quad (66)$$

$$\left.\begin{aligned} [D_s^{(s)}, D_r^{(r)}] &= A^{(s-1)} A^{(s)} \quad r = s \\ &= 0 \qquad r \neq s \end{aligned}\right\}, \quad (67)$$

$$[\pi, D_s^{(s)}] = A_s^{(s)} \quad (68)$$

and that as a consequence

$$[\pi^{(n)}, \pi^{(n)}] = [\pi, \pi^{(n)}] \quad (69)$$

$$= \sum_{s=1}^{n} [A_s^{(s)2}/A^{(s-1)} A^{(s)}]. \quad (70)$$

From Eq. (66) $A^{(1)} = a_{11}$ is a positive quantity since $h^{(1)}$ is not a null solution. Similarly from Eq. (67) using the result that $A^{(1)} > 0$, the fact that $D_s^{(s)}$ cannot be a null solution because of the linear independence of the $h^{(i)}$ and the existence for $h^{(i)}$ of the auxiliary conditions, and the fourth property of the operator $[F, F]$, one can show that $A^{(s)}$ for each successive value of s cannot be negative or zero. Consequently, each term of $[\pi^{(n)}, \pi^{(n)}]$ (Eq. 69) is positive. That $[\pi^{(n)}, \pi^{(n)}]$ is also bounded is proven from the relation

$$\left.\begin{aligned} [\pi - \pi^{(n)}, \pi - \pi^{(n)}] &\geq 0 \\ [\pi, \pi] - 2[\pi, \pi^{(n)}] + [\pi^{(n)}, \pi^{(n)}] &\geq 0 \end{aligned}\right\} \quad (71)$$

and the result of Eq. (69) from which Eq. (71) becomes

$$[\pi, \pi] - \sum_{s=1}^{n} \frac{A_s^{(s)2}}{A^{(s-1)} A^{(s)}} \geq 0.$$

Thus $[\pi^{(n)}, \pi^{(n)}]$ is bounded provided Eqs. (34a and b) have solutions such that the integral $[\pi, \pi]$ is finite. That $[\pi^{(n)}, \pi^{(n)}]$ actually converges to this upper limit as n approaches infinity may be proven in a manner analogous to that used by Enskog in the classical case. One may write then

$$[\pi, \pi] = \lim_{n \to \infty} \sum_{s=1}^{n} \frac{A_s^{(s)2}}{A^{(s-1)} A^{(s)}},$$

which, when introduced into Eq. (43) gives for the heat conductivity coefficient

$$\kappa = \frac{3k}{2m} \frac{(mkT)^{\frac{1}{2}}}{s^2} \frac{2}{3} \sum_{s=1}^{\infty} \frac{A_s^{(s)2}}{A^{(s-1)} A^{(s)}}. \quad (72)$$

The solution of Eq. (34b) is obtained in a similar manner using functions $k^{(r)}$ satisfying conditions analogous to those of $h^{(r)}$ which involve now the solutions π_{ii} instead of π_i. Defining as before the quantities $b_{rs} = [k^{(r)}, k^{(s)}]$ and $\beta_r = [k^{(r)}, \pi]$, constructing the function $\pi^{(n)}$ and the integral $H^{(n)}$ which is then minimized to completely determine $\pi^{(n)}$, one obtains finally for the viscosity coefficient from Eq. (46)

$$\eta = \frac{(mkT)^{\frac{1}{2}}}{s^2} \frac{3}{2} \sum_{s=1}^{\infty} \frac{B_s^{(s)2}}{B^{(s-1)} B^{(s)}}, \quad (73)$$

where $B^{(i)}$ and $B_i^{(i)}$ are determinants analogous to $A^{(i)}$ and $A_i^{(i)}$ defined as before, but with the functions $k^{(r)}$ (b_{rs} and β_r) instead of $h^{(r)}$ (a_{rs} and α_r).

We will now make a choice of the functions $h^{(r)}$ and $k^{(r)}$. The analysis of Part I (§8 and note 4) has shown that the solutions of Eqs. (34a and b) are of the form: $\pi_i = \xi_i \chi_a(\tau^2)$, $\pi_{ii} = (\xi_i^2 - \tau^2/3) \chi_b(\tau^2)$. These functions are ac-

cordingly chosen so as to be proportional to ξ_i and $(\xi_i^2-\tau^2/3)$, respectively, and to depend otherwise only on τ^2 in such a way that the $\pi^{(n)}$ constructed from these functions represent power series in τ^2. Using now further the fact that they must satisfy the auxiliary conditions one obtains as a suitable choice:

$$\left.\begin{aligned} h^{(r)} &= \xi\left[\tau^{2r}-\frac{\Gamma(r+5/2)}{\Gamma(5/2)}\frac{F_{r+1}}{F_1}\right] && \text{a}\\ k^{(r)} &= (\xi^2-\tau^2/3)\tau^{2r-2} && \text{b}\end{aligned}\right\} \quad (74)$$

where

$$F_{r+1}=\frac{1}{\Gamma(r+3/2)}\int_0^\infty \frac{z^{r+1}dz}{(1/A)\exp z-\theta}. \quad (75)$$

3. Evaluation of the Integrals

§ 1. The functions α_r and β_r

Introducing the expression for $h^{(r)}$ into the definition of α_r, and making the substitutions:[8]

$$\frac{f^{(0)2}}{A^2e^{-\tau^2}}=-\frac{1}{2\tau}\frac{\partial f^{(0)}}{\partial\tau}, \qquad p/nkT=F_{3/2}/F_{1/2},$$

$$\int_0^\infty \frac{\partial f^{(0)}}{\partial\tau}\tau^m d\tau=-m\int_0^\infty f^{(0)}\tau^{m-1}d\tau=-\frac{m}{2}\Gamma\left(\frac{m}{2}\right)F_{m/2-1},$$

one obtains

$$\alpha_r=\frac{2\pi}{3A}\Gamma\left(\frac{2r+7}{2}\right)\left[F_{(2r+3)/2}-\frac{5}{2r+5}\frac{F_{(2r+1)/2}F_{3/2}}{F_{1/2}}\right]. \quad (76)$$

But for $A<1$, to which all future considerations will be restricted

$$F_p=A\left[1+\frac{\theta A}{2^{p+1}}+\frac{(\theta A)^2}{3^{p+1}}+\cdots+\frac{(\theta A)^{n-1}}{n^{p+1}}+\cdots\right].$$

Accordingly, for $A\ll 1$

$$\alpha_r=\frac{2\pi r}{3}\Gamma\left(\frac{2r+5}{2}\right)\left[1+\frac{\theta A}{2^{r+5/2}}\left\{\frac{2r+5}{2r}+\frac{5}{r}(2^{r-1}-1)\right\}\right]. \quad (77)$$

Similarly, introducing the expression for $k^{(r)}$ into the definitions of β_r

$$\beta_r=\frac{8\pi}{45A}\Gamma\left(\frac{2r+5}{2}\right)F_{(2r+1)/2} \quad (78)$$

and for $A\ll 1$

$$\beta_r=\frac{8\pi}{45}\Gamma\left(\frac{2r+5}{2}\right)\left[1+\frac{\theta A}{2^{r+1}}\right]. \quad (79)$$

§ 2. The functions a_{rq} and b_{rq}

These functions will be evaluated only for the case of $A\ll 1$. They have been defined in Section 2 in the following manner:

$$a_{rq}=[h^{(r)},h^{(q)}]=\frac{1}{4s^2A^2}\int d\omega\int d\omega_1\int d\Omega\cdot\gamma I(\vartheta\gamma)(h^{(r)}+h_1^{(r)}-h^{(r)\prime}-h_1^{(r)\prime})$$

$$\times(h^{(q)}+h_1^{(q)}-h^{(q)\prime}-h_1^{(q)\prime})f^{(0)}f_1^{(0)}(1+\theta f^{(0)\prime})(1+\theta f_1^{(0)\prime}) \quad (80)$$

with an analogous expression for b_{rq} using $k^{(r)}$ and $k^{(q)}$ for $h^{(r)}$ and $h^{(q)}$. It is convenient now to introduce a transformation of variables from $\xi\eta\zeta\xi_1\eta_1\zeta_1$ to $\gamma\lambda\theta\delta\alpha\epsilon$ where $\gamma=g(m/4kT)^{\frac{1}{2}}$ as previously defined; $\lambda=l(m/kT)^{\frac{1}{2}}$, l being the actual velocity of motion of the center of gravity of the interacting

[8] *Transport Phenomena* I, Eq. (60).

molecules; θ and δ are the polar and azimuthal angles respectively describing the direction of the vector l; and α and ϵ are the polar and azimuthal angles respectively describing the direction of the vector g with respect to the vector l. In collision the only variables of this system which undergo alteration are α and ϵ which after collision become α' and ϵ', and then describe the direction of the vector g' with respect to the vector l. Introducing the considerations of the velocity pyramid, one obtains for the function $h^{(r)}$ in terms of the new variables

$$h^{(r)}=2^{-r-\frac{1}{2}}[\lambda\cos\theta-\gamma(\cos\alpha\cos\theta-\sin\alpha\sin\theta\cos\epsilon)](\lambda^2+\gamma^2-2\gamma\lambda\cos\alpha)^r, \tag{81}$$

$$h_1^{(r)}=2^{-r-\frac{1}{2}}[\lambda\cos\theta+\gamma(\cos\alpha\cos\theta-\sin\alpha\sin\theta\cos\epsilon)](\lambda^2+\gamma^2+2\gamma\lambda\cos\alpha)^r \tag{82}$$

plus terms which contribute nothing to the expression a_{rq}. Similarly, for the function $k^{(r)}$ one obtains

$$k^{(r)}=2^{-r}[(\cos^2\theta-\tfrac{1}{3})(\lambda^2+\gamma^2-2\gamma\lambda\cos\alpha)^r+(\gamma^2\sin^2\theta\sin^2\alpha\cos^2\epsilon-\gamma^2\cos^2\theta\sin^2\alpha$$
$$+2\gamma\lambda\sin\theta\cos\theta\sin\alpha\cos\epsilon+\gamma^2\sin\theta\cos\theta\sin 2\alpha\cos\epsilon)(\lambda^2+\gamma^2-2\gamma\lambda\cos\alpha)^{r-1}], \tag{83}$$

$$k_1^{(r)}=2^{-r}[(\cos^2\theta-\tfrac{1}{3})(\lambda^2+\gamma^2+2\gamma\lambda\cos\alpha)^r+(\gamma^2\sin^2\theta\sin^2\alpha\cos^2\epsilon-\gamma^2\cos^2\theta\sin^2\alpha$$
$$-2\gamma\lambda\sin\theta\cos\theta\sin\alpha\cos\epsilon-\gamma^2\sin\theta\cos\theta\sin 2\alpha\cos\epsilon)(\lambda^2+\gamma^2+2\gamma\lambda\cos\alpha)^{r-1}]. \tag{84}$$

Analogous expressions exist for the primed functions in which α' and ϵ' appear everywhere for α and ϵ. The differential product in the new variable becomes, furthermore

$$d\omega d\omega_1=\lambda^2\gamma^2\sin\theta d\theta d\delta\sin\alpha d\alpha d\epsilon d\gamma d\lambda. \tag{85}$$

Before introducing the new variables into the distribution function $f^{(o)}$, this function is to be expanded in ascending powers of A for values of $A<1$. One obtains finally after retaining only powers of A up to and including the first:

$$f^{(o)}f_1^{(o)}(1+\theta f^{(o)\prime})(1+\theta f_1^{(o)\prime})=A^2e^{-(\lambda^2+\gamma^2)}[1+2\theta Ae^{-\frac{1}{2}(\lambda^2+\gamma^2)}\cdot\{\cosh(\gamma\lambda\cos\alpha)+\cosh(\gamma\lambda\cos\alpha')\}]. \tag{86}$$

The function a_{rq} then becomes

$$a_{rq}=\frac{1}{2s^2}\int_0^\infty\int_0^\infty e^{-(\lambda^2+\gamma^2)}\gamma^3\lambda^2d\gamma d\lambda\int_0^\pi\int_0^{2\pi}\sin\theta d\theta d\delta\int_0^\pi\int_0^{2\pi}\sin\alpha d\alpha d\epsilon\cdot\int_0^\pi\int_0^{2\pi}I(\vartheta\gamma)\sin\vartheta d\vartheta d\varphi$$
$$\cdot(h^{(r)}+h_1^{(r)}-h^{(r)\prime}-h_1^{(r)\prime})(h^{(q)}+h_1^{(q)})+\frac{\theta A}{s^2}\int_0^\infty\int_0^\infty e^{-\frac{1}{2}(\lambda^2+\gamma^2)}\gamma^3\lambda^2d\gamma d\lambda\int_0^\pi\int_0^{2\pi}\sin\theta d\theta d\delta$$
$$\times\int_0^\pi\int_0^{2\pi}\sin\alpha d\alpha d\epsilon\cdot\int_0^\pi\int_0^{2\pi}I(\vartheta\gamma)\sin\vartheta d\vartheta d\varphi\cdot(h^{(r)}+h_1^{(r)}-h^{(r)\prime}-h_1^{(r)\prime})(h^{(q)}+h_1^{(q)})$$
$$\cdot\{\cosh(\gamma\lambda\cos\alpha)+\cosh(\gamma\lambda\cos\alpha')\}, \tag{87}$$

the function b_{rq} being an analogous expression with $k^{(r)}$ and $k^{(q)}$ appearing everywhere for $h^{(r)}$ and $h^{(q)}$.

Integration over all values of the variable φ, the azimuthal collision parameter, is accomplished with the help of the Maxwell theorem of spherical harmonics.[9] The following notation is used in the development of the various functions of the integrand considered as functions of $\alpha\epsilon$ and $\alpha'\epsilon'$ in spherical harmonics: The development coefficients in the functions

$(h^{(r)}+h_1^{(r)})$ are $c_{lp}^{(r)\prime}$, $c_{lp}^{(r)\prime\prime}$

$(h^{(r)}+h_1^{(r)})(h^{(q)}+h_1^{(q)})$ $d_{lp}^{(r,\,q)\prime}$, $d_{lp}^{(r,\,q)\prime\prime}$

[9] Maxwell, *Sc. Papers* II, 681; Boltzmann, *Gastheorie* I, 171.

$\cosh(\gamma\lambda\cos\alpha)$	are e_{lp}', e_{lp}''
$(h^{(r)}+h_1^{(r)})\cosh(\gamma\lambda\cos\alpha)$	$f_{lp}^{(r)'}, f_{lp}^{(r)''}$
$(h^{(r)}+h_1^{(r)})(h^{(q)}+h_1^{(q)})\cosh(\gamma\lambda\cos\alpha)$	$g_{lp}^{(r,q)'}, g_{lp}^{(r,q)''}$

where a typical development is

$$(h^{(r)}+h_1^{(r)})=\sum_{l=0}^{\infty}\sum_{p=0}^{l}(c_{lp}^{(r)'}\cos\epsilon+c_{lp}^{(r)''}\sin\epsilon)P_l^{(p)}(\cos\alpha).$$

Integrating then over φ with the aid of the Maxwell theorem, adding and subtracting suitable series involving $\int_0^\pi I(\vartheta\gamma)\sin\vartheta d\vartheta$, using relations existing among the coefficients to show that the sum of all terms which then do not involve $\int_0^\pi[1-P_l(\cos\vartheta)]I(\vartheta\gamma)\sin\vartheta d\vartheta$ is identically zero, integrating over α and ϵ, and defining a function

$$\theta^{(l)}(\gamma)=\frac{1}{s^2}\int_0^\pi[1-P_l(\cos\vartheta)]I(\vartheta\gamma)\sin\vartheta d\vartheta, \tag{88}$$

where the cross-sectional area effective in transport will be defined then as

$$Q_T^{(l)}(\gamma)=2\pi s^2\theta^{(l)}(\gamma) \tag{89}$$

one obtains finally

$$\begin{aligned}a_{rq}=2\pi^2\sum_{l=1}^{\infty}\frac{2}{2l+1}\Bigg[&\int_0^\infty\int_0^\infty e^{-(\lambda^2+\gamma^2)}\gamma^2\lambda^2\theta^{(l)}(\gamma)d\gamma d\lambda\int_0^\pi\sin\theta d\theta\cdot\Bigg\{2c_{lo}^{(r)'}c_{lo}^{(q)'}\\&+\sum_{m=1}^{l}\frac{(l+m)!}{(l-m)!}(c_{lm}^{(r)'}c_{lm}^{(q)'}+c_{lm}^{(r)''}c_{lm}^{(q)''})\Bigg\}+2\theta A\int_0^\infty\int_0^\infty e^{-\frac{1}{2}(\lambda^2+\gamma^2)}\gamma^2\lambda^2\theta^{(l)}(\gamma)d\gamma d\lambda\\&\times\int_0^\pi\sin\theta d\theta\cdot\Bigg\{2(c_{lo}^{(r)'}f_{lo}^{(q)'}+c_{lo}^{(q)'}f_{lo}^{(r)'}-d_{lo}^{(r,q)'}e_{lo}')+\sum_{m=1}^{l}\frac{(l+m)!}{(l-m)!}\\&\times(c_{lm}^{(r)'}f_{lm}^{(q)'}+c_{lm}^{(r)''}f_{lm}^{(q)''}+c_{lm}^{(q)'}f_{lm}^{(r)'}+c_{lm}^{(q)''}f_{lm}^{(r)''}-d_{lm}^{(r,q)'}e_{lm}'-d_{lm}^{(r,q)''}e_{lm}'')\Bigg\}\Bigg].\end{aligned} \tag{90}$$

Similarly, one finds for b_{rq} an analogous function in which the various coefficients represent the development in spherical harmonics of the expressions just described in which $k^{(r)}$ and $k^{(q)}$ appear everywhere instead of $h^{(r)}$ and $h^{(q)}$.

We restrict our considerations now to the second approximation to the solution of the integral equations. Besides α_r and β_r for $r=1, 2$ one requires for this purpose (Eqs. 72 and 73) the six quantities a_{rq} and b_{rq} with $r, q=1, 2$. Determining then, all of the coefficients required in the various developments in spherical harmonics, integrating over θ and λ and defining

$$P^{(l,p)}(\alpha)=\int_0^\infty e^{-\alpha\gamma^2}\gamma^p\theta^{(l)}(\gamma)d\gamma \tag{91}$$

one obtains the expressions for the a_{rq} and b_{rq} which are given in Appendix 1.

The heat conductivity and viscosity coefficients, κ and η, then become (Eqs. 72 and 73):

$$\kappa=\frac{25}{32\pi^{\frac{1}{2}}}\frac{3k}{2m}\frac{\hbar}{\lambda}\frac{3}{2s^2P^{(2,7)}(1)}(1+\epsilon_1)\left[1+\frac{\pi^{\frac{1}{2}}}{4}n\lambda^3\left\{7-\frac{128}{3^{\frac{1}{2}}}\frac{P^{(2,9)}(4/3)+6P^{(2,7)}(4/3)}{9P^{(2,7)}(1)}+\epsilon_1'\right\}\right], \tag{92}$$

$$\eta=\frac{5}{16\pi^{\frac{1}{2}}}\frac{\hbar}{\lambda}\frac{3}{2s^2P^{(2,7)}(1)}(1+\epsilon_2)\left[1+\frac{\pi^{\frac{1}{2}}}{4}n\lambda^3\left\{\frac{4}{3}-\frac{128}{3^4}\frac{P^{(2,7)}(4/3)}{P^{(2,7)}(1)}+\epsilon_2'\right\}\right], \tag{93}$$

where, as defined in the introduction, λ is the de Broglie wave-length corresponding to the mean temperature motion, and n is the number of molecules per unit volume. The small quantities ϵ_1 and ϵ_2 are given by the following equations:

$$\epsilon_1=\frac{[7/2P^{(2,7)}(1)-P^{(2,9)}(1)]^2}{P^{(2,11)}(1)P^{(2,7)}(1)-[P^{(2,9)}(1)]^2+7[P^{(2,7)}(1)]^2},$$

$$\epsilon_2=\frac{[7/2P^{(2,7)}(1)-P^{(2,9)}(1)]^2}{P^{(2,11)}(1)P^{(2,7)}(1)-[P^{(2,9)}(1)]^2+77/6[P^{(2,7)}(1)]^2}.$$

The small quantities ϵ_1' and ϵ_2' involve $P^{(r,q)}(\alpha)$ with values of α equal to $4/3$ in addition to those with α equal to unity; with $r=4$ in addition to those with r equal to 2; and with q having the series of values 13, 11, 9, and 7. These expressions need not be given since their numerical magnitude is always small compared with the principal term of the density correction, which is already small, and except for light gases at low temperatures negligibly small, compared with the term independent of density. The order of magnitude of ϵ_1' and ϵ_2' will be discussed in connection with the application of these formulae to elastic sphere molecules.

Eqs. (92) and (93) for the gas coefficients have been written only for the case of the Einstein-Bose statistics for which the parameter θ of all previous equations has been put equal to $+1$. In the Fermi-Dirac statistics the equations for κ and η are similar to these with the opposite sign for the term depending on density and with the understanding that the integrals $P^{(r,q)}(\alpha)$ will then be evaluated according to these statistics. The term independent of density in these equations is exactly equivalent to the classical expressions of Enskog and Chapman when in the integrals $P^{(r,q)}(\alpha)$ classical cross-sectional areas are introduced instead of the quantum-mechanically determined areas.

It is of interest to consider the ratio of κ and η in connection with the well-known proportionality in the classical theory of this ratio to the specific heat. Neglecting the second approximation quantities ϵ, this ratio becomes, for the case of rigid elastic spheres, when the classical expression for the differential cross-sectional area is introduced $\kappa/\eta=(5/2)(\partial\epsilon/\partial T)_P$, where ϵ is the energy per unit mass, an expression which degenerates to proportionality with the specific heat only in the classical statistics. In the strict quantum theory, however, for the elastic sphere model as well as for a general force law, the coefficient of $n\lambda^3$ is temperature dependent and there are deviations from this simple result.

4. Application to the Rigid Sphere Model

In order to obtain an indication of the magnitude of the effects introduced by the quantum theory, the viscosity and heat conductivity equations will be applied to the case of the rigid elastic sphere molecule. The procedure is to evaluate first of all the differential cross-sectional area $I(\vartheta\gamma)$, then the function $\theta^{(l)}(\gamma)$ given by Eq. (88), and finally the function $P^{(l,p)}(\alpha)$ given by Eq. (91). The general expression for the differential cross-sectional area is:[10]

$$I(\vartheta g)=(1/4K^2)\,|f(\vartheta g)|^2, \tag{94}$$

where

$$f(\vartheta g)=\sum_l(2l+1)(e^{2i\delta_l}-1)P_l(\cos\vartheta), \tag{95}$$

$$K=2\pi mg/h.$$

g is the relative velocity, m the reduced mass of the molecule, and the δ_l are phase angles determined in the asymptotic solution for large values of r of the radial wave equation. Since Eq. (94) is valid only if the molecules may be considered as similar but not identical, one obtains the correct function in the Einstein-Bose statistics by multiplying by a factor 2 and

[10] Faxen and Holtzmark, Zeits. f. Physik **45**, 307 (1927); Massey and Mohr, Proc. Roy. Soc. **A141**, 434 (1933); Mott and Massey, *The Theory of Atomic Collisions*.

summing over even values of l. Similarly, in the Fermi-Dirac statistics one would sum over only the odd values of l. In all further considerations only the Einstein-Bose statistics will be used.

Having determined $I(\vartheta\gamma)$ one may next evaluate the function $\theta^{(l)}(\gamma)$ and with it the transport cross-sectional area. The latter has been defined by Eq. (89). Putting l equal to 2 one obtains the second order transport cross-sectional area, which becomes simply

$$Q_T^{(2)}(\gamma)=3\pi\int_0^\pi I(\vartheta\gamma)\sin^3\vartheta d\vartheta, \qquad (96)$$

whereas the scattering cross-sectional area is defined by the equation

$$Q_s(\gamma)=2\pi\int_0^\pi I(\vartheta\gamma)\sin\vartheta d\vartheta. \qquad (97)$$

Introducing Eqs. (94) and (95) into Eq. (88) and using the recurrence relations for the Legendre functions one obtains for the second order function in the Einstein-Bose statistics

$$\theta^{(2)}(\gamma)=\frac{12}{K^2s^2}\sum_l\left[\frac{16l^2+12l^2-2l-1}{(4l-1)(4l+3)}\sin^2\delta_{2l}\right.$$
$$-\frac{(2l+2)(2l+1)}{4l+3}\cos(\delta_{2l}-\delta_{2l+2})$$
$$\left.\times\sin\delta_{2l}\sin\delta_{2l+2}\right], \qquad (98)$$

where s, as throughout the theory, is an arbitrary quantity having the dimensions of length. In the Fermi-Dirac statistics one would have a similar expression with $2l$ everywhere replaced by $2l+1$.

Our considerations will be restricted now to the case of the rigid elastic sphere model, and the quantity s will be specialized to represent the molecular diameter. The phase angles δ_l are now determined[2] by the equation:

$$\delta_l=\arctan(-1)^l\frac{J_{l+\frac{1}{2}}(Ks)}{J_{-l-\frac{1}{2}}(Ks)}. \qquad (99)$$

Thus, in the particular case of the elastic sphere model the phase angles and therefore $\theta^{(l)}(\gamma)$ are functions of only the single variable $y=Ks$. Consequently, the function $P^{(l,\,p)}(\alpha)$ defined by Eq. (91) can be a function only of the ratio λ/s where $\lambda=\hbar/(mkT)^{\frac{1}{2}}$. This result follows from the fact that $\gamma=g(m/4kT)^{\frac{1}{2}}=K\lambda=y\cdot\lambda/s$, where $K=\frac{1}{2}mg/\hbar$, m being the actual mass and not the reduced mass of the molecule. One obtains, therefore, from Eq. (91)

$$P^{(l,\,p)}(\alpha)=\left(\frac{\lambda}{s}\right)^{p+1}\int_0^\infty e^{-\alpha(\lambda/s)^2y^2}y^p\theta^{(l)}(y)dy. \qquad (100)$$

Thus, besides an explicit dependence of κ and η on λ and s there is an implicit dependence on these quantities only through the ratio of λ and s.

In order to make the results susceptible of comparison with experiment, the integrals will be evaluated for values of s and m corresponding to hydrogen and helium, of which the masses are 1.66189 and 3.2998×10^{-24} gram per molecule, respectively. The diameter of these molecules will be taken as 2.75 and 2.10×10^{-8} cm, respectively. The phase angles have been determined from Eq. (99) for twelve values of $y=Ks$ between 0.25 and 30.0, and from these phase angles the function $\theta^{(2)}(y)$ of Eq. (97) was determined. The results of this calculation are given in Table I, and a curve showing the dependence of the transport cross-sectional area measured in units of the diameter squared as a function of y is given in Fig. 1. It will be observed that $\theta^{(2)}(y)$ and $Q_T^{(2)}(y)$ approach their classical values as y approaches infinity and a value equal to 8 times the classical values as y

TABLE I.

$y=Ks$	$\theta^{(2)}(y)$
0.000	4.000
0.25	3.91
0.5	3.67
1.0	2.77
1.5	1.78
2.0	1.14
3.0	0.88
4.0	.80
5.0	.74
7.0	.67
10.0	.61
20.0	.58
30.0	.53
∞	.500

TABLE II.

λ/s	$P^{(2,\,2)}(1)$
∞	12.000
1.77	7.98
1.02	4.26
0.79	3.24
.56	2.61
.45	2.37
.39	2.27
.21	1.95
.188	1.90
.136	1.82
.125	1.81
.112	1.77
.107	1.76
.103	1.74
.0000	1.500

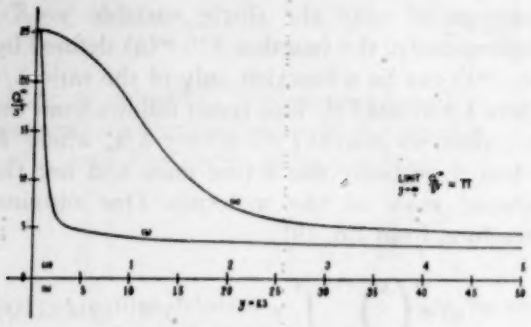

FIG. 1. $Q_T^{(2)}/s^3$ as a function of Ks.

approaches zero. In this respect the transport cross-sectional area differs from the scattering cross section, since the latter, due to the influence of small angle scattering, fails to approach the classical value as y becomes indefinitely large. In the Fermi-Dirac statistics one would find that $\theta^{(2)}(y)$ and $Q_T^{(2)}(y)$ approach the limiting value zero as y approaches zero.

The functions $P^{(l,\,p)}(\alpha)$ are now determined by numerical integration for a series of values of λ/s (a series of values of the temperature). Actually only the integrals with $l=2$, $p=7$, 9 and $\alpha=1$, 4/3 have been evaluated. The remaining integrals appearing in the four ϵ's have not been determined, since it is certain from the form of these expressions that they are somewhat temperature insensitive, and that, consequently, their classical values may be used. These small quantities, when evaluated quantum-mechanically, approach their classical values for $\lambda/s \ll 1$ and $\lambda/s \gg 1$ (limiting case of very high and very low temperatures), and have a slight maximum or minimum at some intermediate temperature depending on the gas. In the case of hydrogen and helium this temperature is in the neighborhood of 1–3° Abs. The quantities ϵ_1 and ϵ_2, for example, exhibit minima equal to zero for s/λ about equal to $\frac{1}{2}$ (T less than 1° Abs. for H_2 and He) and increase monotonously in both directions achieving their classical values of 0.02273 and 0.01485 for s/λ very large and very small. Also the ratio of integrals appearing directly in Eqs. (92) and (93) are temperature insensitive, but in this particular case it is the difference between these ratios and a constant quantity of the same order of magnitude which is of consequence. The direction of the temperature dependence is such as to make the absolute magnitude of this difference increase with decreasing temperature, so that, whereas the ratio of the integrals by themselves vary only by a factor 0.3 between either end of the absolute temperature scale and the temperature at which the maximum is reached, this difference in the case of the heat conductivity coefficient varies by a factor 4.0. Thus, the temperature dependence of the density term in κ and η is by no means confined solely to the appearance of λ^3 in these expressions.

Since the four ϵ's are the quantities coming from the second approximation in the solution of the integral equations, their magnitudes give some idea regarding the nature of convergence of the resulting series. The values of ϵ_1 and ϵ_2 have already been given. Classically, and quantum-mechanically for the case of very high and very low temperatures, ϵ_1' and ϵ_2' add corrections to the density term of about 1.4 and 3.0 percent, respectively. Their temperature dependence has not been investigated, but, as already mentioned, this dependence is certainly small. All of the second approximation corrections are therefore small; in fact, they are of the same order of magnitude as the probable errors in the numerical integrations. In the final numerical results these corrections are, therefore, not included. Various analytical relations exist among the integrals $P^{(l,\,p)}(\alpha)$ which have been helpful as a criterion of the accuracy with which the numerical integration was performed. This accuracy is certainly as good as 3 percent, and is probably somewhat better. Values of all the integrals will not be given, but merely to illustrate the behavior of these functions a set of values of $P^{(2,\,7)}(1)$ is given in Table II, and a curve showing the dependence of $P^{(2,\,7)}(1)$ on s/λ is given in Fig. 2.

The results of the numerical integration are now introduced into Eqs. (92) and (93), and numerical values of κ and η are found as functions of the temperature and density. These results are tabulated as follows: (a) To show the temperature dependence of the principal term. Actually these results should correspond to the limiting case of small densities. For the sake of comparison the best of the available experimental data are also given, most of the experimental data available having been obtained at

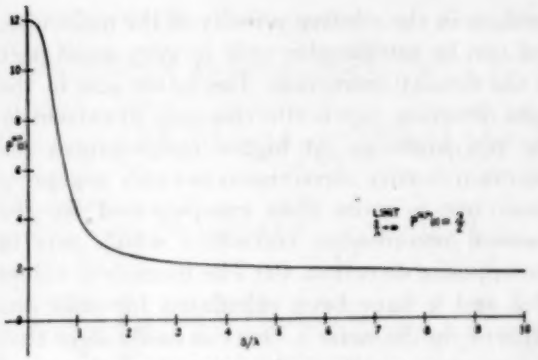

FIG. 2. $P^{(2,\,2)}(1)$ as a function of s/λ.

a pressure of about one atmosphere. These results for the heat conductivity and viscosity coefficients of hydrogen and helium, respectively, appear in Tables III, IV, V and VI. In the case of the viscosity coefficient the calculations leading to these results are a duplication of the published work of Massey and Mohr.[2] These results are given again, however, because they differ from those of Massey and Mohr by an amount exceeding the probable error of the numerical integration. (b) To show the density dependence of the gas coefficients. The results of these calculations appear in Tables VII and VIII for both H_2 and He at temperatures close to the critical temperature. They are tabulated only for one value of the density since the magnitude of the density effect is in first approximation directly proportional to the density. The value of the density chosen corresponds to a value of the degeneracy parameter A equal to 0.1 except at temperatures below the critical value when lower values have been given corresponding to the existence of the vapor phase. Above the critical temperature somewhat higher values of the density than those corresponding to $A=0.1$ may be considered without violating seriously the applicability of the theory. Also, in these tables, for the purpose of comparison with the quantum corrections, appear

TABLE III. *Heat conductivity coefficient of hydrogen, κ in ergs cm^{-2} sec.$^{-1}$ (°C cm^{-1})$^{-1}$.*

T°K	Experiment	Classical theory	Quantum theory ($\rho=0$)
3.0		1.33×10^{3}	0.47×10^{3}
5.0		1.72	0.80
10.0		2.43	1.40
15.4		3.02	1.92
20.9	1.06×10^{3}	3.52	2.38
73.1	4.83	6.58	5.12
123.1	8.12	8.54	6.91
173.1	11.02	10.13	8.36
223.1	13.6	11.50	9.59
273.1	15.9	12.72	10.86
323.1	17.96	13.83	11.97
373.1	20.04	14.53	

TABLE IV. *Heat conductivity coefficient of helium, κ in ergs cm^{-2} sec.$^{-1}$ (°C cm^{-1})$^{-1}$.*

T°K	Experiment	Classical theory	Quantum theory ($\rho=0$)
3.0		1.62×10^{3}	0.62×10^{3}
5.0		2.09	1.03
10.0		2.96	1.76
15.0		3.63	2.31
20.9	2.14×10^{3}	4.28	2.85
73.1	5.55	8.01	6.22
123.1	8.24	10.39	8.31
173.1	10.4	12.32	10.19
223.1	12.3	13.99	11.87
273.1	13.9	15.48	13.49
323.1	15.4	16.83	14.81
373.1	16.7	18.09	

TABLE V. *Viscosity coefficient of hydrogen, η in micropoise.*

T°K	Experiment	Classical theory	Quantum theory ($\rho=0$)
3.0		8.7	3.0
5.0		11.2	5.1
10.0		15.8	9.0
15.4	5.7	20.0	12.4
20.6	8.5	23.0	14.9
70.9	31.9	43.0	32.2
89.6	39.2	48.0	37.2
170.2	60.9	66.0	53.4
273.1	84.2	84.0	70.2
296.1	88.2	88.0	73.6

TABLE VI. *Viscosity coefficient of helium, η in micropoise.*

T°K	Experiment	Classical theory	Quantum theory ($\rho=0$)
3.0		20.8	7.96
5.0		26.8	13.2
10.0		37.9	22.6
15.0	29.46	46.0	29.6
20.2	35.03	52.0	35.7
75.1	81.5	101.0	81.5
88.8	91.8	110	89.7
170.5	139.2	152	129.4
203.1	156.4	167	142.6
250.3	178.8	184	163.4
273.1	187.0	193	173.3
294.5	199.4	200	180.5

TABLE VII. *Density dependence of the viscosity coefficient.*

T°K	A	p (atmos.)	$\left(\frac{\eta_0-\eta_p}{\eta_0}\right)$ Quantum	$\left(\frac{\eta_p-\eta_0}{\eta_0}\right)$ Non-ideal
		Hydrogen		
15.4	0.001	0.068	0.0004	0.0003
20.6	.003	.44	.001	.001
34.0	.1	49.8	.04	.08
		Helium		
3.0	0.03	0.097	0.017	0.0008
5.0	.1	1.15	.05	.006
6.0	.1	1.82	.043	.008
10.0	.1	6.53	.039	.016
15.0	.1	18.0	.037	.03
20.2	.1	37.9	.037	.05

TABLE VIII. *Density dependence of the heat conductivity coefficient.*

T°K	A	p (atmos.)	$\left(\frac{\kappa_0-\kappa_p}{\kappa_0}\right)$ Quantum	$\left(\frac{\kappa_p-\kappa_0}{\kappa_0}\right)$ Non-ideal
		Hydrogen		
20.9	0.003	0.44	0.0003	0.004
34.0	.1	49.8	.009	.27
		Helium		
3.0	0.03	0.096	0.007	0.0026
5.0	.1	1.15	.014	.019
6.0	.1	1.82	.013	.025

the Enskog classical non-ideality corrections discussed in the introduction.

CONCLUSION

Eqs. (92) and (93) are general expressions for the heat conductivity and viscosity coefficients as given by the Einstein-Bose statistics applicable to any gas consisting of molecules whose interaction function is spherically symmetrical. The application of these equations to the rigid sphere type of molecule leads to the following conclusions: (a) As already remarked by Massey and Mohr,[2] the temperature coefficient of viscosity and heat conductivity is not correctly given by the rigid sphere model though the agreement with experiment is considerably better than that given by the classical equations. This improvement is due directly to the increase in the total transport cross-sectional area with decrease in the relative velocity of the molecules, and can be attributable only in very small part to the density correction. The latter acts in the right direction, but is effective only at extremely low temperatures. At higher temperatures the quantum density correction is not only negligibly small but is more than compensated by the classical non-ideality correction which acts in the opposite direction. (b) The numerical values of κ and η have been calculated for only one value of the diameter s. One can easily show that a somewhat smaller value of s than that used would in the case of both H_2 and He give temperature coefficients in better agreement with experiment, but that the numerical values would at nearly all temperatures be somewhat too large. This result follows from the fact that the principal parts of κ and η depend on s and T only through s^3 and s/λ, and that at a particular temperature the derivative of $s^2P^{(2,7)}(1)$ with respect to s is always less than $2sP^{(2,7)}(1)$, its value at the two extremes of the temperature scale. A series development in powers of s/λ would be of interest in determining the exact dependence on s, but such a development has not been obtained. (c) The density correction is by no means negligible under suitable conditions, and seems to be susceptible to experimental test. Such a test leading to an experimental verification of the predictions, would be, also, an experimental verification of the statistics.

It is hoped, now, that the general theory may be extended to include mixtures of gases as well as the simple gases. In concluding this paper I wish to gratefully acknowledge my appreciation and indebtedness to Professor W. Heisenberg for the privilege of working in his Institute where the greater part of this study was made, and for his interest in the problem and the consultations which helped so materially in its eventual solution, and to Professor G. E. Uhlenbeck of the University of Michigan who originally suggested the problem, contributed considerably to the formal portions of the theory, and who was throughout a continual source of valuable criticisms and suggestions.

Appendix 1

The results of the integration in Part 3, §2 are as follows:

$$a_{11}=\frac{8\pi^3\sqrt{\pi}}{9}\left[P^{(2,7)}(1)+\theta A\frac{8}{3}\sqrt{\frac{2}{3}}\left\{\frac{1}{9}P^{(2,9)}\left(\frac{4}{3}\right)+\frac{2}{3}P^{(2,7)}\left(\frac{4}{3}\right)\right\}\right],$$

$$b_{11}=\frac{16\pi^3\sqrt{\pi}}{45}\left[P^{(2,7)}(1)+\theta A\frac{8}{3}\sqrt{\frac{2}{3}}P^{(2,7)}\left(\frac{4}{3}\right)\right],$$

$$a_{21}=\frac{8\pi^3\sqrt{\pi}}{9}\left[P^{(2,9)}(1)+\frac{7}{2}P^{(2,7)}(1)+\theta A\frac{8}{3}\sqrt{\frac{2}{3}}\left\{\frac{26}{189}P^{(2,11)}\left(\frac{4}{3}\right)+\frac{31}{27}P^{(2,9)}\left(\frac{4}{3}\right)+\frac{14}{9}P^{(2,7)}\left(\frac{4}{3}\right)-\frac{4}{945}P^{(4,11)}\left(\frac{4}{3}\right)\right\}\right],$$

$$b_{21}=\frac{8\pi^3\sqrt{\pi}}{45}\left[P^{(2,9)}(1)+\frac{7}{2}P^{(2,7)}(1)+\theta A\frac{8}{3}\sqrt{\frac{2}{3}}\left\{\frac{4}{3}P^{(2,9)}\left(\frac{4}{3}\right)+\frac{7}{3}P^{(2,7)}\left(\frac{4}{3}\right)\right\}\right],$$

$$a_{22}=\frac{8\pi^3\sqrt{\pi}}{9}\left[P^{(2,11)}(1)+7P^{(2,9)}(1)+\frac{77}{4}P^{(2,7)}(1)+\theta A\frac{8}{3}\sqrt{\frac{2}{3}}\left\{\frac{124}{729}P^{(2,13)}\left(\frac{4}{3}\right)+\frac{3260}{1701}P^{(2,11)}\left(\frac{4}{3}\right)+\frac{463}{81}P^{(2,9)}\left(\frac{4}{3}\right)+\frac{154}{27}P^{(2,7)}\left(\frac{4}{3}\right)-\frac{4}{405}P^{(4,13)}\left(\frac{4}{3}\right)-\frac{44}{945}P^{(4,11)}\left(\frac{4}{3}\right)\right\}\right],$$

$$b_{22}=\frac{8\pi^3\sqrt{\pi}}{45}\left[\frac{1}{2}P^{(2,11)}(1)+\frac{7}{2}P^{(2,9)}(1)+\frac{301}{24}P^{(2,7)}(1)+\theta A\frac{8}{3}\sqrt{\frac{2}{3}}\left\{\frac{1528}{1701}P^{(2,11)}\left(\frac{4}{3}\right)+\frac{320}{81}P^{(2,9)}\left(\frac{4}{3}\right)+\frac{301}{54}P^{(2,7)}\left(\frac{4}{3}\right)-\frac{8}{2835}P^{(4,11)}\left(\frac{4}{3}\right)\right\}\right].$$

Errata: On the Paramagnetic Rotation of Tysonite

J. H. Van Vleck and M. H. Hebb, *University of Wisconsin*

(Phys. Rev. **46**, 17, 1934)

In the first line of the second column of the abstract column, and everywhere on pages 26–32, the word *trigonal* should be substituted for *triclinic*.

The Melting Parameters of Nitrogen and Argon under Pressure, and the Nature of the Melting Curve

P. W. BRIDGMAN, *Harvard University*

(Received September 20, 1934)

New measurements have been made of the melting parameters (pressure-temperature coordinates of the melting curve and change of volume) of nitrogen and argon up to 5500 kg/cm², and the latent heat of melting has been calculated from them. The qualitative behavior of these parameters is exactly like those of all other normal substances (with rising melting curves) hitherto measured, so that there is no experimental basis for the expectation of a critical point between liquid and crystalline phases, or of a maximum or of an asymptotic temperature, but all the experimental evidence indicates only a rise of the melting curve to indefinitely high temperature and pressure.

THE question of the nature of the melting curve has been stimulated to fresh consideration recently by the measurements of Simon[1] of the melting curves of helium, hydrogen, neon, argon and nitrogen. These experiments contain an important and novel feature in that a domain of low temperature new for this type of experiment was entered; the pressure domain on the other hand was not as extensive as had been previously explored with respect to this class of phenomena.

The question at issue with regard to the character of the melting curve has at present apparently resolved itself into the question of which one of the following three possibilities corresponds to the facts: does the melting curve end in a critical point like the critical point between liquid and vapor at some finite pressure and temperature, so that continuous passage between liquid and solid (or crystalline) phase would be possible, or does it rise to a maximum temperature at some finite pressure, and from here fall again, so that a substance might be first frozen and then melted again by applying sufficient pressure at constant temperature (hypothesis of Tammann), or does it merely rise to indefinitely high temperatures and pressures, so that no matter how high the temperature a pressure could be found high enough to force crystallization? Obviously in the nature of the case the third possibility can never be proved by direct experiment, but can be indicated only by some plausible method of extrapolation. The first and second possibilities could, on the other hand, be established by reaching experimentally a critical point or a maximum temperature; this however has not been done, so that the existence of a critical point or maximum can at present also be made probable only by some method of extrapolation. The shape of the melting curve by itself gives no necessary information as to the existence of a critical point, for a curve with a form of equation indicating indefinite rise with temperature and pressure might well be terminated by a critical point. An example of this is Simon's own equation which he finds fits very well a large number of melting curves, $\log(p+a)=c\log\tau+b$. On such a curve a critical point can be indicated only by the extrapolation of some other datum, such as for example the difference of volume between the two phases or the latent heat, for both these quantities vanish at the critical point. Simon clearly recognized this. Since his personal opinion was that the curve ends in a critical point, he initiated measurements of the latent heat along the melting curve of helium, hoping to find the decrease that might point to a critical point. Most unfortunately, his experiments at Breslau had to be terminated before any satisfactory results could be obtained. The opinion of Simon, however, that there is a critical point, seems to be shared in a number of quarters, and in any event the opinion seems to be pretty widely spread that the question is still open. Thus in the thesis just published at Leiden of J. H. C. Lisman[2] on the melting curves of condensed

[1] F. Simon, M. Ruhemann and W. A. M. Edwards, Zeits. f. physik. Chemie **B2**, 340 (1929); **6**, 62 (1929); **6**, 331 (1930).

[2] J. H. C. Lisman, *Smeltlijnen van gecondenseerde Gassen*, Thesis published by Eduard Ijdo, Leiden, 1934.

gases, in which there is a discussion of all previous results, the statement is made in conclusion that the grounds do not exist for a decision between a critical point and indefinite rise with pressure and temperature, although a maximum temperature may probably be ruled out.

My personal opinion on this subject, based on experiments made now 20 years ago on the melting of some 25 substances in the extreme temperature range from −38°C to +270°C and to pressures usually four times greater than the highest previously reached,[3] was that the experimental evidence unanimously agrees in giving no indication for the existence of a critical point or maximum, but indicates unequivocally that, unless there is some reversal at pressures at present beyond reach of trends nearly universal in the experimental domain, we must expect that the melting curve rises to indefinitely high temperatures and pressures. The only exceptions are the falling melting curves of the abnormal substances bismuth and gallium, and these evidently should not be given weight in drawing a general conclusion. The fact that this conclusion, which seemed to me to rest on such unexceptional experimental evidence, has not been generally accepted might be taken perhaps to indicate that there was some essential feature which I had overlooked. The suggestion therefore that the permanent gases in the low temperature region might give information qualitatively different in character from the information obtainable at higher temperatures from substances liquid under normal conditions challenged an experimental attack.

I have now succeeded in obtaining the complete melting parameters, that is, the pressure-temperature coordinates of the melting curve, the difference of volume between crystalline and amorphous phases, and the latent heat (this latter by calculation from Clapeyron's equation), of nitrogen and argon down to the temperature of boiling nitrogen (77° Abs.) and up to pressures of 5500 kg/cm², which was also approximately Simon's pressure range. That is, for these two substances I have completed Simon's data by measuring the difference of volume, thus obtaining the additional parameters necessary to indicate by extrapolation which of the three possibilities mentioned above is realized. Lower temperatures were not at my command, so that I could not examine Simon's other three gases.

There were experimental difficulties and modifications in previous technique necessary; no attempt will be made to describe these here, but they will be given in detail elsewhere, probably in *Proceedings of American Academy of Arts and Sciences*. Suffice it to say here that sharp melting curves were obtained, internal evidence of the purity of the gases and the satisfactory functioning of the apparatus. The detailed paper will also contain new data, not presented here, for the p–v–t relations of the amorphous phase in the new domain of temperature and pressure; it would seem that there are no previous measurements on nitrogen below 0°C, and no measurements at all at any temperature of the absolute volume of argon at pressures above 200 kg/cm², although there are measurements of my own on the *change* of volume of argon above 3000 kg/cm².

The melting parameters of nitrogen and argon are presented in Tables I and II. Some of the parameters at atmospheric pressure of nitrogen are bracketed in the table. The reason for this is

TABLE I. *Melting parameters of nitrogen.*

Pressure (kg/cm²)	Temp. Abs.	$d\tau/dp$	ΔV cm³/g	Latent heat kg cm/g	$p\Delta V$
1	63.14°	(.0209)	(.072)	(218)	0
1000	82.3	.0176	.058	271	58
2000	98.6	.0153	.047	302	94
3000	113.0	.0135	.040	334	120
4000	125.8	.0124	.033	335	132
5000	137.8	.0117	.029	342	145
6000	149.2	.0112	.026	346	156

TABLE II. *Melting parameters of argon.*

Pressure kg/cm²	Temp. Abs.	$d\tau/dp$	ΔV cm³/g	Latent heat kg cm/g	$p\Delta V$
1	83.9°	.0238	.0795	280	0
1000	106.3	.0211	.0555	280	55
2000	126.4	.0192	.0425	279	85
3000	144.9	.0178	.0340	277	102
4000	162.0	.0165	.0280	275	112
5000	178.0	.0155	.0240	276	120
6000	193.1	.0146	.0210	277	126

[3] P. W. Bridgman, Phys. Rev. **3**, 126, 153 (1914); **6**, 1, 94 (1915).

that it is probable that the parameters at 1000 kg/cm² and higher refer to α-nitrogen (the modification stable below 35.5°K at atmospheric pressure) rather than to β-nitrogen, which melts at atmospheric pressure at 63.14°K. The point is not entirely certain, however, and cannot be settled until there are more accurate measurements of the density of the solid phases at atmospheric pressure. This matter is discussed at some length in the detailed paper.

As far as the pressure-temperature parameters alone are concerned my melting temperatures are distinctly higher than those of Simon at the same pressure; for argon the maximum discrepancy is about 2.5°, but for nitrogen the discrepancy is more serious, increasing steadily with increasing pressure to a maximum of about 6° at 5500 kg/cm². The direction of the discrepancy is such that it would be accounted for by impurity in Simon's material, but I think that the correct explanation is something else. Simon's method was the method of the plugging of a capillary, first used by Keesom.[4] Solidification is indicated by the failure of an increase of pressure at one end of the capillary to get transmitted to the other end. It is obvious that there must be shearing stresses in the plug of solid which stops the capillary, and it is known from thermodynamics that the melting point is depressed by a shearing stress by an amount proportional to the square of the stress. The shearing stresses would be expected to become larger at higher pressure, since it is general experience that viscosity may increase enormously under pressure. Simon's capillary was only 0.15 mm in diameter, so that there would seem to have been a possibility of fairly large shearing stresses. The point could be settled, if the experiments were repeated, by varying the size of the capillary.

The important data for the question at issue are contained in the ΔV and the latent heat columns of the tables. If there is a critical point, ΔV and latent heat must extrapolate in such a way as to indicate that they will vanish together at some finite temperature and pressure. For argon the latent heat is constant within experimental error over the entire range, and for nitrogen it rises to an approximately constant value; in neither case is there any justification for the supposition that the latent heat will ever vanish. ΔV decreases with rising pressure and temperature, but it is convex toward the pressure or temperature axis in such a way as to give no justification for the expectation that it will vanish at any finite temperature. If the behavior of ΔV were like that on the liquid-vapor curve it would be concave toward the pressure or temperature axis, and would plunge vertically into the axis at the critical point. As an incidental observation it may further be remarked that if ΔV vanishes at infinite pressure it vanishes less strongly than hyperbolically, as shown by the continuous increase of $p\Delta V$ over the entire range.

If there is a maximum temperature on the melting curve (hypothesis of Tammann), then $d\tau/dp$ plotted against temperature should be concave toward the temperature axis and should plunge vertically into it. Actually $d\tau/dp$ against temperature is convex toward the axis with no indication that it will ever cross. If there were an asymptotic temperature at infinite pressure, which is the hypothesis of Schames,[5] not previously mentioned, $d\tau/dp$ would cut the axis at some finite temperature.

In every one of these aspects just mentioned the behavior of nitrogen and argon is exactly like that of all other normal substances hitherto examined, that is, excepting bismuth and gallium, and the general conclusion must therefore be the same. Not one of the positive qualitative criteria demanded by either a critical point, a maximum temperature at finite pressure, or an asymptotic temperature at infinite pressure, is satisfied, but every qualitative feature points unequivocally toward the indefinite rise of the melting curve to continually higher temperatures and pressures.

The almost universal prevalence of these qualitative features appeals to me as something of great significance, which apparently has not yet been appraised at its full theoretical importance. The significance is increased now with the discovery of a new high pressure modification of bismuth,[6] and the certainty that beyond

[4] W. H. Keeson, Communications from Leiden, No. 184b, 1926.

[5] L. Schames, Ann. d. Physik **38**, 830 (1912); **39**, 887 (1912).

[6] P. W. Bridgman, Phys. Rev. **45**, 844 (1934).

25,000 kg/cm² bismuth also has a rising melting curve.

It would of course have been gratifying if I could have extended these measurements to helium also and found its ΔV and latent heat along its melting curve, for Simon stresses the point that exploration of the melting curve of helium over a comparatively low range of pressure and temperature might be expected to give as much information about the essential character of the melting curve as an exploration over a much wider range for other substances. The reason given for this is that such an exploration for helium exceeds the critical temperature by a very much larger factor than is possible for other substances. Thus Simon explicitly comments on the fact that in following the melting curve of helium to 55° Abs. and 5500 kg/cm² he has exceeded the critical temperature by a factor of 8-fold, whereas previously the critical temperature had been exceeded at most by 20 percent in the case of CO_2. I believe, however, that examination will show that these considerations have less pertinence than at first appears. The implication, of course, is that in some way the critical parameters for the change from liquid to vapor are of importance for the phenomenon of freezing to the crystalline phase, and that something analogous to the law of corresponding states for liquid-vapor will carry over to amorphous-crystal, with some connection between the two sets of reduced parameters. Not only is there, so far as I know, no reason theoretically to expect any such connection, but I have previously shown on the basis of the experimental evidence that there can be no law of corresponding states for the freezing of different substances. Until some connection has been established therefore between liquid-vapor and amorphous-crystal phenomena, there would seem to me no reason to ascribe greater significance to the fact that Simon has been able to exceed the critical *temperature* of helium by a factor of 8 than to the fact that the critical *pressure* of CO_2, for example, had previously been exceeded by a factor of 165. It would seem to me on the contrary that any special effects to be shown by helium would be expected in the low temperature domain where degration and similar effects occur, and that having successfully got helium out of this domain into that of normal temperature phenomena, it would be expected to have exhausted its possibilities of giving unique information, and from here on to be of perhaps not much greater significance than other substances. The mere fact that it is possible to bring the melting curve of helium up into the region of normal temperature effects is in itself an argument for the significance of the universal traits of the melting curve discussed above.

Acknowledgment is made of financial assistance from the Rumford Fund of the American Academy of Arts and Sciences.

Erratum: A New Method for Measuring Elastic Moduli and the Variation with Temperature of the Principal Young's Modulus of Rocksalt Between 78°K and 273°K

LEWIS BALAMUTH, *College of the City of New York*

(Phys. Rev. **45**, 715, 1934)

DR. S. L. QUIMBY of Columbia University, New York, has recently pointed out an error in Eq. (13) on page 716 of the above paper. This equation should read

$$f_i = n(G_i^{\frac{1}{2}}/2\rho_i l_i^{\frac{1}{2}})(1 - \pi^2 n^2 \sigma_i^2 \theta_i / 2 l_i^2 A_i)$$

instead of

$$f_i = n(G_i^{\frac{1}{2}}/2\rho_i l_i^{\frac{1}{2}})(1 - \pi^2 n^2 \sigma_i^2 \theta_i / 4 l_i^2 A_i).$$

However, the correct formula was used in computing the results compiled in the various tables in the paper.

LETTERS TO THE EDITOR

Prompt publication of brief reports of important discoveries in physics may be secured by addressing them to this department. Closing dates for this department are, for the first issue of the month, the twentieth of the preceding month; for the second issue, the fifth of the month. The Board of Editors does not hold itself responsible for the opinions expressed by the correspondents.

A Transition in Aluminum at 79°C

Results of thermoelectric measurements in homogeneous aluminum circuits[1] have been analyzed successfully[2] by the theory of Band and Feng[3] with the addition of the hypothesis that there is a discontinuity (irreversible transition) of structure at 79°C. The thermoelectric power difference between the two forms is of the order of 0.005 microvolt per degree, depending slightly on tension.

Direct tests have been performed as follows: A sample of the aluminum wire was mounted under zero tension through the axis of a movable heater, and its ends taken to a thermostat where copper leads connected to a Paschen galvanometer (resistance 13 ohms) adjusted to a sensitivity of 200 mm per microvolt.

Typical results are as follows: Symmetrical heating between two points (A and B) above 80°C was maintained for several hours—no e.m.f. was observed. Immediately after cooling, the heater was shifted over A, and a heating-cooling cycle obtained of e.m.f. against T_A,—see Fig. 1. Immediately after this cycle was completed a second heating-cooling process gave an entirely different cycle above 79°C,—see Fig. 2. Sample curves when the heater was over B (e.m.f. against T_B) are given in Fig. 3.

Heating the whole wire above 80°C for six hours removed all trace of hysteresis, but hysteresis phenomena reappeared in this specimen within twenty-four hours.

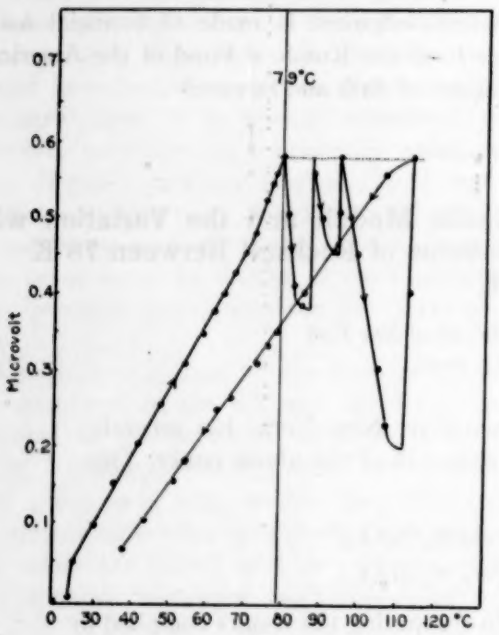

FIG. 1.

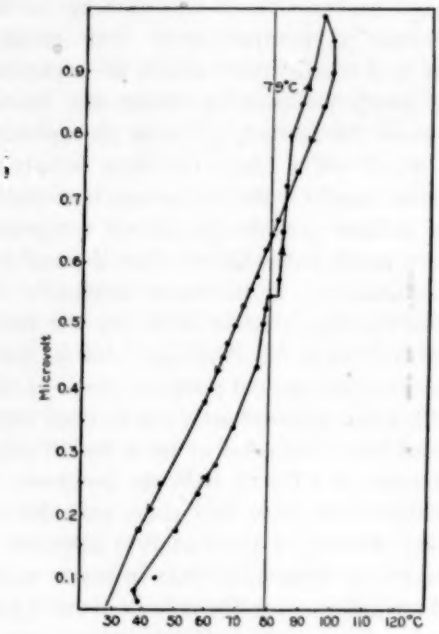

FIG. 2.

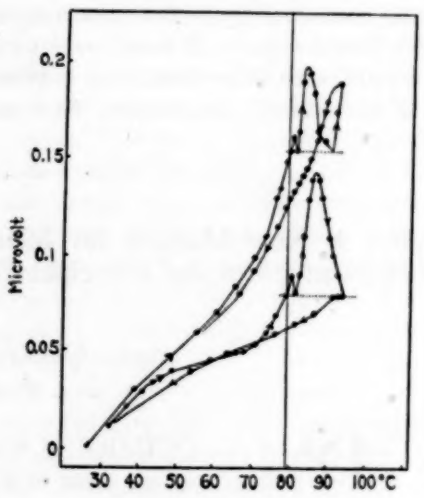

FIG. 3.

The magnitudes of voltages obtained seem to depend upon mechanical treatment of the specimen during mounting in the apparatus, and thus presumably upon small internal strains. A simple recrystallization theory does not seem sufficient to explain the variety of hystereses

observed; it is clear from all results however that there is a transition of some kind at 79°C ±0.5°.

The problem is now being attacked by more refined methods, since the preliminary exploration has given consistently positive results.

WILLIAM BAND
Yenching University,
Peiping,
September 12, 1934.

[1] Band and Li, *Longitudinal Thermoelectric Effect (3) Aluminium* Proc. Phys. Soc. appearing shortly.
[2] Band, *Longitudinal Thermoelectric Effect (4) Aluminium continued*, Proc. Phys. Soc. appearing shortly.
[3] Feng and Band, *Longitudinal Thermoelectric Effect (1) Copper*, Proc. Phys. Soc. **46**, 515 (1934).

Elastic Scattering of Fast Electrons in Mercury and Agreement with Mott's Theory

Jordan[1] has reported good agreement between Mott's theory and the experimentally measured angular distribution of elastically scattered electrons for 2000 volts in mercury in the angle range 0° to 42°. He was unable to go to angles greater than 48°, because he could not measure the small scattered current accurately at large angles and high voltages. Agreement at such a voltage in mercury is not to be expected, since Mott[2] made approximations which are equivalent to assuming that the classical "distance of closest approach," b, of the electron to the nucleus is small compared to the de Broglie wave-length (λ) of the electron. For 2000 volts in mercury, $b=0.57$A, and $\lambda=0.27$A. According to Morse's criterion,[3] which is that the minimum energy for which Mott's equations are accurate is of the order $50Z^2$ (Z is the atomic number), we should not expect good agreement much below 320,000 volts in mercury.

In preliminary experiments, using an apparatus developed to record the angular distribution of scattered electrons photographically, we have found a distinct maximum near 112° at 2000 volts in mercury. Since Mott's theory gives a monotonic curve, we can conclude that there is not good agreement over the whole angular range for 2000 volt electrons in mercury.

A horizontal beam of fast electrons was shot through a vertical molecular beam of mercury. The electrons scattered in a horizontal plane pass through slots in three semicylindrical concentric shields. A retarding potential on the second shield stops all the inelastically scattered electrons, while a high potential on the third shield accelerates the elastically scattered electrons to the film, which is in the form of a semicircular strip. The angular distribution of elastically scattered electrons is thus recorded as the linear distribution of blackening along the strip of film. The decrease in scattered intensity as the incident electron energy is increased, is overcome by increasing the acceleration to the film, which in effect increases its sensitivity.[4] The position of maxima observed at 800 volts in mercury showed good agreement with those observed by Arnot[5] and Jordan and Brode.[6] With increasing electron energy, these maxima moved in to smaller angles, till at 2000 volts only one peak, at 112°, was clearly resolved.

This research is admittedly incomplete because of the transfer of the author to another institution. The investigation was suggested by Professor A. L. Hughes.

W. E. STEPHENS
Washington University,
St. Louis, Missouri,
October 27, 1934.

[1] E. B. Jordan, Phys. Rev. **45**, 47 (1934).
[2] N. F. Mott, Proc. Roy. Soc. **A127**, 658 (1930).
[3] A. L. Hughes and J. H. McMillen, Phys. Rev. **43**, 875 (1933).
[4] B. von Borries and M. Knoll, Phys. Zeits. **35**, 229 (1934).
[5] F. L. Arnot, Proc. Roy. Soc. **A130**, 655 (1931).
[6] E. B. Jordan and R. B. Brode, Phys. Rev. **43**, 112 (1933).

Note on New Bands of the Ionized Nitrogen Molecule

It has been found possible by employing a slit-form cathode to operate a discharge in pure nitrogen so as to develop the $^2\Sigma \rightarrow {}^2\Sigma$ bands of N_2^+ with considerable intensity and great freedom from the troublesome overlapping of spectra of the neutral nitrogen molecule. Measurements on the best plates have enabled the assignment of some 400 new lines to be made including the (2–2), (3–4), (5–7), (6–8), (0–3), (1–4) and (2–5) bands. The locations of the origins have been obtained graphically from the frequencies of the early R and P lines and are given in Table I together with the wave-lengths of the heads.

TABLE I.

Band	Head (A)	Origin (cm^{-1})	Band	Head (A)	Origin (cm^{-1})
(2–2)	λ3857.9	25939.8	(6–8)	λ4466.6	22406.5
(3–4)*	λ4168.0–0.4	24013.8	(0–3)	λ5228.0	19139.7
(3–5)*	λ4554.4–0.2	21971.1	(1–4)	λ5148.8	19434.7
(5–7)	λ4486.2	22305.4	(2–5)	λ5076.5	19710.4

* Double headed due to rotational perturbation.

In addition it has been possible to follow the (3–5) band to the origin and with the help of the data on the (3–4) band to determine with considerable certainty that the $v'=3$ levels are perturbed at only two points (and not three as inferred by Coster and Brons).[1] Densitometer records made from both first and second order plates of these bands indicate pretty definitely that the lines showing the *greater* perturbation (centering at $K'=9$) must originate on $T_1'(K+\frac{1}{2})$ levels while those showing the *smaller* perturbation (centering between $K'=6$ and 7) must originate on the $T_2'(K-\frac{1}{2})$ levels. This reverses the assignment made by Coster and Brons from a study of the (3–5) band alone. It must be borne in mind, however, that these authors were not able, because of the many impurity lines present on their plates, to follow each branch to the origin and admitted that their relative intensity data did not lead unambiguously to their assignment.

The rotational constants and the observed origins are in close agreement with the results predicted by other observers.[1, 2]

A more extended account of the experimental arrangements and the numerical results is appearing in a current number of the *Proceedings of the American Academy of Arts and Sciences.*

F. H. CRAWFORD
P. M. TSAI
Jefferson Physical Laboratory,
Harvard University, Cambridge,
October 26, 1934.

[1] Coster and Brons, Zeits. f. Physik **73**, 747 (1932).
[2] Parker, Phys. Rev. **44**, 914 (1934).

The Quantum Theory of Electromagnetic Fields

Through the kindness of Drs. Darrow and Bozorth I have read the preprint on *Quantum Electrodynamics* presented by Professor Born at the recent International Conference on Physics at London. In section 4 of the paper, he has very kindly referred to a recent paper of mine,[1] but in a manner which may possibly give a wrong impression as to its contents. As the paper in question may not readily be available to those interested in the subject, it seems desirable to point out that there are important differences between Born's treatment[2] and mine, which are primarily not of a mathematical character, as Born seems to suggest, but which are essentially physical (although, of course, they come to mathematical expression). These are:

(1) In I, as opposed to II, the electromagnetic theory of the mass of the electron has no part. Indeed since the positron and proton have the same charge, it is difficult to see how the electromagnetic field, itself determined by the charge, can determine the mass of the singularity in these two different cases, inasmuch as the radius is already fixed by Born's absolute field.

(2) The existence of atoms of electric charge (a hypothesis) seems to me to require us to give up classical ideas of the field of an electron (in much the same way that attempts to construct the e.m. field of a single light quantum have had to be abandoned). On the other hand, Born's success in obtaining a finite mass for a point singularity derives from his use of a particular law of variation of electric intensity in its neighborhood.

(3) It is clearly pointed out in I that the analogues of Schrödinger's operators are to be introduced only if at the same time we introduce the notion of a system of electromagnetic fields—a particular e.m. field is a member of a system just as a particular solution of the Hamilton-Jacobi partial differential equation in dynamics is a member of a system of solutions. This idea of a system of e.m. fields finds no mention at all in Born's work. It is absolutely fundamental to the development of the transformation theory of e.m. fields (analogous to the transformation theory of dynamics) which must be the precursor of a quantum theory of the field.

(4) Born uses the conception due originally to Maxwell of the e.m. field as itself a dynamical system, whereas I have attempted to change drastically the naïve attitude which regards the e.m. field as substantial. It is no more substantial than a momentum vector-field or any other vector field in physics.

(5) The effect of quantizing the field cannot be merely to parcel the charge into bundles $\pm e$, otherwise one might just as well make the simple hypothesis of atoms of charge and leave it at that. One must also look for structure of the field in space and time using a favorable method of analysis, in a way analogous to that in which one shows the wave properties of an electron or atomic beam. This point is not made in II. It may be here remarked that this is the consideration that lacks expression in the commutation rules for the field components due to Heisenberg and Pauli and also in Born's most recent work. The fact that, as Bohr has shown, these rules agree with the uncertainties in field specification which would arise from the mechanical measurements, shows that they do not touch the atomicity of electric charge except insofar as electrons are required for the measurements.

These considerations, however, in a subject which offers so many difficulties, do not detract from the value of Born's contributions to its elucidation.

W. H. Watson

McGill University,
Montreal, Canada,
October 31, 1934.

[1] Watson, Trans. Roy. Soc. Can. Sec. 3, 28 (1934), referred to as I.
[2] Born, Proc. Roy. Soc. **A143**, 410 (1934), especially pp. 410–423, referred to as II.

Proceedings of the New England Section of the American Physical Society

MINUTES OF THE WILLIAMSTOWN MEETING, OCTOBER 13, 1934

THE fifth regular meeting of the New England Section was held at Williams College, Saturday, October 13. The presiding officers at the two morning sessions for contributed papers were Professor W. G. Cady, Chairman of the Section, and Professor G. W. Hull. The presiding officer at the business meeting and afternoon session was Professor Cady, Chairman.

The business meeting, also in the morning, was devoted to the election of officers for the year 1935. The officers for the preceding year were re-elected for a second year. These officers are:

W. G. Cady, Chairman,
Louise McDowell, Vice-Chairman,
P. M. Morse, Secretary-Treasurer,
N. H. Black and F. A. Saunders, Program Committee.

A vote of thanks was extended to the members of the Physics Department at Williams College for their generous hospitality.

Professor Brinsmade then talked on *The Honors Work in Physics at Williams*. There was considerable discussion after the paper.

The Program Committee met after this paper, decided to hold the next meeting of the Section at Massachusetts Institute of Technology on February 2, 1935, and accepted the very kind invitation of Brown University to meet at Providence next fall.

At the luncheon in the gymnasium, President Dennett of Williams gave an address of welcome to the Section.

The afternoon session was devoted to invited papers. Dr. Saul Dushman, of the Research Laboratories of the General Electric Company, gave an address on *The Relationship of Science and Industry*, illustrated by lantern slides and by several very interesting demonstrations.

President Compton of Massachusetts Institute of Technology spoke on *The Scientific Problems of the Nation*, an illuminating discussion of the ways by which the government was helping, and was intending to help, scientific research in this country.

One hundred members attended the morning sessions, and one hundred and forty the afternoon session.

The Program of the Section consisted of 14 papers, the Abstracts of which are given below.

PHILIP M. MORSE
Secretary-Treasurer

ABSTRACTS

1. Ionization Currents Produced by Radon, Ra A and Ra C′ in Cylindrical Ionization Chambers. ROBLEY D. EVANS, National Research Fellow, *University of California*, (now at *Massachusetts Institute of Technology*).—A general theoretical equation is derived for the ionization produced in cylindrical ionization chambers by Rn and its decay products. Where dv/dt = volts per sec. discharge, j = fractional saturation of the ion current, C = electrostatic capacity in cm, A = curies of Rn present at time $t=0$, λ_1 = decay constant of Rn, $1/\mu$ = stopping power of the gas in the ionization chamber, d = cm diameter and h = cm height of the chamber, and $t \geq 3$ hr.:

$$dv/dt = 5.3\times10^{8}(j/C)(3.57-5.00\mu/h - 3.47\mu/d+5.48\mu^{2}/dh)Ae^{-\lambda_1 t},$$

when d and h are greater than twice 6.60μ cm, the range of the Ra C′ alpha-ray. Experimental confirmation employing standard radium solutions is described. Where either C or A is known, the other may be computed, therefore Rn ionization may be employed for absolute capacity measurements. General equations are also derived for alpha-ray ionization (1) above a plane surface due to a homogeneous radioactive substance below the plane, and (2) a radioactive substance uniformly distributed on a wire normal to the plane, and (3) for the ionization outside a dihedral right angle enclosing a homogeneous radioactive substance.

2. The Vapor Pressure of Calcium between 500 and 625°C. ERIK RUDBERG, *Massachusetts Institute of Technology*.—Calcium was deposited in vacuum on thin glass plates exposed to the atomic beam from the open end of a small molybdenum furnace containing the solid metal at constant temperature. From the amount deposited in a given time, determined to 10^{-4} g of Ca by a microchemical method, the vapor pressure p can be calculated. Special tests show that the reflection of atoms at the receiving plate is negligible. The pressures range from 10^{-6} to 10^{-3} mm. They can be represented by the empirical equation $\log p = 8.15 - 9670/T$, where T is the absolute temperature. These pressures are about ten times smaller than those

published by Pilling for the same temperatures. From available data on the specific heat of solid Ca as a function of T, the integrals occurring in the well-known vapor pressure equation of thermodynamics have been computed; from these and from the measured pressures the vapor pressure constant is calculated to be 15.4, as compared with the theoretical value 15.7 from statistical mechanics. The pressure data previously published yield a value 19.3 for this constant.

3. Counter Calibration and Cosmic-Ray Intensity. J. C. STREET AND R. H. WOODWARD, *Harvard.*—An absolute calibration of a set of counters has been obtained by determining their efficiencies and effective volumes. From observations recorded with this calibrated set, the number of ionizing cosmic rays is 0.80 ± 0.028 per cm per minute from unit solid angle at the vertical at sea level. The number of such rays from all directions as obtained by integration over an angular distribution curve is 1.48 ± 0.055 cm^{-2} min.$^{-1}$. This combined with Millikan's ionization chamber measurements gives an average specific ionization of 100 ± 3.7 ion pairs per cm path of a ray. Comparison with previous measurements is given.

4. Transition Effects in the Cosmic Radiation. J. C. STREET AND R. T. YOUNG JR., *Harvard.*—Transition curves similar to those found by Schindler at sea level have been obtained at Cambridge, Massachusetts, and at Lima, Huancayo, and Cerro de Pasca, Peru. The ionization current has been studied as a function of the thicknesses of lead shield above a small ionization chamber at the various stations. The equilibrium under air and lead and their difference, representing the magnitude of the transition, were determined for each location. The magnitude of the transition increases with altitude much more rapidly than the equilibrium ionization under lead. It is shown from the data that the increase of ionization with altitude, usually attributed to a soft primary component, is probably due to a changing equilibrium condition. Comparison with data on showers shows a close parallel between the variations in shower intensity and the transition variations.

5. The General Sum Rule in Intermediate Coupling. GEORGE H. SHORTLEY, National Research Fellow, *Massachusetts Institute of Technology and Harvard.*—The general sum rule—which says that the sum of the strengths of the lines of a transition array, in which the jumping electron is not equivalent to any in the ion, originating in (or terminating on) a level of quantum number J is proportional to $2J+1$—is shown to hold not only for LS and jj couplings but also for all intermediate couplings. Application is made to Ne $2p^53p\rightarrow 2p^53s$. For this array, Ladenburg and Levy obtained the relative strengths of the lines having the same terminal levels from measurements of anomalous dispersion, while lines having different terminal levels were related by direct intensity measurements. For these data a poor agreement is obtained with the general sum rule. If, however, instead of using the measurements of relative intensity, the lines having different final levels are related by the requirement that the general sum rule hold exactly with respect to the final levels, it is also found to hold satisfactorily with respect to the initial levels.

6. Spheroidal Functions. J. A. STRATTON, *Massachusetts Institute of Technology.*—One is led in a number of physical problems to an equation of the type

$$(1-z^2)w''-2(a+1)zw'+(b-c^2z^2)w=0,$$

which may be considered as next in order of complexity to the confluent hypergeometric equation. The problems may be roughly classified into two groups: ones involving spheroidal coordinates, in particular two-center problems such as the hydrogen molecule, and boundary value problems involving spheroidal or elliptical boundary surfaces; and secondly, problems the differential equations of which are characterized by periodic coefficients and which reduce to the above on making the transformation $z=\cos\theta$. As examples of this latter group may be mentioned electric filter problems, problems in rotating electrical machinery, and perturbation problems arising in celestial mechanics. If the condition be imposed that the solutions are to be finite and single valued at the regular points $z=\pm1$, the parameter b is limited to a discrete set of characteristic values. A set of functions satisfying the equation when b assumes a characteristic value has been defined and many of their properties investigated. The Mathieu functions are included as a special case $a=-\frac{1}{2}$, and the spheroidal wave functions correspond to $a=m$, an integer. Otherwise, the parameters a and c may assume any real or complex values. A method is proposed for calculating the characteristic values of b which appear to be applicable to the general study of the characteristic exponents of linear equations with periodic coefficients.

7. Symmetry of the Thermoelectric Effects in Single Crystals. H. P. STABLER, *Williams.*—In a single-crystal rod of a non-cubic metal a transverse temperature gradient produces a longitudinal e.m.f. As a result of this fact the longitudinal thermoelectric power of such a rod must depend not only on its crystallographic orientation but also on the orientation of the temperature gradient. Assuming Kelvin's "axion of the superposition of the thermoelectric effects" it is shown that

$$\tau\frac{dE}{d\tau}l=P_\perp+\frac{\cos\theta\cos\phi}{\cos(\theta-\phi)}(P_{||}-P_\perp),$$

where θ is the angle between the principal crystallographic axis and the geometric axis, ϕ, the angle between the crystallographic axis and the temperature gradient. If the temperature gradient is determined largely by heat flow along the crystal then $\tan\phi=k_{||}/k_\perp\tan\theta$. The above relation has been found to be compatible with all the existing data on thermoelectric symmetry. In particular it explains the apparent deviation from Kelvin's $\cos^2\theta$ law found by Bridgman and others for tin and bismuth. The nonlinearity with $\cos^2\theta$ of the direct measurements of the Peltier heat for bismuth, as reported by Fagan and Collins, may be accounted for by a similar neglected transverse effect.

8. Decrement Investigations of Quartz Resonators. K. S. VAN DYKE AND J. P. HAGEN, *Wesleyan*.—At a meeting of this section two years ago one of the authors reported logarithmic decrements of from 1.1 to 1.4×10^{-3} by a decay method for quartz crystals with finely ground surfaces in vacuum when all mounting losses are eliminated. We now find upon removal of surface imperfections the decrement still further reduced to 5.4×10^{-4}; this is for vibrations at 67.5 kc along the y axis and 27°C. Etching in hydrofluoric acid prior to chemically depositing the silver electrodes is responsible for the elimination of surface losses. The resistance and inductance elements of the equivalent network which the method also yields are 340 ohms and 450 henries for the resonator whose decrement is quoted above. From these, using equations developed in a previous paper (Proc. I.R.E. **16**, 742–764 (1928)), and the dimensions of the resonator ($x=0.491$ cm; $y=4.05$ cm; $z=0.471$ cm) the piezoelectric coefficient and Kimball's internal friction constant are found to be 5.29×10^{4} cgse and 0.007×10^{-15}. The above decrement values are so extreme that their check by some entirely different method is highly desirable. Complete support of the method is found in decrement determinations of another crystal, whose decrement was about 9×10^{-4} at 64.5 kc. These were made alternately by the decay method and by plotting its resonance curve and the two methods found to be in agreement to within a few percent.

9. The Effect of Frequency of Impressed Electromotive Force upon the Power Loss and Dielectric Constant of Various Glasses. LOUISE S. MCDOWELL, PERSIS BULLARD AND MARIAN E. WHITNEY, *Wellesley*.—Power factor, power loss per unit applied potential difference, and dielectric constant for several glasses, at room temperature, with variation in frequency from 60 to 14,000 cycles per sec. and from 100 to 6000 kc per sec. Data are given for five of the six glasses previously investigated by McDowell and Begeman. At frequencies above about 500 kc the power loss in most glasses is found to increase with frequency too rapidly to fit the equation $P/E^2=C\omega\tan=\text{const.}\times f^n$ previously found. Results are compared with those of other investigators and the possibility that the deviation may be due to errors in method is discussed.

10. Band Spectra of LiH, LiD and NaD. F. H. CRAWFORD AND T. JORGENSEN, JR., *Harvard*.—The observations on the $^1\Sigma\rightarrow{}^1\Sigma$ emission bands of lithium hydride (Phys. Rev. **45**, 737 (1934)) have been greatly extended in absorption with the use of both heavy and light hydrogen. The study of densitometer records of the plates has resulted in the identification of nearly 5000 lines including those of Li^7H, Li^6H, Li^7D and Li^6D. The isotope shifts for Li^7H and Li^7D are very large, being for example about 130A for the (14–0) bands. In this case the observed origins are $\nu_{(14,0)}=31{,}066.8$ cm^{-1} and $\nu^1_{(14,0)}=29{,}843.7$ cm^{-1}, whereas the conventional isotope theory predicts the Li^7D origin at 29,834.9 cm^{-1}. The discrepancy seems altogether too large to attribute to experimental error although uncertainty in the vibrational data given in the literature for the upper state is certainly responsible for part of it. It furthermore contains the as yet unknown electronic isotope shift. Improved vibrational constants can unfortunately only be got after most of the lines in the Li^7H spectrum have been measured since no heads are formed and origins must be computed from rotational data. This discrepancy is in the direction predicted by Kronig (Physica **1**, 617, May (1934)) and resulting from the non-identity of the potential energy curves of hydrides and deuterides, whereby the vibrational frequencies of the deuteride molecule are in certain cases slightly greater than those computed from the simple isotope theory. We have recently succeeded in photographing the corresponding spectrum of NaD—a similar appearing headless concourse of lines extending from about λ3500 to λ4500A. Data on this spectrum and comparisons with those of lithium will be reported subsequently.

11. The Spectrum of Calcium Deuteride. WILLIAM W. WATSON, *Yale*.—The several band systems of the CaD molecule have been photographed at high dispersion, by using as a source a Ca arc in an atmosphere of fairly pure deuterium at reduced pressure, in order to get accurate data on the hydrogen isotope effects. Quantum analyses of the 0,0 and 1,1 bands of the "B" system in the red and of the 0,0 band of the ultraviolet "C" system are presented. Although the ratio of the reduced masses for CaH and CaD is 0.51276, the ratio of the B_e constants of the normal $^2\Sigma$ state is 0.51337. The magnitude of this difference, the problem of determining the B_e constants for the B state which interacts strongly with a near-lying electronic state, and the isotope effect on the large ρ-doubling of the B state are discussed. Multiple perturbations of considerable size completely disrupt the usual arrangement of rotational lines in the C system.

12. Honors Work in Physics at Williams College, Professor J. B. BRINSMADE, *Williams College*.

13. The Relationship of Science and Industry, Dr. SAUL DUSHMAN, *General Electric Research Laboratory*.

14. The Scientific Problems of the Nation, President KARL T. COMPTON, *Massachusetts Institute of Technology*.

AUTHOR INDEX TO ABSTRACTS OF THE WILLIAMSTOWN MEETING

Brinsmade, J. B.—No. 12
Bullard, Persis—see McDowell

Compton, Karl T.—No. 14
Crawford, F. H. and T. Jorgensen, Jr.—No. 10

Dushman, Saul—No. 13

Evans, Robley D.—No. 1

Hagen, J. P.—see Van Dyke

Jorgensen, T., Jr.—see Crawford

McDowell, Louise S., Persis Bullard and Marian E. Whitney—No. 9

Rudberg, Erik—No. 2

Shortley, George H.—No. 5
Stabler, H. P.—No. 7
Stratton, J. A.—No. 6
Street, J. C. and R. H. Woodward—No. 3
—— **and R. T. Young, Jr.**—No. 4

Van Dyke, K. S. and J. P. Hagen—No. 8

Watson, William W.—No. 11
Whitney, Marian E.—see McDowell
Woodward, R. H.—see Street

Young, R. T.—see Street